# *Salmonella* induced cell-autonomous immunity

**Dissertation**

**zur Erlangung des Doktorgrades der Naturwissenschaften**

vorgelegt beim Fachbereich 14
Biochemie, Chemie und Pharmazie

der Johann Wolfgang Goethe-Universität
in Frankfurt am Main

von
Marcel Hahn
aus Neuwied

**Frankfurt am Main 2021**
**D30**

vom Fachbereich 14 der
Johann Wolfgang Goethe–Universität als Dissertation angenommen.

Dekan: Prof. Dr. Clemens Glaubitz

Gutachter: Prof. Dr. Volker Dötsch
Prof. Dr. Ivan Dikic

Datum der Disputation:

## Table of Contents

## Zusammenfassung

Die Fähigkeit der spezifischen und kontextabhängigen zellulären Adaption auf intrinsische und/oder extrinsische Signale ist das Fundament zellulärer Homöostase. Verschiedene Signale werden von Membranrezeptoren oder intrazellulären Rezeptoren erkannt und ermöglichen die molekulare Anpassung zellulärer Prozesse. Komplexe, ineinandergreifende Proteinnetzwerke sind dabei elementar in der Regulation der Zelle. Proteine und deren Funktionen werden dabei nach Bedarf reguliert und unterliegen einem ständigen proteolytischen Umsatz.

Die stimulusabhängige Gentranskription und/oder Proteintranslation nimmt hier eine zentrale Stellung ein, da die zugrundeliegende Maschinerie die Komposition und Funktion der Proteinnetzwerke entsprechend anpassen kann. Zusätzlich zur Regulation der Proteinabundanz werden Proteine posttranslational modifiziert, um deren Eigenschaften rasch zu ändern. Zu posttranslationalen Modifikationen zählen die Ubiquitinierung und/oder Phosphorylierung, welche die Proteinfunktionen hochdynamisch regulieren. Deregulierte Proteinnetzwerke werden oft mit Neurodegeneration und Autoimmun- oder Krebserkrankungen assoziiert. Auch Infektionen mit humanpathogenen Bakterien greifen stark in den Regulierungsprozess von Proteinnetzwerken und deren Funktionen ein. Die zelluläre Homöostase wird dadurch herausgefordert.

Bakterien der Gattung *Salmonella* sind zoonotische, gramnegative, fakultativ intrazelluläre Pathogene, welche weltweit millionenfach Salmonellen-erkrankungen hervorrufen. Von besonderer Bedeutung ist dabei *Salmonella enterica serovar* Typhimurium (hiernach *Salmonella*), welches im Menschen, meist durch mangelnde Hygienemaßnahmen, Gastroenteritis auslöst.

Immunität in Epithelzellen wird über das angeborene Immunsystem vermittelt und dient der Pathogenerkennung und -bekämpfung. Die Toll-*like* Rezeptoren (TLR) gehören zu den Mustererkennungsrezeptoren (*pattern recognition receptors*), welche spezifische mikrobielle Strukturen detektieren und eine kontextabhängige zelluläre Antwort generieren. *Danger*-Rezeptoren erkennen hingegen nicht direkt das Pathogen, sondern zelluläre Perturbationen, welche durch Zellschäden oder bakterielle Invasionen verursacht werden. Die intrinsische Fähigkeit der Wirtszelle, sich gegen Infektionen/Gefahren zu wehren

wird dabei als zellautonome Immunität bezeichnet. Dabei nehmen induzierte proinflammatorische Signalwege und zelluläre Stressantworten eine wichtige Stellung ein. Die zelluläre Stressantwort aktiviert unter anderem die selektive Autophagie. Diese kann spezifisch aberrante Organelle, Proteine und invasive Pathogene abbauen. Ein weiterer Stresssignalweg ist die *integrated stress response* (ISR), welche eine selektive Proteintranslation erlaubt und damit die Auflösung des proteintoxischen Stresses ermöglicht.

Zur Penetration von Epithelzellen benötigt *Salmonella* ein komplexes System an Virulenzfaktoren, welches die bakterielle Internalisierung und Proliferation in der Wirtszelle ermöglicht. *Salmonella* nutzt dazu ein Typ-III-Sekretionssystem. Das System sekretiert bakterielle Virulenzfaktoren in die Zelle, sodass eine hochspezifische Modulierung des Wirtes erzwungen wird.

Die Virulenzfaktoren SopE und SopE2 spielen dabei eine Schlüsselrolle, da sie die Pathogenität von *Salmonella* maßgeblich vermitteln. Durch molekulare Mimikry von Wirts GTP (Guanosintriphosphat) -Austauschfaktoren aktivieren SopE und SopE2 die Rho GTPasen CDC42 und Rac1. GTP-geladenes CDC42 und Rac1 wiederum aktivieren das Aktinzytoskelett und stimulieren die Polymerisierung von Aktinfilamenten über den Arp2/3-Komplex an der Invasionsstelle. Das Pathogen wird dadurch in ein membranumhülltes Vesikel, die sogenannte *Salmonella-containing* Vakuole (SCV), aufgenommen. Die SCV stellt eine protektive, replikative, intrazelluläre Nische des Pathogens dar und wird permanent durch verschiedene Virulenzfaktoren moduliert.

Im Allgemeinen führt die Aktivierung von Mustererkennungsrezeptoren und *Danger*-Rezeptoren also zu einer zellulären Stressantwort und Entzündungsreaktion, wodurch es zur Bekämpfung der Infektion kommt. Inflammatorische Signalwege werden meist über den zentralen Transkriptionsfaktor NF-κB (*nuclear factor 'kappa-light-chain-enhancer' of activated B-cells*) vermittelt. NF-κB bewirkt die Induktion von proinflammatorischen Effektoren und Stressgenen. Zellautonome Immunität wird zusätzlich durch antibakterielle Autophagie ermöglicht, wobei *Salmonella* selektiv über das lysosomale System abgebaut werden. Das bakterielle Typ-III-Sekretionssystem verursacht an einigen wenigen SCVs Membranschäden, sodass *Salmonella* das Wirtszytosol penetrieren. Zytosolische Bakterien werden dabei spezifisch ubiquitiniert. Dies erlaubt die Erkennung durch die Autophagie-Maschinerie.

In der vorliegenden Arbeit wurde die zellautonome Immunität von Epithelzellen während einer akuten *Salmonella* Infektion durch quantitative Proteomik untersucht. Dabei konnten wir eine hochdynamische Regulation des Proteoms in qualitativer und quantitativer Weise detektieren.
Wir analysierten dabei die infektionsinduzierten Proteinphosphorylierungsmuster zu unterschiedlichen Zeitpunkten. Die Proteinphosphorylierung stellt eine reversible, amplifizierbare und regulatorische posttranslationale Modifikation dar. Wir konnten dabei zeigen, dass eine *Salmonella* Infektion vorrangig proinflammtatorische, NF-κB-abhängige- und Rho GTPase Signalwege aktiviert. Diese simultane Aktivierung ist ein klassisches Merkmal der akuten *Salmonella* Infektion und ist von zentraler Bedeutung für die bakterielle Pathogenese. Innerhalb der Rho GTPasen nehmen CDC42 und Rac1 eine elementare Rolle ein. Die Virulenzfaktoren SopE und SopE2 aktivieren CDC42 und Rac1, welche die Internalisierung von *Salmonella* bewirken. Innerhalb infektionsassoziierter Rho GTPase Cluster konnten wir dabei erstmalig, im Kontext einer Infektion, die Kinase SIK2 identifizieren. Umfassende biochemische und funktionelle Untersuchungen offenbarten eine bisher unbekannte Schlüsselfunktion von SIK2 in der Aktin-abhängigen, zellautonomen Abwehr während einer *Salmonella* Infektion. Unsere Daten implizieren eine SopE-abhängige Aktivierung von SIK2, welche zellautonome Immunität gewährleistet. SIK2 vermittelt dabei die zelluläre Polymerisierung von Aktinfilamenten, welche vermutlich über den Arp2/3-Komplex katalysiert wird. Dieser Komplex rekrutiert mit SIK2 an die SCV und baut dort einen protektiven Aktinmantel auf. Die Depletion von SIK2 führt zur verstärkten bakteriellen Penetration der SCV, zur Hyperproliferation von *Salmonella* und inhibiert gleichzeitig die antibakterielle Autophagie zytosolischer Bakterien. SIK2 Depletion führt, besonders während einer *Salmonella* Infektion, zum Zusammenbruch des Aktinzytoskeletts und beeinträchtigt dadurch die Abwehrfunktion der Wirtszelle. Obwohl das Aktinzytoskelett während der bakteriellen Invasion manipuliert wird, trägt es kurz nach der Infektion, durch SIK2 vermittelt, zur zellulären Abwehr bei. SIK2 ist daher eine neue, zentrale Kinase der zellautonomen Immunität während einer *Salmonella* Infektion.

Um tiefere Einsicht in die Regulation der infektionsgetriebenen Änderungen der Proteinnetzwerke zu erlangen, analysierten wir die Proteintranslation. Die Kinetik des Translatomes ermöglichte weitreichende Aufschlüsse sowohl über die Regulation des zellulären, als auch des bakteriellen Proteomes unter Infektionsbedingungen. Von besonderer Bedeutung war dabei die konstante translationale Modellierung des NF-κB Signalweges. Diesem wurde bereits eine Schlüsselfunktion in der zellautonomen Immunabwehr von *Salmonella* zugeschrieben. Die zugrundeliegenden molekularen Mechanismen dieser Abwehr waren bis *dato* unbekannt. Wir konnten den molekularen Mechanismus aufklären und einen neuen Signalweg der NF-κB Kinase IKKβ und der *integrated stress response* charakterisieren. Dieser Signalweg vermittelt die zellautonome Immunität der IKKβ Kinase. Biochemische und funktionelle Analysen zeigten, dass die IKKβ Kinase die Aktivität der eIF2α Kinase EIF2AK3/PERK inhibiert und dadurch die ISR reguliert. Dieser molekulare Mechanismus agiert sowohl unter basalen, infektionsunabhängigen als auch unter *Salmonella* Infektionsbedingungen. Wir konnten zeigen, dass die funktionelle Inaktivierung der IKKβ Kinase zu einer PERK Aktivierung führt, welche über eIF2α Phosphorylierung die ISR aktiviert. Diese Aktivierung zieht eine selektive Proteintranslation nach sich, die im Falle der IKKβ Inaktivierung über den stressinduzierten Transkriptionsfaktor ATF4 getrieben wird.

Die funktionale Inaktivierung von IKKβ führt über die Aktivierung der ISR zur Hyperproliferation von *Salmonella*. PERK und ATF4 sind die zentralen Treiber des IKKβ-abhängigen ISR Signalweges. ATF4 Zielgene ändern dabei den Wirtsmetabolismus, wodurch die Hyperproliferation von *Salmonella* begünstigt wird. Darüber hinaus konnten wir zeigen, dass die neu entdeckte Signalachse IKK-PERK-ATF4 zur basalen bakteriellen Proliferation benötigt wird und möglicherweise gezielt von pathogenen Bakterien angesteuert werden kann. In diesem Zusammenhang war zu erkennen, dass ein bereits beschriebener Virulenzfaktor von *Shigella flexneri*, welcher den IKK-Komplex inhibiert, gleichzeitig auch die ISR aktiviert. Dem IKK-Komplex konnten wir somit eine neue, essentielle und protektive Kontrollfunktion der ISR, neben der bereits etablierten NF-κB Funktion, zuschreiben. Diese Entdeckung könnte weitreichende Konsequenzen für andere bakterielle Infektionen haben, da die Interferenz mit dem IKK/NF-κB Signalweg ein verbreiteter Virulenzmechanismus ist. Darüber hinaus könnte die Modulation des IKK-Komplexes zur Steigerung der zellulären Resilienz genutzt werden.

Zur weiteren Aufklärung der *Salmonella* Pathogenität untersuchten wir den Virulenzfaktor SopA. SopA besitzt E3-Ligase-Aktivität und agiert proinflammatorisch. Der zugrundeliegende molekulare Mechanismus war bis *dato* nicht beschrieben. Wir konnten zeigen, dass SopA spezifisch mit den RING-E3-Ligasen TRIM56 und TRIM65 interagiert und kompetitiv dessen Aktivität inhibiert. Zusätzlich katalysiert SopA den proteasomalen Abbau von TRIM56 und TRIM65. Unsere Daten weisen darauf hin, dass SopA die proinflammatorische, zelluläre Funktion über die Regulation der beiden Wirtsproteine TRIM56 und TRIM65 vermittelt.

Zudem konnten wir in Kooperation zur Aufklärung der transkriptionellen Regulation von Autophagie/lysosomalen Genen und deren Funktion durch BRD4 beitragen. BRD4 inhibiert die Expression von Autophagie und lysosomalen Genen. Dadurch trägt BRD4 zur stimulusabhängigen Modulation von Autophagie Signalwegen und deren zellulären Qualitätskontrolle bei.

## Publications

I. Evgenij Fiskin, Sagar Bhogaraju, Lina Herhaus, Sissy Kalayil, **Marcel Hahn**, Ivan Dikic. 2017. Structural basis for the recognition and degradation of host TRIM proteins by *Salmonella* effector SopA. Nature Communications.

II. Jun-ichi Sakamaki, Simon Wilkinson, **Marcel Hahn**, Nilgun Tasdemir, Jim O'Prey, William Clark, Ann Hedley, Colin Nixon, Jaclyn S. Long, Maria New, Tim Van Acker, Sharon A. Tooze, Scott W. Lowe, Ivan Dikic, Kevin M. Ryan. 2017. Bromodomain Protein BRD4 Is a Transcriptional Repressor of Autophagy and Lysosomal Function. Molecular Cell.

III. **Marcel Hahn**, Adriana Covarrubias-Pinto, Lina Herhaus, Shankha Satpathy, Kevin Klann, Keith B. Boyle, Christian Münch, Krishnaraj Rajalingam, Felix Randow, Chunaram Choudhary, Ivan Dikic. 2021. SIK2 orchestrates actin-dependent host response upon *Salmonella* infection. Proceedings of the National Academy of Sciences of the United States of America (PNAS).

IV. **Marcel Hahn***, Kevin Klann*, Ines Gössner, Ivan Dikic[+], Christian Münch[+]. 2021. IKK-β inhibits the integrated stress response to prevent bacterial proliferation. *These authors contributed equally to this work, [+]Corresponding authors. Manuscript submitted.

# Introduction

## 1 *Salmonella* infection of host cells

Human integrity is permanently challenged by microorganisms or viruses, which can infiltrate the body and cause infectious diseases. In order to defend infectious diseases, all higher organisms have developed defense systems, which work both at a systemic and cellular level. This system that can discriminate between self and non-self is called immune system and constitutes of a large variety of molecular and cellular components acting in a spatiotemporal manner.

Today we differentiate between innate immunity and the adaptive immune response. The adaptive immune system, by gene rearrangement in B and T lymphocytes, raises a highly specific response to pathogenic structures and epitopes, which help to eliminate the intruder. This immune response is clonal in nature and becomes part of the body's immunological memory (Murphy *et al*, 2012).

In contrast, innate immunity uses pre-formed, germline encoded receptors known as pattern recognition receptors (PRRs), to detect highly specify microbial molecular structures called pathogen-associated molecular structures (PAMPs). A second family of receptors (danger receptors) detects danger-associated molecular patterns (DAMPs), which sense aberrations in cellular functions as caused by injury or infectious agents. Specialized phagocytotic immune cells, such as macrophages or neutrophils, have a high migratory potential and permanently patrol the environment to clear an infection by phagocytosis. However, the first cells to be contacted by pathogens are non-immune cells, such as epithelial cells in the intestine. Epithelial cells also express PRRs and danger receptors to sense an infection and are able to trigger a multitude of cytoprotective signaling events. The intrinsic ability of host cells to defend themselves from pathogens is referred to as cell-autonomous defense, which is an integral part of the "non-classical" innate immune system (Randow *et al*, 2013).

Bacteria invade host cells either through engulfment by professional phagocytes or they actively invade cells. Most intracellular bacteria such as *Legionella* *pneumophila* (*Legionella*) or *Salmonella enterica* replicate in a vacuolar niche, a membrane-bound compartment called the bacteria-containing vacuole (BCV) (Creasey & Isberg, 2014).

*Salmonella enterica* are rode-shaped, Gram-negative facultative intracellular zoonotic pathogens with around 2,600 serotypes causing salmonellosis with diverse clinical manifestations (Gal-Mor *et al*, 2014; Knodler & Elfenbein, 2019). The genus *Salmonella* was named after Daniel Elmer Salmon (1850–1914), an American veterinary pathologist. He and Theobald Smith isolated the bacterium with from pigs in 1884 for the first time.

Today we differentiate between typhoidal and non-typhoidal *Salmonella* serovars. Non-typhoidal *Salmonella* serovars (S. Typhimurium and S. Enteriditis), display a broad host range and cause a self-limiting neutrophilic gastroenteritis in immunocompetent patients. In contrast, typhoidal, host-adapted and human-specific *Salmonella enterica* serotype Typhi (S. Typhi) causes a severe systemic disease, known as typhoid fever. In total, *Salmonella enterica* annually causes more than 100 million food- and water-borne infections worldwide (Majowicz *et al*, 2010). Nowadays the safety hazard by *Salmonella* species is massively increased by the occurrence of highly virulent and antibiotic-resistant species (Nair *et al*, 2018). In addition, novel non-typhoidal *Salmonella* variants have been reported from sub-Saharan Africa, which cause fatal systemic infections in adults and children (Feasey *et al*, 2012).

## 1.1 S. Thyphimurium infection and intracellular life cycle

In order to colonize the host, *Salmonella enterica* serovar Typhimurium (from here on referred to as *Salmonella*) as well as many other pathogenic bacteria must overcome the intestinal barriers. Following ingestion by co-intake with food, *Salmonella* passages through the stomach.

*Salmonella* is able to survive the acid environment of the stomach (pH 2). Protein-rich food rapidly elevates the stomach pH, which increases survival rate of *Salmonella* (Waterman & Small, 1998; Lawrence, 1998). This finding explains *Salmonella* as a food-borne disease. After stomach passage, vital *Salmonella* colonizes the intestine for proliferation. The latter is achieved by preferentially infecting microfold cells (M cells) and epithelial cells such as enterocytes (Jones *et al*, 1994; Malik-Kale *et al*, 2011).

Depending on the cell type, pathogenic bacteria can penetrate either by an active or passive internalization process. Professional phagocytic cells, such as macrophages, actively phagocytose bacteria. However, most eukaryotic cells are non-phagocytic cells. Such cells are penetrated by sophisticated bacterial strategies, which enforce cellular uptake.

*Listeria monocytogenes* (*Listeria*) or *Yersinia* subspecies engage host cell surface receptors e.g. integrins or cadherins (adhesion receptors) to assist cellular penetration (zipper-based mechanism) (Cossart & Sansonetti, 2004). *Listeria,* for example, by using its leucin-rich repeat proteins internalin A and B, interacts with host membrane-bound receptors such as E-cadherin and Met (Mengaud *et al*, 1996; Bierne & Cossart, 2002). This ligand-receptor engagement leads to receptor clustering, actin polymerization and membrane extension at the internalization site to mediate bacterial uptake.

In contrast, both *Salmonella* and *Shigella flexneri* (*Shigella*) use a distinct trigger-based mechanism to invade epithelial cells. The trigger-based mechanism is mediated by a type III secretion system (T3SS) to inject virulence factors into host cells resulting in forced uptake. This process is accompanied by strong actin cytoskeleton rearrangements, membrane ruffling and ultimately macropinocytic-driven internalization (Fig. 1) (Cossart & Sansonetti, 2004; Galán, 2001).

Subsequent to bacterial internalization most intracellular pathogens trigger coating by a BCV, which in the case of *Salmonella* is called the *Salmonella*-containing vacuole (SCV). In the BCV, bacteria are protected from host defense. BCV-resident bacteria actively defend their compartment and prevent endolysosomal maturation and lysosomal fusion to evade bacterial degradation. A minority of *Salmonella* (around 15%), which escape the SCV and enter the cytosol are now facing cytosolic innate immunity surveillance pathways, such as the cell-autonomous defense (Birmingham *et al*, 2006).

The SCV is characterized by acquiring endolysosomal markers, such as Rab5, Rab7, EEA1 and LAMP1. The SCV is prevented from further maturation to avoid lysosomal degradation of bacteria, but endomembrane compartment interaction is maintained to ensure membrane and nutrient supply (McGourty, 2012; Méresse *et al*, 1999; Steele-Mortimer *et al*, 1999).

At later stages post infection, the SCV is transported to a juxtanuclear position, where bacterial proliferation occurs. *In vivo,* the infection of macrophages helps to spread the disease throughout the body (Haraga *et al*, 2008).
*Salmonella* represents a well-established model organism for studying host-pathogen interactions. It is easy to culture at a fast-growing rate, is amenable for genetic manipulations and robustly infects host cells. Since *Salmonella* is neither highly adapted for a cytosolic entry nor for cytosolic replication, *Salmonella* is efficiently targeted by intrinsic defense mechanisms and thus represents a robust model organism for studying cell-autonomous immunity pathways.
This is in contrast to *Shigella*, which uses rapid escape from the BCV to prevent lysosomal degradation and has developed escape mechanism from cytosolic innate immunity (Fredlund & Enninga, 2014).

## 1.2 Invasion of host cells

For pathogenic bacteria, the extracellular milieu is a hostile environment as they are facing humoral and cellular immunity. Therefore, intracellular pathogenic bacteria have developed a mechanism to evade host immunity. *Salmonella* pathogenesis and its vertebrate host interactions have been shaped by coexistence and coevolution for million years.
Pioneering work from decades ago identified the first *Salmonella* virulence genes, responsible for invasion of non-phagocytic cells (Galan & Curtiss, 1989). Virulence genes are encoded on either plasmids, phage elements or in the genome (McClelland *et al*, 2001). They appear to be acquired horizontally and clustered genomically (McClelland *et al*, 2001; Mills *et al*, 1995).
Today two clusters are known and termed: *Salmonella* pathogenicity islands 1 and 2 (SPI-1/SPI-2) (Collazo & Galán, 1997). These gene loci encode for two type 3 secretion systems (T3SS1 and T3SS2 respectively) with different virulence factors, named bacterial effectors. Upon infection the virulence factors are expressed in a specific spatio- and temporal manner. SPI-1 encoded genes are essential for *Salmonella* invasion of non-phagocytic cells, whereas SPI-2 encoded effector proteins ensure SCV maturation and bacterial proliferation (Hansen-Wester & Hensel, 2001).

### 1.2.1 Bacterial effector proteins

More than 50 years ago, Akio Takeuchi described the infection of guinea pigs by *Salmonella* using electron microscopy. He observed at the pathogen-host contact site in the epithelium local degeneration of microvilli, followed by bacterial internalization into a membrane-bound compartment with subsequent regeneration of the brush boarder (Takeuchi, 1967).

These cellular events represent the morphological hallmarks of *Salmonella* infection. Today we know that these processes are driven by molecular interactions between *Salmonella* effector proteins and the host cell. The delivery of these bacterial effector proteins is achieved by a supramolecular transmembrane complex with a needle-like structure, named type 3 secretion system (Kubori *et al*, 1998; Galán *et al*, 2014).

The T3SS is composed of a rod-like structure, which is anchored in the membrane by an inner and out ring. This structure forms a secretion channel the function of which is strictly controlled. The extramembrane part of the channel mediates host cell membrane sensing and engages translocases to form a pore into the host plasma membrane (Kubori *et al*, 1998; Galán *et al*, 2014). The T3SS injects bacterial effector proteins to hijack various host intracellular processes that promote bacterial replication and modulate host defense. Bacterial effectors often molecularly mimic or modify host proteins (Maculins *et al*, 2016; Galán, 2001). The molecular composition of the T3SS is highly conserved among Gram-negative bacteria. Its delivered content is pathogen specific and depend on the time integrated molecular sequence of events.

For example, the single bacterial effector GtgE (conferring murine host tropism) from S. Typhimurium, is responsible for host restriction of S. Typhi. It has been shown, that host restriction of S. Typhi can be overcome by ectopical expression of GtgE (from S.Typhimurium). Post-transfection, S. Typhi was enabled to proliferate in murine macrophages (Spanò & Galán, 2012). In general, the molecular basis for host restrictions are not well explored. However, this demonstrates that, during evolution and host-adaption, the repertoire of bacterial effector proteins underwent a selection process. This shows, that the functional repertoire of effector proteins is essential for *Salmonella* virulence.

Sensing the change in pH, associated with the passage from the stomach into the intestine (from an acidic to a mild alkaline pH), triggers expression of the SPI-1 effector proteins (Daefler, 1999). The SPI-1 gene locus harbors about 39 genes and is required for epithelial cell invasion (Hansen-Wester & Hensel, 2001). The trigger-based entry mechanism of *Salmonella* depends on a sophisticated machinery of functionally-linked effector proteins, targeting and modulating the host cytoskeleton to prime bacterial internalization into the SCV.

SopB, SopE and SopE2 were recognized as the main effector proteins for mediating *Salmonella* invasion (Zhou *et al*, 2001). It was shown that effector proteins act cooperatively and can exhibit functional redundancy.

SopB is a lipid phosphatase, removing phosphates from the 4´ and 5´position of various phosphatidylinositols resulting in modulation of differential cellular pathways (Hume *et al*, 2017). SopB stimulates bacterial uptake via the RHO GTPase RhoG resulting in actin rearrangements (Zhou *et al*, 2001; Patel & Galán, 2006). In addition, upon invasion, SopB increases phosphatidylinositol-3-phosphate (PI3P) by recruiting Rab5 and VSP34, a PI3-kinase, to the SCV (Mallo *et al*, 2008). The molecular details of this mechanism remains to be further elucidated (Piscatelli *et al*, 2016; Hume *et al*, 2017).

SopE and SopE2 are mimicking host guanine nucleotide exchange factors (GEFs) (Hardt *et al*, 1998; Stender *et al*, 2000). They directly activate the RHO GTPases Rac1 and CDC42 resulting in stimulation of actin polymerization. In the next chapter, I will discuss how *Salmonella* manipulates the actin cytoskeleton by bacterial effector proteins to force cellular entry.

## 1.3 Actin cytoskeleton modulation

Cellular motility and intracellular trafficking are mediated by the cytoskeleton. The eukaryotic cytoskeleton consists of four major components: actin, microtubules, intermediate filaments and septins (Mostowy & Shenoy, 2015). All cytoskeleton compotes are modified by and throughout a bacterial infection, however this chapter will focus exclusively on the role of the actin cytoskeleton during *Salmonella* infection.

The actin cytoskeleton consists of filamentous actin (F-actin), associated with actin binding proteins (ABPs). The latter coordinate the assembly and disassembly of actin. Actin nucleation, meaning aggregation into small oligomers of two to three actin molecules is thermodynamically unfavorable. The cell uses actin nucleation promoting factors (NPFs) to overcome this limitation in order to drive *de novo* actin polymerization. Interestingly, the first discovered NPF was the *Listeria* surface protein ActA. ActA triggers bacterial induced F-actin formation and bacterial motility via actin comet tails (Kühn & Enninga, 2020; Kocks *et al*, 1992).

The WAVE-regulatory complex and N-WASP (neuronal Wiskott–Aldrich Syndrome protein) are host actin nucleation promoting factors.

F-actin polymerization and depolymerization depends on the balance between monomeric globular (G-) actin and F-actin to form actin filaments. Actin fibers are subject to constant assembly and disassembly. In the ATP-bound state, actin monomers bind to the barbed or plus end of actin fibers and nucleate into F-actin elongation. At the pointed or minus end ADP-containing monomers dissociate (Lee & Dominguez, 2010). Hence, actin polymerization is a polar process leading to a fast growing plus end and depolymerizing minus end. This dynamic process is called actin treadmilling and together with ABPs mediates actin polymerization into a double-helical structural filament. Actin filaments provide the mechanical basis for cellular mobility through different highly ordered structures, such as actin stress fibers, lamellipodia, filipodia and membrane ruffles.

The WAVE-regulatory complex and N-WASP activate the multimeric Arp2/3 complex, a major actin polymerization machinery in the cell (Pollard, 2007). The Arp2/3 complex generates branched actin networks, where the newly generated filament branches with a 70° angle from its mother filament. Genetic depletion of the Arp2/3 complex significantly reduced, but did not completely prevent *Salmonella* invasion (Hänisch *et al*, 2011, 2010). Formins, another class of actin nucleating factors, also contribute to F-actin polymerization (Pollard, 2007). The Formin FHOD1, has been found to functionally cooperate with the Arp2/3-complex (Truong *et al*, 2013).

The Rho family of small GTPases are key regulators of the cellular actin cytoskeleton structure (Ridley & Hall, 1992; Sit & Manser, 2011). They represent molecular switches cycling between an active GTP-bound state and an inactive GDP-bound state. The cycling between these two activation states is controlled by guanine nucleotide exchange factors (GEFs). They mediate GTP loading to

activate Rho GTPases. GTPase activating proteins (GAPs) counteract GEFs functions. GAPs increase the intrinsic Rho GTPase activity, hydrolyzing GTP to GDP (Heasman & Ridley, 2008). Once activated, Rho GTPases bind different ABPs or kinases, which directly or indirectly drive actin polymerization. Humans have around 20 different Rho GTPases, among them are Rho, Rac1 and CDC42. Pathogenic bacteria are exploiting and manipulating these intrinsic switches, for instance, through molecularly mimicking host GEF factors. Most prominently, the *Salmonella* T3SS1 effector proteins SopE and SopE2 function as host GEFs. They catalyze GDP release and GTP loading to activate Rho GTPases, such as Rac, RhoG, CDC42. However, SopE/SopE2 lack any sequence- and structural homology to known eukaryotic GEFs (Hardt *et al*, 1998; Patel & Galán, 2005). Nevertheless, it was shown that SopE binds CDC42 and locks the switch I and II region in a confirmation promoting GTP loading, mimicking a Rac1 and Tiam1 interaction (Buchwald *et al*, 2002). *Salmonella* strains devoid of either SopE or SopE2 display only a partial reduction of bacterial invasion, whereas a double depletions shows more pronounced effects suggesting a redundant role SopE and SopE2 (Zhou *et al*, 2001). Despite close structural relationship, SopE and SopE2 show different GEF activity towards Rac1 and CDC42, implicating similar, but distinct functions (Friebel *et al*, 2001). Host CDC42 and Rac1 have been demonstrated to be indispensable for bacterial invasion (Chen *et al*, 1996a).
Active Rac1 and CDC42 recruit the WAVE-regulatory complex to induce Arp2/3 complex–dependent F-actin polymerization (Zhou & Galán, 2001; Humphreys *et al*, 2012). The growing, barbed actin end is directed towards the plasma membrane, initiating the engulfment process of the pathogen.
Post infection the actin cytoskeleton needs to be reestablished in its physiological function. This is achieved by SptP antagonizing SopE/SopE2-driven Rho GTPase activation (Fu & Galán, 1999). SptP targets Rho GTPases (CDC42 and Rac1) via their GAP domain, hydrolyzing GTP rendering the small GTPases inactive. The second functional domain of SptP has a tyrosine phosphatase activity, dephosphorylating villin, a central ABP (Lhocine *et al*, 2015).
Controlled timing and function of these effector molecules is achieved by differential protein half-lives. Despite simultaneously secretion of SopE and SptP into the host cells, SopE shows faster proteasomal turn-over leading to differential activity of both effector proteins (Kubori & Galán, 2003).

The bacterial effector proteins SipC and SipA directly engage actin polymerization. SipC is an integral component of the T3SS1 translocon complex and mediates invasion and effector protein delivery into host cells (Scherer *et al*, 2000). SipC directly binds and bundles actin to drive actin polymerization (Hayward & Koronakis, 1999). SipA cooperates with SipC to nucleate actin and prevents actin depolymerization by antagonizing cofilin, an actin depolymerizing factor (Patel & Galán, 2005; McGhie *et al*, 2001).

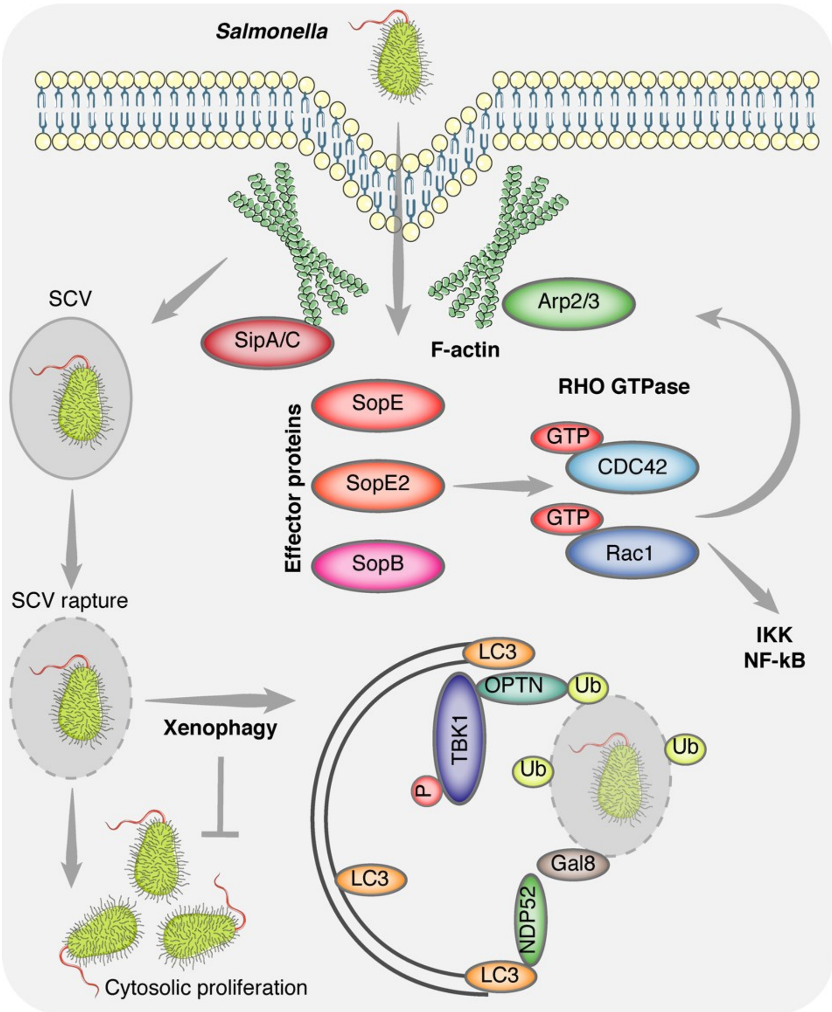


**Figure 1: *Salmonella* infection and intracellular life cycle.** *Salmonella* effector proteins mediate actin-dependent cellular internalization into the SCV. Ubiquitinylation of cytosolic bacteria induces xenophagy via the recruitment of bifunctional autophagy receptors (e.g. OPTN) to degrade the pathogen via the autolysosome (discussed in section 1.6.2).

In summary, *Salmonella* invasion requires a complex and well-orchestrated activity of multiple bacterial effector proteins and host cell Rho GTPases to manipulate actin polymerization (either indirectly via SopE/SopE2, SopB and

SptP or directly by stabilizing F-actin via SipC and SipA) to archive bacterial uptake.

It is important to note that, for *Salmonella* entry, T3SS1-independent invasion pathways have also been described. In this process, *Salmonella* uses two outer membrane proteins Rck and PagN to induce a zipper-based invasion mechanism into host cells (Hume *et al*, 2017). Zipper- or trigger-based invasion mechanisms can be used concomitantly.

## 1.4 Establishing a protective intracellular niche

Internalization of *Salmonella* is mediated by induced membrane ruffles to form the SCV, a specialized intracellular compartment protective to the infective organism. Multiple T3SS1 and T3SS2 effector proteins decorate and shape this compartment, which distinguishes the organelle from regular phagosome or endosomal cellular structures.

The effector protein SopB fulfills a special role, since it modulates phosphoinositide composition, as described earlier, leading to the activation of Rab5 and VPS34 (Mallo *et al*, 2008). VPS34 activation leads to changes in lipid composition subsequently recruiting EEA1 and sorting nexin 1 and 3 (SNX1/SNX3). SNX1/SNX3 are members of the phosphoinositide-binding membrane protein family, important for membrane trafficking (Malik-Kale *et al*, 2011; Steele-Mortimer, 2008). Transient recruitment of EEA1 and transferrin receptors are hallmarks of the early SCV biogenesis (Steele-Mortimer *et al*, 1999). Progressive SCV maturation leads to an exchange of the early SCV markers and replacement by Rab7, LAMP1 and vacuolar ATPases, representing late endosomal/lysosomal markers (Méresse *et al*, 1999). The SCV in contrast to normal lysosomal structures is not enriched in mannose 6-phosphate receptors (M6PR), required for delivering hydrolases such as cathepsins to the lysosome (Garcia-Del Portillo & Finlay, 1995).

Subsequent to *Salmonella* internalization SCV maturation is achieved by sensing the intraphagosomal environment via the two-component regulatory system PhoP-PhoQ (ion and pH sensor) and OmpR-EnvZ (ion sensor). Leading to transcriptional regulation of pro-survival genes conferring resistance to antimicrobial peptides and oxidative stress (Hansen-Wester & Hensel, 2001;

Haraga *et al*, 2008). The SCV is now characterized by low osmolarity (magnesium or phosphate) and low pH, which triggers the SsrA-SsrB system four hours post invasion inducing SPI-2 encoded T3SS2 effector proteins ensuring stabilization of the SCV (Cirillo *et al*, 1998; Hansen-Wester & Hensel, 2001).

During SCV maturation, SPI-1 and SPI-2 co-act to position the SCV to a juxtanuclear location. Coordination of this process is achieved by SopB driven Rho kinase (ROCK) activation. ROCK activation drives actin motor protein myosin II mediated transport (Wasylnka *et al*, 2008). In addition the SPI-2 effectors SseF and SseG use a dynein-mediated transport along microtubules (Salcedo & Holden, 2003; Abrahams *et al*, 2006).

Six hours post invasion, the SCV undergoes major remodeling. A membrane tubular network emanates from the SCV membrane along microtubules towards the cell periphery. This network has been termed *Salmonella*-induced filaments (SIFs) or *Salmonella*-induced tubules (SITs) (Liss & Hensel, 2015; Jennings *et al*, 2017). A major role has been elucidated for the SPI-2 effector SifA (Stein *et al*, 1996). SifA is integrated into the SCV membrane and interacts with host PLEKHM2/SKIP. A second effector protein called PipB2 then tethers the microtubule motor kinesin-1 to the SCV. Activation of the motor protein by SifA-PLEKHM2 results in SCV-microtubular interactions inducing tubulation of the SCV membrane (Boucrot *et al*, 2005; Schroeder *et al*, 2011).

Besides mediating transport SseF and SseG tether the SCV to the Golgi network. This allows SITs and their endosomal connections to supply nutrients and membrane components for *Salmonella* proliferation (Salcedo & Holden, 2003; Schroeder *et al*, 2011; Jennings *et al*, 2017; Liss *et al*, 2017).

Membrane component supply requires SifA to bind the endosomal Rab7 GTPase via the adapter protein PLEKHM1 and the HOPS complex to recruit phagolysosomal membrane elements to the SCV (McEwan *et al*, 2015).

Prior to phagolysosomal membrane fusion with the SCV reduction/neutralization of lysosomal hydrolases is a key requirement.

SifA binds PLEKHM2 and Rab9 to form a trimeric complex on the SCV, sequestering Rab9 from the endosomal system and inhibiting Rab9-dependent retrograde trafficking/recycling of MPRs to the trans-Golgi network (McGourty *et al*, 2012; Jennings *et al*, 2017). This finding explains the paradox that the SCV resembles late endosomal/lysosomal identity, lacking MPRs and associated lysosomal hydrolase enrichment.

SifA can be seen as the master regulator of all key functions associated with SCV maturation, *Salmonella* proliferation and protecting from host innate immunity. Therefore, SifA deletion strains are characterized by a destabilized and ruptured SCV in the late stage of infection (Beuzón *et al*, 2000).

Additional stabilization of the SCV is achieved by SteC, a member of the SPI-2 effector protein family. SteC is a kinase which directly activates MEK1, a MAP (mitogen-activated protein) kinase stimulating via myosin light chain kinase (MLCK) and Myosin IIB F-actin polymerization (Poh *et al*, 2008; Odendall *et al*, 2012). This F-actin network was demonstrated to stabilize the SCV six hours post invasion (Méresse *et al*, 2001; Wasylnka *et al*, 2008). The mechanical processes leading to SCV stabilization remain at present unknown (Unsworth *et al*, 2004; Kühn & Enninga, 2020). Cytosolic *Salmonella*, which have escaped from the SCV, were shown to hyperproliferate in the host cytosol, by exceeding the intravacuolar proliferation rate by far (Brumell *et al*, 2002). Apparently, cytosolic bacteria proliferation is prerequisite to bacterial transmission. Escaped bacteria re-express SPI-1 effector proteins and flagellar structure to be primed for re-infecting cells (Knodler *et al*, 2010; Malik-Kale *et al*, 2011). However, cellular exit strategies and bacterial transmission remain poorly understood on the molecular level.

## 1.5 Pathogen detection and inflammation

Immune recognition is a prerequisite to immune system activation. Pathogen and immune recognition are mediated by PRRs, which mediate the typical signs of inflammation: heat, pain, redness, swelling, and loss of tissue function (Takeuchi & Akira, 2010). PAMPs or DAMPs are required for intracellular immune surveillance. PRRs can be grouped into soluble receptors in the serum (such as complement receptors), membrane-anchored phagocytic receptors, transmembrane signaling receptors and cytoplasmic receptors (Murphy *et al*, 2012). Most of the phagocytosis mediating receptors belong to the family of C-type lectin receptors (CLRs) e.g. highly expressed on macrophages, sensing glucans from fungal cell walls (Murphy *et al*, 2012).

Toll-like receptors represent another family of PRRs exerting multiple functions in both immune recognition and embryonic development (Medzhitov *et al*, 1997). Ten different TLRs (TLR1-10) have been recognized each sensing a distinct set of PAMPs (Takeda & Akira, 2015). TLRs sense pathogens both extracellularly and intracellularly.

TLRs family members are characterized by extracellular leucin-rich repeats (LRR) (important for ligand binding) and a transmembrane region, followed by a cytoplasmic Toll-IL-1 receptor (TIR-) domain mediating receptor signaling into the host cell (Takeuchi & Akira, 2010). Gram-negative bacteria, such as *Salmonella,* are recognized by TLR4 and TLR5 on the cell-surface and via the endosomal TLR9, detecting lipopolysaccharide (LPS), flagellin or unmethylated CpG DNA respectively (Hayashi *et al*, 2001; Hemmi *et al*, 2000; Poltorak *et al*, 1998; Hoshino *et al*, 1999). TLRs act synergistically with cytoplasmic receptors of NOD-like receptor (NLR) and RIG-I-like receptors (RLR) families. RLRs recognizes cytosolic viral double-stranded RNA (dsRNA) during a viral infection. NLR receptors, such as NOD1 and NOD2, detect bacterial peptidoglycans, cell wall components of Gram-positive and Gram-negative bacteria. NLRs are characterized by their nucleotide-binding oligomerization domain (NOD) and LRRs. NOD1/2 have an additional caspase recruitment domain (CARD) crucial for recruitment of downstream molecules such as RIPK2. NLRs are intracellular sensors for bacterial infections and stimulate pro-inflammatory response via nuclear factor kappa-light-chain-enhancer of activated B cells (NF-κB), which is similar to TLR activation.

Upon ligand binding and activation of TLRs exert downstream signaling, mostly via lysine 63- (K63-) and amino-terminal methionine (M1)- linked ubiquitin chains, to assemble a multimeric receptor signaling complex (RSC) (Zinngrebe *et al*, 2013). Ubiquitin-dependent signaling is well-documented in immune signaling pathways and will be described generically by TLR4-RSC signaling, as its ligand LPS is one of the most potent and best characterized endotoxins of Gram-negative bacteria (Fig. 2). LPS is an essential cell wall component of *Salmonella* and induces, if exposed systemically in the body, a septic shock with high mortality. Mice bearing a non-functional mutation in the TLR4 gene are resistant towards LPS induced septic shocks, however they are highly susceptible to *Salmonella* infections (Sultzer, 1968; O'Brien *et al*, 1980; Poltorak *et al*, 1998).

TLR4 detects LPS directly and in co-function with its co-receptor MD-2 indirectly, where MD-2 offers a deep hydrophobic pocket for LPS binding (Kim *et al*, 2007; Park *et al*, 2009). The MD-2/TLR4 heterodimer then induces clustering to activate the receptor complex (Kawai & Akira, 2010). Classical *in vivo* TLR4-mediated immune recognition appear to be even more complex (Kawai & Akira, 2010).

Receptor clustering and TLR4 dimerization allows homophilic protein–protein interactions with TIR-domain containing proteins such as MyD88 (myeloid differentiation primary response protein MyD88), MAL (MyD88-adaptor like), TRIF (TIR domain-containing adapter molecule 1) and TRAM (TRIF-related adaptor molecule). Differential usage of these TIR-domain containing adaptors leads to differential signaling output. E.g. TLR4 signaling via MyD88/MAL and TRIF/TRAM leads to distinct activation of immune system pathways. Myd88-dependent signaling leads to NF-κB and MAP kinase activation, whereas TRIF-signaling triggers IRF3 and the type I interferon pathway (Kawai & Akira, 2010). In addition to its TIR domain, MyD88 harbors a death domain (DD) at the amino-terminus to recruit the serine/threonine kinases IRAK4 and IRAK1 through a series of DD-interactions, forming a signaling platform referred to as the myddosome (Lin *et al*, 2010; Kawasaki & Kawai, 2014). MyD88 and IRAK4 are essential for childhood immunity. Rare mutations in these genes in humans are associated with immunodeficiency and recurrent pyrogenic bacterial infections (Von Bernuth *et al*, 2008; Picard *et al*, 2003). IRAK4 activates IRAK1, which subsequently dissociates from the myddosome. Dissociated, active IRAK1 interacts with the RING-type E3 ligase TRAF6. Subsequently TRAF6 catalyzes K63-linked ubiquitin chain formation (Deng *et al*, 2000; Kawagoe *et al*, 2008). K63 ubiquitin chains serve as a recruitment platform for the TAK1/Tab1-3 kinase complex to activate downstream IKK (IκB kinase)/NF-κB and MAPK/AP-1 (activator protein 1) (Wang *et al*, 2001; Sato *et al*, 2005). In consequence, the E3 ligase Pellino family is recruited in the complex, resulting in amplified ubiquitin chain formation (Ordureau *et al*, 2008). Additionally, the heterotrimeric linear ubiquitin chain assembly complex (LUBAC), containing HOIP as the catalytic E3 ligase subunit, HOIL-1 and Sharpin, recruits to the complex (Sasaki *et al*, 2013; Zinngrebe & Walczak, 2017; Ikeda *et al*, 2011). LUBAC is a unique RING-in-between-RING (RBR) E3 ligase complex, the only complex resulting in the formation of linear- or M1-chains. LUBAC catalyzes a peptide bond between the

C-terminal α-carboxyl group (Gly76) of the incoming ubiquitin and the amino-terminal methionine (M1) of the proceeding ubiquitin molecule (Kirisako *et al*, 2006; Walczak *et al*, 2012). LUBAC has been shown to polyubiquitinate the IKK complex subunit NEMO and to stabilize receptor complex assembly e.g. the tumor necrosis factor α (TNFα) receptor. TNFα ligand binding and LUBAC function drives pro-survival NF-κB and MAPK signaling (Tokunaga *et al*, 2009; Haas *et al*, 2009). Structural analysis of the UBAN (ubiquitin binding in ABIN and NEMO) domain of NEMO revealed a specific binding motif for linear ubiquitin. This provided the basis for decoding ubiquitin signaling by detecting and sensing chain-specific ubiquitin linkages by distinct receptors (Rahighi *et al*, 2009; Dikic *et al*, 2009). The formation of K63-linkages is prerequisite and serves as a substrate for LUBCA recruitment and linear ubiquitin chain formation. Extensive biochemical characterization of receptor signaling components revealed that K63- and M1- ubiquitin chains are often attached to the same substrate or most strikingly, forming K63/M1 mixed or hybrid polyubiquitin chains (Emmerich *et al*, 2013; Cohen & Strickson, 2017). This enables concurrent recruitment of TAK1 and the IKK kinase complex to the same substrates within the signaling complex facilitating TAK1 mediated IKK and NF-κB activation.

TLR4 can also activate pathways associated with TRIF/TRAM to activate IRF3 and NF-κB. TLR4-MyD88 leads to early NF-κB activation, resulting in endocytosis and activation of the TRIF/TRAM signaling from endosomes (late NF-κB activation) (Kagan *et al*, 2008). This sequence of events explains the sequential activation of two distinct pathways emanating from TLR4-RSC. TRIF leads to TRAF6 recruitment, which enables ubiquitin mediated interaction and activation of TAK1 kinase (Sato *et al*, 2003). Additionally, the Rip homotypic interaction motif (RHIM) of TRIF allows recruitment of RIP1 (receptor-interacting protein-1) kinase and the adaptor TRADD required for a late-phase activation of NF-κB (Kawai & Akira, 2010). TRIF engagement recruits TRAF3 and the non-canonical IKK members TBK1 and IKKε to induce type I interferon secretion (Häcker *et al*, 2006; Oganesyan *et al*, 2006). In summary, TLR4 signaling is highly complex and triggers various pathways to balance the pro-inflammatory and type I interferon response. The generic IKK/NF-κB signaling output and the transcriptional gene induction will be described in the next chapter.

In addition to LPS TLR4 senses other ligands e.g. the heat-shock protein 60 (HSP60) (Ohashi *et al*, 2000; Takeda & Akira, 2015). HSP60 represents a classical DAMP or alarmin molecule. In the 1990s Polly Matzinger postulated a novel type of intracellular stressors recognizing DAMPs or alarmins (Matzinger, 1994; Seong & Matzinger, 2004). If DAMPs are released from their respective compartments in the process of cellular injury or death they also trigger an innate immune response. This model lends an elegant explanation for a phenomenon called sterile inflammation, where DAMPs are exposed at the site of injury, recognized by PRRs or danger receptors and trigger an immune reaction in the absence of pathogens (Chen & Nuñez, 2010).

Cellular compartmentalization is a prerequisite and the key to cell-autonomous defense via danger receptors. Each cellular compartment, separated by endomembranes has its own specific molecular composition, enabling the detection of miss-localized DAMPs outside their spatial context (Randow *et al*, 2013). Damage to the endomembranes by *Salmonella* invasion is sensed by a family of β-galactoside-binding lectin proteins, named galectins. Galectin-8 was identified as a danger receptor sensing vesicle-damaging pathogens. This links membrane damage to anti-bacterial autophagy induction, which restricts *Salmonella* proliferation (Thurston *et al*, 2012).

Recruitment of galectin-8 is not specific to pathogen invasion but associated in general with endomembrane damage, indicating them as danger receptors rather than pathogen receptors (Paz *et al*, 2010; Thurston *et al*, 2012; Maejima *et al*, 2013). The association of the danger receptor galectin-8 and anti-bacterial autophagy will be described further in the section 1.6.2.

*Salmonella* induced inflammation is typically explored in *in vivo* mouse models. The gut microbiome is competitive to pathogens for nutrients and epithelial contact sites (defense effect known as colonization resistance). To break the colonization resistance, *Salmonella* is able to use inflammation-derived metabolites to gain a selective metabolic growth advantage (Stecher *et al*, 2007; Thiennimitr *et al*, 2011). *Salmonella* Typhimurium infection in mice exhibits a typhoid-like phenotype resulting in systemic infection. Especially, depletion of commensal bacteria by pre-treatment with antibiotics, *Salmonella* Typhimurium is able to exert a gastroenteritis with local inflammation and breaking colonization resistance (Barthel *et al*, 2003; Gal-Mor *et al*, 2014).

### 1.5.1 IKK/NF-κB signaling

Highly regulated protein networks ensure cellular homeostasis. During this process proteins are permanently synthesized, post-translationally modified by a plethora of post-translational modifications (PTMs) and/or degraded. Receptor-mediated signaling ensures cellular communication including gene activation/inactivation in response to extrinsic and/or intrinsic factors. In innate immunity PRRs senses PAMPs and DAMPs allowing tailored responses to specific input.

Most signals from PRRs are integrated via IKK/NF-κB signaling (Fig. 2) (Mitchell *et al*, 2016; Hayden & Ghosh, 2008). NF-κB has been recognized as family of transcription factors regulating gene activation in response to PRR activation (Sen & Baltimore, 1986b, 1986a). NF-κB is an active and rich field for research since dysregulated signaling impacts various human disease conditions (Oeckinghaus & Ghosh, 2009).

The NF-κB family comprises five members: RelA (known as p65), RelB and c-Rel, and the precursor proteins NF-κB1 (p105) and NF-κB2 (p100). The precursor proteins are proteolytically processed into p50 and p52, respectively. All members are characterized by an amino-terminal Rel-homology domain (RHD) (two immunoglobulin-like beta barrel subdomains) mediating DNA-binding (binding to the NF-κB consensus sequence) and homo-or heterodimerization (Ghosh *et al*, 1995). Furthermore, the RHD domain mediates nuclear translocation and interaction with inhibitors of NF-κB (IκBs). Additionally, RelA, RelB and c-Rel contain carboxy-terminal transactivation domain (TAD) necessary for target gene expression. Multiple PTMs within the RHD and TAD regulate dimerization and target DNA affinity (Hayden & Ghosh, 2008). 15 different NF-κB homo-, heterodimer combinations have been described. Not all dimers were found to activate gene transcription (Hoffmann & Baltimore, 2006). Non-activating NF-κB dimers, such as p50-p50, were found to inhibit gene transcription. The prototypical dimer consists of p50 and RelA/p65.

Inhibitory factors (IκBs) via their RHD domain sequester cytosolic NF-κB. The IκB family comprises six different proteins, three canonical IκBs (IκBα, IκBβ and IκBε) and three non-canonical (IκBζ, IκBγ and Bcl-3) (Oeckinghaus & Ghosh, 2009).

All members are characterized by multiple ankyrin repeats responsible for binding the RHD of NF-κB, thus masking their nuclear localization sequence (NLS). In general, non-proteolytically processed NF-κB1/2 function as inhibitory proteins for their processed forms.

Two distinct NF-κB pathways have been described: the canonical and non-canonical NF-κB pathway. Subsequently, I will focus on the canonical NF-κB pathway, since the non-canoncial pathway is of lesser importance for *Salmonella* infection in epithelial cells (Fig. 2).
PRR activation leads to the recruitment of the IKK complex composed of the two IκB kinases (IKK1/2 or IKKα and IKKβ) and the regulatory subunit IKKγ or NEMO (Chen *et al*, 1996b; Wertz & Dixit, 2010). IKKα and IKKβ have an amino-terminal kinase domain, followed by a leucine zipper (required for dimerization) and helix-loop-helix domain (HLH), needed for optimal kinase activation. The carboxy-terminal region interacts with NEMO. The molecular mechanisms of IKK complex activation is still not fully elucidated. The complex can be activated either by the upstream TAK1 kinase or NEMO-mediated clustering. Both results in IKK kinase auto-phosphorylation within the receptor signaling complex (Mitchell *et al*, 2016; Wertz & Dixit, 2010). IKKβ was shown to be essential and sufficient to phosphorylate IκBα on serine 32 and serine 36 (Li *et al*, 1999; Chen *et al*, 1996b). IκBα phosphorylation induces its degradation, a hallmark of NF-κB activation. The βTrCP containing Skp1-Culin-Roc1/Rbx1/ Hrt-1-F-box (SCF) E3 ubiquitin ligase complexes ($SCF^{\beta TrCP}$) directly binds to phosphorylated IκBα and polyubiquitinates (lysine 21&22) the inhibitor with lysine 48-linked ubiquitin chains, serving as proteolytic signal for the 26S proteasome (Yaron *et al*, 1998; Scherer *et al*, 1995; Hayden & Ghosh, 2004). Proteasomal degradation of IκBα results in dissociation of the respective NF-κB dimer, unmasking the NLS. This allows nuclear translocation and binding to κB sites within the promotor regions of NF-κB target genes (Hoffmann & Baltimore, 2006).

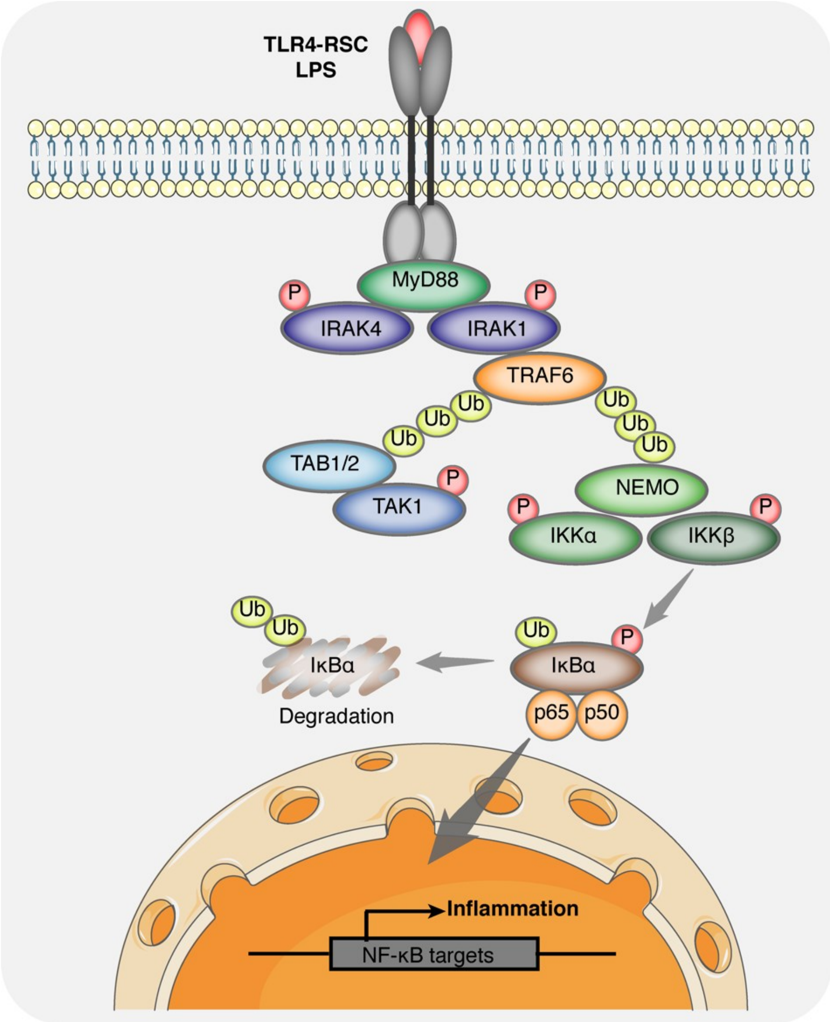


**Figure 2: TLR4 receptor signaling complex upon LPS binding.** Receptor activation assembles a multimeric signaling complex to activate the IKK/NF-κB pathway. IKKβ phosphorylates IκBα inducing its degradation and liberating the respective NF-κB dimer (p65/p50). NF-κB induces a pro-inflammatory host response.

Other IκB proteins such as IκBβ are degraded in an analogous manner to activate NF-κB gene transcription (Kanarek *et al*, 2010). The list of NF-κB target genes is extensive, indicative of the fundamental impact of this signaling pathway (Pahl, 1999). Additional regulators of NF-κB are target genes e.g. IκBα or NF-κB1 (p105) generating a negative feedback-loop for fine-tuning of the pathway.

Cooperation of IKK/NF-κB and MAPK/AP-1 signaling pathways regulates the production of pro-inflammatory cytokines (TNFα, IL-1β and IL-6), chemokines (IL-8), autophagy- and other pro-survival genes protecting the cell and surrounding tissue.

## 1.6 Stress response pathways

Bacterial infection elicits cellular stress pathways of the host to maintain and/or reestablish cellular homeostasis and pathogen defense (LaRock et al, 2015; Kroemer et al, 2010). This following chapters focus on the integrated stress response (ISR) and the selective autophagy of pathogens, called xenophagy.

### 1.6.1 Integrated stress response

The central dogma of molecular biology describes the flow of genetic information from DNA into functional proteins. The molecular protein synthesis machinery is subject to tight regulation. Cellular homeostasis ensures synthesis, folding, modification, processing and degradation of proteins in an adequate manner und is subjected to extensive quality control mechanisms. The integrated stress response senses both cellular stress out of the ER lumen and cytosolic stress exerted by nutrient deprivation or endoplasmic reticulum (ER) stress (accumulation of unfolded proteins) (Fig. 3) (Costa-Mattioli & Walter, 2020; Ron, 2002).

To raise an appropriate ISR signals from four different kinases need to be integrated. Phosphorylation of the eukaryotic translation initiation factor 2 alpha (eIF2α or EIF2S1) reduces the overall translation initiation rate, while increasing the translation of specific ISR effector genes. Dynamic reprogramming of the cellular translation rate helps resolving cellular stress. However, if the stressor signal is excessive or sustained, the ISR switches from pro-survival program to an apoptotic outcome. In general the four eIF2α kinases (EIF2AK1-4) are sensing heme deprivation (EIF2AK1/HRI), viral infection (EIF2AK2/PKR), ER stress (EIF2K3/PERK) and amino acid deprivation (EIF2AK4/GCN2) (Pakos-Zebrucka *et al*, 2016; Taniuchi *et al*, 2016). The eIF2α kinases display a common activation mechanism, which is characterized by carboxy-terminal domain mediated dimerization and auto-phosphorylation/-activation. The amino-terminal surveys environment conditions to trigger the ISR (Donnelly *et al*, 2013).

To initiate translation, the eIF2 complex (eIF2α, eIF2β, and eIF2γ) binds GTP and the initiator methionine transfer RNA (Met-tRNA$_i^{Met}$) to form the ternary complex (TC). Subsequently the TC interacts with the 40S ribosomal subunit and other translation initiation factors such as eIF4F to bind the 5´methylguanine Cap of mRNA. The pre-initiation complex (PIC) migrates to the start codon and upon base pair matching (AUG and the tRNA) the $tRNA_i^{Met}$ is released and GTP-loaded eIF2α is hydrolyzed (Pakos-Zebrucka *et al*, 2016). GDP-eIF2α dissociates from the complex and is re-loaded by the GEF eIF2B, allowing to repeat the cycle (Pakos-Zebrucka *et al*, 2016). Translation of the loaded mRNA starts after 60S ribosomal subunit recruitment to the 40S subunit, forming the functional 80S ribosome.

Upon ISR activation the eIF2α kinases phosphorylates serine 51 (S51) of eIF2α (Kaufman *et al*, 1989; Colthurst *et al*, 1987). This converts eIF2α from an eIF2B substrate to a competitive inhibitor by blocking eIF2B GEF activity (Rowlands *et al*, 1988). Cellular eIF2B supply is limited, therefore inactivation of eIF2α by phosphorylation leads to a rapid blockage of Cap-depended protein translation. Paradoxically, this leads to a preferential translation of genes harboring an upstream open reading frame (uORF) in their 5´untranslated region (5´UTR) due to persistent ribosomal scanning (Lee *et al*, 2009; Palam *et al*, 2011). ISR specific effector genes, such as ATF4, CHOP/DDIT3 and GADD34/PPP1R15A, alleviate stress and amplify the effects of stress response genes. The feedback-loop from GADD34 activates the protein phosphatase 1 (PP1) complex to dephosphorylate eIF2α, terminating the ISR and reinitiating physiological translation (Novoa *et al*, 2001). ATF4 is a basic leucine zipper transcription factor and key regulator of the stress response and impacts on amino acid metabolism, oxidative stress etc. (Karpinski *et al*, 1992; Vallejo *et al*, 1993; Ameri & Harris, 2008).

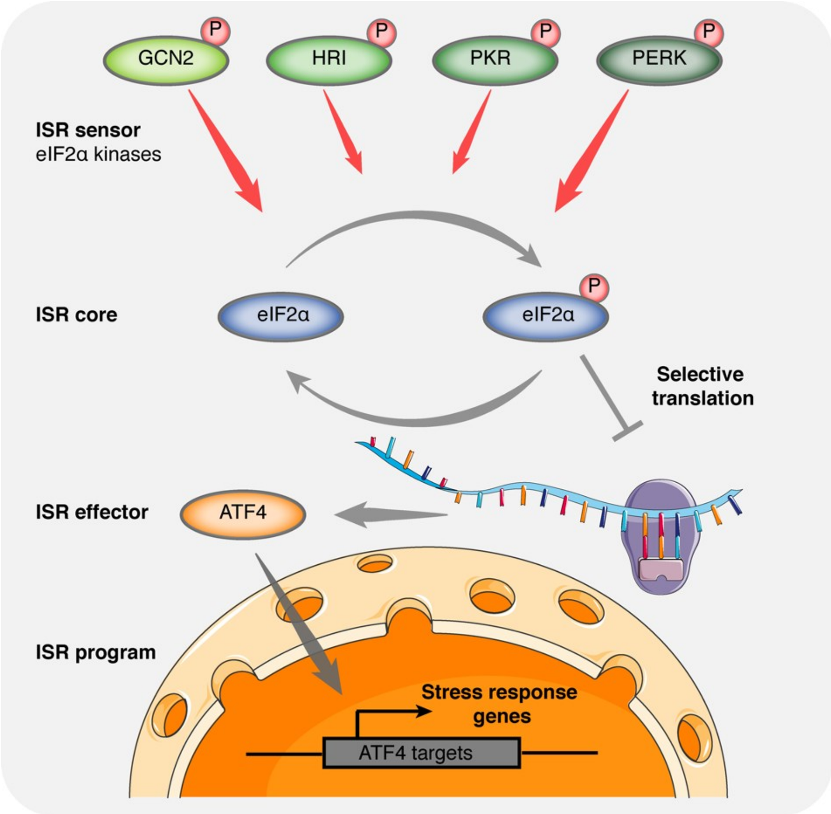


**Figure 3: Integrated stress response signaling.** Activated GCN2, HRI, PKR and PERK induce eIF2α S51 phosphorylation to inhibit protein synthesis. ISR signaling leads to a selective translation by preferentially translating ISR-specific mRNAs. The transcription factor ATF4 is a key mediator of the ISR by regulating expression of stress response genes. Figure adapted from (Pakos-Zebrucka *et al*, 2016).

Stress responses involving the ISR system are critical to both viral and bacterial infections (Balachandran *et al*, 2000; Dauber & Wolff, 2009; Knowles *et al*, 2021).

### 1.6.2 Selective autophagy of *Salmonella*

Previously macroautophagy (hereafter autophagy) has been considered a non-specific bulk pathway for the degradation of cellular components, such as proteins, carbohydrates and lipids. Autophagy is dependent on lysosomal degradation: the cargo is engulfed in a *de novo* formed double membrane compartment known as the autophagosome prior to fusion with the lysosome (Yang & Klionsky, 2010; De Duve & Wattiaux, 1966).

It is established that autophagy is a conserved, adaptive and highly selective catabolic pathway for the break-down of biomolecules or organelles and for recycling of resulting metabolites. This process is default in nature and amplified upon cellular stress. Autophagy represents a major component of cellular homeostasis and together with the ubiquitin-proteasome pathway constitutes the major cellular degradation pathway (Dikic, 2017).

Autophagy relies on the integrated activity of around 30 evolutionarily conserved autophagy genes (ATG, in yeast Atg). They function hierarchically to regulate autophagosome formation. Seminal work identified those genes in yeast genetic screens during starvation (Tsukada & Ohsumi, 1993).

To initiate phagophore formation, the Atg1/ULK1 (Unc-51-like kinase 1) complex composed of ULK1, FIP200 (focal adhesion kinase family interacting protein of 200kDa), ATG13 and ATG101 are required. This initiation complex is negatively regulated by the mTOR (mammalian target of rapamycin) complex 1 (mTORC1). mTORC1 phosphorylates ULK1 and ATG13, keeping them in their inactive form (Hosokawa *et al*, 2009). Upon amino acid deprivation, mTORC1, a major nutrient and stress sensor within the cell is inactivated, leading to release of ULK1-ATG13, which in turn activates the ULK1 complex. The kinase ULK1 phosphorylates Beclin 1 within the class III phosphatidylinositol-3-kinase (PI3K) complex I containing ATG14 and the catalytic subunit VP34 to enhance PI3K activity (Russell *et al*, 2013). VPS34 subsequently phosphorylates phosphatidylinositol to generate phosphatidylinositol 3-phosphate (PI3P), leading to local enrichment of PI3P, finally resulting in phagophore assembly. ATG9-positive vesicles are recruited to the phagophore assembly site, which is hypothesized to form at the ER (Nishimura *et al*, 2017). In addition, PI3P serves as a binding site for WD-repeat domain phosphoinositide interacting 1/2 (WIPI1/2) proteins. WIPI1/2 further recruits the ubiquitin-like conjugation machinery ATG12-ATG5–ATG16L complex to the phagophore (Dooley *et al*, 2014; Kuma *et al*, 2002). Phagophore elongation is driven by the E3 ligase activity of this complex to conjugate the autophagy-specific ubiquitin-like family (Atg8 in yeast) of microtubule-associated protein light chain 3 (MAP1LC3) and the γ-aminobutyric acid receptor-associated protein (GABARAP) to phosphatidylethanolamine (PE) (Dikic & Elazar, 2018). In contrast to yeast encoding for only one Atg8 member, mammalian cells encode for 6 paralogs from two ATG8 isogenes building the LC3- (LC3A, LC3B, LC3C) and GABRARAP- (GABARAP, GABARAPL1, GABARAPL2) family. This significantly expands the conjugation repertoire. Conjugation of ATG8 proteins allows expansion and closing of the phagophore to form a functional autophagosome (Weidberg *et al*, 2011).

In addition to its homeostatic functions, autophagy is implicated in innate immunity and the cell-autonomous defense. In the context of bacterial infection it is referred to as xenopahgy (Fig. 1) (Gomes & Dikic, 2014; Nakagawa *et al*, 2004; Randow *et al*, 2013). *Salmonella* infection in cell culture is used as a model system for the role of autophagy in cell-autonomous defense and will be described below in detail.

The SCV is prone to rupture caused by translocase proteins of T3SS1, most prominently by SipC (Du *et al*, 2016; Kreibich *et al*, 2015). Pioneering work identified a sub-fraction of intracellular *Salmonella* (15%) to cause rupture of the SCV one to two hours post infection. These cytosolic bacteria are characterized by ubiquitin decoration (Perrin *et al*, 2004; Birmingham *et al*, 2006).

Work from our laboratory proposed a role for ubiquitin as a selective "eat me"/degradation signal for different cargos by linking ubiquitylation structures to the autophagy machinery (Kirkin *et al*, 2009b). This hypothesis is derived from the discovery of selective autophagy receptors, which can function as bifunctional molecules. For example, NBR1 (neighbor of BRCA1 gene 1) has been recognized in the context of selective autophagy as a receptor for aggerated proteins containing a ubiquitin-binding domain (UBD) and a LIR (LC3-interacting motif)-region (Kirkin *et al*, 2009a). Thus, linking ubiquitinated cargo to selective autophagy receptors and ATG8 molecules to the nascent phagophore.

Additional bifunctional autophagy receptors have been identified: p62/SQSTM1 (sequestosome-1), OPTN (optineurin), NDP52 (nuclear dot protein 52 and TAX1BP1 (tax1-binding protein 1) were shown to be recruited to ubiquitinated intracellular *Salmonella*, thus bridging the bacteria to ATG8 and the nascent phagophore (Zheng *et al*, 2009; Wild *et al*, 2011; Tumbarello *et al*, 2015; Thurston *et al*, 2009). Furthermore, the existence of various forms of ubiquitin linkages was demonstrated, resulting in the formation of specialized ubiquitin patches on the bacterial surface (van Wijk *et al*, 2012; Van Wijk *et al*, 2017). Analogous microdomains are formed by the autophagy receptors p62 and NDP52 (Cemma *et al*, 2011).

The UBAN domain of OPTN binds K63 and M1-chains, although with different affinities. NDP52 binds K63 ubiquitin chains via a ubiquitin-binding zinc finger

(Wild *et al*, 2011; Thurston *et al*, 2009). E3 ligases ubiquitinating *Salmonella* are LRSAM1 (leucine rich repeat and sterile alpha motif containing 1), LUBAC and ARIH1 (ariadne RBR E3 ubiquitin protein ligase 1), which act in cooperation to form a complex ubiquitin coat around the bacteria (Huett *et al*, 2012; Noad *et al*, 2017; Polajnar *et al*, 2017; Herhaus & Dikic, 2017). Substrates for bacterial surface ubiquitylation still need to be identified, but global PTM ubiquitin profiling identified bacterial outer membrane proteins as candidates for bacterial surface ubiquitylation (Fiskin *et al*, 2016).

An atypical LIR motif of the autophagy receptor NDP52 results in binding of LC3C and additionally binds galectin-8 via a galectin-interacting region, linking damaged SCV remnants to the autophagy machinery (Thurston *et al*, 2012; von Muhlinen *et al*, 2012; Li *et al*, 2013). Therefore, NDP52 not only detects cytosolic bacteria via ubiquitin but also senses endomembrane damage via galectin-8 on the SCV to induce anti-bacterial autophagy. The multi-modular nature of NDP52 via adaptor proteins allows for co-recruitment of TBK1 (Thurston *et al*, 2009). TBK1 signaling establishes multiple feed-forward loops amplifying autophagic degradation. TBK1 was shown to phosphorylate OPTN in the UBAN domain as well as in the LIR motif, thereby enhancing ubiquitin- and LC3 affinity and autophagic recruitment kinetics (Wild *et al*, 2011; Richter *et al*, 2016; Heo *et al*, 2015). Additionally, TBK1 signaling further impacts autophagy progression by triggering WIPI2- and ULK1 complex recruitment to stimulate phagophore growth (Thurston *et al*, 2016; Ravenhill *et al*, 2019). TBK1 is central to positive feed-forward stimulation and amplification of autophagy signaling.

Elimination of any of the anti-bacterial autophagy system (ATG5, ULK1, NDP52, OPTN, LUBAC and TBK1) enable cytosolic bacterial hyperproliferation (Ravenhill *et al*, 2019; Thurston *et al*, 2009; Noad *et al*, 2017; Thurston *et al*, 2016; Wild *et al*, 2011)

# 2 Infection induced protein dynamics

Quantitative analysis of protein dynamics resulting of host-pathogen interaction on a molecular level is the key to the understanding of pathogenicity and host defense systems.

Upon infection not only total protein levels are modulated, but also quantity and quality of post-translational modifications are altered. These dynamic changes demonstrate the host cells capacity to react to the pathogen. Regulatory signaling pathways integrate the infection-driven cellular stress response to functionally adapt the host protein network. A technical approach to measure these dynamic changes in the host proteome is quantitative mass spectrometry.

## 2.1 Bacterial infection shapes the proteomic profile

*Salmonella* virulence is centrally mediated by T3SS1 and its interaction with host cells (Galán, 2001). The main purpose if this interaction is to drive bacterial uptake subsequent to actin cytoskeleton rearrangement. In response to the pathogen intrusion the host cell establishes an inflammatory innate immune response, which in turn converts to its advantage. The molecular interplay of host and pathogen is fine-tuned through extensive coevolution and requires a complex, concerted action of bacterial effectors. Pioneering work demonstrated that *Salmonella* provokes a transcriptional response, driven by a subset of T3SS1 effector proteins (Hobbie *et al*, 1997; Bruno *et al*, 2009). This resembles a PRR driven response: SopE/E2 and SopB activate Rho GTPases and resulting in a transcriptional response mediated by MAPK and NF-κB (Fig. 1) (Chen *et al*, 1996a; Bruno *et al*, 2009). These findings link bacterial invasion and actin cytoskeleton rearrangements to a pathogen-driven transcriptional host response. Subsequent to *Salmonella* infection, ribosomal profiling has been performed, however results demonstrated that mRNA levels do not necessarily correlate to protein levels in the host cell (Hannemann *et al*, 2013; Fortelny *et al*, 2017). Thus, quantitative proteome profiling was required. Experimental analysis using this technology was fundamental for results described in manuscript IV (Klann *et al*, 2020; Klann & Munch, 2020)

We infected HeLa cells with *Salmonella* and took samples at an hourly interval, which were then analyzed to measure dynamic changes in protein translation rate and resulting protein levels. Analyzing bacterial protein synthesis and total protein profiles, we were able to demonstrate protein dynamics that was biphasic in nature. First phase ranged from one to four hours post infection, resembling a bacterial lag-phase characterized by low protein synthesis rate and constant protein levels. The second phase ranged from five to eight hours post infection and showed a burst of bacterial *de novo* protein synthesis. The majority of newly synthesized proteins belonged to the class of RNA-binding proteins e.g. ribosomal proteins. Increased bacterial proliferation correlated with increased bacterial *de novo* ribosomal protein synthesis (Cirillo *et al*, 1998; Hansen-Wester & Hensel, 2001). Our findings are in accordance with published data indicating the upregulation of SPI-2 effector proteins and bacterial proliferation.

Subsequent to quantitative proteome analysis of the pathogen, we also analyzed the host proteome in an analogous way. One hour post infection, we were unable to detect any significant changes in the host proteome. Differences could only be displayed by focusing on protein *de novo* synthesis rather than overall protein levels. This indicates that measurements of total protein dynamics is limited by low intensity and half-live of the signal of interest (Klann & Münch, 2020; Schwanhäusser *et al*, 2011).

Functional pathway analysis revealed that in the early phase of translational modulation mainly proteins associated with RNA processing and extracellular matrix proteins (ECM; required for pathogen adherence and invasion) are affected (Singh *et al*, 2012). In contrast, the second late phase of translation coincided with the observed burst of bacterial proliferation and was mainly characterized by significant upregulation of proteins from the NF-κB signaling pathway. This finding, together with the observed role of NF-κB signaling for the cell-autonomous defense against *Salmonella* infection prompted us to further investigate this regulatory mechanism (Noad *et al*, 2017; Van Wijk *et al*, 2017).

## 2.2 PTM-driven signaling

A bacterial infection does not only affect protein synthesis and degradation, but also triggers post-translational modification, either directly through bacterial effector proteins or indirectly via host-pathway activation (LaRock *et al*, 2015). Previous work using stable isotope of amino acids in cell culture (SILAC)-labeling in combination with diGly-remnant immunoprecipitations indicated a central role for the cellular ubiquitinome, warranting additional exploration (Fiskin *et al*, 2016).

### 2.2.1 Phosphorylation-dependent signaling

Protein phosphorylation is an effective and reversible post-translational modification regulating protein function and turn-over (Cohen, 2002). Protein phosphorylation occurs under basal conditions and can be amplified upon various stimuli. Analysis of the phosphoproteome is technical challenging since post cell lysis protein phosphorylation pattern may change artificially (Macek *et al*, 2009). Precise mapping of protein phosphorylation sites is critical to the understanding of differential protein functions and to delineate cellular downstream signaling networks (Macek *et al*, 2009).
In manuscript III, we applied a quantitative SILAC-based labeling approach, for HeLa cells that were differentially labeled with natural occurring heavy isotopes and infected with *Salmonella*. To monitor SPI-1 dependent PTM dynamics, cells were lysed at 30 minutes and two hours post infection, respectively. Previous work from our laboratory demonstrated that, shortly after infection, SPI-1 proteins affected ubiquitin signaling and that the NF-κB pathway played a central role. It was also recognized that the RHO GTPase system network contributed to the actin cytoskeleton modulation, the precise molecular mechanism of which was not yet defined (Fiskin *et al*, 2016).
Therefore, we aimed to extend our knowledge on PTM-driven signaling networks by applying phosphoproteomics. 30 minutes post infection phosphoproteome changes were most pronounced, affecting a total of 17,900 sites, 10% of which were regulated by the experimental conditions. Functional pathway enrichment analysis identified Rho GTPase signaling with CDC42 and Rac1 as the most prominent GTPases that were modulated. In addition, upregulation of NLR- and

TNFα-receptor signaling with downstream NF-κB activation was recognized. This finding was in accordance with previous data obtained in model systems of *Salmonella* and *Shigella* infections (Rogers *et al*, 2011; Schmutz *et al*, 2013).
Within RHO GTPase signaling clusters, we identified SIK2 to have an, as yet undescribed protective role in host cells in *Salmonella* infections (discussed in section 4) (manuscript III) (Hahn *et al*, 2021).
PTM cross-talk of pathogen driven host pathways requires complex, integrated analysis of PTM systems (phosphorylation, ubiquitylation etc.) to fully understand the molecular relationships (Venne *et al*, 2014; Herhaus & Dikic, 2015).
Novel experiments using tandem mass tag (TMT)-based phosphoproteome profiling compared molecular PTM signatures across multiple conditions (Mertins *et al*, 2018). TMT allows the quantitative analysis of up to 16 multiplexed and pooled samples mixed at equimolar ratios. As described in manuscript III we used this method to determine the impact of SIK2 signaling during *Salmonella* infection. Cluster and functional pathway analysis revealed a dysregulation of phosphorylation depended signaling signatures centered around the actin cytoskeleton (Hahn *et al*, 2021).
In manuscript IV, by applying this method and an IKK inhibitor (TPCA-1) to the experimental system, we were able to discriminate between the unfolded protein response (UPR) and ISR signaling. Applying extensive bioinformatic analysis to the data set obtained, allowed the identification of a signaling pattern distinct from UPR signaling. This indicates that IKK inhibition does not prefer UPR signaling, but results in ISR activation. In parallel, screening the phosphorylation pattern of the four eIF2α kinases, we noted a specific, significant downregulation of the EIF2AK3/PERK kinase, the functional implications of which needed to be defined (manuscript IV). In general, this finding was key to unravel the molecular signaling circuit between IKKβ kinase and the integrated stress repose pathway (see section 5).

### 2.2.2 Ubiquitin-dependent signaling

Covalent attachment of ubiquitin to target proteins to form mono- or polymeric post-translational modification represents a default mechanism to regulate the functions and the life cycle of proteins.

Ubiquitylation is an elaborate and reversible PTM in eukaryotic cells, requiring the activation of three enzymes: a ubiquitin-activating enzyme (E1), a ubiquitin-conjugation system (E2) and, finally, a ubiquitin ligase (E3) attaching the ubiquitin molecule to its respective target (Hershko & Ciechanover, 1998). Ubiquitin ligation is catalyzed by three distinct E3 ligase classes: 1) the HECT ligases (homologous to E6–AP carboxy-terminus), 2) RING (really interesting new gene) and 3) RING-in-between-RING (RBR) ligases.

Defined by the acceptor lysine or the amino-terminus, ubiquitin attachment occurs via various forms of homo- or hetero-linkages: K6, K11, K27, K29, K33, K48, K63 and M1 (Yau & Rape, 2016). Ubiquitin receptors (proteins harboring a UBD) specifically recognize ubiquitinylated proteins and propagate the appropriate signal depending on the type of modification (Husnjak & Dikic, 2012). *Salmonella*, like many prokaryotic bacteria, do not have a prototypic ubiquitin system. They encode bacterial effector proteins which harbor E3 ligase activity, exploiting the host ubiquitin system via molecular mimicry (Ashida *et al*, 2014; Maculins *et al*, 2016).

For instance, the carboxy-terminus of *Salmonella* E3-like effector protein SopA is structurally similar to the eukaryotic HECT-type E3, mimicking their ligase function (Diao *et al*, 2008). *Salmonella* SopA mimics the EHEC/EPEC effector protein NleL (Lin *et al*, 2012). Both, NleL as well as SopA, are T3SS1 secreted proteins. SopA was demonstrated to be pro-inflammatory by evoking neutrophilic trans-epithelial migration, a hallmark of *Salmonella* mediated gastroenteritis (Wood *et al*, 2000). Molecular substrates for SopA remain to be defined. First candidates have been identified: the tripartite-motif containing (TRIM) E3 ligases TRIM56 and TRIM65, as described in manuscript I (Kamanova *et al*, 2016; Fiskin *et al*, 2017).

The functional interaction of SopA with TRIM56/65 was confirmed using different proteomic approaches. TRIM proteins represent a large family of RING E3 ligases implicated in host defense and PRR signaling (Versteeg *et al*, 2013). It can be speculated that the TRIM ligases TRIM56 and TRIM65 are mediating the observed pro-inflammatory effect of SopA.

Protein-protein interaction studies using truncated mutants of SopA and TRIM proteins revealed that the amino-terminal β-helix of SopA interacts specifically with the RING-domain of TRIM56/65. Given the generic nature of a RING E3 ligase domain, it is surprising to see specific interactions between SopA and TRIM 56/65 (Deshaies & Joazeiro, 2009). To further explore this, we generated a minimal domain binding construct and co-crystalized the TRIM56 amino-terminal RING-domain and the amino-terminal β-helix of SopA. Resolution of this crystalized complex revealed the precise interacting motif as described in manuscript I. We recognized that other RING ligases , such as TRIM32 or RNF4, sterically clashed with SopA β-helix and N-lobe preventing interaction. In addition, SopA binding obstructs the E2 binding surface on TRIM56, potentially indicating an inhibitory function. Indeed, in the *in vitro* ubiquitin assays, diminishing TRIM56 E3 ligase activity has been observed with increasing amounts of SopA. Additional biochemical analysis showed a SopA-mediated ubiquitylation of TRIM56 with proteolytic K48 chains, marking the E3 ligase for potential proteasomal degradation. Along this line, infection and cycloheximide pulse-chase experiments demonstrated SopA-mediated TRIM56/65 ubiquitylation followed by subsequent degradation.

Results indicate a dual mechanism of action for bacterial effector proteins with E3 ligase activity: Inhibition of E2-E3 interaction by TRIM ligases and downregulation of TRIM proteins by degradation via the ubiquitin-proteasome system. Degradation of TRIM56/65 upon SopA interaction needs to be confirmed. It can be speculated that TRIM56/65 acts as an inhibitor for the type I interferon signaling cascade, therefore the degradation may result in activation. Our extensive proteomic analysis confirmed the upregulation of the type I interferon as a critical component of *Salmonella* infection (Robinson *et al*, 2012) (manuscript IV). Timely integration of these opposing signals may result in an initial stimulatory effect on type I interferon signaling, followed by termination of the pro-inflammatory signaling by degradation of TRIM56/65 (Galán, 2021).

In addition to molecular mimicry of host E3 ligases, pathogenic bacteria evolved a different class of E3 ligase (novel E3 ligase (NEL)). They do not share structural homology with any known eukaryotic E3 ligase (Maculins *et al*, 2016).

Both *Salmonella* and *Shigella* encode NELs: SspH1/2 (*Salmonella*) and IpaH4.5 and IpaH9.8 (both *Shigella*). IpaH9.8 has been reported to interfere with the NF-κB mediated pro-inflammatory host response (Ashida *et al*, 2010). *In vivo* infections with a *Shigella* mutant strain (expressing a catalytic inactive IpaH9.8) exhibited decreased bacterial proliferation while displaying an augmented and persisting inflammation (Ashida *et al*, 2010). IpaH9.8 interacts with both A20-binding inhibitor of NF-κB activation 1 (ABIN-1) and NEMO, an essential subunit of the IKK complex. IpaH9.8 promotes NEMO polyubiquitylation via K27-linkages, facilitating proteasomal degradation. Thereby, *Shigella* attenuates NF-κB activation to perturbate protective host inflammatory signaling. The precise mechanism, how these K27-linkages facilitate NEMO degradation it not fully understood. In manuscript IV we confirmed the above-mentioned finding, since IpaH9.8 overexpression resulted in ISR activation, the implications of which will be further discussed in section 5.

We demonstrated the importance of IKK/NF-κB for the *Salmonella* infection process. This pathway is strongly activated by phosphorylation (manuscript III) and results in perpetuated activation of this pathways throughout the infection (manuscript IV). Pharmacological inhibition of IKKβ, the central kinase of the IKK complex, results in *Salmonella* hyperproliferation in an ISR-dependent way (manuscript IV).

Ubiquitinylation of cytosolic bacteria induces xenophagy via the recruitment of bifunctional autophagy receptors (e.g. OPTN) to degrade the pathogen via the autolysosome (Wild *et al*, 2011). T3SS1 induced SCV damage promotes escape of bacteria into the host cytosol, where *Salmonella* is rapidly marked with ubiquitin (Du *et al*, 2016; Kreibich *et al*, 2015; Perrin *et al*, 2004). Ubiquitin co-localized with *Salmonella* serves as an autophagy marker of cytosolic bacteria (manuscript III) (van Wijk *et al*, 2012; Van Wijk *et al*, 2017).

We and others demonstrated that ubiquitin patches (microdomains) on *Salmonella* serve as a recruiting platform for host defense mechanism (Noad *et al*, 2017; Van Wijk *et al*, 2017). Linear ubiquitin chains catalyzed by LUBAC on the bacterial surface serve as a docking station for NEMO and the IKK complex. Juxtaposing results in IKK/NF-κB pathway activation for restriction of bacterial proliferation (Van Wijk *et al*, 2017). Recent findings indicate that the IKK complex mediates additional functions outside the receptor signaling complex, independent of downstream NF-κB signaling (Antonia *et al*, 2021). In manuscript IV, we also report a novel NF-κB independent function of the IKK complex.

# 3 Regulation of autophagy

Upon host invasion, *Salmonella* secrets effector proteins into the host cell via an SPI-1 encoded T3SS1 complex (Cossart & Sansonetti, 2004).
During this process, a pore called translocon is formed, causing membrane leakage. The leakage results in the loss of intracellular amino acids, causing an acute amino acid starvation stress, which is sensed by the mTORC1 complex (Tattoli *et al*, 2012). mTORC1 mediates dual function: nutrient concentration sensing and regulation of autophagy. Inactivation of mTORC1 is associated with the activation of the ULK1 complex, which in turn simulates an anti-bacterial host response (Hosokawa *et al*, 2009; Tattoli *et al*, 2012). mTORC1 inhibition is transient in nature leading to re-localization of mTORC1 to the SVC. SCV-localized mTORC1 suppresses autophagy, which is speculated to support the *Salmonella* escape. mTORC1 regulates autophagosome and lysosome biogenesis via the master transcription factor EB (TFEB) (Settembre *et al*, 2011).

Manuscript II, describes the identification of a novel and TFEB-independent transcriptional regulator of autophagy and autophagosomal-lysosomal genes, BRD4 (bromodomain containing 4) (Sakamaki *et al*, 2017). BRD4 is a member of the BET (bromodomain and extra terminal domain) family, binding to acetylated lysine through bromodomains (Shi & Vakoc, 2014).
TFEB stimulates autophagy via the nutrient-sensing mTORC1 complex. In contrast, the active BRD4 is inhibitory. Functional depletion of BRD4 increased autophagy flux and autophagosome formation and lysosomal fusion (manuscript II). Transcriptional analysis after depletion showed a marked upregulation of transcription and translation of multiple autophagy genes (LC3B, ATG9, OPTN, p62 etc.). This upregulation occurred independently of TFEB, since anti-TFEB siRNA did not abolished gene or protein induction nor autophagy flux.
Binding of BRD4 via histone H4 lysine 16 (H4K16) acetylation to the promotor of autophagy genes represses gene transcription. This specific acetylation site was shown to be regulated by the deacetylase sirtuin 1 (SIRT1). SIRT1 activity is regulated by the AMP-activated protein kinase (AMPK), displacing SIRT1 from its inhibitor DBC1 (deleted in breast cancer protein 1) (Chang *et al*, 2015). Besides mTOR, AMPK functions as an independent nutrient sensor, which can

activate autophagy directly (Hardie *et al*, 2012). Using starvation or rapamycin treatment as a model system for autophagy induction, we recognized extended and amplified phases of autophagy in the absence of BRD4. This paradoxical finding is explained by the observation that BRD4 depletion increases the expression of autophagy genes, such as p62 and OPTN. We subsequently analyzed associated pathways. In the model used BRD4 depletion had no functional impact on anti-bacterial autophagy and mitophagy. This was an unexpected finding. In contrast, protein aggregates induced by the overexpression of polymorphic huntingtin protein (containing the aggregation-causing expansion of poly-glutamines) were shown to be more efficiently degraded by depletion of BRD4. Despite a general role of BRD4 on the transcription of autophagy genes were only able to demonstrate a direct role for BRD4 in some, but not all autophagy pathways.

Autophagy pathways are diverse and selective, depending on the cargo nature to be removed. The molecular regulation of these diverse pathways requires further work.

Recent work identified the bacterial effector protein SopF (Xu *et al*, 2019). SopF mediates a novel autophagy initiation cascade and represents an integral part of a bacterial host evasion mechanism.

Autophagy initiation occurs via the vacuolar-type ATPase (v-ATPase), which, upon membrane damage, recruits the ATG8 conjugation complex around ATG5 and ATG16L to the SCV. This recruitment jumpstarts autophagosome formation by directly promoting LC3 lipidation to the SCV (Pao & Rape, 2019). *Salmonella* SopF blocks ATG16L recruitment promoting autophagy escape and subversion. This process is independent of essential canonical upstream autophagy machinery. This was confirmed by FIP200 depletion, which had no effect on xenophagy. Additional work indicated that selective autophagy can bypass the need for an upstream activation by AMPK or mTOR by direct recruiting ULK1 via NDP52 and TBK1 to mitochondria or *Salmonella* (Ravenhill *et al*, 2019; Vargas *et al*, 2019).

It is tempting to speculate that these novel insights into the process of *Salmonella* invasion/proliferation may promote novel therapies for selective stimulation of autophagy targeting pathogens or disease associated intracellular protein aggregates.

## 4 Regulation of the actin cytoskeleton upon infection

T3SS function is central to the pathogenesis of *Salmonella*. Pathogen effector proteins interact and modify host pathways to ensure pathogen survival and intracellular proliferation. SopB/SopE/SopE2 are essential for the invasion of epithelial cells (Fig. 1) (Zhou *et al*, 2001). Drugs inhibiting actin polymerization block *Salmonella* invasion (Galán & Zhou, 2000; Kihlstrom & Nilsson, 1977).
30 minutes post infection, extensive phosphorylation of the Rho GTPase system and target proteins regulating the actin cytoskeleton during *Salmonella* infection is demonstrated in manuscript III. The WAVE-regulatory complex and N-WASP have been identified as the major actin nucleation promoting factors downstream of the Rho GTPases Rac1 and CDC42 (Pollard, 2007).
We identified SIK2 as a novel signaling network component, which regulates the actin cytoskeleton and host defense (manuscript III) (Hahn *et al*, 2021). *Salmonella* invasion results in SIK2 kinase phosphorylation and activation. The kinase responsible for SIK2 phosphorylation remains to be identified. Ectopic expression of *Salmonella* SPI-1 effector proteins (SopA and SopE) induce SopE-dependent SIK2 phosphorylation. SIK2 depletion revealed a higher percentage of SCV damage and enabling cytosolic escape of bacteria. Thus, SIK2 depletion resulted in strong *Salmonella* hyperproliferation in HeLa cells. Furthermore, we demonstrated that SIK2 kinase activity is required to minimize intracellular *Salmonella* proliferation and to assure actin cytoskeleton integrity.
The molecular mechanism of SIK2 activation remains to be defined. Experiments using *Salmonella* SopE/E2 deletion strains may enable elucidation of this pathway. SIK2 PTM modifications are of specific interest to define basal conditions and to define modulations during pathogen infection.
We speculate that SopE activates p21-activated kinase 1 (PAK1) via CDC42 in an analogy to a described non-canonical signaling complex (Sun *et al*, 2018; Galán, 2021). This complex includes PAK1, TRAF6 and TAK1, which in consequence activates NF-κB signaling. In addition, this complex may be

responsible for SIK2 phosphorylation. Activated TAK1 resulted as a top hit in the *Salmonella* induced phosphoproteome (manuscript III) and was shown to restrict *Salmonella* proliferation (Liu *et al*, 2018).

SIK2 interactomics indicated that, under basal conditions SIK2 interacts with approximately 20 proteins. In contrast, upon pathogen infection, SIK2 interacts with more than 170 proteins, indicating the high degree of complexity of the infection pathway. Bioinformatic analysis identified novel and known prime targets involved in *Salmonella* invasion and host colonization (Vorwerk *et al*, 2014; Hume *et al*, 2017). SPI-1 effector proteins target RHO GTPases (CDC42) and regulators of the actin cytoskeleton (Arp2/3-complex) to enable pathogen uptake and SCV formation. The novel discovered SIK2 kinase was demonstrated to be indispensable for F-actin formation. SIK2 depletion caused monomeric G-actin accumulation and reduction in F-actin. This is in agreement with the well-established action of SopE and the speculated connection to SIK2 (Hardt *et al*, 1998; Patel & Galán, 2005).

Post invasion, SIK2 assumes multiple functions; most importantly SIK2 via the Arp2/3 complex recruits F-actin to the SCV to prevent cytosolic hyperproliferation. At late stages of infection, a dense actin network surrounds the SCV for stabilization of this compartment (Méresse *et al*, 2001; Wasylnka *et al*, 2008; Odendall *et al*, 2012). The actin meshwork forms in a SPI-2 dependent manner six hours post invasion (Poh *et al*, 2008). The precise molecular interactions, that result in the formation of the actin network, remain to be defined (Unsworth *et al*, 2004; Kühn & Enninga, 2020). We demonstrated that SIK2 and the actin machinery recruits to the SCV shortly after internalization and stabilizes the vacuole to restrict *Salmonella* proliferation. In the early phase of *Salmonella* infection the actin cytoskeleton aids bacterial invasion, whereas subsequently the actin cytoskeleton acts as a major component of the host innate immunity limiting proliferation by shielding bacteria in the SCV (Hahn *et al*, 2021). It would be interesting to test if active SIK2 is also required for actin meshwork formation at six hours post invasion.

We aimed at identifying SIK2 kinase specific substrates. A chemical genetic SIK2 screen identified components of the PI3K kinase pathway as potential candidates (Miranda *et al*, 2016). The PI3K kinase pathway was demonstrated to be linked to actin polymerization via CDC42. SopB has been identified as one of the mediating effector proteins (Hume *et al*, 2017; Mallo *et al*, 2008; Chamberlain *et al*, 2004). Additional reports suggest also a regulatory role for the Arp2/3-complex phosphorylation by PAK kinase (Vadlamudi *et al*, 2004). In manuscript III, we described the modulation of the PTM pattern of the Arp2/3 complex and other proteins, which are required for F-actin formation.

# 5 IKKβ controls the ISR and mediates cell-autonomous immunity

In manuscript IV, we identified that the entire NF-κB pathway is subject to modulation resulting in pronounced upregulation of e.g. IKKβ and NF-κB family proteins. We and others recognized and reported a role for NF-κB signaling in the cell-autonomous defense to restrict *Salmonella* proliferation (Noad *et al*, 2017; Van Wijk *et al*, 2017). The underlying molecular mechanism remained largely unknown. Therefore, we examined the effects of IKK/NF-κB signaling on the host cell translatome.

Combining pharmacological inhibition of the IKK complex by blocking IKKβ and mePROD proteomics, we observed a global attenuation of translation in our assays. While IKKβ inhibition resulted in *Salmonella* hyperproliferation, the IKK complex also proved to be critical to mediate shutdown of protein synthesis. Detailed analysis of the events leading to the inhibition of protein synthesis was performed. Titration of low doses of cycloheximide during *Salmonella* infection did not impact on basic intracellular proliferation rate. This indicates that, upon IKK inhibition, *Salmonella* hyperproliferation is not the simple consequence of protein translation shutdown.

Analogous changes are observed under cellular stress conditions mediated via the ISR or mTORC1 (Klann *et al*, 2020; Pakos-Zebrucka *et al*, 2016; Thoreen *et al*, 2012). Under cellular stress conditions mediated by the ISR and mTORC1 translational shutdown is selective. In contrast stress response related genes are selectively upregulated (Klann *et al*, 2020).

Upon IKK inhibition ATF4 target genes were selectively upregulated. We hypothesized that IKK inhibition results in ISR induction causing translational reprograming in favor of *Salmonella* proliferation. Currently, most reports speculate on a cytoprotective role of the ISR system (Knowles *et al*, 2021; Tattoli *et al*, 2012).

IKK inhibition resulted in ISR activation by inducing eIF2α S51 phosphorylation and ATF4 expression. IKK inhibition did not affect the mTORC1 target EIF4EBP1, indicating that IKK inhibition triggers the ISR without causing mTORC1 activation. ISR induction is inhibited by IKKβ. A dominate negative mutant of IKKβ was sufficient to activate the ISR. IKKβ function appears to be independent of the NF-κB system, since depletion of RelA/p65 did not affect IKK induced ISR signaling. We demonstrated that ISR effector genes (CHOP/DDIT3 and ATF4) were upregulated by IKK inhibition. However, we were unable to detect ER-stress or UPR activation upon IKK inhibition.

Additional experiments revealed EIF2AK3/PERK kinase as the mediator of IKK induced ISR signaling. We showed PERK activation subsequent to IKK inhibition and reduced ATF4 and eIF2α S51 phosphorylation following PERK depletion. Interaction between PERK and IKKβ suggested a functional relationship. This defines an as yet unknown IKK/PERK/ISR regulatory axis, the functional consequences of which were investigated.

Infection-induced ISR activation was observed (eIF2α S51 phosphorylation and ATF4 induction). IKK induced hyperproliferation was prevented by depletion of the ISR core proteins PERK and ATF4. This proves the central role of IKKs in cell-autonomous immunity by controlling the ISR. Previous work suggested that the induction of the UPR response favors *Salmonella* proliferation (Antoniou *et al*, 2019). In contrast, our data show that IKK signaling dampens the ISR activity and reduces bacterial proliferation. The UPR was shown to activate NF-κB via the ER kinase IRE1 (Hu *et al*, 2006; Schmitz *et al*, 2018). In addition, we show that IKK inhibition affects transcription and translational via PERK and ISR signaling, in a manner different from UPR and IRE1 activation. PERK and ATF4 mediate both basic and hyperproliferation of *Salmonella*.

However, we failed to demonstrate that pathogenic bacteria in general interfere with IKK signaling to induce the ISR. As discussed in section 2.2.2, the *Shigella* NEL effecter protein IpaH9.8 was shown to target the IKK complex for degradation in order to dampen NF-κB signaling and the pro-inflammatory response (Ashida *et al*, 2010, 2014). We were able to show that IpaH9.8 overexpression triggers ISR activation via ATF4 and eIF2α S51 phosphorylation.

We tested the closest *Salmonella* structural homolog of IpaH9.8, called SspH1, implicated in NF-κB signaling, suggesting also functional homology (Haraga & Miller, 2003). However, we failed to measure a SspH1 mediated ISR induction. Impact of SspH1 on NF-κB signaling has been demonstrated by others to be indirectly mediated (Keszei *et al*, 2014). Therefore, homology of SspH1 to IpaH9.8 remains on the structural level only.

# 6 Conclusion and future directions

As described in detail in the introduction a sophisticated regulatory mechanism between *Salmonella* and the host has evolved. In our work, we exclusively focused on *Salmonella* epithelial cell interaction.

Our work identified the AMPK-related kinase SIK2 as a central regulator of host defense. Future work needs to address the molecular events leading to activation of SIK2 kinase and its effect on the regulation of F-actin. Here, we provide first evidence that SIK2 activates a Rho GTPase cluster with CDC42 and the Arp2/3-complex as major components. The bacterial effector protein SopE mediates SIK2 phosphorylation and activation. Given the structural homology of 70% between SopE and SopE2, it is of interest to know if SopE2 can (partially) replace SopE function (Friebel *et al*, 2001). SopE and SopE2 target the Rho GTPases Rac1 and CDC42 with different GEF kinetics (Friebel *et al*, 2001). Additionally, SIK2 was shown to impact on the PI3K pathway (Miranda *et al*, 2016), thus potentially regulating F-actin formation. SopB through Rho GTPases regulates phospholipid flux, which also affects F-actin linkage to membrane components (Scott *et al*, 2005; Bakowski *et al*, 2010). Differential linkage via lipids may have a major impact on establishing the actin network to protect the SCV. Work from others involving *Chlamydia* and *Shigella* infection have described F-actin network similarities. It would be of relevance to know if the newly identified SIK2 plays a similarly important role in these model systems. (Kumar & Valdivia, 2008; Méresse *et al*, 2001; Kühn *et al*, 2020). Variations of the host cell type (e.g. macrophages) may lead to additional novel scientific insight.

Pro-inflammatory IKK/NF-κB signaling is a central component of *Salmonella* infection. We were able to assign a novel and central role to the IKK complex in mediating NF-κB-independent cell-autonomous immunity. IKK signaling impacts on both NF-κB- and ISR signaling to restrict *Salmonella* proliferation.

We demonstrated the functional effect of the *Shigella* IpaH9.8 ligase to activate the ISR. A *Salmonella* effector homolog has not been identified, yet. Other work reported the function of YopJ, an *Yersinia* effector to acetylate threonine residue in the activation loop of IKKα and IKKβ inactivating the kinase complex (Mittal *et al*, 2006). In general, pathogenic interferences with IKK/NF-κB is a broad virulence mechanism, calling for a systematic analysis of the identified IKK/ISR axis upon infections (Rahman & McFadden, 2011).

IKKβ kinase activity via PERK inhibition is required to limit the ISR. IKK kinase activity has been found to be associated via PERK phosphorylation with PERK activity. Reduced PERK activity is associated with phosphorylation on its serine 1,094 site. To date, it is unknow whether this represents a causal relationship. Because of the extreme carboxy-terminus location of the serine 1,094 site it has proven not well accessible for experimental exploration. E.g. the crystal structure analysis failed to solve the very carboxy-terminal structure (Cui *et al*, 2011). The serine 1,094 is speculated to be involved in PERK dimerization, which is prerequisite to PERK activity. The precise mechanism remains to be resolved.

ISR and UPR activity are triggered by different events, however share some functional implications (Costa-Mattioli & Walter, 2020). PERK is sensing protein misfolding in the ER with its luminal domain to activate an ATF4-mediated stress response (Harding *et al*, 2003). However, PERK activity can also be induced by bypassing the need of the luminal stress-sensing domain (Volmer *et al*, 2013; Costa-Mattioli & Walter, 2020). This provides evidence for an alternative model regulating PERK activity. In general, the molecular mechanism for PERK activation still remains unclear (Donnelly *et al*, 2013). Since PERK is the only ISR regulator with overlapping UPR functions (translation inhibition), it is surprising to see that PERK is the key molecule to regulate the IKK/ISR axis causing a response distinct from UPR activation.

In analogy to our data, IKK complex restricting PERK, previous work showed that AKT kinase phosphorylates PERK to inhibit its function (Mounir *et al*, 2011). It is tempting to speculate that AKT exerts a indirect PERK inhibitory function via the

IKK complex, since AKT regulates IKK activity and subsequently NF-κB signaling (Bai *et al*, 2009).

Rewarding future research may focus on the precise mechanism of IKK controlling PERK and its impact on bacterial infections. More detail insight may help to develop specific modulators of the IKK complex of therapeutic value. We also noticed that under basal conditions (without pathogen infection), inhibition of the IKK complex elicits a stress response. In general, cellular stress response can be seen as a means for cell survival. Eliciting a stress response as a therapeutic measure may elevate cellular resilience. Such therapies may find home to fight neurodegenerative diseases.

## Present Investigation

Except where stated otherwise by reference or acknowledgment, the work presented was generated by myself under the supervision of my advisors during my doctoral studies. All contributions from colleagues are explicitly referenced in the thesis. The material listed below was obtained in the context of collaborative research:

I. Evgenij Fiskin, Sagar Bhogaraju, Lina Herhaus, Sissy Kalayil, **Marcel Hahn**, Ivan Dikic, 2017. Structural basis for the recognition and degradation of host TRIM proteins by *Salmonella* effector SopA. **Nature Communications**.

Aim: Identification of host substrates of *Salmonella* effector protein SopA (HECT E3 ligase-type) and their structural and functional characterization upon *Salmonella* infection.

Contributions:

a) Generation of TRIM56 and TRIM65 knock-out cell lines using CRISPR/Cas9.
b) Establishing a type I interferon (IFN) reporter gene assay to measure INF-beta induction of TRIM56, TRIM65 and SopA in conjunction with nucleic acid-sensing receptors such as MDA5.
c) ELISA assays in TRIM56, TRIM65 over-expression or KO cell lines to measure cytokine (IL-1β and TNFa) and chemokine release (IL-8).
d) To biochemically assess SopA influenced pro-inflammatory signaling monitoring for instance IRF3 activation via phosphorylation.
e) To demonstrate the specificity of SopA towards TRIM56 and TRIM65 by co-expressing SopA with different RING-domain containing E3 ligases and subsequent co-immunoprecipitations.
f) Commenting on and editing the manuscript.

II. Jun-ichi Sakamaki, Simon Wilkinson, **Marcel Hahn**, Nilgun Tasdemir, Jim O'Prey, William Clark, Ann Hedley, Colin Nixon, Jaclyn S. Long, Maria New, Tim Van Acker, Sharon A. Tooze, Scott W. Lowe, Ivan Dikic and Kevin M. Ryan. 2017. Bromodomain Protein BRD4 Is a Transcriptional Repressor of Autophagy and Lysosomal Function. **Molecular Cell**.

Aim: Identifying novel transcriptional regulators of autophagy and their impact on selective autophagy pathways as well as their implications in autophagy and lysosomal biogenesis.

Contributions:

a) Establishing *Salmonella* infection conditions in human pancreatic ductal adenocarcinoma KP-4 cells.
b) Establishing xenophagy readouts in BRD4 depleted cells under infection conditions.
c) To demonstrate the influence of BRD4 on selective autophagy pathways such as xenophagy using *Salmonella* infection in KP-4 cells by proliferation assays and microscopy analysis of anti-bacterial autophagy markers.

III. **Marcel Hahn**, Adriana Covarrubias-Pinto, Lina Herhaus, Shankha Satpathy, Kevin Klann, Keith B. Boyle, Christian Münch, Krishnaraj Rajalingam, Felix Randow, Chunaram Choudhary, Ivan Dikic. 2021. SIK2 orchestrates actin-dependent host response upon *Salmonella* infection. **Proceedings of the National Academy of Sciences of the United States of America (PNAS)**.

Aim: PTM-profiling of infected human epithelial cells to identify novel key players upon *Salmonella* infection as well as functional characterization of the identified SIK2 kinase and its cytoprotective role by controlling actin polymerization under infection conditions.

Contributions:

a) Designing and conducting most of the experiments.
b) Conceiving the study together with Ivan Dikic.
c) Writing the manuscript with Ivan Dikic with input from all authors.
d) A SILA-based phosphoproteome workflow and large-scale *Salmonella* infections of HCT116 cells, lysis, and protein precipitations.
e) PTM-profiling to identify novel signaling networks and key players upon *Salmonella* infections in human epithelial cells (SILAC-based phosphopeptide enrichment, fractionation and subsequent MS/MS was performed by Shankha Satpathy).
f) All generated data was quantitively analyzed using MaxQuant, Proteome Discoverer and Perseus software.
g) Functional protein-protein interactions and pathway enrichment analysis using Cytoscape software with additional plug-ins such as ReactomeFI or STRING.
h) Establishing siRNA transfection conditions for depleting SIK2 in HeLa cells.
i) Establishing intracellular *Salmonella* proliferation experiments in SIK2 depleted cells.
d) Generation of inducible HA-tagged and siRNA-resistant SIK2 WT, K44A, S117A, S117D HeLa cells.
e) To demonstrate the impact of SIK2 expression and its kinase activity on restricting intracellular *Salmonella* proliferation.

f) Establishing confocal microscopy using endogenous xenophagy markers such as LC3B, Galectin-8, LAMP1 and ubiquitin in SIK2 depleted and infected cells.
g) To demonstrate SIK2 function by stabilizing the *Salmonella*-containing vacuole and to promote actin-dependent xenophagy in infected cells.
h) Generation of an endogenously tagged SIK2 HeLa cell line, using CRISPR/Cas12–assisted PCR- tagging.
i) To identify the SIK2 interactome profile under basal as well as under infection conditions.
j) IP-MS using the endogenously tagged SIK2 HeLa cell line for quantitative TMT-based interactome profiling to elucidate the functional role of SIK2 during a *Salmonella* infection.
k) Co-immunoprecipitation of endogenous SIK2 and subsequent Western-blot analysis of SIK2 interaction partners.
l) A TMT-based phosphoproteome workflow of infected HeLa after SIK2 depletion. Cells were siRNA transfected, infected with *Salmonella* subsequently lysed followed by protein precipitation, tryptic digest, peptide desalting and lyophilization, TMT labeling, phosphopeptide enrichment, high pH reverse phase fractionation and peptide resuspension for LC-MS.
m) PTM-profiling to identify the impact of SIK2 driven phosphorylation events during a *Salmonella* infection on previously identified actin cytoskeleton targets.
n) Establishing an endogenous SIK2, Arp2/3-complex and Cortactin confocal microscopy read-out in MEFs to study compartmentalization and localization/recruitment behavior under basal as well infection conditions.
o) Determine the function of SIK2 on the cytoskeleton by measuring F-actin polymerization biochemically (G/F-actin fractionation by ultra-centrifugation).
p) Microscopy of Phalloidin positive F-actin structures.
q) Endogenous PTM analysis of SIK2 using Phos-tag gels to study SIK2 phosphorylation upon infection.
r) To assess the role of *Salmonella* effector proteins such as SopA and SopE on SIK2 modification.
s) To determine the effect of SPI-1 *Salmonella* effector proteins on the phosphorylation of pro-inflammatory key players.
t) Other experiments were performed by co-authors.

IV. **Marcel Hahn***, Kevin Klann*,Ines Gössner, Ivan Dikic⁺,Christian Münch⁺. 2021. IKK-β inhibits the integrated stress response to prevent bacterial proliferation.

*These authors contributed equally to this work, +Corresponding authors. **Manuscript submitted.**

Aim: Profiling the translatomic host-pathogen landscape in *Salmonella* infected epithelial cells as well as the characterization of the novel IKK/PERK/ATF4 signaling axis, which functionally links pro-inflammatory IKK signaling to the integrated stress response and controls an acute infection.

Contributions:

a) Designing, conducting all experiments and analyzing all data together with Kevin Klann.
b) Conceiving the study and writing the manuscript together with Kevin Klann, Ivan Dikic and Christian Münch.
c) Time-resolved translatomics of *Salmonella* infected HeLa cells. Cells were SILAC-pulsed one hour before lysis and profiled over the time of 8 hours post infection.
d) For translatomics cells were lysed, proteins precipitated, tryptically digested, peptides desalted, lyophilized, TMT labeled and mixed in equimolar ratios. MS-Data analysis was performed by Kevin Klann.
e) Kinetic profiling of *Salmonella* and host translation rates to determine infection phases.
f) Translatomics in triplicates with two different time points from each infection phase to study proteomic profile in detail.
g) Intracellular *Salmonella* proliferation assays to study the effect of IKK inhibition.
h) Intracellular *Salmonella* proliferation assays with cycloheximide titration to study the effect of a translation shut-down on *Salmonella* proliferation.
i) Establishing IKK inhibitor (TPCA-1 and IKK-16) treatment in HeLa cells.
j) Using IKK inhibitor to study the effect of IKK/NF-κB signaling on cellular translation rates under basal as well as infection conditions. MS-Data analysis was performed by Kevin Klann.
k) Generation of an ATF4-GFP reporter cell line (together with Kevin Klann).
l) To demonstrate the influence of IKK inhibition on the integrated stress response using a FACS-based read out (ATF4-GFP induction) (together with Kevin Klann).
m) Western blot analysis of integrated stress response markers such as EIF2S1 S51 phosphorylation or ATF4 induction (together with Kevin Klann).
n) Using IKKβ wild type or a dominate negative catalytic inactive IKKβ mutant (K44A) to test, if the IKKβ kinase activity is controlling the ISR.
o) To demonstrate PERK activation upon IKK inhibition by studying PERK mobility in an SDS-PAGE.
p) Co-immunoprecipitation of Flag-IKKβ and Myc-PERK to demonstrate a functional protein interaction.
q) *Salmonella* infection of MEFs to study the ISR activation upon infection at different time points post infection.
r) Intracellular *Salmonella* proliferation assays in PERK or ATF4 siRNA transfected or ATF4 knock-out cells to demonstrate the dependency of *Salmonella* proliferation on the ISR pathway.
s) Intracellular *Salmonella* proliferation assays in PERK or ATF4 siRNA transfected or ATF4 knock-out cells treated with IKK inhibitors to demonstrate that the IKK dependent bacterial hyperproliferation is caused by an ISR activation.

t) Molecular cloning of *Salmonella* effector proteins isolated from genomic DNA and in frame cloning into various expression vectors for functional characterization.
u) Over-expression of IpaH9.8 a *Shigella flexneri* effector protein belonging to the novel E3 ligase family (NEL) to demonstrate that pathogenic bacteria interfere with IKK signaling to activate the ISR besides dampening NF-κB signaling.
v) To biochemically assess the impact of NF-κB signaling on the ISR and the TPCA-1 mediated ISR induction using RNAi against RELA (p65).
w) To biochemically assess the PERK mediated EIF2S2 S51 phosphorylation in PERK knock-out cells upon TPCA-1 treatment.
x) Other experiments were performed by Kevin Klann.
y) HeLa ATF4 knock-out cell line was generated by Ines Gössner.

## Abbreviations

| | |
|---|---|
| ABIN | A20-binding inhibitor of NF-κB activation |
| ABP | Actin binding protein |
| ADP | Adenosine diphosphate |
| AMPK | AMP-activated protein kinase |
| AP-1 | Activator protein 1 |
| ARIH1 | Ariadne RBR E3 ubiquitin protein ligase 1 |
| Arp2/3 complex | Actin related protein 2/3 complex |
| ATF4 | Activating Transcription Factor 4 |
| ATG | Autophagy gene |
| ATP | Adenosine triphosphate |
| BCV | Bacteria-containing vacuole |
| BRD4 | Bromodomain containing 4 |
| CARD | Caspase recruitment domain |
| CLR | C-type lectin receptor |
| DAMP | Danger-associated molecular pattern |
| DBC1 | Deleted in breast cancer protein 1 |
| DD | Death domain |
| DDIT3 | DNA damage-inducible transcript 3 protein |
| dsRNA | Double-stranded RNA (ribonucleic acid) |
| ECM | Extracellular matrix protein |
| EEA1 | Early endosome antigen 1 |
| EHEC | Enterohaemorrhagic E. coli |
| eIF | Eukaryotic translation initiation factor |
| EIF2AK | eIF2α kinase |
| EIF4EBP1 | Eukaryotic translation initiation factor 4E-binding protein 1 |
| EPEC | Enteropathogenic E. coli |
| ER | Endoplasmic reticulum |
| F-actin | Filamentous actin |
| FHOD1 | FH1/FH2 domain-containing protein 1 |
| FIP200 | Focal adhesion kinase family interacting protein of 200kDa |
| G-actin | Globular actin |
| GABARAP | γ-aminobutyric acid type A (GABA) receptor-associated protein |
| GAP | GTPase-activating protein |
| GDP | Guanosine diphosphate |
| GEF | Guanine nucleotide exchange factor |
| GFP | Green fluorescent protein |
| GTP | Guanosine-5'-triphosphate |
| HECT | Homologous to E6–AP carboxy terminus |
| HLH | Helix-loop-helix domain |
| HOIL-1 | Heme-oxidized iron-responsive element binding protein 2 ligase-1 |
| HOIP | HOIL-1L interacting protein |
| HOPS complex | Homotypic fusion and protein sorting (HOPS)-tethering complex |
| HSP | Heat-shock protein |
| IFN | Interferon |
| IKK | IκB kinase |

| | |
|---|---|
| IKK-16 | N-(4-Pyrrolidin-1-yl-piperidin-1-yl)-[4-(4-benzo[b]thiophen-2-yl-pyrimidin-2-ylamino)phenyl]carboxamide hydrochloride |
| IL | Interleukin |
| IRAK | Interleukin-1 receptor-associated kinase |
| IRF | Interferon regulatory factor |
| IRF3 | Interferon regulatory factor 3 |
| ISR | Integrated stress response |
| IκB | Inhibitors of NF-κB |
| KO | Knock-out |
| LAMP1 | Lysosome-associated membrane glycoprotein 1 |
| LC-MS | Liquid chromatography–mass spectrometry |
| LIR | LC3-interacting motif |
| LPS | Lipopolysaccharide |
| LRR | Leucin-rich repeats |
| LRSAM1 | Leucine rich repeat and sterile alpha motif containing 1 |
| LUBAC | Linear ubiquitin chain assembly complex |
| M cells | Microfold cells |
| M6PR | Mannose 6-phosphate receptor |
| MAL | MyD88-adaptor like |
| MAP1LC3 | Microtubule-associated protein light chain 3 |
| MAPK | Mitogen-activated protein kinase |
| MD-2 | Myeloid differentiation factor 2 |
| MEK1 | MAPK/ERK kinase 1 |
| mePROD | Multiplexed enhanced protein dynamics |
| MLCK | Myosin light chain kinase |
| mRNA | Messenger ribonucleic acid |
| MS | Mass spectrometry |
| mTOR | Mammalian target of rapamycin |
| mTORC1 | mTOR complex 1 |
| MyD88 | Myeloid differentiation primary response protein MyD88 |
| N-WASP | Neuronal Wiskott–Aldrich Syndrome protein |
| NBR1 | Neighbor of BRCA1 gene 1 |
| NDP52 | Nuclear dot protein 52 |
| NEL | Novel E3 ligase |
| NEMO | NF-kappa-B essential modulator |
| NF-κB | Nuclear factor kappa-light-chain-enhancer of activated B cells |
| NLR | Nucleotide-binding oligomerization domain-like receptor |
| NLS | Nuclear localization sequence |
| NOD | Nucleotide-binding oligomerization domain |
| NPF | Nucleation promoting factor |
| OPTN | Optineurin |
| p62 | Phosphotyrosine-independent ligand for the Lck SH2 domain of 62 kDa |
| PAMP | Pathogen-associated molecular structure |
| PE | Phosphatidylethanolamine |
| PI3K | Phosphatidylinositol-3-kinase |
| PI3P | Phosphatidylinositol-3-phosphate |
| PIC | Pre-initiation complex |
| PLEKHM | Pleckstrin homology domain-containing family M member |

| | |
|---|---|
| PP1 | Protein phosphatase 1 |
| PPP1R15A | Protein phosphatase 1 regulatory subunit 15A |
| PRR | Pattern recognition receptor |
| PTM | Post-translational modification |
| RBR | RING-in-between-RING |
| RHD | Rel homology domain |
| RHIM | Rip homotypic interaction motif |
| RING | Really interesting new gene |
| RIPK | Receptor-interacting serine/threonine-protein kinase |
| RLR | Retinoic acid-inducible gene-I-like receptor |
| RNAi | RNA interference |
| ROCK | Rho kinase |
| RSC | Receptor signaling complex |
| $SCF^{\beta TrCP}$ | βTrCP containing Skp1-Culin-Roc1/Rbx1/ Hrt-1-F-box |
| SCV | *Salmonella*-containing vacuole |
| SIF | *Salmonella*-induced filament |
| SILAC | Stable isotope of amino acids in cell culture |
| SIRT1 | Sirtuin 1 |
| SIT | *Salmonella*-induced tubule |
| SNX | Sorting nexin |
| SPI-1 | *Salmonella* pathogenicity islands 1 |
| SPI-2 | *Salmonella* pathogenicity islands 2 |
| T3SS | Type III secretion system |
| TAB | TAK1 binding protein |
| TAD | Transactivation domain |
| TAK1 | TGF-beta-activated kinase 1 |
| TAX1BP1 | Tax1-binding protein 1 |
| TC | Ternary complex |
| TFEB | Transcription factor EB |
| TIR | Toll-IL-1 receptor |
| TLR | Toll-like receptor |
| TMT | Tandem mass tag |
| TNFα | Tumor necrosis factor alpha |
| TPCA-1 | 2-[(Aminocarbonyl)amino]-5-(4-fluorophenyl)-3-thiophenecarboxamide |
| TRADD | TNF receptor type 1-associated DEATH domain protein |
| TRAF | TNF receptor associated factor |
| TRAM | TRIF-related adaptor molecule |
| TRIF | TIR domain-containing adapter molecule 1 |
| TRIM | Tripartite motif-containing |
| UBAN | Ubiquitin binding in ABIN and NEMO |
| UBD | Ubiquitin-binding domain |
| ULK1 | Unc-51-like kinase 1 |
| uORF | Upstream open reading frame |
| UPR | Unfolded protein response |
| UTR | Untranslated region |
| vATPase | Vacuolar-type ATPase |
| VPS34 | Vacuolar protein sorting 34 |
| WIPI | WD repeat domain phosphoinositide interacting |
| WT | Wild type |

Acknowledgements

## References

Abrahams GL, Müller P & Hensel M (2006) Functional dissection of SseF, a type III effector protein involved in positioning the salmonella-containing vacuole. *Traffic* 7: 950–965

Ameri K & Harris AL (2008) Activating transcription factor 4. *Int J Biochem Cell Biol* 40: 14–21

Antonia RJ, Hagan RS & Baldwin AS (2021) Expanding the View of IKK: New Substrates and New Biology. *Trends Cell Biol* 31: 166–178

Antoniou AN, Lenart I, Kriston-Vizi J, Iwawaki T, Turmaine M, McHugh K, Ali S, Blake N, Bowness P, Bajaj-Elliott M, *et al* (2019) Salmonella exploits HLA-B27 and host unfolded protein responses to promote intracellular replication. *Ann Rheum Dis* 78: 74–82

Ashida H, Kim M & Sasakawa C (2014) Exploitation of the host ubiquitin system by human bacterial pathogens. *Nat Rev Microbiol* 12: 399–413

Ashida H, Kim M, Schmidt-Supprian M, Ma A, Ogawa M & Sasakawa C (2010) A bacterial E3 ubiquitin ligase IpaH9.8 targets NEMO/IKKγ to dampen the host NF-κB-mediated inflammatory response. *Nat Cell Biol* 12: 66–73

Bai D, Ueno L & Vogt PK (2009) Akt-mediated regulation of NFκB and the essentialness of NFκB for the oncogenicity of PI3K and Akt. *Int J Cancer* 125: 2863–2870

Bakowski MA, Braun V, Lam GY, Yeung T, Heo W Do, Meyer T, Finlay BB, Grinstein S & Brumell JH (2010) The phosphoinositide phosphatase SopB manipulates membrane surface charge and trafficking of the Salmonella-containing vacuole. *Cell Host Microbe* 7: 453–462

Balachandran S, Roberts PC, Brown LE, Truong H, Pattnaik AK, Archer DR & Barber GN (2000) Essential role for the dsRNA-dependent protein kinase PKR in innate immunity to viral infection. *Immunity* 13: 129–141

Barthel M, Hapfelmeier S, Quintanilla-Martínez L, Kremer M, Rohde M, Hogardt M, Pfeffer K, Rüssmann H & Hardt WD (2003) Pretreatment of mice with streptomycin provides a Salmonella enterica serovar Typhimurium colitis model that allows analysis of both pathogen and host. *Infect Immun* 71: 2839–2858

Von Bernuth H, Picard C, Jin Z, Pankla R, Xiao H, Ku CL, Chrabieh M, Mustapha

I Ben, Ghandil P, Camcioglu Y, *et al* (2008) Pyogenic bacterial infections in humans with MyD88 deficiency. *Science (80- )* 321: 691–696

Beuzón CR, Méresse S, Unsworth KE, Ruíz-Albert J, Garvis S, Waterman SR, Ryder TA, Boucrot E & Holden DW (2000) Salmonella maintains the integrity of its intracellular vacuole through the action of SifA. *EMBO J* 19: 3235–3249

Bierne H & Cossart P (2002) InlB, a surface protein of Listeria monocytogenes that behaves as an invasin and a growth factor. *J Cell Sci* 115: 3357–3367

Birmingham CL, Smith AC, Bakowski MA, Yoshimori T & Brumell JH (2006) Autophagy Controls Salmonella Infection in Response to Damage to the Salmonella-containing Vacuole. *J Biol Chem* 281: 11374–11383

Boucrot E, Henry T, Borg JP, Gorvel JP & Méresse S (2005) The intracellular fate of Salmonella depends on the recruitment of kinesin. *Science (80- )* 308: 1174–1178

Brumell JH, Tang P, Zaharik ML & Finlay BB (2002) Disruption of the Salmonella-containing vacuole leads to increased replication of Salmonella enterica serovar typhimurium in the cytosol of epithelial cells. *Infect Immun* 70: 3264–3270

Bruno VM, Hannemann S, Lara-Tejero M, Flavell RA, Kleinstein SH & Galán JE (2009) Salmonella Typhimurium Type III Secretion Effectors Stimulate Innate Immune Responses in Cultured Epithelial Cells. *PLOS Pathog* 5: e1000538

Buchwald G, Friebel A, Galán JE, Hardt WD, Wittinghofer A & Scheffzek K (2002) Structural basis for the reversible activation of a Rho protein by the bacterial toxin SopE. *EMBO J* 21: 3286–3295

Cemma M, Kim PK & Brumell JH (2011) The ubiquitin-binding adaptor proteins p62/SQSTM1 and NDP52 are recruited independently to bacteria-associated microdomains to target Salmonella to the autophagy pathway. *Autophagy* 7: 341–345

Chamberlain MD, Berry TR, Pastor MC & Anderson DH (2004) The p85α subunit of phosphatidylinositol 3′-kinase binds to and stimulates the GTPase activity of Rab proteins. *J Biol Chem* 279: 48607–48614

Chang C, Su H, Zhang D, Wang Y, Shen Q, Liu B, Huang R, Zhou T, Peng C, Wong CCL, *et al* (2015) AMPK-Dependent Phosphorylation of GAPDH Triggers Sirt1 Activation and Is Necessary for Autophagy upon Glucose

Starvation. *Mol Cell* 60: 930–940
Chen GY & Nuñez G (2010) Sterile inflammation: Sensing and reacting to damage. *Nat Rev Immunol* 10: 826–837
Chen LM, Hobbie S & Galán JE (1996a) Requirement of CDC42 for Salmonella-induced cytoskeletal and nuclear responses. *Science (80- )* 274: 2115–2118
Chen ZJ, Parent L & Maniatis T (1996b) Site-specific phosphorylation of IκBα by a novel ubiquitination- dependent protein kinase activity. *Cell* 84: 853–862
Cirillo DM, Valdivia RH, Monack DM & Falkow S (1998) Macrophage-dependent induction of the Salmonella pathogenicity island 2 type III secretion system and its role in intracellular survival. *Mol Microbiol* 30: 175–188
Cohen P (2002) The origins of protein phosphorylation. *Nat Cell Biol* 4: E127–E130
Cohen P & Strickson S (2017) The role of hybrid ubiquitin chains in the MyD88 and other innate immune signalling pathways. *Cell Death Differ* 268: 22723
Collazo CM & Galán JE (1997) The invasion-associated type-III protein secretion system in Salmonella - A review. *Gene* 192: 51–59
Colthurst DR, Campbell DG & Proud CG (1987) Structure and regulation of eukaryotic initiation factor eIF-2. Sequence of the site in the alpha subunit phosphorylated by the haem-controlled repressor and by the double-stranded RNA-activated inhibitor. *Eur J Biochem* 166: 357–363
Cossart P & Sansonetti PJ (2004) Bacterial Invasion: The Paradigms of Enteroinvasive Pathogens. *Science (80- )* 304: 242 LP – 248
Costa-Mattioli M & Walter P (2020) The integrated stress response: From mechanism to disease. *Science* 368
Creasey EA & Isberg RR (2014) Maintenance of vacuole integrity by bacterial pathogens. *Curr Opin Microbiol* 17: 46–52
Cui W, Li J, Ron D & Sha B (2011) The structure of the PERK kinase domain suggests the mechanism for its activation. *Acta Crystallogr Sect D Biol Crystallogr* 67: 423–428
Daefler S (1999) Type III secretion by Salmonella typhimurium does not require contact with a eukaryotic host. *Mol Microbiol* 31: 45–51
Dauber B & Wolff T (2009) Activation of the antiviral kinase PKR and viral countermeasures. *Viruses* 1: 523–544
Deng L, Wang C, Spencer E, Yang L, Braun A, You J, Slaughter C, Pickart C &

Chen ZJ (2000) Activation of the Iκb kinase complex by TRAF6 requires a dimeric ubiquitin-conjugating enzyme complex and a unique polyubiquitin chain. *Cell* 103: 351–361

Deshaies RJ & Joazeiro CAP (2009) RING domain E3 ubiquitin ligases. *Annu Rev Biochem* 78: 399–434

Diao J, Zhang Y, Huibregtse JM, Zhou D & Chen J (2008) Crystal structure of SopA, a Salmonella effector protein mimicking a eukaryotic ubiquitin ligase. *Nat Struct Mol Biol* 15: 65–70

Dikic I (2017) Proteasomal and autophagic degradation systems. *Annu Rev Biochem* 86: 193–224

Dikic I & Elazar Z (2018) Mechanism and medical implications of mammalian autophagy. *Nat Publ Gr*

Dikic I, Wakatsuki S & Walters KJ (2009) Ubiquitin-binding domains — from structures to functions. *Nat Rev Mol Cell Biol* 10: 1–13

Donnelly N, Gorman AM, Gupta S & Samali A (2013) The eIF2α kinases: Their structures and functions. *Cell Mol Life Sci* 70: 3493–3511

Dooley HC, Razi M, Polson HEJ, Girardin SE, Wilson MI & Tooze SA (2014) WIPI2 links LC3 conjugation with PI3P, autophagosome formation, and pathogen clearance by recruiting Atg12-5-16L1. *Mol Cell* 55: 238–252

Du J, Reeves AZ, Klein JA, Twedt DJ, Knodler LA & Lesser CF (2016) The type III secretion system apparatus determines the intracellular niche of bacterial pathogens. *Proc Natl Acad Sci U S A* 113: 4794–4799

De Duve C & Wattiaux R (1966) Functions of lysosomes. *Annu Rev Physiol* 28: 435–492

Emmerich CH, Ordureau A, Strickson S, Arthur JSC, Pedrioli PGA, Komander D & Cohen P (2013) Activation of the canonical IKK complex by K63/M1-linked hybrid ubiquitin chains. *Proc Natl Acad Sci U S A* 110: 15247–15252

Feasey NA, Dougan G, Kingsley RA, Heyderman RS & Gordon MA (2012) Invasive non-typhoidal salmonella disease: An emerging and neglected tropical disease in Africa. *Lancet* 379: 2489–2499

Fiskin E, Bhogaraju S, Herhaus L, Kalayil S, Hahn M & Dikic I (2017) Structural basis for the recognition and degradation of host TRIM proteins by Salmonella effector SopA. *Nat Commun* 8: 14004

Fiskin E, Bionda T, Dikic I & Behrends C (2016) Global Analysis of Host and

Bacterial Ubiquitinome in Response to Salmonella Typhimurium Infection. *Mol Cell* 62: 967–981

Fortelny N, Overall CM, Pavlidis P & Freue GVC (2017) Can we predict protein from mRNA levels? *Nature* 547: E19–E20

Fredlund J & Enninga J (2014) Cytoplasmic access by intracellular bacterial pathogens. *Trends Microbiol* 22: 128–137

Friebel A, Ilchmann H, Aepfelbacher M, Ehrbar K, Machleidt W & Hardt WD (2001) SopE and SopE2 from Salmonella typhimurium Activate Different Sets of RhoGTPases of the Host Cell. *J Biol Chem* 276: 34035–34040

Fu Y & Galán JE (1999) A Salmonella protein antagonizes Rac-1 and Cdc42 to mediate host-cell recovery after bacterial invasion. *Nature* 401: 293–297

Gal-Mor O, Boyle EC & Grassl GA (2014) Same species, different diseases: How and why typhoidal and non-typhoidal Salmonella enterica serovars differ. *Front Microbiol* 5: 391 doi:10.3389/fmicb.2014.00391 [PREPRINT]

Galán JE (2001) Salmonella Interactions with Host Cells: Type III Secretion at Work. *Annu Rev Cell Dev Biol* 17: 53–86

Galán JE (2021) Salmonella Typhimurium and inflammation: a pathogen-centric affair. *Nat Rev Microbiol*

Galan JE & Curtiss R (1989) Cloning and molecular characterization of genes whose products allow Salmonella typhimurium to penetrate tissue culture cells. *Proc Natl Acad Sci U S A* 86: 6383–6387

Galán JE, Lara-Tejero M, Marlovits TC & Wagner S (2014) Bacterial type III secretion systems: Specialized nanomachines for protein delivery into target cells. *Annu Rev Microbiol* 68: 415–438

Galán JE & Zhou D (2000) Striking a balance: modulation of the actin cytoskeleton by Salmonella. *Proc Natl Acad Sci* 97: 8754–8761

Garcia-Del Portillo F & Finlay BB (1995) Targeting of Salmonella typhimurium to vesicles containing lysosomal membrane glycoproteins bypasses compartments with mannose 6-phosphate receptors. *J Cell Biol* 129: 81–97

Ghosh G, Van Duyne G, Ghosh S & Sigler PB (1995) Structure of nf-κb p50 homodimer bound to a κb site. *Nature* 373: 303–310

Gomes LC & Dikic I (2014) Autophagy in antimicrobial immunity. *Mol Cell* 54: 224–233

Haas TL, Emmerich CH, Gerlach B, Schmukle AC, Cordier SM, Rieser E, Feltham R, Vince J, Warnken U, Wenger T, *et al* (2009) Recruitment of the Linear Ubiquitin Chain Assembly Complex Stabilizes the TNF-R1 Signaling Complex and Is Required for TNF-Mediated Gene Induction. *Mol Cell* 36: 831–844

Häcker H, Redecke V, Blagoev B, Kratchmarova I, Hsu LC, Wang GG, Kamps MP, Raz E, Wagner H, Häcker G, *et al* (2006) Specificity in Toll-like receptor signalling through distinct effector functions of TRAF3 and TRAF6. *Nature* 439: 204–207

Hahn M, Covarrubias-Pinto A, Herhaus L, Satpathy S, Klann K, Boyle KB, Münch C, Rajalingam K, Randow F, Choudhary C, *et al* (2021) SIK2 orchestrates actin-dependent host response upon Salmonella infection. *Proc Natl Acad Sci U S A* 118: e2024144118

Hänisch J, Ehinger J, Ladwein M, Rohde M, Derivery E, Bosse T, Steffen A, Bumann D, Misselwitz B, Hardt WD, *et al* (2010) Molecular dissection of Salmonella-induced membrane ruffling versus invasion. *Cell Microbiol* 12: 84–98

Hänisch J, Kölm R, Wozniczka M, Bumann D, Rottner K & Stradal TEB (2011) Activation of a RhoA/myosin II-dependent but Arp2/3 complex-independent pathway facilitates Salmonella invasion. *Cell Host Microbe* 9: 273–285

Hannemann S, Gao B & Galán JE (2013) Salmonella Modulation of Host Cell Gene Expression Promotes Its Intracellular Growth. *PLoS Pathog* 9: e1003668–e1003668

Hansen-Wester I & Hensel M (2001) Salmonella pathogenicity islands encoding type III secretion systems. *Microbes Infect* 3: 549–559

Haraga A & Miller SI (2003) A Salmonella enterica serovar Typhimurium translocated leucine-rich repeat effector protein inhibits NF-κB-dependent gene expression. *Infect Immun* 71: 4052–4058

Haraga A, Ohlson MB & Miller SI (2008) Salmonellae interplay with host cells. *Nat Rev Microbiol* 6: 53–66

Hardie DG, Ross FA & Hawley SA (2012) AMPK: A nutrient and energy sensor that maintains energy homeostasis. *Nat Rev Mol Cell Biol* 13: 251–262

Harding HP, Zhang Y, Zeng H, Novoa I, Lu PD, Calfon M, Sadri N, Yun C, Popko B, Paules R, *et al* (2003) An Integrated Stress Response Regulates Amino Acid Metabolism and Resistance to Oxidative Stress. *Mol Cell* 11: 619–633

Hardt W-D, Chen L-M, Schuebel KE, Bustelo XR & Galán JE (1998) S. typhimurium Encodes an Activator of Rho GTPases that Induces Membrane Ruffling and Nuclear Responses in Host Cells. *Cell* 93: 815–826

Hayashi F, Smith KD, Ozinsky A, Hawn TR, Yi EC, Goodlett DR, Eng JK, Akira S, Underhill DM & Aderem A (2001) The innate immune response to bacterial flagellin is mediated by Toll-like receptor 5. *Nature* 410: 1099–1103

Hayden MS & Ghosh S (2004) Signaling to NF-kappaB. *Genes & Dev* 18: 2195–2224

Hayden MS & Ghosh S (2008) Shared Principles in NF-κB Signaling. *Cell* 132: 344–362

Hayward RD & Koronakis V (1999) Direct nucleation and bundling of actin by the SipC protein of invasive Salmonella. *EMBO J* 18: 4926–4934

Heasman SJ & Ridley AJ (2008) Mammalian Rho GTPases: New insights into their functions from in vivo studies. *Nat Rev Mol Cell Biol* 9: 690–701

Hemmi H, Takeuchi O, Kawai T, Kaisho T, Sato S, Sanjo H, Matsumoto M, Hoshino K, Wagner H, Takeda K, *et al* (2000) A Toll-like receptor recognizes bacterial DNA. *Nature* 408: 740–745

Heo J-M, Ordureau A, Paulo JA, Rinehart J & Harper JW (2015) The PINK1-PARKIN Mitochondrial Ubiquitylation Pathway Drives a Program of OPTN/NDP52 Recruitment and TBK1 Activation to Promote Mitophagy. *Mol Cell* 60: 7–20

Herhaus L & Dikic I (2015) Expanding the ubiquitin code through post-translational modification. *EMBO Rep* 16: 1071–1083

Herhaus L & Dikic I (2017) Regulation of Salmonella-host cell interactions via the ubiquitin system. *Int J Med Microbiol* 308: 176–184

Hershko A & Ciechanover A (1998) The ubiquitin system. *Annu Rev Biochem* 67: 425–479

Hobbie S, Chen LM, Davis RJ & Galán JE (1997) Involvement of mitogen-activated protein kinase pathways in the nuclear responses and cytokine production induced by Salmonella typhimurium in cultured intestinal epithelial cells. *J Immunol* 159: 5550–9

Hoffmann A & Baltimore D (2006) Circuitry of nuclear factor κB signaling. *Immunol Rev* 210: 171–186

Hoshino K, Takeuchi O, Kawai T, Sanjo H, Ogawa T, Takeda Y, Takeda K &

Akira S (1999) Cutting edge: Toll-like receptor 4 (TLR4)-deficient mice are hyporesponsive to lipopolysaccharide: evidence for TLR4 as the Lps gene product. *J Immunol* 162: 3749–52

Hosokawa N, Hara T, Kaizuka T, Kishi C, Takamura A, Miura Y, Iemura SI, Natsume T, Takehana K, Yamada N, *et al* (2009) Nutrient-dependent mTORCI association with the ULK1-Atg13-FIP200 complex required for autophagy. *Mol Biol Cell* 20: 1981–1991

Hu P, Han Z, Couvillon AD, Kaufman RJ & Exton JH (2006) Autocrine Tumor Necrosis Factor Alpha Links Endoplasmic Reticulum Stress to the Membrane Death Receptor Pathway through IRE1α-Mediated NF-κB Activation and Down-Regulation of TRAF2 Expression. *Mol Cell Biol* 26: 3071–3084

Huett A, Heath RJ, Begun J, Sassi SO, Baxt LA, Vyas JM, Goldberg MB & Xavier RJ (2012) The LRR and RING domain protein LRSAM1 is an E3 ligase crucial for ubiquitin-dependent autophagy of intracellular salmonella typhimurium. *Cell Host Microbe* 12: 778–790

Hume PJ, Singh V, Davidson AC & Koronakis V (2017) Swiss army pathogen: The Salmonella entry toolkit. *Front Cell Infect Microbiol* 7: 2700

Humphreys D, Davidson A, Hume PJ & Koronakis V (2012) Salmonella Virulence Effector SopE and Host GEF ARNO Cooperate to Recruit and Activate WAVE to Trigger Bacterial Invasion. *Cell Host Microbe* 11: 129–139

Husnjak K & Dikic I (2012) Ubiquitin-binding proteins: decoders of ubiquitin-mediated cellular functions. *Annu Rev Biochem* 81: 291–322

Ikeda F, Deribe YL, Skånland SS, Stieglitz B, Grabbe C, Franz-Wachtel M, Van Wijk SJL, Goswami P, Nagy V, Terzic J, *et al* (2011) SHARPIN forms a linear ubiquitin ligase complex regulating NF-κB activity and apoptosis. *Nature* 471: 637–641

Jennings E, Thurston TLMM & Holden DW (2017) Salmonella SPI-2 Type III Secretion System Effectors: Molecular Mechanisms And Physiological Consequences. *Cell Host Microbe* 22: 217–231

Jones BD, Ghori N & Falkow S (1994) Salmonella typhlrnurium initiates murine infection by penetrating and destroying the specialized epithelial M cells of the peyer’s patches. *J Exp Med* 180: 15–23

Kagan JC, Su T, Horng T, Chow A, Akira S & Medzhitov R (2008) TRAM couples endocytosis of Toll-like receptor 4 to the induction of interferon-β. *Nat Immunol* 9: 361–368

Kamanova J, Sun H, Lara-Tejero M & Galán JE (2016) The Salmonella Effector Protein SopA Modulates Innate Immune Responses by Targeting TRIM E3 Ligase Family Members. *PLOS Pathog* 12: e1005552

Kanarek N, London N, Schueler-Furman O & Ben-Neriah Y (2010) Ubiquitination and degradation of the inhibitors of NF-kappaB. *Cold Spring Harb Perspect Biol* 2

Karpinski BA, Morle GD, Huggenvik J, Uhler MD & Leiden JM (1992) Molecular cloning of human CREB-2: An ATF/CREB transcription factor that can negatively regulate transcription from the cAMP response element. *Proc Natl Acad Sci U S A* 89: 4820–4824

Kaufman RJ, Davies M V, Pathak VK & Hershey JW (1989) The phosphorylation state of eucaryotic initiation factor 2 alters translational efficiency of specific mRNAs. *Mol Cell Biol* 9: 946–958

Kawagoe T, Sato S, Matsushita K, Kato H, Matsui K, Kumagai Y, Saitoh T, Kawai T, Takeuchi O & Akira S (2008) Sequential control of Toll-like receptor-dependent responses by IRAK1 and IRAK2. *Nat Immunol* 9: 684–691

Kawai T & Akira S (2010) The role of pattern-recognition receptors in innate immunity: Update on toll-like receptors. *Nat Immunol* 11: 373–384

Kawasaki T & Kawai T (2014) Toll-like receptor signaling pathways. *Front Immunol* 5: 461 doi:10.3389/fimmu.2014.00461 [PREPRINT]

Keszei AFA, Tang X, McCormick C, Zeqiraj E, Rohde JR, Tyers M & Sicheri F (2014) Structure of an SspH1-PKN1 complex reveals the basis for host substrate recognition and mechanism of activation for a bacterial E3 ubiquitin ligase. *Mol Cell Biol* 34: 362–373

Kihlstrom E & Nilsson L (1977) Endocytosis of Salmonella typhimurium 395 MS and MR10 by HeLa cells. *Acta Pathol Microbiol Scand - Sect B Microbiol Immunol* 85: 322–328

Kim HM, Park BS, Kim JI, Kim SE, Lee J, Oh SC, Enkhbayar P, Matsushima N, Lee H, Yoo OJ, *et al* (2007) Crystal Structure of the TLR4-MD-2 Complex with Bound Endotoxin Antagonist Eritoran. *Cell* 130: 906–917

Kirisako T, Kamei K, Murata S, Kato M, Fukumoto H, Kanie M, Sano S, Tokunaga F, Tanaka K & Iwai K (2006) A ubiquitin ligase complex assembles linear polyubiquitin chains. *EMBO J* 25: 4877–4887

Kirkin V, Lamark T, Sou Y, Bjorkoy G, Nunn JL, Bruun J-A, Shvets E, McEwan DG, Clausen TH, Wild P, *et al* (2009a) A role for NBR1 in autophagosomal degradation of ubiquitinated substrates. *Mol Cell* 33: 505–516

Kirkin V, McEwan DG, Novak I & Dikic I (2009b) A role for ubiquitin in selective autophagy. *Mol Cell* 34: 259–269

Klann K & Munch C (2020) Instrument Logic Increases Identifications during Mutliplexed Translatome Measurements. *Anal Chem*: acs.analchem.0c01749

Klann K & Münch C (2020) Unbiased translation proteomics upon cell stress. *Mol Cell Oncol* 7: 1763150

Klann K, Tascher G & Münch C (2020) Functional Translatome Proteomics Reveal Converging and Dose-Dependent Regulation by mTORC1 and eIF2α. *Mol Cell* 77: 913-925.e4

Knodler LA & Elfenbein JR (2019) Salmonella enterica. *Trends Microbiol*

Knodler LA, Vallance BA, Celli J, Winfree S, Hansen B, Montero M & Steele-Mortimer O (2010) Dissemination of invasive Salmonella via bacterial-induced extrusion of mucosal epithelia. *Proc Natl Acad Sci U S A* 107: 17733–17738

Knowles A, Campbell S, Cross N & Stafford P (2021) Bacterial Manipulation of the Integrated Stress Response: A New Perspective on Infection. *Front Microbiol* 12: 463 doi:10.3389/fmicb.2021.645161 [PREPRINT]

Kocks C, Gouin E, Tabouret M, Berche P, Ohayon H & Cossart P (1992) L. monocytogenes-induced actin assembly requires the actA gene product, a surface protein. *Cell* 68: 521–531

Kreibich S, Emmenlauer M, Fredlund J, Rämö P, Münz C, Dehio C, Enninga J & Hardt W-D (2015) Autophagy Proteins Promote Repair of Endosomal Membranes Damaged by the Salmonella Type Three Secretion System 1. *Cell Host Microbe* 18: 527–537

Kroemer G, Mariño G & Levine B (2010) Autophagy and the Integrated Stress Response. *Mol Cell* 40: 280–293

Kubori T & Galán JE (2003) Temporal regulation of Salmonella virulence effector function by proteasome-dependent protein degradation. *Cell* 115: 333–342

Kubori T, Matsushima Y, Nakamura D, Uralil J, Lara-Tejero M, Sukhan A, Galán

JE & Aizawa SI (1998) Supramolecular structure of the salmonella typhimurium type III protein secretion system. *Science (80- )* 280: 602–605

Kühn S, Bergqvist J, Gil M, Valenzuela C, Barrio L, Lebreton S, Zurzolo C & Enninga J (2020) Actin Assembly around the Shigella-Containing Vacuole Promotes Successful Infection. *Cell Rep* 31: 107638

Kühn S & Enninga J (2020) The actin comet guides the way: How Listeriaactin subversion has impacted cell biology, infection biology and structural biology. *Cell Microbiol* 22: 2877

Kuma A, Mizushima N, Ishihara N & Ohsumi Y (2002) Formation of the ∼350-kDa Apg12-Apg5·Apg16 multimeric complex, mediated by Apg16 oligomerization, is essential for autophagy in yeast. *J Biol Chem* 277: 18619–18625

Kumar Y & Valdivia RH (2008) Actin and Intermediate Filaments Stabilize the Chlamydia trachomatis Vacuole by Forming Dynamic Structural Scaffolds. *Cell Host Microbe* 4: 159–169

LaRock DL, Chaudhary A & Miller SI (2015) Salmonellae interactions with host processes. *Nat Publ Gr* 13: 191–205

Lawrence E (1998) How salmonella survive the stomach. *Nature*

Lee SH & Dominguez R (2010) Regulation of actin cytoskeleton dynamics in cells. *Mol Cells* 29: 311–325

Lee YY, Cevallos RC & Jan E (2009) An upstream open reading frame regulates translation of GADD34 during cellular stresses that induce eIF2phosphorylation. *J Biol Chem* 284: 6661–6673

Lhocine N, Arena ET, Bomme P, Ubelmann F, Prévost MC, Robine S & Sansonetti PJ (2015) Apical invasion of intestinal epithelial cells by salmonella typhimurium requires villin to remodel the brush border actin cytoskeleton. *Cell Host Microbe* 17: 164–177

Li S, Wandel MP, Li F, Liu Z, He C, Wu J, Shi Y & Randow F (2013) Sterical hindrance promotes selectivity of the autophagy cargo receptor NDP52 for the danger receptor galectin-8 in antibacterial autophagy. *Sci Signal* 6: ra9

Li ZW, Chu W, Hu Y, Delhase M, Deerinck T, Ellisman M, Johnson R & Karin M (1999) The IKKβ subunit of IκB kinase (IKK) is essential for nuclear factor κB activation and prevention of apoptosis. *J Exp Med* 189: 1839–1845

Lin DYW, Diao J & Chen J (2012) Crystal structures of two bacterial HECT-like

E3 ligases in complex with a human E2 reveal atomic details of pathogen-host interactions. *Proc Natl Acad Sci U S A* 109: 1925–1930

Lin SC, Lo YC & Wu H (2010) Helical assembly in the MyD88-IRAK4-IRAK2 complex in TLR/IL-1R signalling. *Nature* 465: 885–890

Liss V & Hensel M (2015) Take the tube: Remodelling of the endosomal system by intracellular Salmonella enterica. *Cell Microbiol* 17: 639–647

Liss V, Swart AL, Kehl A, Hermanns N, Zhang Y, Chikkaballi D, Böhles N, Deiwick J & Hensel M (2017) Salmonella enterica Remodels the Host Cell Endosomal System for Efficient Intravacuolar Nutrition. *Cell Host Microbe* 21: 390–402

Liu W, Jiang Y, Sun JJ, Geng S, Pan Z, Prinz RA, Wang C, Sun JJ, Jiao X & Xu X (2018) Activation of TGF-beta-activated kinase 1 (TAK1) restricts Salmonella Typhimurium growth by inducing AMPK activation and autophagy. *Cell death & Dis* 9: 570

Macek B, Mann M & Olsen J V. (2009) Global and site-specific quantitative phosphoproteomics: Principles and applications. *Annu Rev Pharmacol Toxicol* 49: 199–221

Maculins T, Fiskin E, Bhogaraju S & Dikic I (2016) Bacteria-host relationship: ubiquitin ligases as weapons of invasion. *Cell Res* 26: 499–510

Maejima I, Takahashi A, Omori H, Kimura T, Takabatake Y, Saitoh T, Yamamoto A, Hamasaki M, Noda T, Isaka Y, *et al* (2013) Autophagy sequesters damaged lysosomes to control lysosomal biogenesis and kidney injury. *EMBO J* 32: 2336–2347

Majowicz SE, Musto J, Scallan E, Angulo FJ, Kirk M, O'Brien SJ, Jones TF, Fazil A, Hoekstra RM & Studies for the IC on ED "Burden of I (2010) The Global Burden of Nontyphoidal Salmonella Gastroenteritis. *Clin Infect Dis* 50: 882–889

Malik-Kale P, Jolly CE, Lathrop S, Winfree S, Luterbach C & Steele-Mortimer O (2011) Salmonella - at home in the host cell. *Front Microbiol* 2: 125

Mallo G V., Espina M, Smith AC, Terebiznik MR, Alemán A, Finlay BB, Rameh LE, Grinstein S & Brumell JH (2008) SopB promotes phosphatidylinositol 3-phosphate formation on Salmonella vacuoles by recruiting Rab5 and Vps34. *J Cell Biol* 182: 741–752

Matzinger P (1994) Tolerance, danger, and the extended family. *Annu Rev*

*Immunol* 12: 991–1045

McClelland M, Sanderson KE, Spieth J, Clifton SW, Latreille P, Courtney L, Porwollik S, Ali J, Dante M, Du F, *et al* (2001) Complete genome sequence of Salmonella enterica serovar Typhimurium LT2. *Nature* 413: 852–856

McEwan DG, Richter B, Claudi B, Wigge C, Wild P, Farhan H, McGourty K, Coxon FP, Franz-Wachtel M, Perdu B, *et al* (2015) PLEKHM1 regulates Salmonella-containing vacuole biogenesis and infection. *Cell Host Microbe* 17: 58–71

McGhie EJ, Hayward RD & Koronakis V (2001) Cooperation between actin-binding proteins of invasive Salmonella: SipA potentiates SipC nucleation and bundling of actin. *EMBO J* 20: 2131–2139

McGourty K (2012) Salmonella inhibits retrograde trafficking of mannose-6-phosphate receptors and lysosome function (Science (963)). *Science (80- )* 338: 1287

McGourty K, Thurston TL, Matthews SA, Pinaud L, Mota LJ & Holden DW (2012) Salmonella inhibits retrograde trafficking of mannose-6-phosphate receptors and lysosome function. *Science* 338: 963–967

Medzhitov R, Preston-Hurlburt P & Janeway CA (1997) A human homologue of the Drosophila toll protein signals activation of adaptive immunity. *Nature* 388: 394–397

Mengaud J, Ohayon H, Gounon P, Mege RM & Cossart P (1996) E-cadherin is the receptor for internalin, a surface protein required for entry of L. monocytogenes into epithelial cells. *Cell* 84: 923–932

Méresse S, Steele-Mortimer O, Finlay BB & Gorvel JP (1999) The rab7 GTPase controls the maturation of Salmonella typhimurium-containing vacuoles in HeLa cells. *EMBO J* 18: 4394–4403

Méresse S, Unsworth KE, Habermann A, Griffiths G, Fang F, Martínez-Lorenzo MJ, Waterman SR, Gorvel J-P & Holden DW (2001) Remodelling of the actin cytoskeleton is essential for replication of intravacuolar Salmonella. *Cell Microbiol* 3: 567–577

Mertins P, Tang LC, Krug K, Clark DJ, Gritsenko MA, Chen L, Clauser KR, Clauss TR, Shah P, Gillette MA, *et al* (2018) Reproducible workflow for multiplexed deep-scale proteome and phosphoproteome analysis of tumor tissues by liquid chromatography-mass spectrometry. *Nat Protoc* 13: 1632–1661

Mills DM, Bajaj V & Lee CA (1995) A 40 kb chromosomal fragment encoding Salmonella typhimurium invasion genes is absent from the corresponding region of the Escherichia coli K-12 chromosome. *Mol Microbiol* 15: 749–759

Miranda F, Mannion D, Liu S, Zheng Y, Mangala LS, Redondo C, Herrero-Gonzalez S, Xu R, Taylor C, Chedom DF, *et al* (2016) Salt-Inducible Kinase 2 Couples Ovarian Cancer Cell Metabolism with Survival at the Adipocyte-Rich Metastatic Niche. *Cancer Cell* 30: 273–289

Mitchell S, Vargas J & Hoffmann A (2016) Signaling via the NFkappaB system. *Wiley Interdiscip Rev Syst Biol Med* 8: 227–241

Mittal R, Peak-Chew SY & McMahon HT (2006) Acetylation of MEK2 and IκB (IKK) activation loop residues by YopJ inhibits signaling. *Proc Natl Acad Sci U S A* 103: 18574–18579

Mostowy S & Shenoy AR (2015) The cytoskeleton in cell-autonomous immunity: structural determinants of host defence. *Nat Rev Immunol* 15: 559–573

Mounir Z, Krishnamoorthy JL, Wang S, Papadopoulou B, Campbell S, Muller WJ, Hatzoglou M & Koromilas AE (2011) Akt determines cell fate through inhibition of the PERK-eIF2α phosphorylation pathway. *Sci Signal* 4: ra62

von Muhlinen N, Akutsu M, Ravenhill BJ, Foeglein Á, Bloor S, Rutherford TJ, Freund SM V, Komander D & Randow F (2012) LC3C, Bound Selectively by a Noncanonical LIR Motif in NDP52, Is Required for Antibacterial Autophagy. *Mol Cell* 48: 329–342

Murphy K, Travers P, Walport M, Janeway C, Mowat A & Weaver CT (2012) Janeway's immunobiology New York: Garland Science

Nair DVT, Venkitanarayanan K & Johny AK (2018) Antibiotic-resistant Salmonella in the food supply and the potential role of antibiotic alternatives for control. *Foods* 7: 167

Nakagawa I, Amano A, Mizushima N, Yamamoto A, Yamaguchi H, Kamimoto T, Nara A, Funao J, Nakata M, Tsuda K, *et al* (2004) Autophagy defends cells against invading group A Streptococcus. *Science (80- )* 306: 1037–1040

Nishimura T, Tamura N, Kono N, Shimanaka Y, Arai H, Yamamoto H & Mizushima N (2017) Autophagosome formation is initiated at phosphatidylinositol synthase-enriched ER subdomains . *EMBO J* 36: 1719–1735

Noad J, von der Malsburg A, Pathe C, Michel MA, Komander D & Randow F

(2017) LUBAC-synthesized linear ubiquitin chains restrict cytosol-invading bacteria by activating autophagy and NF-κB. *Nat Microbiol* 2: 17063

Novoa I, Zeng H, Harding HP & Ron D (2001) Feedback inhibition of the unfolded protein response by GADD34-mediated dephosphorylation of eIF2α. *J Cell Biol* 153: 1011–1021

O'Brien AD, Rosenstreich DL, Scher I, Campbell GH, MacDermott RP & Formal SB (1980) Genetic control of susceptibility to Salmonella typhimurium in mice: Role of the LPS gene. *J Immunol* 124: 20–24

Odendall C, Rolhion N, Förster A, Poh J, Lamont DJ, Liu M, Freemont PS, Catling AD & Holden DW (2012) The salmonella kinase SteC targets the MAP kinase MEK to regulate the host actin cytoskeleton. *Cell Host Microbe* 12: 657–668

Oeckinghaus A & Ghosh S (2009) The NF-kappaB family of transcription factors and its regulation. *Cold Spring Harb Perspect Biol* 1: a000034–a000034

Oganesyan G, Saha SK, Guo B, He JQ, Shahangian A, Zarnegar B, Perry A & Cheng G (2006) Critical role of TRAF3 in the Toll-like receptor-dependent and -independent antiviral response. *Nature* 439: 208–211

Ohashi K, Burkart V, Flohé S & Kolb H (2000) Cutting Edge: Heat Shock Protein 60 Is a Putative Endogenous Ligand of the Toll-Like Receptor-4 Complex. *J Immunol* 164: 558–561

Ordureau A, Smith H, Windheim M, Peggie M, Carrick E, Morrice N & Cohen P (2008) The IRAK-catalysed activation of the E3 ligase function of Pellino isoforms induces the Lys63-linked polyubiquitination of IRAK1. *Biochem J* 409: 43–52

Pahl HL (1999) Activators and target genes of Rel/NF-κB transcription factors. *Oncogene* 18: 6853–6866

Pakos-Zebrucka K, Koryga I, Mnich K, Ljujic M, Samali A & Gorman AM (2016) The integrated stress response. *EMBO Rep* 17: 1374–1395

Palam LR, Baird TD & Wek RC (2011) Phosphorylation of eIF2 facilitates ribosomal bypass of an inhibitory upstream ORF to enhance CHOP translation. *J Biol Chem* 286: 10939–10949

Pao KC & Rape M (2019) Tug of War in the Xenophagy World. *Trends Cell Biol* 29: 767–769

Park BS, Song DH, Kim HM, Choi BS, Lee H & Lee JO (2009) The structural basis of lipopolysaccharide recognition by the TLR4-MD-2 complex. *Nature*

458: 1191–1195

Patel JC & Galán JE (2005) Manipulation of the host actin cytoskeleton by Salmonella - All in the name of entry. *Curr Opin Microbiol* 8: 10–15

Patel JC & Galán JE (2006) Differential activation and function of Rho GTPases during Salmonella–host cell interactions . *J Cell Biol* 175: 453–463

Paz I, Sachse M, Dupont N, Mounier J, Cederfur C, Enninga J, Leffler H, Poirier F, Prevost MC, Lafont F, *et al* (2010) Galectin-3, a marker for vacuole lysis by invasive pathogens. *Cell Microbiol* 12: 530–544

Perrin AJ, Jiang X, Birmingham CL, So NSY & Brumell JH (2004) Recognition of bacteria in the cytosol of mammalian cells by the ubiquitin system. *Curr Biol* 14: 806–811

Picard C, Puel A, Bonnet M, Ku CL, Bustamante J, Yang K, Soudais C, Dupuis S, Feinberg J, Fieschi C, *et al* (2003) Pyogenic bacterial infections in humans with IRAK-4 deficiency. *Science (80- )* 299: 2076–2079

Piscatelli HL, Li M & Zhou D (2016) Dual 4- and 5-phosphatase activities regulate SopB-dependent phosphoinositide dynamics to promote bacterial entry. *Cell Microbiol* 18: 705–719

Poh J, Odendall C, Spanos A, Boyle C, Liu M, Freemont P & Holden DW (2008) SteC is a Salmonella kinase required for SPI-2-dependent F-actin remodelling. *Cell Microbiol* 10: 20–30

Polajnar M, Dietz MS, Heilemann M & Behrends C (2017) Expanding the host cell ubiquitylation machinery targeting cytosolic Salmonella. *EMBO Rep*

Pollard TD (2007) Regulation of actin filament assembly by Arp2/3 complex and formins. *Annu Rev Biophys Biomol Struct* 36: 451–477

Poltorak A, He X, Smirnova I, Liu MY, Van Huffel C, Du X, Birdwell D, Alejos E, Silva M, Galanos C, *et al* (1998) Defective LPS signaling in C3H/HeJ and C57BL/10ScCr mice: Mutations in Tlr4 gene. *Science (80- )* 282: 2085–2088

Rahighi S, Ikeda F, Kawasaki M, Akutsu M, Suzuki N, Kato R, Kensche T, Uejima T, Bloor S, Komander D, *et al* (2009) Specific Recognition of Linear Ubiquitin Chains by NEMO Is Important for NF-κB Activation. *Cell* 136: 1098–1109

Rahman MM & McFadden G (2011) Modulation of NF-κB signalling by microbial pathogens. *Nat Rev Microbiol* 9: 291–306

Randow F, MacMicking JD & James LC (2013) Cellular self-defense: how cell-autonomous immunity protects against pathogens. *Science* 340: 701–706

Ravenhill BJ, Boyle KB, von Muhlinen N, Ellison CJ, Masson GR, Otten EG, Foeglein Á, Williams R & Randow F (2019) The Cargo Receptor NDP52 Initiates Selective Autophagy by Recruiting the ULK Complex to Cytosol-Invading Bacteria. *Mol Cell*

Richter B, Sliter DA, Herhaus L, Stolz A, Wang C, Beli P, Zaffagnini G, Wild P, Martens S, Wagner SA, *et al* (2016) Phosphorylation of OPTN by TBK1 enhances its binding to Ub chains and promotes selective autophagy of damaged mitochondria. *Proc Natl Acad Sci* 113: 201523926–201524044

Ridley AJ & Hall A (1992) The small GTP-binding protein rho regulates the assembly of focal adhesions and actin stress fibers in response to growth factors. *Cell* 70: 389–399

Robinson N, McComb S, Mulligan R, Dudani R, Krishnan L & Sad S (2012) Type I interferon induces necroptosis in macrophages during infection with Salmonella enterica serovar Typhimurium. *Nat Immunol* 13: 954–962

Rogers LD, Brown NF, Fang Y, Pelech S & Foster LJ (2011) Phosphoproteomic analysis of Salmonella-infected cells identifies key kinase regulators and SopB-dependent host phosphorylation events. *Sci Signal* 4: rs9–rs9

Ron D (2002) Translational control in the endoplasmic reticulum stress response. *J Clin Invest* 110: 1383–1388

Rowlands AG, Panniers R & Henshaw EC (1988) The catalytic mechanism of guanine nucleotide exchange factor action and competitive inhibition by phosphorylated eukaryotic initiation factor 2. *J Biol Chem* 263: 5526–5533

Russell RC, Tian Y, Yuan H, Park HW, Chang YY, Kim J, Kim H, Neufeld TP, Dillin A & Guan KL (2013) ULK1 induces autophagy by phosphorylating Beclin-1 and activating VPS34 lipid kinase. *Nat Cell Biol* 15: 741–750

Sakamaki J, Wilkinson S, Hahn M, Tasdemir N, O’Prey J, Clark W, Hedley A, Nixon C, Long JS, New M, *et al* (2017) Bromodomain Protein BRD4 Is a Transcriptional Repressor of Autophagy and Lysosomal Function. *Mol Cell* 66: 517-532.e9

Salcedo SP & Holden DW (2003) SseG, a virulence protein that targets Salmonella to the Golgi network. *EMBO J* 22: 5003–5014

Sasaki Y, Sano S, Nakahara M, Murata S, Kometani K, Aiba Y, Sakamoto S, Watanabe Y, Tanaka K, Kurosaki T, *et al* (2013) Defective immune responses in mice lacking LUBAC-mediated linear ubiquitination in B cells. *EMBO J* 32: 2463–2476

Sato S, Sanjo H, Takeda K, Ninomiya-Tsuji J, Yamamoto M, Kawai T, Matsumoto K, Takeuchi O & Akira S (2005) Essential function for the kinase TAK1 in innate and adaptive immune responses. *Nat Immunol* 6: 1087–1095

Sato S, Sugiyama M, Yamamoto M, Watanabe Y, Kawai T, Takeda K & Akira S (2003) Toll/IL-1 Receptor Domain-Containing Adaptor Inducing IFN-β (TRIF) Associates with TNF Receptor-Associated Factor 6 and TANK-Binding Kinase 1, and Activates Two Distinct Transcription Factors, NF-κB and IFN-Regulatory Factor-3, in the Toll-Like Receptor S. *J Immunol* 171: 4304–4310

Scherer CA, Cooper E & Miller SI (2000) The Salmonella type III secretion translocon protein SspC is inserted into the epithelial cell plasma membrane upon infection. *Mol Microbiol* 37: 1133–1145

Scherer DC, Brockman JA, Chen Z, Maniatis T & Ballard DW (1995) Signal-induced degradation of IκBα requires site-specific ubiquitination. *Proc Natl Acad Sci U S A* 92: 11259–11263

Schmitz ML, Shaban MS, Albert BV, Gökçen A & Kracht M (2018) The crosstalk of Endoplasmic Reticulum (ER) stress pathways with NF-κB: Complex mechanisms relevant for cancer, inflammation and infection. *Biomedicines* 6 doi:10.3390/biomedicines6020058 [PREPRINT]

Schmutz C, Ahrne E, Kasper CA, Tschon T, Sorg I, Dreier RF, Schmidt A & Arrieumerlou C (2013) Systems-level overview of host protein phosphorylation during Shigella flexneri infection revealed by phosphoproteomics. *Mol & Cell Proteomics* 12: 2952–2968

Schroeder N, Mota LJ & Méresse S (2011) Salmonella-induced tubular networks. *Trends Microbiol* 19: 268–277

Schwanhäusser B, Busse D, Li N, Dittmar G, Schuchhardt J, Wolf J, Chen W & Selbach M (2011) Global quantification of mammalian gene expression control. *Nature* 473: 337–342

Scott CC, Dobson W, Botelho RJ, Coady-Osberg N, Chavrier P, Knecht DA, Heath C, Stahl P & Grinstein S (2005) Phosphatidylinositol-4, 5-bisphosphate hydrolysis directs actin remodeling during phagocytosis. *J Cell Biol* 169: 139–149

Sen R & Baltimore D (1986a) Multiple nuclear factors interact with the immunoglobulin enhancer sequences. *Cell* 46: 705–716

Sen R & Baltimore D (1986b) Inducibility of κ immunoglobulin enhancer-binding protein NF-κB by a posttranslational mechanism. *Cell* 47: 921–928

Seong SY & Matzinger P (2004) Hydrophobicity: An ancient damage-associated molecular pattern that initiates innate immune responses. *Nat Rev Immunol* 4: 469–478

Settembre C, Di Malta C, Polito VA, Arencibia MG, Vetrini F, Erdin S, Erdin SU, Huynh T, Medina D, Colella P, *et al* (2011) TFEB links autophagy to lysosomal biogenesis. *Science (80- )* 332: 1429–1433

Shi J & Vakoc CR (2014) The Mechanisms behind the Therapeutic Activity of BET Bromodomain Inhibition. *Mol Cell* 54: 728–736

Singh B, Fleury C, Jalalvand F & Riesbeck K (2012) Human pathogens utilize host extracellular matrix proteins laminin and collagen for adhesion and invasion of the host. *FEMS Microbiol Rev* 36: 1122–1180

Sit S-T & Manser E (2011) Rho GTPases and their role in organizing the actin cytoskeleton. *J Cell Sci* 124: 679

Spanò S & Galán JE (2012) A Rab32-dependent pathway contributes to Salmonella typhi host restriction. *Science (80- )* 338: 960–963

Stecher B, Robbiani R, Walker AW, Westendorf AM, Barthel M, Kremer M, Chaffron S, Macpherson AJ, Buer J, Parkhill J, *et al* (2007) Salmonella enterica serovar typhimurium exploits inflammation to compete with the intestinal microbiota. *PLoS Biol* 5: 2177–2189

Steele-Mortimer O (2008) The Salmonella-containing vacuole: moving with the times. *Curr Opin Microbiol* 11: 38–45

Steele-Mortimer O, Méresse S, Gorvel JP, Toh BH & Finlay BB (1999) Biogenesis of Salmonella typhimurium-containing vacuoles in epithelial cells involves interactions with the early endocytic pathway. *Cell Microbiol* 1: 33–49

Stein MA, Leung KY, Zwick M, Garcia-del Portillo F & Finlay BB (1996) Identification of a Salmonella virulence gene required for formation of filamentous structures containing lysosomal membrane glycoproteins within epithelial cells. *Mol Microbiol* 20: 151–164

Stender S, Friebel A, Linder S, Rohde M, Mirold S & Hardt W-D (2000) Identification of SopE2 from Salmonella typhimurium, a conserved guanine nucleotide exchange factor for Cdc42 of the host cell. *Mol Microbiol* 36:

1206–1221

Sultzer BM (1968) Genetic control of leucocyte responses to endotoxin [17]. *Nature* 219: 1253–1254

Sun H, Kamanova J, Lara-Tejero M & Galán JE (2018) Salmonella stimulates pro-inflammatory signalling through p21-activated kinases bypassing innate immune receptors. *Nat Microbiol* 3: 1122–1130

Takeda K & Akira S (2015) Toll-Like receptors. *Curr Protoc Immunol* 2015: 14.12.1-14.12.10

Takeuchi A (1967) Electron microscope studies of experimental Salmonella infection. I. Penetration into the intestinal epithelium by Salmonella typhimurium. *Am J Pathol* 50: 109–136

Takeuchi O & Akira S (2010) Pattern Recognition Receptors and Inflammation. *Cell* 140: 805–820

Taniuchi S, Miyake M, Tsugawa K, Oyadomari M & Oyadomari S (2016) Integrated stress response of vertebrates is regulated by four eIF2α kinases. *Sci Rep* 6: 32886

Tattoli I, Sorbara MT, Vuckovic D, Ling A, Soares F, Carneiro LAM, Yang C, Emili A, Philpott DJ & Girardin SE (2012) Amino acid starvation induced by invasive bacterial pathogens triggers an innate host defense program. *Cell Host Microbe* 11: 563–575

Thiennimitr P, Winter SE, Winter MG, Xavier MN, Tolstikov V, Huseby DL, Sterzenbach T, Tsolis RM, Roth JR & Bäumler AJ (2011) Intestinal inflammation allows Salmonella to use ethanolamine to compete with the microbiota. *Proc Natl Acad Sci U S A* 108: 17480–17485

Thoreen CC, Chantranupong L, Keys HR, Wang T, Gray NS & Sabatini DM (2012) A unifying model for mTORC1-mediated regulation of mRNA translation. *Nature* 485: 109–113

Thurston TL, Boyle KB, Allen M, Ravenhill BJ, Karpiyevich M, Bloor S, Kaul A, Noad J, Foeglein Á, Matthews SA, *et al* (2016) Recruitment of TBK1 to cytosol-invading Salmonella induces WIPI2-dependent antibacterial autophagy. *EMBO J* 35: e201694491-1792

Thurston TLM, Ryzhakov G, Bloor S, von Muhlinen N & Randow F (2009) The TBK1 adaptor and autophagy receptor NDP52 restricts the proliferation of ubiquitin-coated bacteria. *Nat Immunol* 10: 1215–1221

Thurston TLM, Wandel MP, von Muhlinen N, Foeglein Á & Randow F (2012) Galectin 8 targets damaged vesicles for autophagy to defend cells against bacterial invasion. *Nature* 482: 414–418

Tokunaga F, Sakata SI, Saeki Y, Satomi Y, Kirisako T, Kamei K, Nakagawa T, Kato M, Murata S, Yamaoka S, *et al* (2009) Involvement of linear polyubiquitylation of NEMO in NF-κB activation. *Nat Cell Biol* 11: 123–132

Truong D, Brabant D, Bashkurov M, Wan LCK, Braun V, Heo W Do, Meyer T, Pelletier L, Copeland J & Brumell JH (2013) Formin-mediated actin polymerization promotes Salmonella invasion. *Cell Microbiol* 15: 2051–2063

Tsukada M & Ohsumi Y (1993) Isolation and characterization of autophagy-defective mutants of Saccharomyces cerevisiae. *FEBS Lett* 333: 169–174

Tumbarello DA, Manna PT, Allen M, Bycroft M, Arden SD, Kendrick-Jones J & Buss F (2015) The Autophagy Receptor TAX1BP1 and the Molecular Motor Myosin VI Are Required for Clearance of Salmonella Typhimurium by Autophagy. *PLOS Pathog* 11: e1005174-26

Unsworth KE, Way M, McNiven M, Machesky L & Holden DW (2004) Analysis of the mechanisms of Salmonella-induced actin assembly during invasion of host cells and intracellular replication. *Cell Microbiol* 6: 1041–1055

Vadlamudi RK, Li F, Barnes CJ, Bagheri-Yarmand R & Kumar R (2004) p-41-Arc subunit of human Arp2/3 complex is a p21-activated kinase-1-interacting substrate. *EMBO Rep* 5: 154–160

Vallejo M, Ron D, Miller CP & Habener JF (1993) C/ATF, a member of the activating transcription factor family of DNA- binding proteins, dimerizes with CAAT/enhancer-binding proteins and directs their binding to cAMP response elements. *Proc Natl Acad Sci U S A* 90: 4679–4683

Vargas JNS, Wang C, Bunker E, Hao L, Maric D, Schiavo G, Randow F & Youle RJ (2019) Spatiotemporal Control of ULK1 Activation by NDP52 and TBK1 during Selective Autophagy. *Mol Cell* 74: 347-362.e6

Venne AS, Kollipara L & Zahedi RP (2014) The next level of complexity: Crosstalk of posttranslational modifications. *Proteomics* 14: 513–524

Versteeg GA, Rajsbaum R, Sanchez-Aparicio MT, Maestre AM, Valdiviezo J, Shi M, Inn K-S, Fernandez-Sesma A, Jung J & Garcia-Sastre A (2013) The E3-ligase TRIM family of proteins regulates signaling pathways triggered by innate immune pattern-recognition receptors. *Immunity* 38: 384–398

Volmer R, Van Der Ploeg K & Ron D (2013) Membrane lipid saturation activates endoplasmic reticulum unfolded protein response transducers through their transmembrane domains. *Proc Natl Acad Sci U S A* 110: 4628–4633

Vorwerk S, Krieger V, Deiwick J, Hensel M & Hansmeier N (2014) Proteomes of Host Cell Membranes Modified by Intracellular Activities of Salmonella enterica. *Mol & Cell Proteomics* 14: 81–92

Walczak H, Iwai K & Dikic I (2012) Generation and physiological roles of linear ubiquitin chains. *BMC Biol* 10: 23–26

Wang C, Deng L, Hong M, Akkaraju GR, Inoue JI & Chen ZJ (2001) TAK1 is a ubiquitin-dependent kinase of MKK and IKK. *Nature* 412: 346–351

Wasylnka JA, Bakowski MA, Szeto J, Ohlson MB, Trimble WS, Miller SI & Brumell JH (2008) Role for myosin II in regulating positioning of Salmonella-containing vacuoles and intracellular replication. *Infect Immun* 76: 2722–2735

Waterman SR & Small PLC (1998) Acid-sensitive enteric pathogens are protected from killing under extremely acidic conditions of pH 2.5 when they are inoculated onto certain solid food sources. *Appl Environ Microbiol* 64: 3882–3886

Weidberg H, Shpilka T, Shvets E, Abada A, Shimron F & Elazar Z (2011) LC3 and GATE-16 N Termini Mediate Membrane Fusion Processes Required for Autophagosome Biogenesis. *Dev Cell* 20: 444–454

Wertz IE & Dixit VM (2010) Signaling to NF-kappaB: regulation by ubiquitination. *Cold Spring Harb Perspect Biol* 2

van Wijk SJL, Fiskin E, Putyrski M, Pampaloni F, Hou J, Wild P, Kensche T, Grecco HE, Bastiaens P & Dikic I (2012) Fluorescence-Based Sensors to Monitor Localization and Functions of Linear and K63-Linked Ubiquitin Chains in Cells. *Mol Cell* 47: 797–809

Van Wijk SJLL, Fricke F, Herhaus L, Gupta J, Hötte K, Pampaloni F, Grumati P, Kaulich M, Sou YS, Komatsu M, *et al* (2017) Linear ubiquitination of cytosolic Salmonella Typhimurium activates NF-kappaB and restricts bacterial proliferation. *Nat Microbiol* 2: 17066

Wild P, Farhan H, McEwan DG, Wagner S, Rogov V V, Brady NR, Richter B, Korac J, Waidmann O, Choudhary C, *et al* (2011) Phosphorylation of the autophagy receptor optineurin restricts Salmonella growth. *Science (80- )*

333: 228–233

Wood MW, Jones MA, Watson PR, Siber AM, McCormick BA, Hedges S, Rosqvist R, Wallis TS & Galyov EE (2000) The secreted effector protein of Salmonella dublin, SopA, is translocated into eukaryotic cells and influences the induction of enteritis. *Cell Microbiol* 2: 293–303

Xu Y, Zhou P, Cheng S, Lu Q, Nowak K, Hopp A-K, Li L, Shi X, Zhou Z, Gao W, *et al* (2019) A Bacterial Effector Reveals the V-ATPase-ATG16L1 Axis that Initiates Xenophagy. *Cell* 178: 552-566.e20

Yang Z & Klionsky DJ (2010) Eaten alive: A history of macroautophagy. *Nat Cell Biol* 12: 814–822

Yaron A, Hatzubai A, Davis M, Lavon I, Amit S, Manning AM, Andersen JS, Mann M, Mercurio F & Ben-Neriah Y (1998) Identification of the receptor component of the IκBα-ubiquitin ligase. *Nature* 396: 590–594

Yau R & Rape M (2016) The increasing complexity of the ubiquitin code. *Nat Cell Biol* 18: 579–586

Zheng YT, Shahnazari S, Brech A, Lamark T, Johansen T & Brumell JH (2009) The Adaptor Protein p62/SQSTM1 Targets Invading Bacteria to the Autophagy Pathway. *J Immunol* 183: 5909–5916

Zhou D, Chen LM, Hernandez L, Shears SB & Galán JE (2001) A Salmonella inositol polyphosphatase acts in conjunction with other bacterial effectors to promote host cell actin cytoskeleton rearrangements and bacterial internalization. *Mol Microbiol* 39: 248–260

Zhou D & Galán J (2001) Salmonella entry into host cells: the work in concert of type III secreted effector proteins. *Microbes Infect* 3: 1293–1298

Zinngrebe J, Montinaro A, Peltzer N & Walczak H (2013) Ubiquitin in the immune system. *EMBO Rep* 15: 28–45

Zinngrebe J & Walczak H (2017) TLRs Go Linear - On the Ubiquitin Edge. *Trends Mol Med*

nature COMMUNICATIONS

ARTICLE

Received 6 Jul 2016 | Accepted 21 Nov 2016 | Published 13 Jan 2017

DOI: 10.1038/ncomms14004 OPEN

# Structural basis for the recognition and degradation of host TRIM proteins by *Salmonella* effector SopA

Evgenij Fiskin[1,*], Sagar Bhogaraju[1,2,*], Lina Herhaus[1], Sissy Kalayil[1,2], Marcel Hahn[1] & Ivan Dikic[1,2,3]

The hallmark of *Salmonella* Typhimurium infection is an acute intestinal inflammatory response, which is mediated through the action of secreted bacterial effector proteins. The pro-inflammatory *Salmonella* effector SopA is a HECT-like E3 ligase, which was previously proposed to activate host RING ligases TRIM56 and TRIM65. Here we elucidate an inhibitory mechanism of TRIM56 and TRIM65 targeting by SopA. We present the crystal structure of SopA in complex with the RING domain of human TRIM56, revealing the atomic details of their interaction and the basis for SopA selectivity towards TRIM56 and TRIM65. Structure-guided biochemical analysis shows that SopA inhibits TRIM56 E3 ligase activity by occluding the E2-interacting surface of TRIM56. We further demonstrate that SopA ubiquitinates TRIM56 and TRIM65, resulting in their proteasomal degradation during infection. Our results provide the basis for how a bacterial HECT ligase blocks host RING ligases and exemplifies the multivalent power of bacterial effectors during infection.

[1] Institute of Biochemistry II, Goethe University School of Medicine, Theodor-Stern-Kai 7, 60590 Frankfurt am Main, Germany. [2] Buchmann Institute for Molecular Life Sciences, Goethe University, Max-von-Laue-Strasse 15, 60438 Frankfurt am Main, Germany. [3] Department of Immunology and Medical Genetics, School of Medicine, University of Split, Soltanska 2, 21000 Split, Croatia. * These authors contributed equally to this work. Correspondence and requests for materials should be addressed to I.D. (email: Ivan.Dikic@biochem2.de).

*Salmonella enterica* serovar Typhimurium is a Gram-negative pathogenic bacterium, which represents a major cause of food- and water-borne disease. Non-typhoidal *Salmonella* strains, including *S.* Typhimurium, cause severe gastroenteritis in immunocompetent individuals, whereas systemic infection can arise in immunosuppressed hosts. *S.* Typhimurium invasion and the concomitant induction of intestinal inflammation are initiated by secreted bacterial effector proteins, which are translocated into host cells via a channel-forming multi-protein complex known as the type-3 secretion system (T3SS)[1].

Bacterial infection is sensed by host pattern recognition receptor-mediated detection of pathogen-associated molecular patterns, such as lipopolysaccharide or bacteria-derived nucleic acids, and induces a pro-inflammatory state to combat infection[2]. The propagation of this innate immune response requires posttranslational modification of assembled receptor signalling complexes with ubiquitin (Ub)[3], which in eukaryotes is catalysed by three distinct classes of E3 Ub ligases known as homologous to E6–AP carboxy terminus (HECT), really interesting new gene (RING) and RING-between-RING.

To counteract Ub-dependent induction of host inflammatory signalling and microbicidal programmes, a wide range of bacteria have acquired strategies to subvert the host Ub proteasome system. Despite lacking the canonical Ub proteasome system, prokaryotic pathogens encode various families of virulence promoting E3 ligases. After their T3SS-mediated translocation, these ligase effectors hijack the host ubiquitination machinery and use their intrinsic catalytic activity to modify specific cellular targets[4–7]. The *Salmonella* T3SS effector protein SopA is a HECT-like E3 ligase that promotes *Salmonella* infection-induced inflammation[8–11]. Lacking noticeable primary sequence homology to eukaryotic HECT enzymes, the crystal structure of SopA showed the characteristic bi-lobal architecture of HECT ligases[9,12,13]. SopA-catalysed ubiquitination proceeds via a thioester-linked SopA$\sim$Ub intermediate and requires an active site cysteine in its C terminus[8]. Subsequently solved structures of SopA in complex with E2 Ub-conjugating enzymes revealed an E2-binding site located within the N-lobe of SopA and further indicate a high structural flexibility of its C-lobe[14]. Structural characterization of SopA also uncovered the presence of an amino-terminal β-helix domain, whose function so far remains unknown[9].

Recent work implicates SopA in the regulation of two tripartite-motif containing (TRIM) E3 ligases TRIM56 and TRIM65 (ref. 15). TRIM proteins constitute a large family of $\sim$70 RING-type E3 ligases, which plays a pivotal role in the host innate immune response against various pathogens[16,17]. TRIM56 and TRIM65 in particular have been demonstrated to stimulate type I interferon expression in conjunction with nucleic acid-sensing receptors such as STING, RIG-I and MDA5 (refs 15,18,19). TRIMs are characterized by the presence of three common structural features, consisting of an N-terminal catalytic RING domain, one or two B-boxes and a coiled-coil[20]. Multiple studies demonstrated that the coiled-coil of various TRIMs mediates anti-parallel dimer formation[21–24]. Furthermore, catalytic activity of TRIM proteins is enhanced by coiled-coil-dependent dimerization and, more recently, was shown to require RING domain dimerization for the proper activation of the E2$\sim$Ub conjugate[25,26].

Here, using quantitative proteomics, structural and biochemical analysis we elucidate how *Salmonella* HECT-like ligase SopA specifically targets and inhibits human TRIM56 and TRIM65. We present the structure of the SopA–TRIM56 RING complex providing the molecular basis for SopA target specificity. Analysis of this complex further reveals that SopA occludes the E2 binding site of TRIM56 RING and inhibits TRIM ligase activity. Finally, we demonstrate that SopA directly mediates ubiquitination and proteasomal degradation of TRIM56 and TRIM65.

## Results

**Identification of TRIM56 and TRIM65 as SopA interactors**. Aiming to understand the molecular basis of SopA function during *Salmonella* pathogenesis, we set out to identify SopA host interactions using affinity purification coupled mass spectrometry (MS). To this end, we generated a stable HeLa Flp-In T-REx cell line inducibly expressing GFP-SopA upon the addition of doxycycline (Supplementary Fig. 1a). These cells were differentially labelled using stable isotope labelling by amino acids in cell culture (SILAC) and then either left untreated or treated with doxycycline to induce GFP-SopA expression. Next, SopA-containing complexes were immunoprecipitated using anti-green fluorescent protein (GFP) beads, subjected to tryptic in-gel digest and extracted peptides were analysed by liquid chromatography-coupled MS/MS on an Orbitrap mass spectrometer (Fig. 1a and Supplementary Fig. 1b). We reproducibly identified two TRIM E3 ligases, TRIM56 and TRIM65, as the most significant SopA-enriched hits (Fig. 1b, Supplementary Fig. 1c and Supplementary Data 1). Subsequent immunoblotting experiments confirmed these MS data and revealed that endogenous TRIM56 and TRIM65 indeed specifically co-precipitated with transiently expressed GFP-SopA, but not with its enterohemorrhagic *Escherichia coli* homologue NleL (Fig. 1c). To additionally identify SopA interactors in the course of infection, we isolated SopA from cells infected with *S.* Typhimurium strains expressing tagged SopA–HA or empty vector controls. Consistent with results from heterologous expression experiments, we recovered TRIM56 and TRIM65 as major interacting proteins of bacterially secreted SopA in *Salmonella*-infected cells (Fig. 1d,e and Supplementary Data 2).

Given the reported ability of TRIM proteins to form hetero-oligomers[27], we tested whether TRIM56 and TRIM65 interact with each other. We did not detect complex formation between these two TRIM proteins after transient expression of tagged TRIM versions (Supplementary Fig. 1e,f). To further characterize the interaction mode between TRIM56/TRIM65 and SopA, we expressed different truncation constructs of both TRIM proteins individually and tested them for the ability to co-immunoprecipitate SopA (Fig. 2a and Supplementary Fig. 1d). Whereas ablation of both coiled-coil and substrate-binding domains had no effect, deletion of the RING domain in case of both TRIM56 and TRIM65 completely abolished SopA interaction (Fig. 2c,d). Analogously, we expressed SopA truncations to determine the requirements for TRIM56/65 interaction (Fig. 2b). Interestingly, the capacity of SopA to associate with both TRIM56/65 mapped to the N-terminal β-helix domain (Fig. 2e). Consistently, pull-down experiments using recombinant TRIM56 and SopA proteins revealed that SopA directly interacts with the RING of TRIM56 or TRIM65 via its β-helix domain (Fig. 2f and Supplementary Fig. 1g).

**Crystal structure of the SopA–TRIM56 complex**. To understand the molecular basis of the interaction between SopA and TRIMs, we set out to determine the crystal structure of the SopA–TRIM56 complex. Initial attempts to co-purify bacterially expressed SopA (163–782) and TRIM56 RING domain (1–94) did not yield stoichiometric complex in size-exclusion chromatography (Supplementary Fig. 2a), due to the low affinity binding between these molecules with a dissociation constant of $\sim$9 μM (Fig. 2g). To circumvent this problem, we fused the minimal binding regions of TRIM56 (1–94) and SopA (163–425) using a

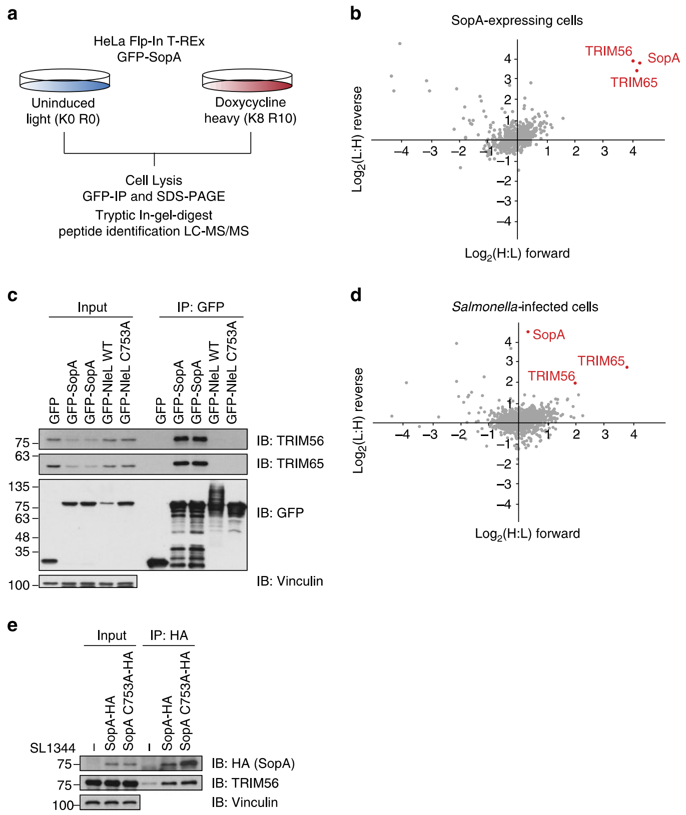


**Figure 1 | Identification of TRIM56 and TRIM65 as SopA-interacting proteins.** (**a**) Workflow for SILAC-coupled SopA interactome analysis from inducible HeLa Flp-In T-REx GFP-SopA-expressing cells. (**b**) SopA interacts with TRIM56 and TRIM65. Scatter plot of forward and reverse SILAC SopA interactome. Proteins situated in the upper left quadrant include contaminants. (**c**) Endogenous TRIM56 and TRIM65 specifically interact with SopA. Lysates from HEK293T cells expressing GFP, GFP-SopA or GFP-NleL constructs were subjected to anti-GFP IP, followed by SDS–PAGE and immunoblotting. (**d**) Bacterially translocated SopA interacts with TRIM56/65. Scatter plot of forward and reverse SILAC interactome experiments from *Salmonella*-infected HeLa cells. Proteins situated in the upper left quadrant include contaminants. (**e**) Endogenous TRIM56 interacts with bacterially secreted SopA during infection. Lysates from HeLa cells infected with SL1344 WT, SopA–HA or catalytic-dead SopA C753A-HA-expressing strains were subjected to anti-HA IP, followed by SDS–PAGE and immunoblotting.

flexible linker (Supplementary Fig. 2b). Such end-to-end fusion of two different proteins with short flexible linkers is a commonly employed method in crystallization of low-affinity protein complexes[28]. This fusion construct was purified and crystallized in the space group P $3_1$ 1 2 and the optimized crystals diffracted to $\sim$2.9 Å resolution (Supplementary Fig. 2c). The structure was determined by molecular replacement and refined until convergence (Fig. 3a and Table 1).

The asymmetric unit contained one copy of the SopA–TRIM56 dimer. The structure reveals that the first $Zn^{2+}$-binding loop in the TRIM56 RING domain is packed in a cleft at the interface of the β-helix and the N-lobe domains of SopA (Fig. 3b). The structure of SopA in complex with TRIM56 overlays well with the SopA apo structure with a mean root mean squared deviation (r.m.s.d.) of 0.9 Å over all the C-α atoms[9]. Both the linker residues between TRIM56 and SopA, as well as the 17 N-terminal residues of TRIM56 were disordered and could not be observed in the electron density. Comparison of the TRIM56 RING domain structure with all the structures in PDB using DALI revealed that it is most similar to the RING domain of RNF146 with a mean r.m.s.d. of 2.5 Å over all the C-α atoms[29]. Moreover, the RING domains of TRAF6, RING1B, TRIM32 and RNF4 also closely resemble the TRIM56 RING domain with mean r.m.s.d. of 2.6, 1.8, 2.1 and 1.9 Å over >90% of C-α atoms, respectively. The interface of SopA and TRIM56 contains a mix of hydrophobic/hydrophilic interactions with a buried surface area of 750 $Å^2$ (Fig. 3b). In TRIM56, residues Leu25 and Glu26 contribute majorly towards interaction with SopA. Although Glu26 makes polar contacts with Arg296, His297 and Lys298 of SopA, Leu25 inserts into a hydrophobic pocket of SopA involving Phe345 and Pro334.

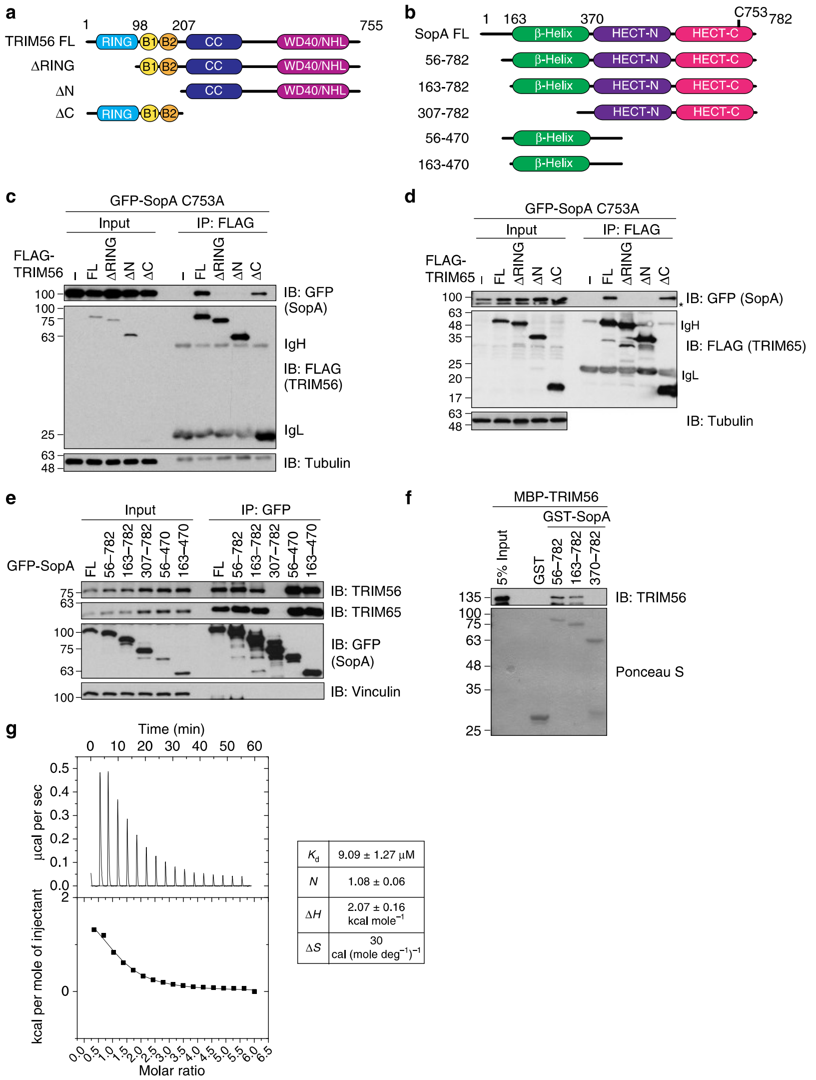


**Figure 2 | TRIM56 and TRIM65 RING domains directly interact with the β-helix region of SopA.** (**a**,**b**) Domain organization of TRIM56 (**a**) and SopA (**b**), and corresponding truncation constructs. B1 and B2, B-box type zinc fingers; CC, coiled-coil domain; HECT-N, N-lobe; HECT-C, C-lobe. (**c**,**d**) TRIM56/TRIM65 RING domain is required for SopA interaction. Lysates from HEK293T cells co-expressing GFP-SopA C753A and indicated FLAG-TRIM56 (**c**) or FLAG-TRIM65 (**d**) constructs were subjected to anti-FLAG IP, followed by SDS-PAGE and immunoblotting. (**e**) Intact SopA β-helix is required for TRIM56/TRIM65 interaction. Lysates from HEK293T cells expressing indicated GFP-SopA constructs were subjected to anti-GFP IP, followed by SDS-PAGE and immunoblotting. (**f**) SopA-TRIM56/65 interaction is direct. Recombinant MBP-TRIM56 was incubated with GST or different GST-SopA proteins and subjected to glutathione sepharose pull-down followed by SDS-PAGE and immunoblotting. (**g**) Isothermal titration calorimetry (ITC) measurement of SopA-TRIM56 RING interaction. 1,000 μM TRIM56 (1-94) was injected gradually into 20 μM SopA (163-782) present in the sample cell. Raw ITC data were plotted and analysed using Origin 7 software. The table shows values obtained for various parameters of the SopA-TRIM56 interaction. $\Delta H$, heat change; $K_d$, dissociation constant; $N$, occupancy; $\Delta S$, entropy change.

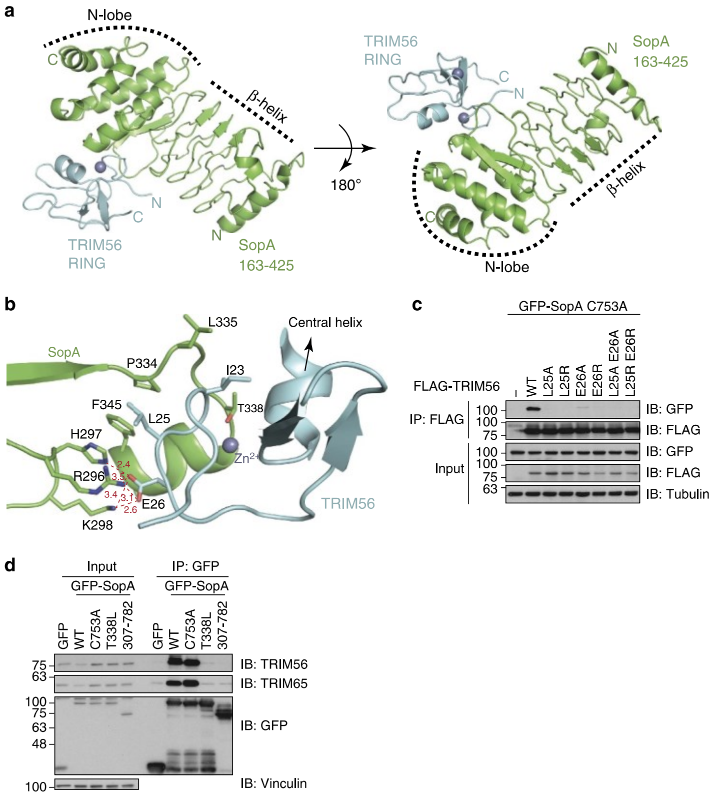


**Figure 3 | Structure of SopA β-helix in complex with TRIM56 RING domain.** (**a**) Crystal structure of SopA–TRIM56 complex shown in cartoon representation. SopA is shown in green and TRIM56 in cyan, two orientations rotated by *x*:180° are shown. (**b**) Enlarged view of the interface of SopA and TRIM56 showing the important residues involved in the interaction. Right conformation depicted in **a** was rotated by *y*: 140°, *x*: 145° and *z*: 35° and zoomed in; residues 18–48 in TRIM56 RING and 295–299, as well as 330–345 in SopA are shown. Hydrogen bonds with corresponding distances are depicted in deep red. (**c**) TRIM56 RING mutations abolish SopA interaction. Lysates from cells co-expressing GFP-SopA C753A and indicated FLAG-TRIM56 RING domain mutants were subjected to anti-FLAG IP, followed by SDS–PAGE and immunoblotting. (**d**) SopA T338L mutation abolishes SopA–TRIM56 and SopA–TRIM65 interaction. Lysates from cells expressing indicated GFP-SopA β-helix point mutants were subjected to anti-GFP IP, followed by SDS–PAGE and immunoblotting.

The central α-helix present in TRIM56 also makes several hydrophobic contacts and packs tightly against SopA (Fig. 3b).

Structure-guided point mutations in the first $Zn^{2+}$-binding loop of TRIM56 RING confirmed the requirement of Leu25 and Glu26 for SopA–TRIM complex formation. The corresponding TRIM56 single and double mutants were unable to co-precipitate SopA upon transient expression, while retaining functional RING E3 activity (Fig. 3c and Supplementary Fig. 2d). Thr338 of SopA is in close proximity to the central α-helix in TRIM56 (Fig. 3b) and we predicted that mutating it to Leucine would create steric clashes and impair the interaction. Indeed, a T338L point mutation in SopA completely abolished interaction with endogenous TRIM56 (Fig. 3d). Interestingly, SopA T338L mutation also prevented binding of SopA to TRIM65, indicating that SopA recognizes both TRIM56 and TRIM65 in a similar manner.

**Structural basis of SopA specificity for TRIM56 and TRIM65.** Sequence comparison of SopA and its *E. coli* homologue NleL revealed that NleL lacks all the residues involved in SopA–TRIM56 binding (Supplementary Fig. 2e). This readily explained why NleL does not target TRIM proteins (Fig. 1c). On the other hand, multiple sequence alignment of several TRIM proteins and other closely related RING domain-containing proteins revealed that residues Leu25 and Glu26, which are essential for TRIM56-SopA interaction, show a conservation of 75% and 50%, respectively (Fig. 4a). Despite this conservation, no other detected TRIM protein was found significantly enriched in our SopA interactome studies (Supplementary Data 1,2), indicating that the primary sequence of TRIM proteins may not determine SopA specificity. Other factors influencing SopA selectivity may include subcellular targeting and expression levels of various TRIMs.

**Table 1 | Data collection and refinement statistics.**

| | SopA–Trim56 complex |
|---|---|
| Wavelength (Å) | 0.99987 |
| Resolution range (Å) | 43.48–2.849 (2.95–2.85) |
| Space group | P 31 1 2 |
| *Unit cell* | |
| *a, b, c* (Å) | 71.01, 71.01, 122.94 |
| *α, β, γ* (°) | 90, 90, 120 |
| Unique reflections | 8,375 (833) |
| Multiplicity | 20.0 (19.0) |
| Completeness (%) | 98.37 (84.05) |
| Mean *Iσ(I)* | 31.15 (3.64) |
| Wilson B-factor (Å$^2$) | 77.87 |
| *R*-merge | 0.074 (0.834) |
| CC1/2 | 1 (0.985) |
| *R*-work | 0.2234 (0.3022) |
| *R*-free | 0.2780 (0.3269) |
| Number of atoms | 2395 |
| Macromolecules | 2392 |
| Ligands | 2 |
| Water | 1 |
| Protein residues | 325 |
| Root mean square (bonds; Å) | 0.004 |
| Root mean square (angles; °) | 0.97 |
| Ramachandran favoured (%) | 92 |
| Ramachandran outliers (%) | 0.94 |
| Clashscore | 6.51 |
| Average B-factor (Å$^2$) | 86.30 |
| Macromolecules | 86.30 |
| Ligands | 88.50 |
| Solvent | 46.80 |

Statistics for the highest-resolution shell are shown in parentheses.

Here we investigated whether the crystal structure of the SopA–TRIM56 complex explains the specificity of SopA. We superimposed the TRIM56 RING domain with RINGs of various TRIM proteins (only TRIM32 and TRIM39 are shown as representatives), as well as RNF4 and TRAF6 (Fig. 4b–e). Although, the first $Zn^{2+}$-binding loop of all the aligned RING domains fits into the cavity between the β-helix domain and the N-lobe of SopA without sterical clashes, the central α-helix of various RING domains appears to be clashing with SopA and rendering the binding unfavourable. Hence, positioning of the central α-helix of RING domains relative to the first $Zn^{2+}$-binding loop is one of the crucial factors defining the specificity of SopA. Consistent with these data, SopA was not able to bind and co-precipitate TRIM32, TRIM39 and RNF4 (Fig. 4f). In essence, a combination of sequence and structural features determine SopA-binding specificity towards the RING domains of TRIM56 and TRIM65.

**SopA inhibits TRIM56 ligase activity**. To gain more insights from the structure of SopA–TRIM56 complex, we superimposed TRIM56 RING with the RNF4 RING bound to UbcH5a (PDB: 4AP4)[30] (Fig. 5a). Surprisingly, this revealed that both SopA-binding and potential E2-binding surfaces on TRIM56 are overlapping, suggesting that SopA may hinder the interaction of E2 and TRIM56. In other words, SopA may negatively regulate the Ub ligase activity of TRIM56 by masking its E2-binding surface. To address this hypothesis, we first tested if the bacterially purified TRIM56 constructs harbour E3 ligase activity *in vitro*. Various TRIM56 constructs were incubated in the presence of three different E2s: UbcH5a, UbcH5b and UbcH7 (Fig. 5b). All TRIM56 constructs including the minimal RING domain used for crystallization of the SopA–TRIM56 complex were active and robustly synthesized free Ub chains in the presence of UbcH5a and UbcH5b, but not in the presence of UbcH7. We then examined how increasing amounts of SopA affect the Ub ligase activity of full-length TRIM56 (Fig. 5c). SopA (163–425) lacking its E2-binding region[14] was used in this assay to negate the possibility of SopA-mediated E2 recruitment. Although a previous report proposed SopA to activate TRIM56 and TRIM65 activity[15], we observed that SopA (163–425) inhibited the ligase activity of TRIM56 as seen by the decrease in free Ub chains and especially di-Ub formation (Fig. 5c).

**SopA mediates degradative ubiquitination of TRIM56**. To identify SopA substrates, we compared the diGly-modified proteome of cells infected with wild-type *Salmonella* (SL1344 WT) or a *sopA* deletion strain (*ΔsopA*) (Fig. 6a and Supplementary Fig. 3a). Two replicate SILAC diGly proteomics experiments resulted in the quantification of ~9,000 diGly sites in ~4,500 proteins (Supplementary Fig. 3b). Importantly, we identified multiple ubiquitination sites in TRIM56 (K87, K270 and K377) and TRIM65 (K206) as SopA-regulated events with the highest SILAC ratios of all quantified peptides (Fig. 6b, Supplementary Fig. 3c and Supplementary Data 3). To elaborate these findings, we purified ubiquitinated proteins from cells, which were infected with SL1344 WT, a non-invasive mutant defective in effector secretion (*ΔSPI1*) or with various *sopA* deletion (*ΔsopA*) and complemented strains (*ΔsopA + sopA*, *ΔsopA + sopA C753A*) in the presence or absence of the proteasome inhibitor MG132 using tandem Ub-binding entities (TUBEs; Fig. 6c)[31]. Indeed, we observed the appearance of ubiquitinated high molecular weight species of endogenous TRIM56 upon *Salmonella* infection (Fig. 6c). Infection of cells with complemented *sopA* deletion strains, expressing higher amounts of SopA relative to SL1344 WT *Salmonella* (Supplementary Fig. 3g), resulted in increased modification of TRIM56. Interestingly, ubiquitination of TRIM56 increased upon proteasome inhibition and was completely dependent on the presence of catalytically competent SopA. Moreover, infection of cells with *Salmonella* expressing the binding-deficient SopA T338L mutant did not result in TRIM56 modification (Fig. 6d). In agreement with the results obtained from infected cells, we were able to reconstitute SopA-mediated ubiquitination of TRIM56 *in vitro* using recombinant proteins. Importantly, to monitor SopA catalytic activity and to exclude TRIM-mediated chain formation, we used the E2 enzyme UbcH7 in these experiments (Fig. 5b). Both the isolated RING domain and full-length TRIM56 were robustly ubiquitinated by SopA *in vitro* (Fig. 6e and Supplementary Fig. 3d), whereas TRIM56 RING mutants unable to interact with SopA were not modified (Supplementary Fig. 3e). As conjugation of substrates with different types of polyubiquitin chains can have distinct functional outcomes[32], we decided to examine the Ub linkage preference of SopA as well as TRIM56. For this purpose, we performed *in vitro* ubiquitination reactions using Ub mutants harbouring single lysine residues. Although TRIM56 catalytic activity showed a bias towards K11- and K63-linked polyubiquitin (Supplementary Fig. 3f), SopA preferentially modified TRIM56 with K48- and K11-linked Ub chains implicated in proteasomal targeting (Fig. 6f).

**Infection induces proteasomal turnover of TRIM56/TRIM65**. Given the MG132-sensitive nature of SopA-mediated TRIM56 ubiquitination and its preference for the synthesis of mostly degradative K48- and K11-chain types, we monitored the abundance of TRIM56 and TRIM65 proteins after infection of cells with *S.* Typhimurium WT, *sopA*-deficient or *sopA*-complemented

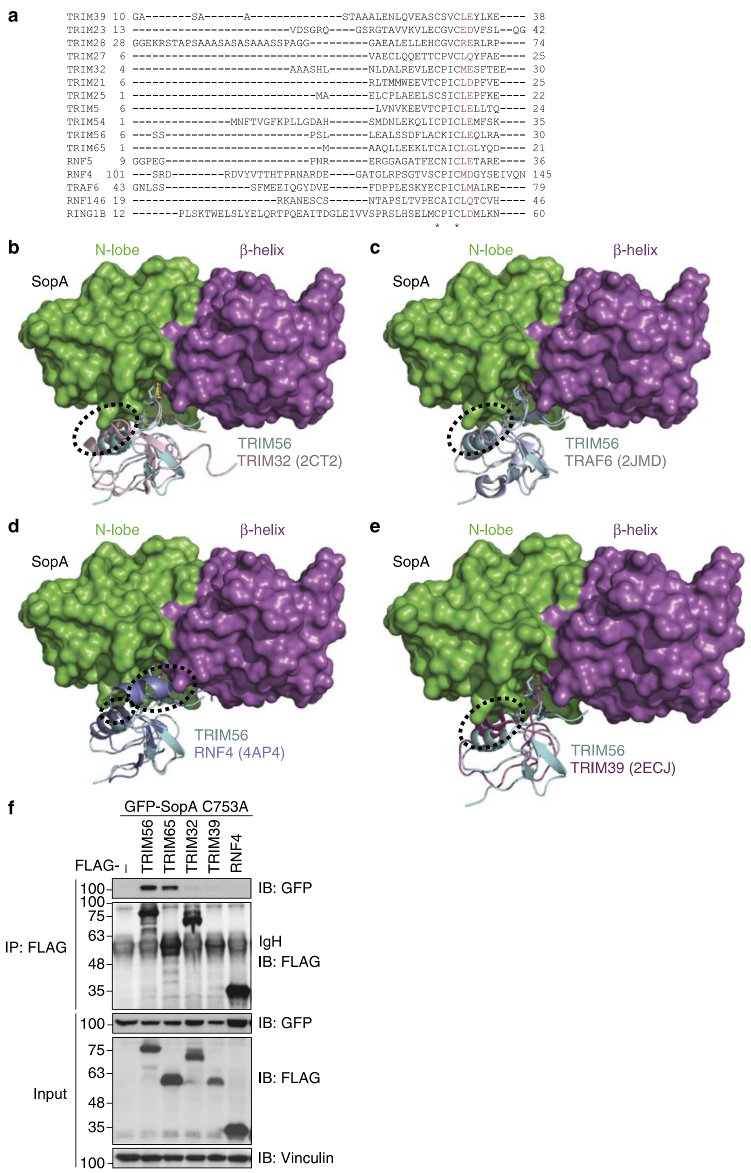


**Figure 4 | Structural features of TRIMs define specificity of SopA towards TRIM56.** (**a**) Multiple sequence alignment of the first $Zn^{2+}$-binding loop region from various TRIMs and the closely related RING domain-containing proteins reveal Glu25 and Leu26 (residues in TRIM56 that are involved in binding to SopA) are fairly conserved (coloured in red). $Zn^{2+}$-coordinating cysteines are indicated using an asterisk. (**b**,**c**,**d**,**e**) TRIM56 RING domain was aligned with various closely related RINGs showing the clashes (circled) of SopA with the central α-helix of various RING domains (**b**, TRIM32; **c**, TRAF6; **d**, RNF4; **e**, TRIM39). PDB codes of the structures used in the alignment are indicated in brackets: (2JMD)[47], (4AP4)[30]. (**f**) SopA does not bind TRIM32, TRIM39 and RNF4. Lysates from cells co-expressing GFP-SopA C753A and indicated FLAG-RING E3 ligase constructs were subjected to anti-FLAG IP, followed by SDS–PAGE and immunoblotting.

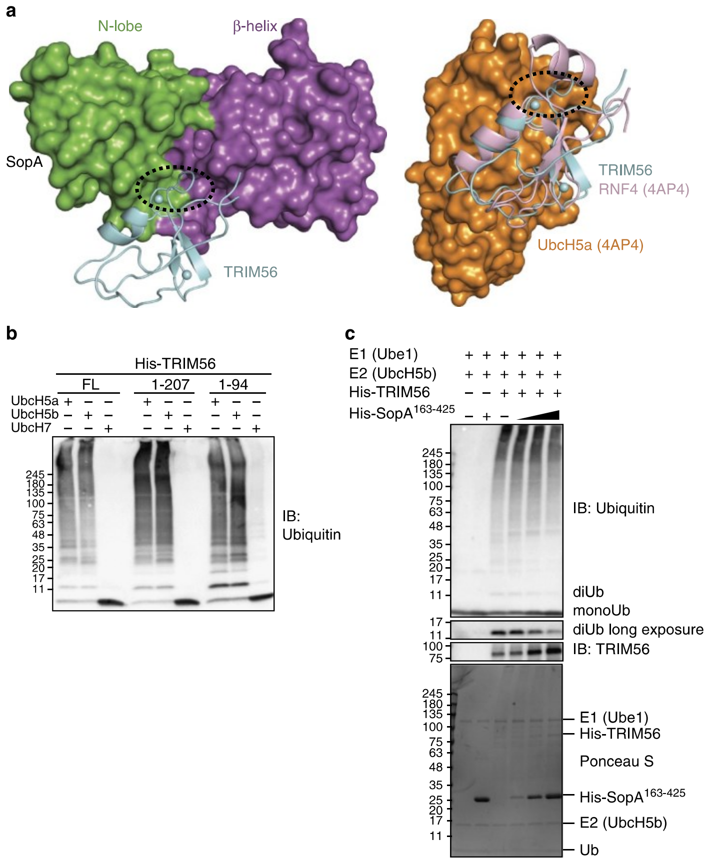


**Figure 5 | SopA inhibits TRIM56-mediated ubiquitin chain formation.** (**a**) SopA occupies the potential E2-binding site on TRIM56. Left, crystal structure of SopA–TRIM56 with SopA shown in surface representation. β-Helix and part of the N-lobe are coloured differently as indicated. Right, TRIM56 RING domain is superimposed with RNF4 RING domain bound to UbcH5a (PDB code: 4AP4)[30]. First $Zn^{2+}$-binding loop of TRIM56 RING domain is circled to highlight overlapping binding interfaces of SopA and E2. (**b**) Ubiquitin ligase activity of various TRIM56 constructs in the presence of UbcH5a, UbcH5b and UbcH7. (**c**) Effect of SopA-binding on the ligase activity of TRIM56 full-length protein. SopA (163–425) was added at 1×, 5× and 10× molar excess of E2. Inhibition of TRIM56 activity was monitored by free ubiquitin chain formation. Apparent increase in TRIM56 full-length levels with increasing SopA is due to a decrease in auto-ubiquitination of TRIM56.

strains. These experiments revealed that protein levels of both TRIMs decreased in a SopA ligase activity-dependent manner (Fig. 7a). To address whether SopA-mediated reduction of TRIM56 and TRIM65 arises due to diminished protein translation or due to destabilization of TRIM56 and TRIM65 proteins, we performed cycloheximide chase experiments. Infection of cycloheximide-treated cells induced robust SopA-driven degradation of TRIM56 and TRIM65 (Fig. 7b). We were able to recapitulate these findings in doxycycline-inducible SopA-expressing cells, in which SopA induction triggered TRIM56 and TRIM65 degradation. Additional treatment of these cells with MG132 restored TRIM protein levels and resulted in the appearance of high molecular weight ubiquitinated species (Fig. 7c). Interestingly, a previous study suggested SopA targeting of TRIM56 and TRIM65 to be non-degradative[15]. Here we provide multiple lines of evidence, which strongly support the notion that SopA-mediated ubiquitination inhibits and triggers the proteasomal degradation of TRIM56 and TRIM65 during *Salmonella* infection (Fig. 8).

## Discussion

By using an unbiased multi-layered proteomics approach in *Salmonella*-infected cells, we recovered two host TRIM RING ligases, TRIM56 and TRIM65, as interactors and substrates of the *Salmonella* HECT-like ligase SopA. Using co-immunoprecipitation of various constructs of SopA and TRIMs, we showed that the N-terminal RING domains of TRIM proteins are both

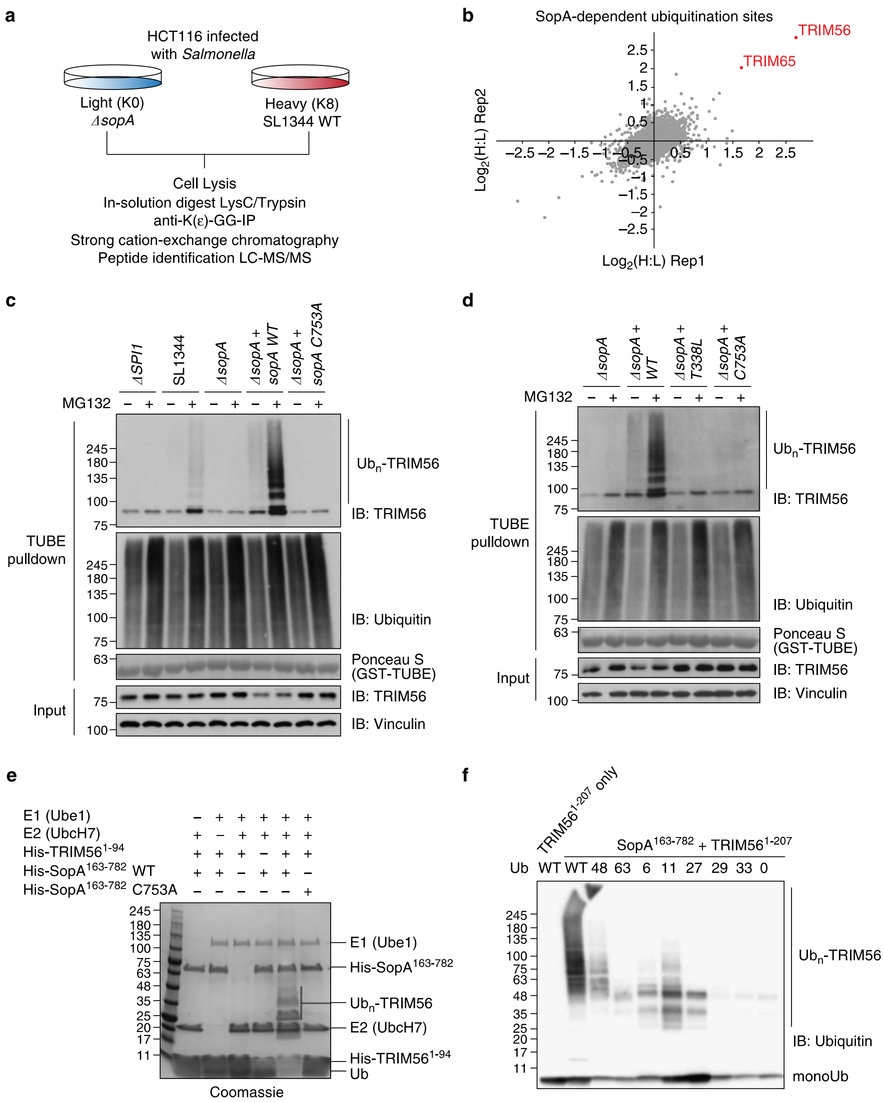


**Figure 6 | TRIM56 and TRIM65 are substrates of degradative SopA ubiquitination.** (**a**) Workflow for SopA-dependent ubiquitinome analysis using SILAC diGly proteomics of *Salmonella* SL1344 WT and *ΔsopA*-infected HCT116 cells 30 min post infection. (**b**) SopA ubiquitinates TRIM56 and TRIM65. Scatter plot of replicate SopA ubiquitinome experiments. (**c**,**d**) SopA-mediated ubiquitination of TRIM56 on infection is MG132 sensitive and depends on SopA catalytic activity (**c**) and on SopA–TRIM56 binding (**d**). Lysates from HeLa cells infected with *Salmonella* SL1344 WT or indicated mutant strains in the absence or presence of 20 μM proteasome inhibitor MG132 were subjected to TUBE pulldown followed by SDS–PAGE and immunoblotting. (**e**) SopA ubiquitinates TRIM56 RING domain *in vitro.* Purified SopA WT and catalytic mutant (C753A) were incubated with E1, UbcH7, ubiquitin, ATP and TRIM56 RING domain. TRIM56 ubiquitination is seen with WT SopA but not in the presence of catalytic-dead SopA. (**f**) Testing SopA ubiquitin chain specificity. WT SopA was incubated with TRIM56 (1–207) and WT ubiquitin or various ubiquitin mutants that contain only a single surface lysine. E1, UbcH7, ubiquitin and ATP were added to all the reactions. TRIM56 alone is not active under these conditions (lane 1).

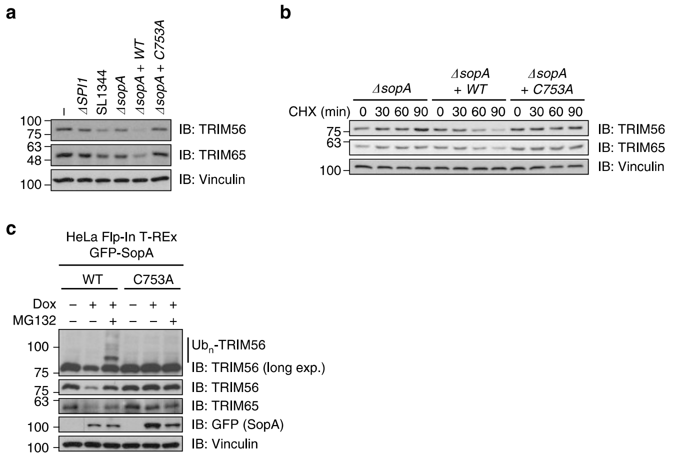


**Figure 7 | *Salmonella* infection induces proteasomal degradation of TRIM56 and TRIM65.** (**a**) TRIM56 and TRIM65 protein levels decrease in SopA activity-dependent manner. Lysates from HCT116 cells infected with *Salmonella* SL1344 WT, ΔSPI1 or indicated *sopA* mutant strains were subjected to SDS-PAGE and immunoblotting. (**b**) SopA-mediated degradation of TRIM56 and TRIM65 on infection. Lysates from HCT116 cells treated with 100 μg ml$^{-1}$ cycloheximide and infected with the indicated *sopA* mutant *Salmonella* strains for indicated time points were subjected to SDS-PAGE and immunoblotting. (**c**) SopA-mediated degradation of TRIM56 and TRIM65 on heterologous expression. Lysates from inducible HeLa Flp-In T-REx GFP-SopA cells left untreated or treated with indicated combinations of 1 μg ml$^{-1}$ doxycycline and 20 μM MG132 were subjected to SDS-PAGE and immunoblotting.

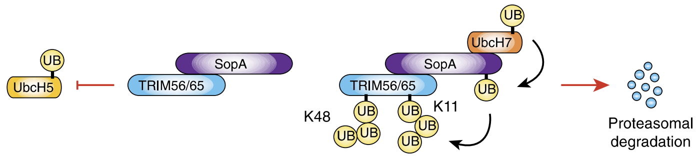


**Figure 8 | Model for dual SopA-mediated targeting of TRIM56 and TRIM65.** Binding of SopA to the RING domains of TRIM56 and TRIM65 impedes TRIM E3 Ub ligase activity by occluding the RING-E2 interaction surface (left panel). The SopA HECT ligase activity deposits degradative ubiquitin chains linked via K48 and K11 on TRIM56 and TRIM65, resulting in their proteasomal degradation during *Salmonella* infection (right panel).

necessary and sufficient for binding to the N terminus of SopA. It is interesting to note that SopA specifically interacts with the RING domains of TRIM56 and TRIM65 amongst a large number of expressed RING domain-containing human proteins[33] (Supplementary Fig. 4a,b). To understand the basis for this remarkable specificity, we determined the crystal structure of SopA (residues 163–425) and TRIM56 (residues 1–94) in complex. The structure revealed the interface of SopA and TRIM56 in atomic detail and also provided an explanation for the specificity of SopA towards TRIM56 and TRIM65. The placement of the central α-helix in various RING domains in combination with the defined sequence features of the first $Zn^{2+}$-binding loop appears to determine the specificity for SopA binding. Comparison of our SopA–TRIM56 complex structure with a previously determined SopA structure carrying the C-lobe[9] uncovers that the catalytic cysteine in the C-lobe is positioned in close proximity to the C terminus of the TRIM56 RING (Supplementary Fig. 4c). Strikingly, we found that the ubiquitination site at Lys87 in the RING domain of TRIM56 is one of the most upregulated modification events in cells infected with SopA-containing *Salmonella* (Fig. 6b and Supplementary Data 3), thus supporting the juxtaposition of these domains in our model (Supplementary Fig. 4c). However, Lys87 is disordered in the crystal structure of SopA–TRIM56, indicating that Ub conjugation to the HECT-active site may be necessary to stabilize the substrate lysine. Structural investigation of TRIM56 in complex with Ub-conjugated SopA will provide more insights into the SopA mechanism of action and HECT catalytic mechanism in general.

Interestingly, a recent study demonstrated the requirement of RING dimerization for the E3 ligase activity of TRIM25 and TRIM32 (ref. 26). We did not observe a dimer of TRIM56 RING in our crystal structure, raising the possibility that SopA binding may interfere with TRIM56 RING dimerization. To address this, we aligned one RING domain of the TRIM32 dimer with TRIM56 RING in the SopA–TRIM56 complex structure (Supplementary Fig. 4d). In this setup, we observed only minor clashes between the TRIM32 dimer and SopA, indicating that SopA interaction may be compatible with TRIM56 dimerization in solution. Accordingly, we predict the potential TRIM56 dimer to bind two molecules of SopA under saturating conditions. The absence of dimerization of the TRIM56 RING in our structure might therefore be a result of the C-terminal fusion of SopA to the RING domain for the purpose of crystallization.

Further analysis of the SopA–TRIM56 structure indicated that SopA binding to the RING domain obstructs the E2-binding site of TRIM56. This led us to hypothesize that SopA interferes with TRIM ligase activity. Titration experiments indeed provided support for SopA interaction-mediated inhibition of TRIM56 activity. It should be noted that in our assays SopA (residues 163–425) was added at 1 ×, 5 × and 10 × molar excess compared with E2 and the effective inhibition was only achieved with the last two conditions. It remains to be seen whether the inhibitory action of SopA on TRIM56 ligase activity is promoted by localized interactions in the context of full size proteins during infection. This interaction mode of SopA is however an effective way for proteins to ubiquitinate E3 ligases in general without getting ubiquitinated themselves. This is achieved, because binding of SopA and E2 to the TRIM56 RING domain is mutually exclusive. Moreover, acute inhibition of TRIM56 and TRIM65 by binding of SopA functions in conjunction with SopA-mediated degradative ubiquitination of TRIM56/65 to downregulate activity and abundance of TRIM proteins *in vivo*. Taken together, our results provide evidence for an inhibitory mechanism underlying targeting of TRIM56/65 via SopA.

It is interesting to note that a recent study proposed a different model of action for SopA-mediated TRIM56/65 ubiquitination[15]. SopA-catalysed ubiquitination of TRIM56 and TRIM65 was suggested to be non-degradative and to promote TRIM56 and TRIM65 activity towards their respective targets RIG-I and MDA5, resulting in an increased transcription of type I interferon. Here we provide multiple lines of evidence in support of SopA-mediating degradation of TRIM56 and TRIM65. We observed that SopA-dependent ubiquitination of TRIM56 is robustly increased after treatment of infected cells with proteasome inhibitor. Moreover, both proteomics and biochemical data revealed that TRIM56 and TRIM65 are degraded in the course of infection and heterologous SopA expression with protein levels being restored by proteasome inhibition. *In vitro* ubiquitination experiments further indicated that SopA preferentially modifies TRIM56 with K48- and K11-linked polyubiquitin, two chain types known to confer proteasomal turnover[32]. Importantly, we did not detect stimulation of TRIM56 or TRIM65-mediated type I interferon expression by SopA, but observed that SopA activity confers decreased interferon-β transcription instead. Although it can not be excluded that the relative expression levels and E3 ligase activities of secreted SopA and host TRIM56 and TRIM65 *in vivo* determine the outcome of this host–pathogen targeting event and account for the discrepancy in presented findings and previous data, our observations in cultured epithelial cells indicate a progressive decay of endogenous TRIM56 and TRIM65 protein levels upon standard *Salmonella* infection conditions.

In general, structural information of proteins has proven instrumental to the identification and design of lead compounds for the inhibition of enzymatic activities and interaction interfaces[34]. Given that *Salmonella* pathogenesis *in vivo* requires the induction of mucosal inflammation to establish a proliferative niche, we envision that the structure of the SopA–TRIM56 complex presented here could aid approaches for the chemical modulation of this host–pathogen interaction.

## Methods

**Cell lines.** HeLa, HCT116 and HEK293T cells were obtained from ATCC and cultured in DMEM medium (Thermo Scientific) with 10% fetal bovine serum (Thermo Scientific), 0.2 mM L-glutamine (Thermo Scientific) and penicillin/streptomycin (Sigma Aldrich) at 37 °C and 5% $CO_2$. HeLa FRT/TO cells for the generation of stable cell lines using the Flp-In T-REx System (Thermo Scientific) were generously provided by S. Taylor (Faculty of Life Sciences, University of Manchester, UK) and maintained in medium containing 15 μg ml$^{-1}$ Blasticidin. Stable HeLa Flp-In T-REx GFP-SopA cells were generated by transfection of HeLa FRT/TO cells with Flp-recombinase expression vector pOG44 and pcDNA5 FRT/TO GFP-SopA constructs in a 9:1 ratio. Thirty-six hours post transfection, cells were trypsinized and seeded in selection medium containing 15 μg ml$^{-1}$ Blasticidin and 250 μg ml$^{-1}$ Hygromycin. Resistant cell colonies were expanded and tested for doxycycline inducibility of the transgene. For SILAC labelling, HeLa and HCT116 cells were cultured in lysine/arginine-free DMEM (Thermo Scientific) with 10% dialysed fetal bovine serum, 2 mM L-glutamine, penicillin/streptomycin and light lysine (73 μg ml$^{-1}$) and light arginine (42 μg ml$^{-1}$). For heavy medium heavy isotope-enriched amino acids K8-lysine (L-lysine, 2HCl U-$^{13}C_6$ U-$^{15}N_2$, Cambridge Isotope Laboratories, Inc.) and R10-arginine (L-arginine U-$^{13}C_6$ U-$^{15}N_4$) were used. Cells were cultured in corresponding SILAC medium for at least seven passages and the incorporation of labelled amino acids to at least 95% was verified.

**Plasmids and bacterial strains.** All generated plasmids and *Salmonella* strains in this study are listed in Supplementary Table 1. *S.* Typhimurium strains are all in the SL1344 background. The *invA* deletion strain (*ΔSPI1*) was a kind gift of Jorge Galan and described previously[35]. The *sopA* deletion strain was generated using the lambda Red recombination method[36]. Herefore, lambda Red recombinase expressing temperature-sensitive plasmid pKD46 (kind gift from Dirk Bumann) was introduced into SL1344 at 30 °C. Electrocompetent SL1344 carrying pKD46 was then electroporated with PCR products harbouring the kanamycin resistance gene from pKD4 flanked by 40 bp overhangs homologous to the 5′- and 3′-ends of the *sopA* gene. After electroporation, bacteria were plated on kanamycin-containing lysogeny broth (LB) plates at 37 °C to prevent pKD46 propagation. Resistant clones were recovered, grown overnight at 37 °C, 180 r.p.m. and genomic DNA was isolated using GenElute Bacterial Genomic DNA Kit (Sigma Aldrich). SopA knockout was verified by PCR using primers flanking the *sopA* gene. For complementation of the *ΔsopA* strain, the *sopA* coding sequence and its promoter-containing upstream region encompassing 638 bp were amplified from SL1344 genomic DNA and cloned into the low-copy vector pWSK29. Complementation was performed with empty vector or with untagged or C-terminally haemagglutinin (HA)-tagged SopA WT and catalytic-dead C753A mutant. Mammalian SopA expression constructs were generated by amplifying *sopA* coding sequence from SL1344 genomic DNA and cloning it into pEGFP-C1 in frame with the N-terminal GFP tag. GFP-SopA WT and mutants were then transferred *en bloc* into pcDNA5 FRT/TO used for stable cell line generation. Plasmids for transient mammalian expression of TRIM ligases were constructed using corresponding complementary DNAs of human TRIM56 (MGC clone: 52308) and TRIM65 (MGC clone: 4385873), and cloning them into pcDNA5 FRT/TO in frame with an N-terminal FLAG tag. The pcDNA5 FRT/TO FLAG-TRIM32 construct was obtained from the University of Dundee (DU25291). TRIM39-FLAG-expressing plasmid was purchased from Hölzel. For recombinant protein production, full-length SopA and TRIM56 were cloned into pGEX-6P1 and pMAL-C2X with an N-terminal glutathione *S*-transferase (GST)- or maltose binding protein (MBP)-tag, respectively.

Following plasmids were made for purification of various proteins for use in *in vitro* ubiquitination assays, binding studies and crystallization experiments. Plasmids of mouse Ube1 and human UbcH7 in pET28a vector with C-terminal HIS tag were used for expression/purification in *E. coli* BL21 DE3 and subsequently used in *in vitro* ubiquitination assays. SopA (163–782), various constructs of TRIM56 (full-length, 1–94, 1–207 and 95–207) were cloned into a modified pET15b vector with an N-terminal HIS tag cleavable by 3C protease. The fusion construct of SopA (163–425) and TRIM56 (1–94) was generated by inserting a linker sequence coding for GSGSENLYFQGGSGS between both proteins using overlapping primers and cloned into a modified pET21a vector with C-terminal CPD-HIS tag. SopA (163–782) and TRIM56 (1–94) were also cloned into the modified pET21a vector.

All point mutations and truncations in SopA and TRIM proteins were introduced by site-directed mutagenesis according to standard protocols.

**X-ray data collection and structure determination.** Purified SopA (163–425)/TRIM56 (1–94) fusion was used at 20 mg ml$^{-1}$ in vapour diffusion crystallization trials. Crystals were grown in 28% w/v Polyacrylate 2100 sodium salt, 0.2 M NaCl and 0.1 M MES pH 6. Optimized crystals were flash frozen in liquid nitrogen. Mother liquor supplemented with 25% glycerol was used as a cryo protectant. Diffraction data were collected at Swiss Light Source (Villigen, Switzerland) and processed by XDS[37]. SopA structure (PDB code: 2QZA)[9] trimmed to contain only the residues 163–425 and TRIM32 structure (PDB code 2CT2) were used as search models in molecular replacement by PHASER[38]. To aid in model building, positions of $Zn^{2+}$ atoms were determined using ANODE[39]. Iterative model building and refinement cycles were carried out until convergence using COOT[40] and PHENIX[41], respectively. A side-by-side stereo view of the electron density covering the SopA–TRIM56 interface is provided in Supplementary Fig. 5.

**Immunoblotting and antibodies.** Proteins were separated by SDS–PAGE and transferred to nitrocellulose membranes (GE Healthcare) using wet blot transfer. Total protein was stained using Ponceau S and membranes were blocked and incubated with antibodies either in 5% milk or 5% BSA in TBS (150 mM NaCl and 20 mM Tris pH 8.0). Washes were performed in TBS-T (TBS and 0.1% Tween20).

After incubation with horesradish peroxidase-conjugated secondary antibodies, membranes were developed using chemiluminescence reagents ImmunoCruz (Santa Cruz) or TMA-6 (Lumigen). The following commercial primary antibodies were used: α-HA (16B12, Covance MMS-101, 1:1,000), α-GFP (B-2, Santa Cruz sc-9996, 1:1,000), α-FLAG (M2, Sigma F3165, 1:5,000), α-Ub (P4D1, Santa Cruz sc-8017, 1:1,000), α-TRIM56 (Abcam ab154862, 1:10,000), α-TRIM65 (Sigma HPA021578, 1:500), α-Tubulin (Sigma T9026, 1:5,000) and α-Vinculin (Sigma hVIN-1, 1:2,000). Uncropped scans of developed membranes are provided in Supplementary Figs 6,7,8 and 9 as part of the Supplementary Information.

***Salmonella* infection.** Cultures of *S.* Typhimurium strains were inoculated from single colonies in LB with 0.3 M NaCl and grown overnight for 16 h at 37 °C with shaking 180 r.p.m. The next day, bacteria were diluted 1:33 and grown at 37 °C and 180 r.p.m. for 3 h until an optical density $OD_{600}$ of 1.8 was reached. Cell lines were grown to 80–90% confluency in DMEM + 10% FCS with penicillin and streptomycin. Before infection, cells were washed and incubated in antibiotics-free medium. Infections were performed for 30 min at 37 °C at a multiplicity of infection of 50 in DMEM + 10% FCS. The infection medium was aspirated and cells were incubated for 1 h in DMEM + 10% FCS containing 100 μg ml$^{-1}$ gentamicin to kill extracellular bacteria. For the remainder of the experiment, cells were kept in full medium with 16 μg ml$^{-1}$ gentamicin.

**Protein immunoprecipitation.** For transient co-expression experiments, $8 \times 10^5$ HEK293T cells were seeded in six-well plates. Transfection was performed 24 h later with 1 μg of corresponding plasmid DNA using GeneJuice (Novagen) according to manufacturer's instructions. Cells were harvested and lysed 24 h after transfection. For stable inducible protein expression, corresponding cells were treated with 1 μg ml$^{-1}$ doxycycline for 8 h. Cells were washed once in ice-cold PBS and subsequently lysed for 10 min on ice in immunoprecipitation (IP) lysis buffer (10 mM Tris-HCl pH 7.5, 100 mM KCl, 2 mM $MgCl_2$, 0.5% NP-40 and 1 × Protease Inhibitor Cocktail EDTA-free (Roche)). Insoluble material was pelleted by centrifugation for 10 min at 15,000 r.p.m., 4 °C and supernatants were applied to lysis buffer-equilibrated antibody-coupled resin. For respective IPs, anti-FLAG (Sigma) and anti-GFP (Chromotek) matrices were used and incubated for 2 h at 4 °C with gentle rotation. Protein-bound beads were washed 5 × with IP lysis buffer and eluted by boiling in 2 × Laemmli buffer. For SILAC-coupled IP, the same amount of heavy and light labelled cells were harvested and proteins were immunoprecipitated separately. SILAC-IPs from differently labelled conditions were pooled during the last wash step and eluted together.

**Recombinant protein expression and purification.** GST- or MBP-fusion coding plasmids were transformed into *E. coli* BL21 (DE3). Overnight cultures were diluted 1:40 in LB medium with 200 μM $ZnSO_4$ and cells were grown to $OD_{600}$ of 0.6 at 37 °C and 140 r.p.m. Cultures were cooled down to 16 °C and protein expression was induced with 0.25 mM isopropyl-β-D-thiogalactoside. After overnight incubation (> 18 h), cells were lysed by sonication in lysis buffer (20 mM Tris-HCl pH 7.5, 150 mM NaCl, 1 mM phenylmethylsulfonyl fluoride and 0.1% β-mercaptoethanol) and incubated in lysis buffer with 0.5% Triton X-100 for 5 min on ice. Lysates were cleared by centrifugation and the supernatants were incubated with glutathione sepharose 4B beads (GE Healthcare) or amylose resin (NEB) at 4 °C with gentle rotation. Fusion protein-bound beads were washed 3 × with lysis buffer containing 0.1% Triton X-100. MBP-fusion proteins were eluted from resin in maltose-containing buffer (25 mM Tris-HCl pH 7.5 and 10 mM maltose).

C-terminal CPD-HIS-tagged fusion of TRIM56 (1–94) and SopA (163–425) was expressed in Rosetta DE3 *E. coli* cells. Cells were lysed in Buffer A containing 50 mM Tris pH 7.5, 10% glycerol and 300 mM NaCl. Cleared lysate was incubated with pre-equilibrated Talon beads for an hour at 4 °C. After discarding the flowthrough, the protein-bound beads were washed thoroughly with Buffer A and incubated with 100 μM of Inositol hexakisphosphate (Sigma) in Buffer A containing 50 mM NaCl, to induce the CPD self-cleavage and the release of TRIM56-SopA fusion from the beads. Protein was loaded onto anion exchange column Q-sepharose (GE Healthcare) and eluted using a linear gradient of salt from 50 mM NaCl to 1 M NaCl in Buffer A. Protein was concentrated and injected into a Superdex 200 10/300 size-exclusion column and eluted in buffer containing 10 mM HEPES pH 7.5, 150 mM NaCl and 1 mM tris(2-carboxyethyl)phosphine (TCEP). Eluted protein was buffer exchanged into 10 mM HEPES pH 7.5, 50 mM NaCl, 1 mM TCEP and concentrated to 20 mg ml$^{-1}$ using Amicon ultrafiltration device and used for crystallization. All SopA and TRIM56 constructs used in *in vitro* biochemical assays and isothermal titration calorimetry were purified as described above, without the ion-exchange chromatography and the final buffer exchange steps.

**Pull-down with recombinant proteins.** GST pull-down experiments were performed in 600 μl pull-down buffer (150 mM NaCl, 50 mM Tris pH 7.5, 5 mM dithiothreitol (DTT), 0.1% NP-40 and 0.5 mg ml$^{-1}$ BSA). GST-fusion proteins coupled to beads (5 mg) were incubated with soluble MBP-TRIM56 (500 μg) overnight at 4 °C with gentle rotation. Beads were washed with PDB, eluted with Laemmli buffer and analysed by SDS–PAGE and immunoblotting.

For Ni pull-down experiment, untagged SopA (163–782) and various constructs of HIS-tagged TRIM56 were expressed in BL21 DE3 *E. coli* cells. Lysates containing HIS-tagged TRIM proteins and untagged SopA were mixed and incubated with Talon beads for 1 h at 4 °C in buffer containing 50 mM Tris pH 7.5, 100 mM NaCl, 5% glycerol and 10 mM imidazole. Beads were subsequently washed and bound proteins were eluted using Laemmli buffer and analysed by SDS–PAGE.

For TUBE pull-down *Salmonella*-infected HeLa cells either left untreated or treated with 20 μM MG132 were harvested 30 min post infection, washed with ice-cold PBS and lysed on ice in IP lysis buffer containing the deubiquitinase inhibitor N-ethylmaleimide (10 mM Tris-HCl pH 7.5, 100 mM KCl, 2 mM $MgCl_2$, 0.5% NP-40, 1 × Protease Inhibitor Cocktail EDTA-free (Roche) and 10 mM N-ethylmaleimide). Cell debris was pelleted by centrifugation for 10 min at 15,000 r.p.m., 4 °C and supernatants were added to GST-tagged tandem UBA (TUBE1)-coupled resin (LifeSensors). Pull-down reactions were incubated for 2 h at 4 °C with gentle rotation, beads were washed five times with PBS–Tween20 (0.1%) and bound material was eluted by boiling in Laemmli buffer.

***In vitro* ubiquitination.** Unless otherwise mentioned, *in vitro* ubiquitination reaction mixture contained 300 nM purified Ube1 (E1), 3 μM E2 (UbcH7 or UbcH5a/b), 1 μM SopA (163–782) WT or C753A mutant and ~8 μM of various TRIM56 constructs. Ub was added to a final concentration of 25 μM and the reaction was initiated by adding 2.5 mM ATP. Ubiquitination buffer contained 50 mM Tris pH 7.5, 50 mM NaCl, 10 mM $MgCl_2$ and 0.5 mM DTT. Reaction was allowed to proceed for 1 h at 37 °C and stopped by the addition of Laemmli buffer. Samples were analysed by SDS–PAGE followed by western blotting. For the *in vitro* ubiquitination experiment shown in Supplementary Fig. 3e, bacterial lysates expressing WT and various mutants of TRIM56 RING domain were used instead of purified TRIM56 constructs.

**MS sample preparation.** For SILAC interactome analysis, IP eluates were subjected to in-gel trypsin digest[42]. To this end, eluates were run on a 10% Tris-glycine SDS–PAGE and lanes were cut into six slices each. Proteins were reduced with 10 mM DTT, alkylated with 55 mM chloroacetamide and digested overnight with 12.5 ng μl$^{-1}$ trypsin. The next day, peptides were sequentially extracted from gel pieces using 30, 80 and 100% acetonitrile-containing solvents. For proteomics and diGly proteomics experiments, SILAC labelled cells were washed twice with ice-cold PBS and lysed under denaturing conditions in 5 ml denaturation buffer (8 M Urea, 1% SDS, 50 mM Tris pH 8, 50 mM NaCl, 1 × Protease Inhibitor Cocktail EDTA-free (Roche) and 50 μM DUB inhibitor PR-619). To fragment DNA, lysates were sonicated 2 × 90 s with 1 s pulses. Protein content was measured using BCA assay (Thermo Scientific) and differentially labelled lysates were mixed in a 1:1 ratio (> 20 mg total protein). Proteins were precipitated using methanol/chloroform and resuspended in 7 ml thiourea-containing denaturation buffer (6 M Urea, 2 M Thiourea and 50 mM Tris-HCl pH 8). Samples were reduced using 5 mM DTT and alkylated with 10 mM chloroacetamide. Proteolytic digest was performed initially with Lys-C (Wako; 1:200 substrate-enzyme ratio) for at least 4 h at room temperature. To reduce urea concentration, digests were diluted 1:5 with 25 mM Tris-HCl pH 8 and incubated for at least 16 h with trypsin (Promega; 1:200 substrate-enzyme ratio) at room temperature. Digests were stopped by addition of trifluoroacetic acid (TFA) to 0.4% and diGly proteomics samples were desalted using tC18-Sep-Paks (Whatman), eluted in 50% acetonitrile and dried by lyophilization.

**Purification of diGly-modified peptides.** After lyophilization, peptides were resuspended in 1.5 ml IAP buffer (50 mM MOPS pH 7.4, 10 mM $Na_2HPO_4$ and 50 mM NaCl). The pH of the peptide solution was adjusted using 1 M Tris pH 10 and insoluble material was removed (9,000 *g*/8 min). Supernatants were incubated with 128 μg IAP buffer equilibrated α-Lys(ε)-GG antibody coupled agarose (Cell Signaling) for 4 h at 4 °C. Beads were washed 3 × with IAP buffer and twice with MilliQ water. Bound diGly peptides were eluted 2 × with 80 μl 0.15% TFA by centrifugation and were further separated into multiple fractions using pH-based strong cation exchange chromatography[43]. Each peptide fraction was desalted using C18 material containing stage tips[44].

**Peptide identification and data analysis.** Each peptide sample was applied onto an EasyLC nano-HPLC-coupled Orbitrap Elite setup (Thermo Scientific). Peptides were injected in 0.5% acetic acid on a 15 cm-long C18-filled fused silica capillary column. Samples were separated at a flow of 200 nl min$^{-1}$ using a 226 min gradient of 5–33% solvent B (80% acetonitrile and 0.5% acetic acid). Peptide MS spectra were acquired in the Orbitrap ranging from *m/z* 300 to 2,000 with a resolution of 120,000. The mass spectrometer was operated in data-dependent acquisition mode. For each cycle, the 20 peptide ions with highest intensity were sequentially isolated and CID MS/MS spectra were acquired in the Iontrap. The target values of the mass analysers were $10^6$ (Orbitrap) and $5 \times 10^3$ (Iontrap). Peptide ions with unassigned charge state and in case of diGly proteomics samples below + 3 were excluded from fragmentation. Raw data were processed with MaxQuant (1.3.0.5)[45,46] and fragment peaks were searched against human and *Salmonella* SL1344 UNIPROT databases. Up to two missed tryptic cleavages were allowed. Carbamidomethylation of cysteine was set as fixed modification. Variable modifications included N-terminal acetylation, methionine oxidation and GlyGly modification. For protein quantification, a minimum of two quantified peptides was required. Both protein and peptide false discovery rate were set to 1%. Perseus was used for data sorting.

**Isothermal titration calorimetry.** Purified SopA (163–782) and TRIM56 (1–94) were buffer exchanged into 10 mM HEPES, 100 mM NaCl and 1 mM TCEP. Using VP-ITC Microcal calorimeter (GE Healthcare), 1.4 ml of 20 μM SopA was titrated with 1 mM of TRIM56 at 25 °C with 5 μl injections with a gap of 5 min between each injection. Heat of dilution was also measured by injecting 1 mM TRIM56 into the buffer and the resulting values were subtracted from the SopA–TRIM56 titration curve. Data were analysed using Origin 7 software provided by Microcal.

**Data availability.** The atomic coordinates of the SopA–TRIM56 structure have been deposited in the Protein Data Bank under accession number 5JW7. All the remaining data can be obtained from the corresponding author upon reasonable request. The following reported PDB files were used: 4AP4, 2JMD, 2QZA and 2CT2.

## References

1. Galan, J. E. & Wolf-Watz, H. Protein delivery into eukaryotic cells by type III secretion machines. *Nature* **444,** 567–573 (2006).
2. Bryant, C. E. *et al.* International Union of Basic and Clinical Pharmacology. XCVI. Pattern recognition receptors in health and disease. *Pharmacol. Rev.* **67,** 462–504 (2015).
3. Gomes, L. C. & Dikic, I. Autophagy in antimicrobial immunity. *Mol. Cell* **54,** 224–233 (2014).
4. Ashida, H., Kim, M. & Sasakawa, C. Exploitation of the host ubiquitin system by human bacterial pathogens. *Nat. Rev. Microbiol.* **12,** 399–413 (2014).
5. Tanner, K., Brzovic, P. & Rohde, J. R. The bacterial pathogen-ubiquitin interface: lessons learned from *Shigella*. *Cell Microbiol.* **17,** 35–44 (2015).
6. Maculins, T., Fiskin, E., Bhogaraju, S. & Dikic, I. Bacteria-host relationship: ubiquitin ligases as weapons of invasion. *Cell Res.* **26,** 499–510 (2016).
7. Huibregtse, J. & Rohde, J. R. Hell's BELs: bacterial E3 ligases that exploit the eukaryotic ubiquitin machinery. *PLoS Pathog.* **10,** e1004255 (2014).
8. Zhang, Y., Higashide, W. M., McCormick, B. A., Chen, J. & Zhou, D. The inflammation-associated *Salmonella* SopA is a HECT-like E3 ubiquitin ligase. *Mol. Microbiol.* **62,** 786–793 (2006).
9. Diao, J., Zhang, Y., Huibregtse, J. M., Zhou, D. & Chen, J. Crystal structure of SopA, a *Salmonella* effector protein mimicking a eukaryotic ubiquitin ligase. *Nat. Struct. Mol. Biol.* **15,** 65–70 (2008).
10. Wood, M. W. *et al.* The secreted effector protein of Salmonella dublin, SopA, is translocated into eukaryotic cells and influences the induction of enteritis. *Cell Microbiol.* **2,** 293–303 (2000).
11. Zhang, S. *et al.* The *Salmonella* enterica serotype typhimurium effector proteins SipA, SopA, SopB, SopD, and SopE2 act in concert to induce diarrhea in calves. *Infect. Immun.* **70,** 3843–3855 (2002).
12. Huang, L. *et al.* Structure of an E6AP-UbcH7 complex: insights into ubiquitination by the E2-E3 enzyme cascade. *Science* **286,** 1321–1326 (1999).
13. Verdecia, M. A. *et al.* Conformational flexibility underlies ubiquitin ligation mediated by the WWP1 HECT domain E3 ligase. *Mol. Cell* **11,** 249–259 (2003).
14. Lin, D. Y., Diao, J. & Chen, J. Crystal structures of two bacterial HECT-like E3 ligases in complex with a human E2 reveal atomic details of pathogen-host interactions. *Proc. Natl Acad. Sci. USA* **109,** 1925–1930 (2012).
15. Kamanova, J., Sun, H., Lara-Tejero, M. & Galan, J. E. The *Salmonella* effector protein sopa modulates innate immune responses by targeting TRIM E3 ligase family members. *PLoS Pathog.* **12,** e1005552 (2016).
16. Versteeg, G. A., Benke, S., Garcia-Sastre, A. & Rajsbaum, R. InTRIMsic immunity: positive and negative regulation of immune signaling by tripartite motif proteins. *Cytokine Growth Factor Rev.* **25,** 563–576 (2014).
17. Davis, M. E. & Gack, M. U. Ubiquitination in the antiviral immune response. *Virology* **479-480,** 52–65 (2015).
18. Tsuchida, T. *et al.* The ubiquitin ligase TRIM56 regulates innate immune responses to intracellular double-stranded DNA. *Immunity* **33,** 765–776 (2010).
19. Versteeg, G. A. *et al.* The E3-ligase TRIM family of proteins regulates signaling pathways triggered by innate immune pattern-recognition receptors. *Immunity* **38,** 384–398 (2013).
20. Meroni, G. & Diez-Roux, G. TRIM/RBCC, a novel class of 'single protein RING finger' E3 ubiquitin ligases. *Bioessays* **27,** 1147–1157 (2005).
21. Goldstone, D. C. *et al.* Structural studies of postentry restriction factors reveal antiparallel dimers that enable avid binding to the HIV-1 capsid lattice. *Proc. Natl Acad. Sci. USA* **111,** 9609–9614 (2014).
22. Li, Y. *et al.* Structural insights into the TRIM family of ubiquitin E3 ligases. *Cell Res.* **24,** 762–765 (2014).
23. Sanchez, J. G. *et al.* The tripartite motif coiled-coil is an elongated antiparallel hairpin dimer. *Proc. Natl Acad. Sci. USA* **111,** 2494–2499 (2014).
24. Weinert, C., Morger, D., Djekic, A., Grutter, M. G. & Mittl, P. R. Crystal structure of TRIM20 C-terminal coiled-coil/B30.2 fragment: implications for the recognition of higher order oligomers. *Sci. Rep.* **5,** 10819 (2015).
25. Streich, Jr F. C., Ronchi, V. P., Connick, J. P. & Haas, A. L. Tripartite motif ligases catalyze polyubiquitin chain formation through a cooperative allosteric mechanism. *J. Biol. Chem.* **288,** 8209–8221 (2013).
26. Koliopoulos, M. G., Esposito, D., Christodoulou, E., Taylor, I. A. & Rittinger, K. Functional role of TRIM E3 ligase oligomerization and regulation of catalytic activity. *EMBO J.* **35,** 1204–1218 (2016).
27. Napolitano, L. M. & Meroni, G. TRIM family: pleiotropy and diversification through homomultimer and heteromultimer formation. *IUBMB Life* **64,** 64–71 (2012).
28. Reddy Chichili, V. P., Kumar, V. & Sivaraman, J. Linkers in the structural biology of protein-protein interactions. *Protein Sci.* **22,** 153–167 (2013).
29. Holm, L., Kaariainen, S., Wilton, C. & Plewczynski, D. Using Dali for structural comparison of proteins. *Curr. Protoc. Bioinformatics*. Chapter 5, Unit 5 5 (2006).
30. Plechanovova, A., Jaffray, E. G., Tatham, M. H., Naismith, J. H. & Hay, R. T. Structure of a RING E3 ligase and ubiquitin-loaded E2 primed for catalysis. *Nature* **489,** 115–120 (2012).
31. Hjerpe, R. *et al.* Efficient protection and isolation of ubiquitylated proteins using tandem ubiquitin-binding entities. *EMBO Rep.* **10,** 1250–1258 (2009).
32. Grabbe, C., Husnjak, K. & Dikic, I. The spatial and temporal organization of ubiquitin networks. *Nat. Rev. Mol. Cell Biol.* **12,** 295–307 (2011).
33. Deshaies, R. J. & Joazeiro, C. A. RING domain E3 ubiquitin ligases. *Annu. Rev. Biochem.* **78,** 399–434 (2009).
34. Simmons, K. J., Chopra, I. & Fishwick, C. W. Structure-based discovery of antibacterial drugs. *Nat. Rev. Microbiol.* **8,** 501–510 (2010).
35. Bruno, V. M. *et al.* *Salmonella* Typhimurium type III secretion effectors stimulate innate immune responses in cultured epithelial cells. *PLoS Pathog.* **5,** e1000538 (2009).
36. Datsenko, K. A. & Wanner, B. L. One-step inactivation of chromosomal genes in *Escherichia coli* K-12 using PCR products. *Proc. Natl Acad. Sci. USA* **97,** 6640–6645 (2000).
37. Kabsch, W. XDS. *Acta Crystallogr. D Biol. Crystallogr.* **66,** 125–132 (2010).
38. Storoni, L. C., McCoy, A. J. & Read, R. J. Likelihood-enhanced fast rotation functions. *Acta Crystallogr. D Biol. Crystallogr.* **60,** 432–438 (2004).
39. Thorn, A. & Sheldrick, G. M. ANODE: anomalous and heavy-atom density calculation. *J. Appl. Crystallogr.* **44,** 1285–1287 (2011).
40. Emsley, P. & Cowtan, K. Coot: model-building tools for molecular graphics. *Acta Crystallogr. D Biol. Crystallogr.* **60,** 2126–2132 (2004).
41. Adams, P. D. *et al.* PHENIX: a comprehensive Python-based system for macromolecular structure solution. *Acta Crystallogr. D Biol. Crystallogr.* **66,** 213–221 (2010).
42. Shevchenko, A., Tomas, H., Havlis, J., Olsen, J. V. & Mann, M. In-gel digestion for mass spectrometric characterization of proteins and proteomes. *Nat. Protoc.* **1,** 2856–2860 (2006).
43. Wagner, S. A. *et al.* A proteome-wide, quantitative survey of *in vivo* ubiquitylation sites reveals widespread regulatory roles. *Mol. Cell Proteomics* **10,** M111 013284 (2011).
44. Rappsilber, J., Ishihama, Y. & Mann, M. Stop and go extraction tips for matrix-assisted laser desorption/ionization, nanoelectrospray, and LC/MS sample pretreatment in proteomics. *Anal. Chem.* **75,** 663–670 (2003).
45. Cox, J. & Mann, M. MaxQuant enables high peptide identification rates, individualized p.p.b.-range mass accuracies and proteome-wide protein quantification. *Nat. Biotechnol.* **26,** 1367–1372 (2008).
46. Cox, J. *et al.* Andromeda: a peptide search engine integrated into the MaxQuant environment. *J. Proteome Res.* **10,** 1794–1805 (2011).
47. Mercier, P. *et al.* Structure, interactions, and dynamics of the RING domain from human TRAF6. *Protein Sci.* **16,** 602–614 (2007).

## Acknowledgements

We thank D. Bumann and B. Claudi for advice, and P. Kraiczy and V. Kempf for help with infections and all members of the Dikic lab for support and constructive discussions. We thank the Swiss Light Source staff for their support during diffraction data collection. This work was supported by grants from the DFG (SFB 1177 on selective autophagy), the SPP 1580 programme 'Intracellular compartments as places of pathogen-host-interactions', the Cluster of Excellence 'Macromolecular Complexes' of the Goethe University Frankfurt (EXC 115), LOEWE grant Ub-Net and LOEWE Centrum for Gene and Cell Therapy Frankfurt. L.H. is supported by an European Molecular Biology Organization (EMBO) long-term postdoctoral fellowship. E.F. is supported by a Boehringer Ingelheim Fonds PhD fellowship.

## Author contributions

E.F. and I.D. conceived the study and initiated the project. I.D. supervised the project. E.F. performed and analysed MS experiments, *Salmonella* infections, immunoprecipitation experiments, biochemical experiments with GST- and MBP-fusion proteins, cycloheximide chase assays, generated stable cell lines and *Salmonella sopA* knockout and complemented strains. S.B. performed and analysed crystallography experiments including protein purification of SopA–TRIM56 fusion and HIS-tagged proteins, crystallization, structure determination, isothermal titration calorimetry, nickel pull-down experiments, modelling and *in vitro* ubiquitination experiments. L.H. and M.H. performed immunoprecipitation and infection experiments. S.K. performed *in vitro* ubiquitination experiments. E.F., S.B. and I.D. wrote and all authors edited the manuscript.

## Additional information

**Supplementary Information** accompanies this paper at http://www.nature.com/naturecommunications

**Competing financial interests:** The authors declare no competing financial interests.

**Reprints and permission** information is available online at http://npg.nature.com/reprintsandpermissions/

**How to cite this article:** Fiskin, E. *et al.* Structural basis for the recognition and degradation of host TRIM proteins by *Salmonella* effector SopA. *Nat. Commun.* **8,** 14004 doi: 10.1038/ncomms14004 (2017).

**Publisher's note**: Springer Nature remains neutral with regard to jurisdictional claims in published maps and institutional affiliations.

Molecular Cell

Article

# Bromodomain Protein BRD4 Is a Transcriptional Repressor of Autophagy and Lysosomal Function

## Graphical Abstract

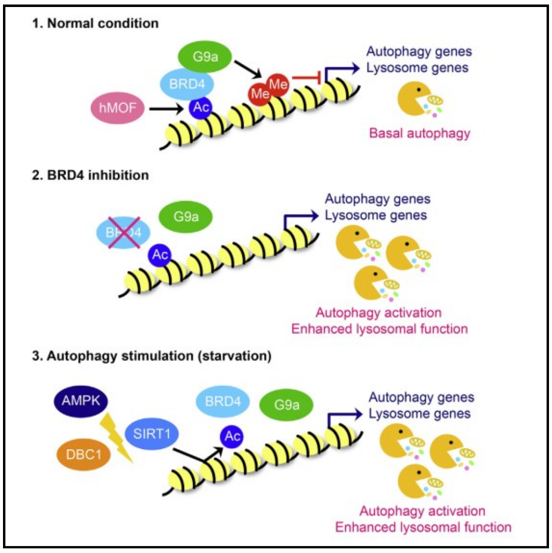


## Highlights

- BRD4 represses a program of autophagy and lysosome genes independently of MiT/TFE
- BRD4 de-repression promotes certain types of autophagy, but not others
- Nutrient deprivation de-represses BRD4 via AMPK signaling to promote cell survival
- Oncoprotein BRD4-NUT is a potent repressor of autophagy and lysosome function

## Authors

Jun-ichi Sakamaki, Simon Wilkinson, Marcel Hahn, ..., Scott W. Lowe, Ivan Dikic, Kevin M. Ryan

## Correspondence

k.ryan@beatson.gla.ac.uk

## In Brief

Sakamaki et al. show that BRD4 represses autophagy and lysosome gene expression. This repression is alleviated during nutrient deprivation through AMPK-SIRT1 signaling, allowing autophagy activation. BRD4 inhibition enhances autophagic flux and lysosomal function and promotes the degradation of protein aggregates.

Sakamaki et al., 2017, Molecular Cell 66, 517–532
May 18, 2017 
http://dx.doi.org/10.1016/j.molcel.2017.04.027

CellPress

Molecular Cell
Article

# Bromodomain Protein BRD4 Is a Transcriptional Repressor of Autophagy and Lysosomal Function

Jun-ichi Sakamaki,[1] Simon Wilkinson,[1,8] Marcel Hahn,[2] Nilgun Tasdemir,[3] Jim O'Prey,[1] William Clark,[1] Ann Hedley,[1] Colin Nixon,[1] Jaclyn S. Long,[1] Maria New,[4] Tim Van Acker,[4] Sharon A. Tooze,[4] Scott W. Lowe,[3,5] Ivan Dikic,[2,6,7] and Kevin M. Ryan[1,9,*]
[1]Cancer Research UK Beatson Institute, Garscube Estate, Switchback Road, Glasgow G61 1BD, UK
[2]Institute of Biochemistry II, Goethe University School of Medicine, 60590 Frankfurt, Germany
[3]Department of Cancer Biology and Genetics, Memorial Sloan Kettering Cancer Center, New York, NY 10065, USA
[4]Molecular Cell Biology of Autophagy, Francis Crick Institute, London NW1 1AT, UK
[5]Howard Hughes Medical Institute, New York, NY 10065, USA
[6]Buchmann Institute for Molecular Life Sciences, Goethe University, 60438 Frankfurt, Germany
[7]Institute of Immunology, School of Medicine, University of Split, 21 000 Split, Croatia
[8]Present address: Edinburgh Cancer Research UK Centre, MRC Institute of Genetics and Molecular Medicine, University of Edinburgh, Edinburgh EH4 2XR, UK
[9]Lead Contact
*Correspondence: k.ryan@beatson.gla.ac.uk
http://dx.doi.org/10.1016/j.molcel.2017.04.027

## SUMMARY

**Autophagy is a membrane-trafficking process that directs degradation of cytoplasmic material in lysosomes. The process promotes cellular fidelity, and while the core machinery of autophagy is known, the mechanisms that promote and sustain autophagy are less well defined. Here we report that the epigenetic reader BRD4 and the methyltransferase G9a repress a TFEB/TFE3/MITF-independent transcriptional program that promotes autophagy and lysosome biogenesis. We show that BRD4 knockdown induces autophagy in vitro and in vivo in response to some, but not all, situations. In the case of starvation, a signaling cascade involving AMPK and histone deacetylase SIRT1 displaces chromatin-bound BRD4, instigating autophagy gene activation and cell survival. Importantly, this program is directed independently and also reciprocally to the growth-promoting properties of BRD4 and is potently repressed by BRD4-NUT, a driver of NUT midline carcinoma. These findings therefore identify a distinct and selective mechanism of autophagy regulation.**

## INTRODUCTION

(Macro) autophagy is a catabolic process that delivers intracellular constituents and organelles to lysosomes for degradation (Mizushima et al., 2008). This process operates at basal levels in virtually all cells and contributes to the preservation of cellular fidelity. Autophagy can also be activated by various stresses and signaling cues to promote the degradation of specific species to bring about selective desired effects within cells (Khaminets et al., 2016; Rabinowitz and White, 2010). The importance of the process is exemplified by the fact that its dysregulation is implicated in various diseases, including neuronal degeneration, immune diseases, and cancer (Mizushima et al., 2008).

Autophagy is initiated by the formation of double-membraned structures called phagophores that originate from endoplasmic reticulum (ER)-derived omegasomes as well as other sources (Ktistakis and Tooze, 2016). As phagophores grow, they form sphere-like structures called autophagosomes that sequester and entrap cytoplasmic components. Autophagosomes can then fuse with other organelles, such as endosomes, but ultimately, fusion occurs with lysosomes forming autolysosomes within which cargo digestion occurs (Ktistakis and Tooze, 2016). Intensive studies have identified the genes involved in the various steps of autophagy, which has led to an established basic machinery for this complicated vesicular trafficking system (Ktistakis and Tooze, 2016; Lamb et al., 2013).

Numerous signaling pathways that regulate autophagy in response to specific stimuli have been identified (Lamb et al., 2013). Recent accumulating evidence has also highlighted the importance of transcriptional regulation of autophagy to sustain prolonged autophagy and/or maintain basal autophagy (Baek and Kim, 2017; Füllgrabe et al., 2014, 2016). The precise control of suppression and de-repression of autophagy is essential as both excess and insufficient autophagy activation has been shown to be deleterious to cells (Mizushima et al., 2008). However, the detailed regulatory mechanisms controlling autophagy in both general and specific contexts remain largely unknown.

Successful completion of autophagy also requires functional lysosomes, acidic organelles that contain various acid hydrolases for the degradation of macromolecules (Shen and Mizushima, 2014). Lysosomal dysfunction impairs the degradation of autophagic cargo, as well as molecules delivered by the

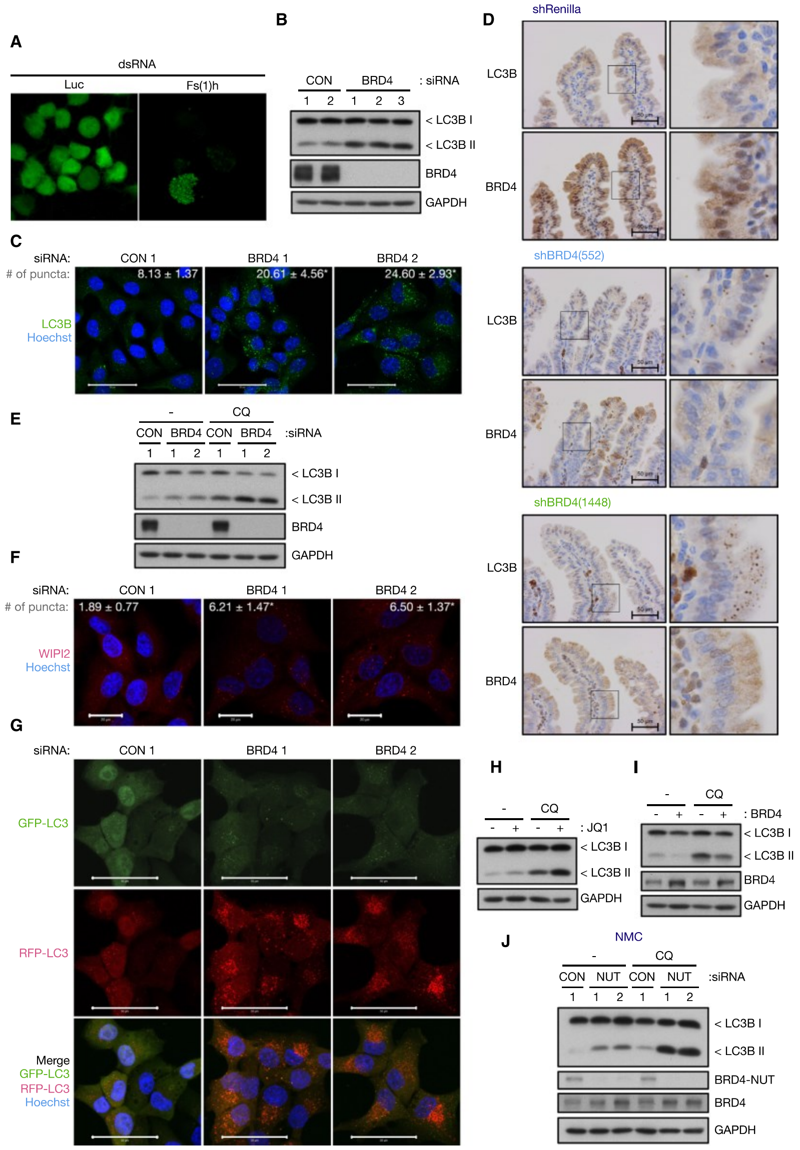


*(legend on next page)*

endocytic pathway, macropinocytosis, and chaperone-mediated autophagy, which in turn causes diseases, including neuronal degeneration and lysosomal storage disorders (Shen and Mizushima, 2014). In the course of an increased autophagic response, lysosome biogenesis and function must also be enhanced to support increased cargo degradation, yet the mechanism underlying this effect is poorly understood. Recent reports have shown that the coordinated activation of the autophagy-lysosome pathway is governed by several transcription factors, including transcription factor EB (TFEB) (Settembre et al., 2011). Following certain autophagic stimuli, TFEB translocates to the nucleus and activates a subset of autophagy and lysosome genes. This enhances autophagosome formation, their fusion with lysosomes, and lysosome biogenesis and function (Settembre et al., 2011).

Bromodomain-containing protein 4 (BRD4) is a member of the bromodomain and extraterminal (BET) family proteins characterized by two N-terminal bromodomains and an extraterminal (ET) domain (Shi and Vakoc, 2014). BRD4 binds to acetylated histones and transcription factors through bromodomains and recruits transcriptional regulators such as positive transcription elongation factor b (P-TEFb) and Mediator complex (Shi and Vakoc, 2014). BRD4 is involved in the activation of genes involved in cell growth and cell cycle progression (Wang and Filippakopoulos, 2015). As a result, intensive studies have been focused on the role of BRD4 in cancer, and BET inhibitors have been proven to have efficacy against various types of tumors (Wang and Filippakopoulos, 2015). Intriguingly, recent accumulating evidence has shown that BRD4 also plays a role in different biological processes, including memory formation, mitochondrial oxidative phosphorylation, and DNA damage response (Barrow et al., 2016; Floyd et al., 2013; Korb et al., 2015). However, our understanding of the biological role of BRD4 requires further investigation.

Here, by using RNAi screening and transcriptome analysis, we have identified BRD4 as a transcriptional repressor of autophagy and lysosomal function. We show that BRD4 suppresses the expression of a subset of autophagy and lysosome genes by binding to the promoter regions under normal growth conditions and that this repression is alleviated in response to certain autophagic stimuli. Inhibition of BRD4 enhances autophagic flux and lysosomal function, which consequently promotes the degradation of pathogenic protein aggregates and confers the resistance to starvation-induced cell death. These observations therefore provide important insights into a regulatory mechanism controlling autophagy and lysosome function.

## RESULTS

### BRD4 Is a Repressor of Autophagy

To understand the regulatory mechanisms of autophagy, we conducted an RNAi screen using *Drosophila* S2R$^{+}$ cells stably expressing GFP-LC3 (Wilkinson et al., 2011). Double-stranded RNA targeting female sterile (1) homeotic (Fs(1)h) was one of the hits that increased GFP-LC3 puncta (Figure 1A). Fs(1)h is a BET protein that functions as a scaffold protein bridging acetylated histones and transcriptional regulators (Kellner et al., 2013). The mammalian BET family consists of four members: ubiquitously expressed BRD2, BRD3, and BRD4 and testis-specific BRDT (Shi and Vakoc, 2014). To validate the screening results, we knocked down the genes encoding BRD2, BRD3, or BRD4 in human pancreatic ductal adenocarcinoma KP-4 cells and determined their effects on autophagy by monitoring the levels of the lipidated form of LC3 (LC3II)—a marker of autophagosome formation/accumulation (Klionsky et al., 2016). This revealed that knockdown of BRD4, but not BRD2 and BRD3, led to an increase in LC3II levels (Figure 1B; Figures S1A and S1B). The generality of this finding was confirmed using a panel of different cell lines (Figure S1C). Consistent with LC3II accumulation, the number of LC3 puncta, an indicator of autophagosome formation (Klionsky et al., 2016), was also increased in BRD4 knockdown cells (Figure 1C). Furthermore, analysis of intestinal sections from mice expressing an inducible BRD4 shRNA revealed that LC3 lipidation and puncta also increased in vivo upon knockdown of BRD4 (Figure 1D; Figure S1D).

There are three BRD4 isoforms reported—isoform A (referred to as long isoform) that possesses a carboxy-terminal domain (CTD) containing the binding site for P-TEFb, isoform B that lacks the CTD and has a unique 77 amino acid extension at its C terminus, and isoform C (referred to as short isoform) that is the shortest isoform lacking the CTD (Figure S1E). Isoform-specific function of BRD4 has been described (Floyd et al., 2013). Knockdown of either the short or the long isoform of BRD4 had no effect on LC3II, while simultaneous depletion of both isoforms promoted LC3 lipidation (Figures S1F and S1G), indicating that BRD4 short and long isoforms are functionally redundant in the regulation of autophagy. Of note, we could not detect BRD4 isoform B in KP-4 cells.

**Figure 1. BRD4 Silencing Enhances Autophagic Flux**

(A) *Drosophila* S2R$^{+}$ cells expressing GFP-LC3 were transfected with double-stranded RNA (dsRNA) targeting control luciferase (Luc) or Fs(1)h.

(B and C) KP-4 cells transfected with control or BRD4 siRNA for 72 hr were subjected to western blot analysis (B) and stained for LC3B (C). The number of LC3 puncta normalized to cell number is shown. CON: n = 94 cells, BRD4 1: n = 97 cells, BRD4 2: n = 74 cells. Scale bars, 50 μm.

(D) Immunohistochemistry of small intestinal sections from transgenic mice harboring inducible renilla luciferase or BRD4 shRNA. Sections were stained for LC3 (upper) and BRD4 (lower). Cytoplasmic signal in BRD4 panels is due to non-specific staining. Scale bars, 50 μm.

(E) KP-4 cells transfected with BRD4 siRNA were treated with 10 μM CQ for 4 hr.

(F) KP-4 cells transfected with BRD4 siRNA were stained for WIPI2. The number of WIPI2 puncta normalized to cell number is shown. CON: n = 119 cells, BRD4 1: n = 107 cells, BRD4 2: n = 109 cells. Scale bars, 20 μm.

(G) KP-4 cells stably expressing RFP-GFP-LC3 were transfected with BRD4 siRNA. Scale bars, 50 μm.

(H) KP-4 cells were treated with 500 nM JQ1 for 9 hr in the presence or absence of CQ (10 μM, 4 hr).

(I) KP-4 cells overexpressing BRD4 were treated with 10 μM CQ for 4 hr.

(J) TY-82 cells transfected with NUT siRNA for 5 days were treated with 10 μM CQ for 8 hr. BRD4-NUT was detected using NUT antibody.

All data are shown as mean ± SD. $^{*}p < 0.01$. See also Figure S1.

As LC3II accumulation is attributed to either increased autophagy induction or impaired autophagosome turnover, the effect of BRD4 knockdown on autophagic flux was examined in the presence of chloroquine (CQ), an inhibitor of lysosomal degradation (Klionsky et al., 2016). As shown in Figures 1E, S1H, and S1I, BRD4 silencing increased LC3II levels in the presence of CQ, suggesting that BRD4 knockdown enhances autophagic flux.

To further examine the stage at which BRD4 affects autophagy, we first examined the recruitment of WD repeat domain phosphoinositide interacting 2 (WIPI2) to phosphatidylinositol 3-phosphate (PI3P)-enriched membrane—an event that precedes LC3 lipidation and which is used as a marker of early stages of autophagy induction (Klionsky et al., 2016). This revealed that an increased number of WIPI2 puncta were also observed in BRD4-silenced cells (Figure 1F). In addition, we performed a detailed examination of LC3 localization by using RFP-GFP-tandem-tagged LC3 (Kimura et al., 2007). Due to the acid lability of GFP in (auto)lysosomes, this revealed an increase in $GFP^{-}/RFP^{+}$ autolysosomes and also, to lesser extent, $GFP^{+}/RFP^{+}$ phagophores/autophagosomes in BRD4 knockdown cells (Figure 1G), suggesting that BRD4 knockdown promotes the formation of autophagosomes and subsequent fusion with lysosomes. Autophagy receptors, such as p62/SQSTM1, are degraded together with cargos and are used as readouts of autophagic degradation (Klionsky et al., 2016). Consistently, BRD4 silencing led to a reduction in exogenously expressed GFP-p62 levels, and this p62 degradation was blocked by CQ (Figure S1J).

BET inhibitors displace BRD proteins from promoter and enhancer regions, thereby interfering with BRD-mediated transcriptional regulation (Shi and Vakoc, 2014). Similar to the results we obtained in BRD4 knockdown cells, BET inhibitor JQ1 (Filippakopoulos et al., 2010) increased LC3II levels (Figure 1H; Figures S1K and S1L). As this did not occur in the absence of BRD4 (Figure S1M), we conclude that autophagy activation by JQ1 is attributed to BRD4 inhibition. In addition, increased LC3 lipidation and puncta formation were observed in mice treated with JQ1 (Figures S1N and S1O). Similarly, we found that the BET degrader ARV-825 (Lu et al., 2015) also activates autophagy (Figure S1P). Conversely, overexpression of BRD4 suppressed autophagic flux (Figure 1I; Figure S1Q). Collectively, these results identify BRD4 as a conserved negative regulator of autophagy.

Chromosomal translocation of *BRD4* to the locus encoding nuclear protein in testis (NUT) causes NUT midline carcinoma (NMC), a rare aggressive subtype of squamous cell carcinoma (French, 2010). The fusion gene product BRD4-NUT possesses two N-terminal bromodomains, an ET domain, and almost the full length of NUT at its C terminus (Figure S1E) (French, 2010). As a result, we were interested to know whether BRD4-NUT also functions as a suppressor of autophagy. By taking advantage of the testis-specific expression of NUT, we used small interfering RNA (siRNA) against NUT to knockdown BRD4-NUT (Schwartz et al., 2011). Inhibition of BRD4-NUT by NUT siRNAs or JQ1 caused accumulation of LC3II in the presence of CQ in the TY-82 NMC cell line (Figure 1J; Figures S1R and S1S), and the effect of JQ1 treatment on LC3 lipidation was comparable to that of BRD4-NUT knockdown (Figure S1T). BRD4-NUT knockdown also increased the formation of $GFP^{-}/RFP^{+}$ LC3 puncta, indicating an accumulation of autolysosomes (Figure S1U). Interestingly, knockdown of BRD4 expressed from the unaffected allele had little effect on autophagy compared to BRD4-NUT knockdown (Figure S1V), suggesting that BRD4-NUT fusion protein is a dominant repressor of autophagy in NMC.

## BRD4 Is a Negative Regulator of Autophagy Gene Expression

As BRD4 is a transcriptional regulator, we hypothesized that BRD4 regulates autophagy at the transcriptional level. RNA sequencing (RNA-seq) analysis followed by reverse transcriptase quantitative PCR (RT-qPCR) validation revealed that a significant number of autophagy genes were upregulated upon knockdown of BRD4 (Figures 2A and 2B; Figures S2A–S2D). These include genes that encode proteins involved in autophagosome formation (BECN1, VMP1, PIK3C3, WIPI1, ATG2A, ATG9B, and MAP1LC3B) (Lamb et al., 2013), autophagy cargo recruitment (SQSTM1 and OPTN), autophagosome-lysosome fusion (PLEKHM1, TECPR1, and HOPS complex components) (McEwan et al., 2015a), and maintenance of functional ER exit sites and autophagosome formation (MAP1LC3C, TECPR2, and SEC24D) (Stadel et al., 2015). BET inhibitors also led to upregulation of autophagy genes (Figure 2C). Of note, de-repression of autophagy genes was observed almost immediately after JQ1 addition (Figure 2D), implying that these autophagy genes are directly regulated by BRD4. In addition, we found that overexpression of BRD4 repressed autophagy gene expression (Figure 2E; Figure S2E). As it is well established that BRD4 can form a complex with P-TEFb and facilitate productive elongation at promoter-proximal regions (Shi and Vakoc, 2014), we considered that the effect on autophagy may also be through this mechanism. We found, however, that knockdown of cyclin-dependent kinase 9 (CDK9), a subunit of P-TEFb, had no effect on LC3II levels (Figures S2F and S2G). This rules out the involvement of P-TEFb in this response and indicates that BRD4 modulates autophagy through a distinct pathway.

## BRD4 Regulates Lysosome Gene Expression and Lysosomal Function

As significant changes in lysosome gene expression occur upon BRD4 knockdown (Figure 2A), this prompted us to examine whether these alterations enhance lysosomal function and support increased autophagic flux. First, we validated the RNA-seq results by conducting RT-qPCR analyses, which showed that BRD4 knockdown significantly upregulated a number of lysosome genes involved in proteolysis, glycan degradation, and lysosome biogenesis (Figure 3A). Consistent with this, we observed an increase in lysosomal protein levels, including lysosomal-associated membrane protein 1 (LAMP1), LAMP2, acid sphingomyelinase (ASM), $\alpha$-glucosidase (GAA), and heavy chain of mature cathepsin B (CTSB HC) and cathepsin D (CTSD HC) (Figure 3B; Figure S3A). Staining of lysosomal compartments with anti-LAMP1 antibody and LysoTracker red also revealed an expanded lysosomal area in BRD4 knockdown cells (Figures 3C and 3D, upper panels). To assess the activity of lysosomal enzymes, we employed the use of Magic Red CTSB, a CTSB substrate that produces a cresyl violet fluorophore upon proteolytic

A

| GO term | GO ID | P value | Gene # |
|---|---|---|---|
| Lysosome | GO:0005764 | 3.00E-012 | 53 |
| Lysosomal lumen | GO:0043202 | 3.34E-012 | 22 |
| Endosome | GO:0005768 | 4.77E-005 | 53 |
| Autophagy | GO:0006914 | 2.65E-004 | 31 |
| Regulation of autophagy | GO:0010506 | 2.65E-002 | 22 |

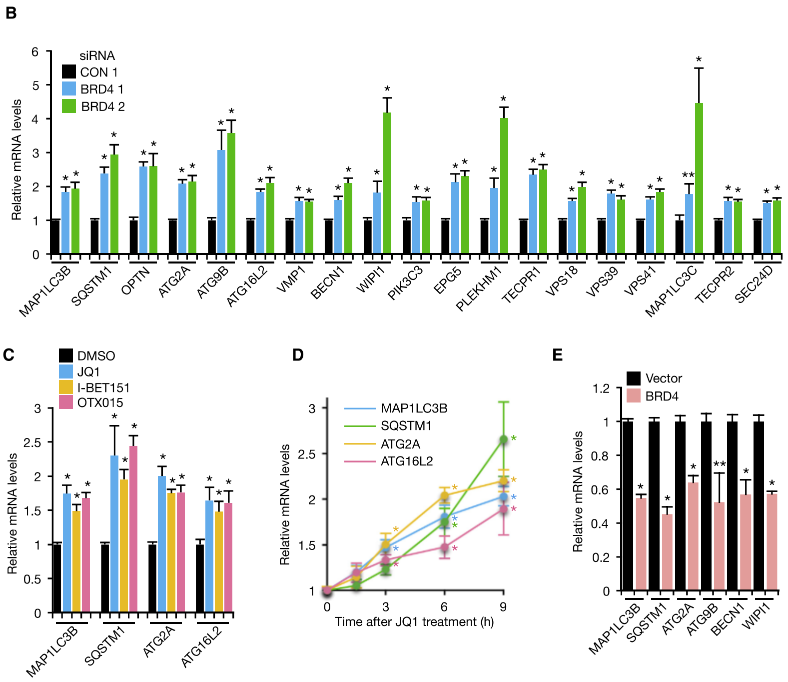


**Figure 2. BRD4 Is a Negative Regulator of Autophagy Gene Expression**

(A and B) KP-4 cells transfected with control or BRD4 siRNA were subjected to RNA-seq and gene ontology analyses (A) and RT-qPCR analysis (B).

(C) RT-qPCR analysis of KP-4 cells treated with DMSO, 500 nM JQ1, 500 nM I-BET151, or 500 nM OTX015 for 9 hr.

(D) RT-qPCR analysis of KP-4 cells treated with 500 nM JQ1 for the indicated time.

(E) RT-qPCR analysis of KP-4 cells overexpressing BRD4.

All data are shown as mean ± SD. In (A)–(D), n = 3 independent experiments; in (E), data are representative of two independent experiments performed in triplicate. *$p < 0.01$, **$p < 0.05$. See also Figure S2.

cleavage. As shown in Figure 3D's lower panels, a significant increase in CTSB substrate cleavage was seen in BRD4 knockdown cells. In addition, we also observed increased enzymatic activity of β-hexosaminidase, a lysosomal enzyme that catalyzes the hydrolysis of ganglioside monosialic 2, in BRD4 knockdown cells (Figure 3E). These results indicate that not only autophagic flux, but also lysosomal biogenesis and function are enhanced by BRD4 knockdown. Furthermore, we also observed upregulation of autophagy and lysosomal gene expression upon BRD4-NUT inhibition by NUT siRNA and JQ1 and an increase in lysosomal protein levels and LysoTracker+ acidic compartments in BRD4-NUT knockdown NMC cells (Figures 3F and 3G; Figures S3B and S3C), suggesting that BRD4-NUT also suppresses the autophagy-lysosome pathway in NMC.

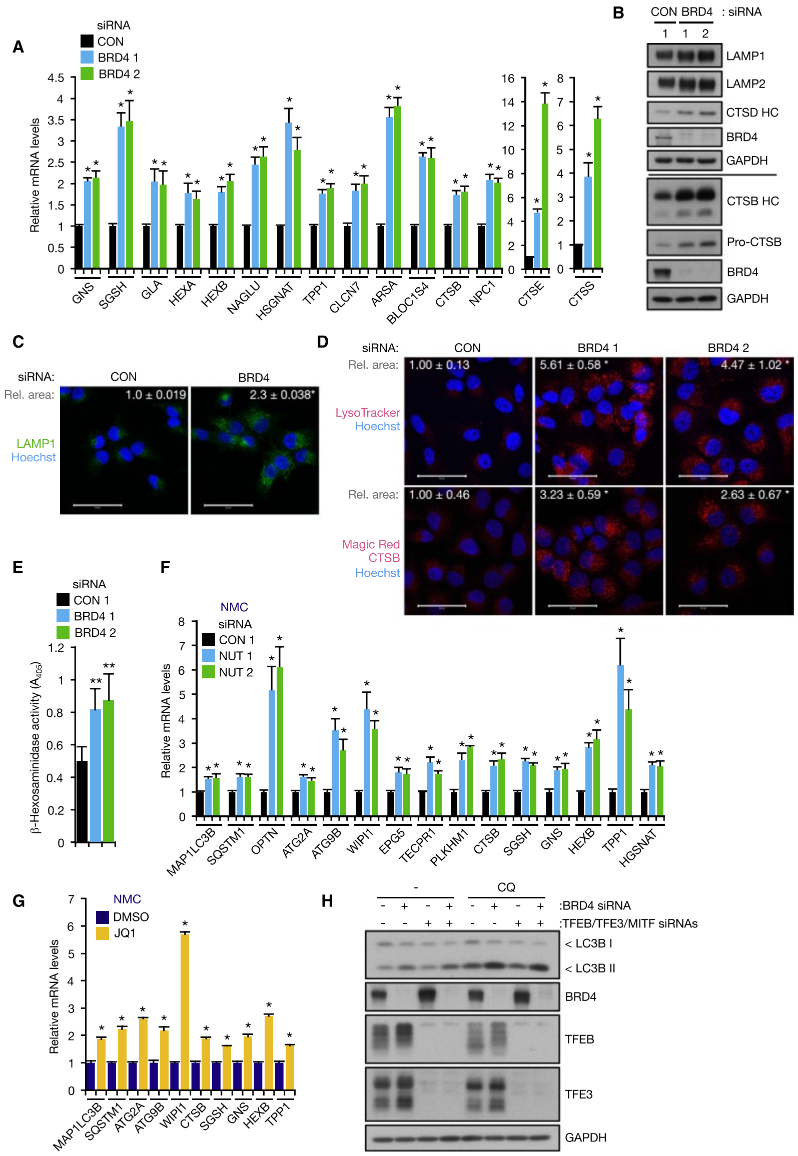


*(legend on next page)*

Activation of the autophagy-lysosome pathway in BRD4 knockdown cells is reminiscent of the phenotype observed by activation of TFEB (Settembre et al., 2011). We therefore tested the possibility that BRD4 knockdown stimulates autophagy through activation of TFEB and its related members TFE3 and MITF. However, BRD4 knockdown cells were capable of activating autophagy in the absence of TFEB (Figures S3D–S3F). Furthermore, BRD4 knockdown still activated autophagy and lysosome gene transcription and enhanced autophagic flux in cells where all MiT/TFE members (TFEB, TFE3, and MITF) were simultaneously silenced (Figure 3H; Figures S3G–S3J), indicating that BRD4 regulates autophagy independently of MiT/TFE transcription factors.

## BRD4 Is Recruited to Autophagy Gene Promoters and Its Dissociation Leads to Transcriptional Activation of Autophagy Genes

We next examined the molecular mechanism by which BRD4 represses autophagy and lysosome gene expression. Given that BET inhibitor dissociates BRD4 from acetylated histones and rapidly upregulates autophagy genes (Figure 2D), we hypothesized that BRD4 binds to acetylated histones at autophagy and lysosome gene promoter regions. Indeed, BRD4 was found at autophagy and lysosome gene promoter regions, and its enrichment was reduced after JQ1 treatment (Figures S4A and S4B). BRD4 occupation at autophagy and lysosome gene promoters was also significantly decreased during starvation, and this BRD4 dissociation was correlated with upregulation of gene expression (Figures 4A and 4B).

Interestingly, histone H4 lysine 16 (H4K16) acetylation that is recognized by BRD4 (Zippo et al., 2009) is downregulated upon autophagic stimulation (Füllgrabe et al., 2013). H4K16 acetylation and its acetyltransferase human males absent on the first (hMOF) have been described as both positive and negative regulators of autophagy (Füllgrabe et al., 2013; Hale et al., 2016). Therefore, we tested whether BRD4 recruitment is regulated by hMOF. CRISPR/CRISPR-associated protein 9 (Cas9)-mediated editing of *hMOF* efficiently reduced hMOF protein levels and H4K16Ac status at autophagy gene promoters (Figures S4C and S4D). Depletion of hMOF also caused BRD4 dissociation from autophagy gene promoters, upregulation of autophagy gene expression, and increased LC3 lipidation (Figure 4C; Figures S4E and S4F). Consistent with the previous study (Füllgrabe et al., 2013), H4K16Ac declined upon starvation (Figure 4D), implying that BRD4 dissociation is attributed to H4K16 deacetylation in response to starvation. However, analysis of hMOF protein levels revealed that they did not change during starvation (Figure S4G). As a result, we hypothesized instead that the decrease in H4K16 acetylation and subsequent BRD4 dissociation during starvation may be driven by the deacetylase Sirtuin 1 (SIRT1) (Vaquero et al., 2007). In line with this hypothesis, H4K16 deacetylation and BRD4 dissociation by starvation were not seen in cells infected with Cas9/single-guide RNA (sgRNA) targeting SIRT1 (Figure 4E; Figure S4H). In addition, SIRT1 depletion suppressed starvation-induced autophagy gene expression and LC3 lipidation (Figure 4F; Figure S4I), underscoring the importance of this enzyme in this response.

It is known that SIRT1 is activated by nutrient deprivation via its dissociation from the inhibitory molecule Deleted in Breast Cancer protein 1 (DBC1) and an increase in nicotinamide adenine dinucleotide ($NAD^+$) levels in a manner dependent on AMP-activated protein kinase (AMPK) (Cantó et al., 2009; Chang et al., 2015). As expected, AMPK phosphorylation at Thr172, which is required for its activation, increased during nutrient starvation (Figure S4J). Consistent with these observations, we found that BRD4 forms a complex with SIRT1 and DBC1 and that starvation disrupts the SIRT1-DBC1 interaction (Figures S4K and S4L). The dissociation of this interaction was not observed in cells treated with AMPK inhibitor Compound C and infected with Cas9/sgRNAs targeting AMPK$\alpha$ catalytic subunits (Figure 4G; Figure S4M). Moreover, disruption of *AMPK$\alpha$* genes prevented BRD4 dissociation from autophagy gene promoters in response to starvation (Figure S4N). As a consequence, AMPK inhibition blocked autophagy gene expression and autophagic flux induced by starvation (Figure 4H; Figures S4O and S4P). Collectively, these results detail a signaling cascade from nutrient deprivation to de-repression of autophagy gene transcription, which involves the disruption of SIRT1-DBC1 interaction by AMPK and SIRT1-mediated BRD4 dissociation from autophagy gene promoters.

## BRD4 Represses Autophagy Gene Expression through Binding to G9a

In contrast to its well-established role as a positive transcriptional regulator of genes involved in cell growth (Shi and Vakoc, 2014), BRD4 represses expression of a subset of autophagy genes. We therefore investigated the molecular mechanism by which BRD4 suppresses autophagy gene expression. From previous interactome analyses of BRD4 (Dawson et al., 2011), we searched for BRD4 interacting protein(s) that are known to be involved in gene repression. Different from the majority of interacting proteins, histone lysine methyltransferase G9a has been shown to both promote and repress transcription by catalyzing mono- and di-methylation of histone H3 at lysine 9 (H3K9),

**Figure 3. BRD4 Knockdown Enhances Lysosomal Function**

(A) RT-qPCR analysis of KP-4 cells transfected with control or BRD4 siRNA.

(B–D) KP-4 cells transfected with BRD4 siRNA were subjected to western blot analysis with antibodies against lysosomal proteins (B) and stained with LAMP1 antibody (C), LysoTracker Red (100 nM, 2 hr) (D, upper panels), and Magic Red CTSB (1 hr) (D, lower panels). Area of LAMP1$^+$, LysoTracker$^+$, and Magic Red CTSB$^+$ area normalized to cell number is shown (C, CON: n = 115 cells, BRD4: n = 130 cells; D upper, CON: n = 66 cells, BRD4 1: n = 52 cells, BRD4 2: n = 50 cells; D lower, CON: n = 164 cells, BRD4 1: n = 109 cells, BRD4 2: n = 53 cells). Scale bars, 50 $\mu$m.

(E) Hexosaminidase activity was measured using lysates from control and BRD4 knockdown KP-4 cells.

(F and G) RT-qPCR analysis of TY-82 cells transfected with NUT siRNA for 72 hr (F) or treated with 500 nM JQ1 for 9 hr (G).

(H) KP-4 cells were transfected with BRD4 and/or MiT/TFE (TFEB, TFE3, MITF) siRNAs and treated with 10 $\mu$M CQ for 4 hr.

All data are shown as mean ± SD. In (A) and (F), n = 3 independent experiments. In (E), n = 4 independent experiments. In (G), data are representative of two independent experiments performed in triplicate. $^*p < 0.01$, $^{**}p < 0.05$. See also Figure S3.

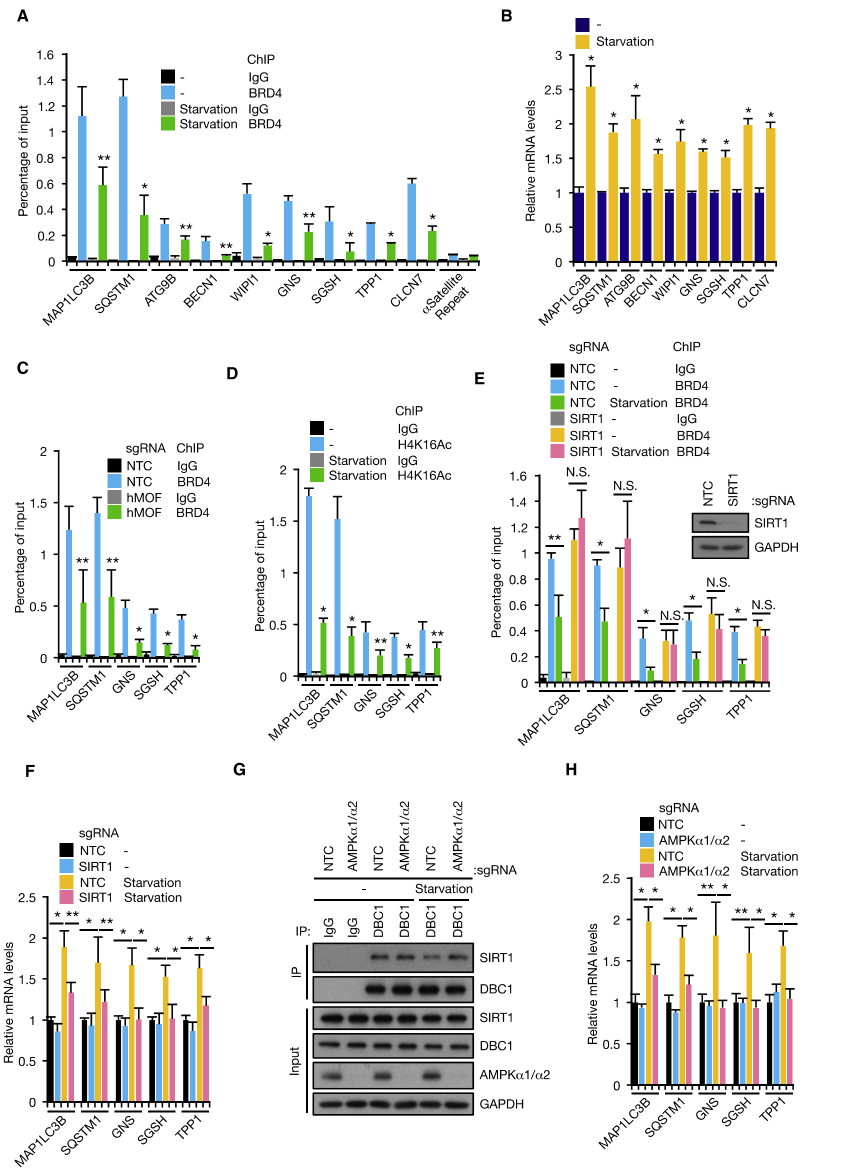

(legend on next page)

respectively (Shinkai and Tachibana, 2011). We first confirmed the interaction between BRD4 and G9a by reciprocal co-immunoprecipitation (Figure 5A). G9a interacted with the long and short isoforms of BRD4 (Figure S5A), which is consistent with our observations that both isoforms contribute to autophagy repression (Figure S1F). Importantly, we observed that the interaction between BRD4 and G9a was disrupted by starvation (Figure 5B). In addition, G9a recruitment to autophagy gene promoters was abolished by JQ1 treatment and BRD4 knockdown (Figures 5C and 5D; Figures S5B and S5C). Consequently, H3K9diMe status was also reduced in these settings (Figures 5E and 5F). Consistent with a functional role in the regulation of autophagy, G9a silencing upregulated autophagy gene expression and enhanced autophagic flux (Figures 5G and 5H; Figures S5D and S5E). Furthermore, simultaneous knockdown of BRD4 and G9a did not cause further accumulation of LC3II and autophagy gene transcripts (Figures 5G and 5H; Figure S5E), and G9a silencing largely abolished autophagy suppression by BRD4 overexpression (Figure 5I; Figure S5F), suggesting that BRD4 and G9a act on the same pathway. In addition, we found that autophagy regulation by H4K16 acetylation and G9a is also conserved in NMC. Depletion of hMOF decreased H4K16 acetylation and increased LC3II levels in TY-82 cells (Figures S5G–S5I). Starvation led to a SIRT1-dependent H4K16 deacetylation at autophagy gene promoters (Figure S5J). BRD4-NUT interacts with G9a, and G9a silencing promoted LC3 lipidation (Figures S5K and S6L), implying that, like BRD4, BRD4-NUT suppresses autophagy through G9a.

## BRD4 Knockdown Modulates Specific Types of Autophagy

Bulk degradation of cytoplasmic components by autophagy, termed bulk autophagy, is thought to feed energy sources during nutrient shortage, whereas degradation of specific substrates, such as protein aggregates, damaged mitochondria and pathogens, called selective autophagy, serves as an intracellular quality control mechanism (Khaminets et al., 2016; Rabinowitz and White, 2010). We were therefore interested in understanding the contribution of BRD4 to the control of stimulus-dependent and selective autophagy.

In the first instance, we examined starvation- and rapamycin-induced autophagy and found that they were augmented by BRD4 silencing (Figures 6A and 6B; Figures S6A and S6B). Reduction of both LC3I and II after 2 hr of starvation in BRD4 knockdown cells suggests enhanced LC3I conversion to LC3II and subsequent degradation (Figure 6A; Figure S6A). Conversely, BRD4 overexpression suppressed LC3I conversion to LC3II induced by starvation and rapamycin (Figure S6C). In addition, BRD4 knockdown further activated autophagy induced by glucose starvation, hypoxia, trehalose, and oncogenic Ras mutant (Figures 6C–6F; Figures S6D–S6G). Similarly, TFEB and TFE3-mediated autophagy activation was also augmented by BRD4 and G9a silencing (Figures S6H and S6I). We next determined whether BRD4 knockdown would promote the autophagic degradation of protein aggregates (aggrephagy). To test this, we analyzed aggregates caused by mutant Huntingtin (HTT) and found that BRD4 silencing promoted the degradation of poly-glutamine (Q)-expanded HTT (HTT 94Q) (Figure 6G). Conversely, BRD4 overexpression exacerbated the accumulation of HTT 94Q in the insoluble fraction (Figure S6J). Similar to the previous reports (Williams et al., 2008), induction of polyQ-expanded HTT caused a reduction in cell number, and BRD4 knockdown ameliorated this effect (Figure S6K).

In contrast, modulation of BRD4 did not promote or prevent the clearance of *Salmonella enterica* serovar Typhimurium by xenophagy (Figure 6H; Figure S6L) or mitochondria by mitophagy (Figure 6I; Figures S6M and S6N). In fact, we actually observed an accumulation of mitochondrial proteins in BRD4 knockdown cells, which may be due to transcriptional upregulation of mitochondrial genes as recently described (Barrow et al., 2016). A similar effect was also observed with p62/SQSTM1 mRNA and protein levels upon BRD4 knockdown (Figure 2B; Figure S6O), thereby complicating its utility as a marker of autophagic activity modulated by BRD4. In conclusion, our collective results show that BRD4 knockdown affects some, but not all, types of autophagy, indicating that it is a regulator of this response in specific contexts.

## BRD4 Knockdown Sustains mTOR Activity during Starvation and Confers Resistance to Starvation-Induced Cell Death

Autophagic degradation of intracellular proteins produces amino acids, leading to activation of the amino acid sensor mechanistic target of rapamycin complex1 (mTORC1), and these nutrient sources can be used to maintain cell survival during periods of starvation (Perera et al., 2015; Rabinowitz and White, 2010). We observed that BRD4 knockdown sustained the phosphorylation status of S6K, a substrate of mTORC1 and established readout of mTORC1 activity (Perera et al., 2015), during amino acid starvation (Figure 7A). This sustained S6K phosphorylation was abolished by CQ and CRISPR/Cas9-mediated ATG5 gene disruption (Figures 7B and 7C), suggesting that BRD4 knockdown activates mTORC1 through the autophagy-lysosome pathway during amino acid shortage. Therefore, we next examined whether autophagy activation by BRD4 knockdown affects cell growth and cell survival during nutrient deprivation. As reported previously (Shi and Vakoc, 2014; Zuber et al.,

**Figure 4. Starvation Leads to BRD4 Dissociation from Autophagy Gene Promoters**

(A and B) KP-4 cells were starved for 4 hr followed by chromatin immunoprecipitation (ChIP) assay with BRD4 antibody (A) and RT-qPCR analysis (B).

(C) KP-4 cells infected with Cas9/hMOF sgRNA were subjected to ChIP assay with BRD4 antibody.

(D) KP-4 cells were starved for 4 hr followed by ChIP assay with H4K16Ac antibody.

(E and F) KP-4 cells infected with Cas9/SIRT1 sgRNA were starved for 4 hr followed by ChIP assay with BRD4 antibody (E) and RT-qPCR analysis (F). Western blot shows efficient SIRT1 depletion in Cas9/SIRT1 sgRNA-infected cells.

(G and H) KP-4 cells infected with Cas9/AMPK$\alpha$1 and $\alpha$2 sgRNAs were starved for 4 hr followed by immunoprecipitation with DBC1 antibody (G) and RT-qPCR analysis (H).

All data are shown as mean ± SD. In (A)–(F) and (H), n = 3 independent experiments. *p < 0.01, **p < 0.05, N.S., no significance. See also Figure S4.

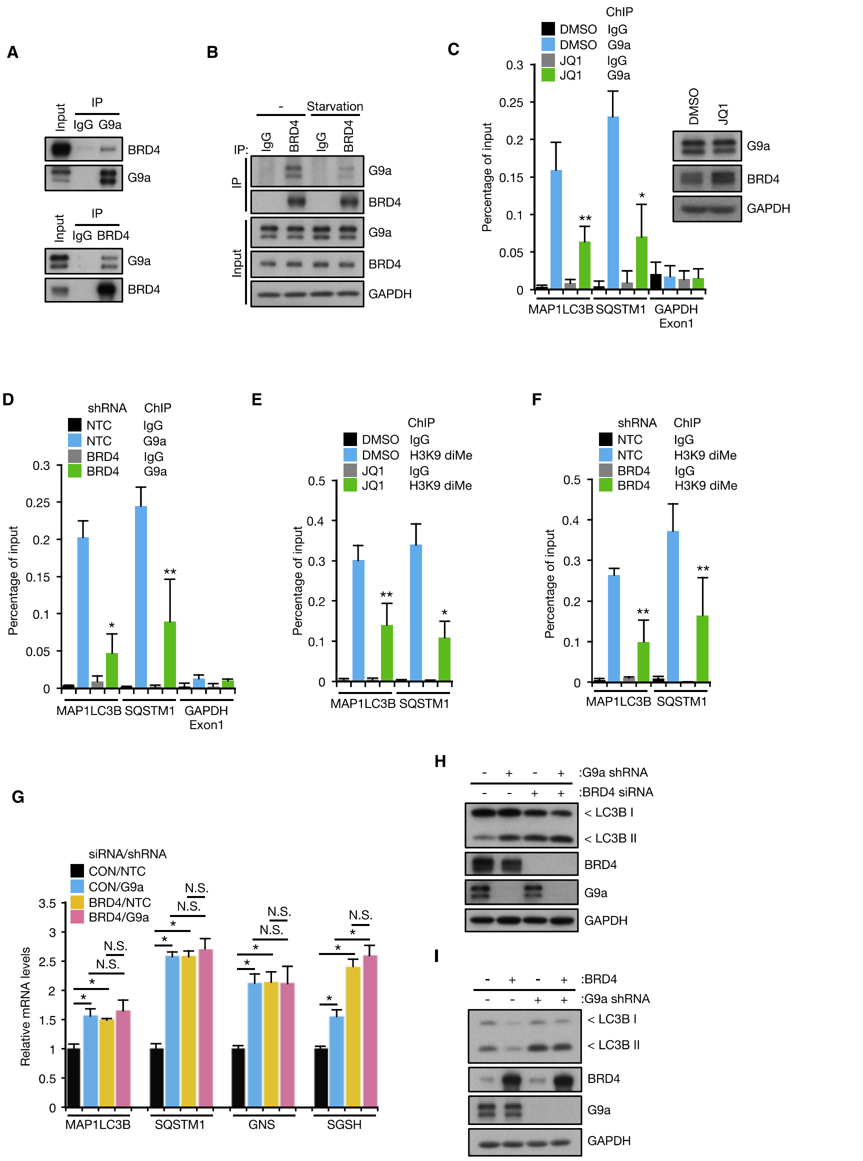


(legend on next page)

2011), BRD4 knockdown caused downregulation of c-Myc, altered cell cycle gene expression, and decreased cell proliferation due to cell cycle retardation under nutrient-replete conditions (Figures S7A–S7D). We found, however, that this growth retardation was caused independently of autophagic activity (Figures S7E and S7F). In contrast to these effects on cell growth, we found that starvation-induced cell death was significantly suppressed in BRD4 knockdown cells, and this protective effect was abolished by ATG5 gene disruption and CQ treatment (Figures 7D–7G; Figure S7G). These data therefore suggest that the modulation of autophagy by BRD4 inhibition maintains cell survival under starvation conditions by providing nutrient source.

## DISCUSSION

In this study, we show that a series of autophagic processes, including autophagosome formation, fusion of autophagosomes with lysosomes, and lysosome biogenesis and function, is transcriptionally repressed by BRD4. BRD4 knockdown upregulates a subset of autophagy and lysosome genes, which in turn enhances autophagic flux and lysosome biogenesis and activity. Interestingly, the effect of this transcriptional program only affects certain forms of autophagy. We found that knockdown of BRD4 promoted autophagy induced by stimuli, such as nutrient deprivation, rapamycin, and protein aggregates, but this did not affect the autophagic removal of mitochondria or bacteria. This indicates that the program is selectively engaged, adding another layer of complexity to the control of this ubiquitous and yet multifaceted process.

As different types of selective autophagy utilize their designated receptors to recruit the cargos, we examined whether the aggrephagy receptor(s) are specifically upregulated by BRD4 and found that the expression of p62 and Optineurin increased upon BRD4 knockdown (Figure 2B; Figure S7H). However, these receptors capture ubiquitinated mitochondria and pathogens, as well as protein aggregates (Khaminets et al., 2016); therefore, these alterations do not provide a mechanistic explanation for the autophagy specificity conferred by BRD4 knockdown. Since mechanisms of selective autophagy are not fully elucidated, the future identification of selective autophagy-specific regulators will help solve this question.

In the case of autophagy induced by nutrient availability, it is already clear that the process is orchestrated by different mechanisms. The acute response to nutrient deprivation includes nutrient sensing by mTORC1 and AMPK and activation of the UNC-51-like kinase (ULK) and class III phosphatidylinositol-3 kinase (PI3K) complexes. This subsequently leads to the formation of a PI3P-enriched membrane compartment, recruitment of the ATG12-5-16L1 complex, and LC3 lipidation (Lamb et al., 2013). More recently, it has become clear that the transcriptional activation of autophagy and lysosome genes plays an important role in prolonged autophagy (Füllgrabe et al., 2014). Although the link between nutrient sensing by mTORC1 and TFEB-mediated autophagy/lysosome gene activation is now well recognized, other signaling pathways that mediate the nutrient regulation of autophagy genes are not fully understood. In this regard, we report that a signaling cascade consisting of two nutrient sensor molecules—AMPK and SIRT1—integrate the nutrient status of the cell to autophagy gene regulation via BRD4. Nutrient deprivation causes the dissociation of SIRT1 from its inhibitory molecule DBC1 in an AMPK-dependent manner and may also activate SIRT1 via an increase in $NAD^+$/NADH ratio (Cantó et al., 2009), which in turn leads to SIRT1-mediated BRD4 dissociation from autophagy gene promoters and de-repression of autophagy gene expression. Our findings suggest that BRD4 suppresses autophagy and lysosome gene expression under nutrient-replete conditions to prevent excess autophagy, and BRD4 dissociation allows cells to maintain autophagic activity during prolonged nutrient shortage. Interestingly, a recent report showing that JQ1 increases LC3 lipidation and autophagosome formation implicates the involvement of BET proteins in autophagy regulation (Jang et al., 2016). Importantly, however, the detailed mechanism by which JQ1 modulates autophagy and the molecule that mediates this effect were not explored.

Currently, TFEB is thought to be a "master" regulator of autophagy and lysosome gene transcription (Settembre et al., 2011). Importantly, BRD4 inhibition activates autophagy in the absence of TFEB and its related molecules TFE3 and MITF. This observation suggests that BRD4 orchestrates a distinct transcriptional program and is therefore another crucial regulator of autophagy and lysosome gene expression. Interestingly, a recent report has shown that AMPK activates TFEB-mediated transcription by inducing the transcriptional coactivator, Coactivator associated arginine (R) methyltransferase 1 (CARM1) (Shin et al., 2016). These findings, taken together, suggest that AMPK activation upon nutrient deprivation stimulates TFEB-mediated transcription and suppresses BRD4 function to cooperatively activate the autophagy-lysosome pathway.

BRD4 has been proposed as a positive regulator of transcription that bridges histone acetylation and transcriptional regulators such as P-TEFb and the Mediator complex (Shi and Vakoc, 2014). We observed, as previously reported, that this positive effect on transcription is particularly important for the regulation of genes involved in the promotion of cell growth (Zuber et al., 2011), and so it is interesting that BRD4 at the same time reciprocally represses genes involved in major catabolic processes at the lysosome and vice versa. Interestingly, although this is not the first report to show that BRD4 functions as a transcriptional

**Figure 5. BRD4 Represses Autophagy Gene Expression through G9a**
(A) Cell extracts from KP-4 cells were subjected to immunoprecipitation with G9a (upper) and BRD4 (lower) antibodies.
(B) KP-4 cells were starved for 4 hr followed by immunoprecipitation with BRD4 antibody.
(C–F) KP-4 cells were treated with 500 nM JQ1 for 9 hr (C and E). KP-4 cells harboring inducible control or BRD4 shRNA were treated with 500 ng/mL doxycycline (DOX) for 4 days (D and F). ChIP assays were performed using G9a (C and D) and H3K9diMe (E and F) antibodies.
(G and H) KP-4 cells infected with shRNA targeting G9a were transfected with BRD4 siRNA followed by RT-qPCR (G) and western blot (H).
(I) KP-4 cells overexpressing BRD4 were infected with shRNA targeting G9a.
All data are shown as mean ± SD. In (C)–(G), n = 3 independent experiments. *p < 0.01, **p < 0.05, N.S., no significance. See also Figure S5.

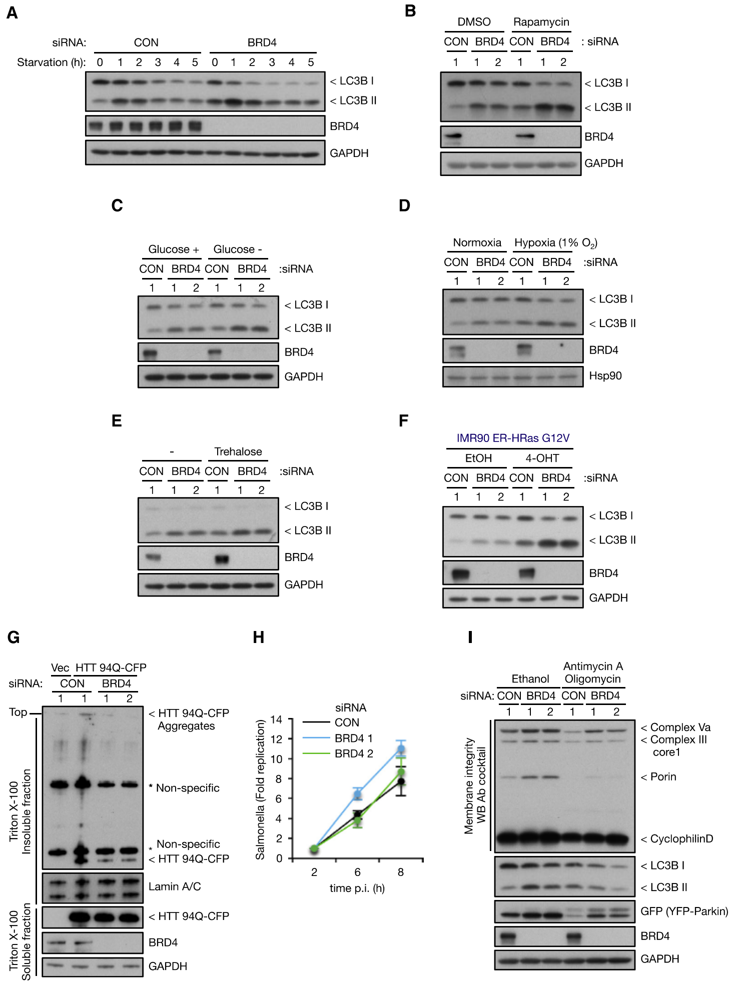


**Figure 6. Effect of BRD4 Silencing on Stimulus-Dependent and Selective Autophagy**

(A–F) Cells transfected with BRD4 siRNA were starved for 1–5 hr (KP-4 cells, A), treated with 500 nM rapamycin for 24 hr (KP-4 cells, B), starved of glucose for 4 hr (KP-4 cells, C), cultured under hypoxic (1% $O_2$) conditions for 48 hr (SUIT2 cells, D), treated with 100 mM Trehalose for 4 hr (KP-4 cells, E), or treated with 500 nM 4-Hydroxytamoxifen (4-OHT) for 48 hr (IMR90 ER-HRas G12V cells, F).

(G) KP-4 cells harboring rtTA and Tre-tight-HTT Q94-CFP were transfected with BRD4 siRNA. At 12 hr after transfection, cells were treated with 1 $\mu$g/mL DOX for 10 hr. At 48 hr after removal of DOX, cells were separated into Triton X-100 soluble and insoluble fractions.

(H) KP-4 cells transfected with BRD4 siRNA were infected with *Salmonella enterica* serovar Typhimurium. The number of *Salmonella* was determined by performing colony-forming unit assays at 2, 6, and 8 hr after infection and normalized to the numbers at 2 hr. Data are shown as mean ± SEM; n = 4 independent experiments.

(I) KP-4 cells expressing YFP-parkin were transfected with BRD4 siRNA followed by treatment with 1 $\mu$M Antimycin A and 1 $\mu$M Oligomycin for 8 hr.

See also Figure S6.

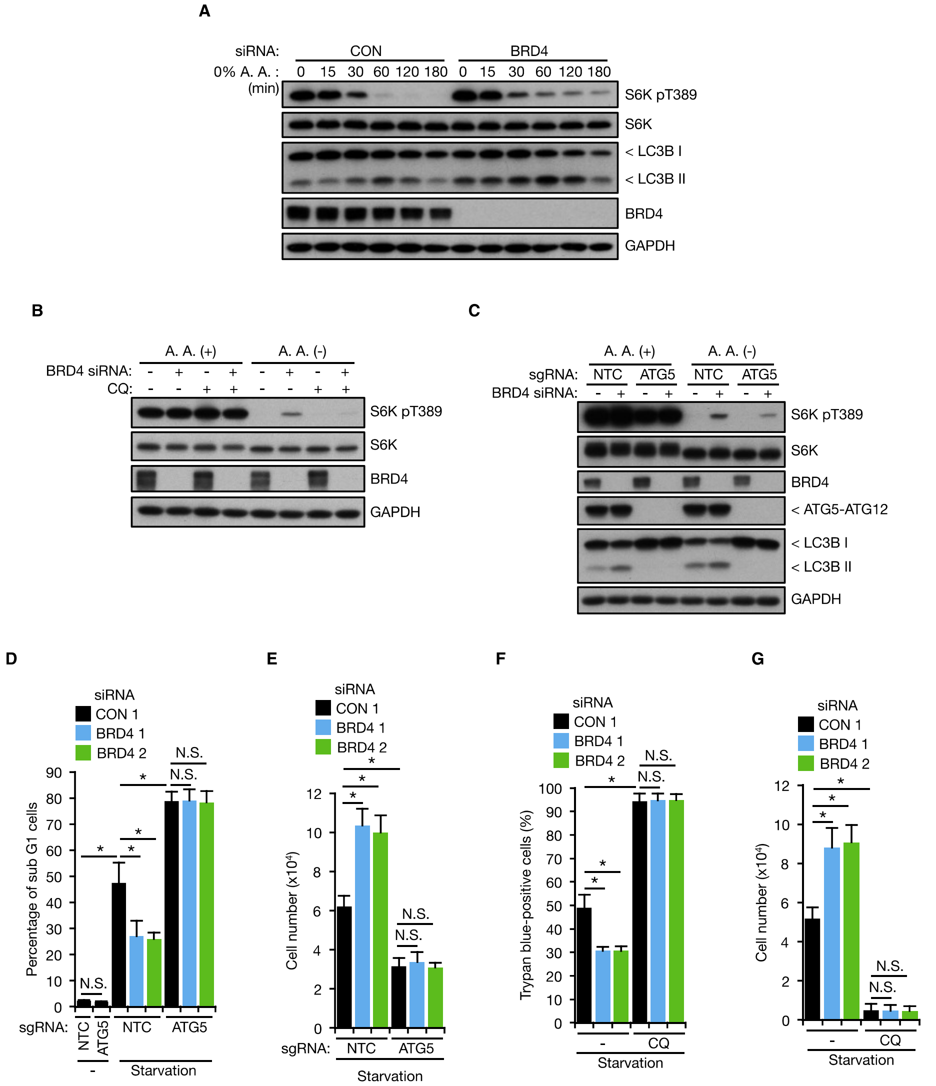


**Figure 7. BRD4 Knockdown Sustains mTOR Activity during Starvation and Confers Resistance to Starvation-Induced Cell Death**

(A and B) KP-4 cells transfected with BRD4 siRNA were starved of amino acids (A). Cells pre-treated with CQ (10 μM, 4 hr) were subjected to amino acid starvation for 2 hr in the presence of CQ (B).

(C) KP-4 cells infected with Cas9/ATG5 sgRNA were transfected with BRD4 siRNA and subjected to amino acid starvation for 2 hr.

(legend continued on next page)

CellPress

repressor, the mechanisms behind this effect were largely unknown (Barrow et al., 2016). We show that BRD4 is recruited to autophagy and lysosome gene promoter regions and interacts with G9a that deposits a repressive H3K9diMe mark. However, our finding that G9a knockdown largely, but not completely, abrogates autophagy repression by BRD4 overexpression implies that there are other mechanism(s) that mediate the autophagy suppression by BRD4. Different transcriptional activators (i.e., FOXO family and p53 family), repressors (i.e., ZKSCAN3 and FOXK), and histone modifications (i.e., H3K27triMe and H2BK120Ub) are also involved in the transcriptional regulation of autophagy (Baek and Kim, 2017; Füllgrabe et al., 2016). Therefore, it remains possible that BRD4 affects the recruitment of these transcription factors and histone-modifying enzymes to suppress autophagy gene expression.

Modulation of autophagic activity is thought to be a potential therapeutic strategy for various diseases, including neuronal degeneration, infectious diseases, and cancer (Rubinsztein et al., 2012). In this regard, identification of druggable autophagy regulators would be an attractive strategy to treat these diseases. BET inhibitors exhibit anti-tumor effects in various types of cancers and have been tested in phase one and two clinical trials (Wang and Filippakopoulos, 2015). Our findings also potentially indicate that BET inhibitors may have beneficial effects in diseases, such as neurodegeneration, where promotion of autophagy is being explored for therapy.

There has been much interest in whether autophagy represses or promotes tumor development (Galluzzi et al., 2015) and so the fact that the product of a chromosomal translocation considered to be the driver of NMC is a repressor of autophagy is an interesting discovery. Interestingly, we found that, in NMC cells, BRD4 expressed from the unaffected allele has little contribution to the regulation of autophagy, indicating a dominant role of BRD4-NUT in autophagy repression. How this enhanced repression is achieved and how much, if at all, the repression of autophagy is a contributing factor in the development of NMC are beyond the scope of this current study but undoubtedly worthy of future investigation.

Taken together, the findings we present here detail a mechanism of transcriptional regulation of autophagy and lysosome function. The mechanism facilitates some forms of autophagy, but not others, and this therefore highlights an additional control point of autophagy regulation that may be relevant to various forms of human disease.

## STAR★METHODS

Detailed methods are provided in the online version of this paper and include the following:



## SUPPLEMENTAL INFORMATION

Supplemental Information includes seven figures and two tables and can be found with this article online at http://dx.doi.org/10.1016/j.molcel.2017.04.027.

## AUTHOR CONTRIBUTIONS

J.S. designed the project, conducted most of the experiments, analyzed data, and wrote the manuscript. S.W. conducted the RNAi screening in *Drosophila* S2R+ cells. M.H. conducted xenophagy experiments under the supervision of I.D. N.T. generated BRD4 knockdown mice, performed JQ1 treatment in mice, and prepared tissue sections under the supervision of S.W.L. J.O. generated pBabe-mRFP-GFP-LC3 and lentiCRISPR-NTC, ATG5 plasmids, and KP-4 cells expressing Cas9/ATG5 sgRNA and helped with experiments. W.C. performed RNA-seq. A.H. conducted analysis of the RNA-seq data. C.N. performed immunohistochemistry staining. J.S.L. generated KP-4 cells expressing YFP-parkin and helped with experiments. M.N. and T.V.A. conducted the initial evaluation of autophagic flux in cell lines used in this study and provided advice regarding the autophagy experiments under the supervision of S.A.T. K.M.R. conceived and supervised the project and wrote the manuscript.


## ACKNOWLEDGMENTS

We thank members of the Ryan Laboratory for helpful discussions. We also thank Direna Alonso Curbelo for advice on BRD4 IHC staining and Peter


(D and E) KP-4 cells infected with Cas9/ATG5 sgRNA were transfected with BRD4 siRNA. Following 48 hr starvation, percentage of subG1 cells (D) and cell number (E) were determined (n = 3 independent experiments).

(F and G) KP-4 cells transfected with BRD4 siRNA were starved for 48 hr in the presence or absence of 10 μM CQ. Percentage of dead (F) and surviving (G) cells was determined by trypan blue exclusion test (n = 4 independent experiments).

All data are shown as mean ± SD. *p < 0.01, N.S., no significance. See also Figure S7.

CellPress

Adams and David Rubinsztein for advice. Work in the Ryan laboratory is supported by Cancer Research UK (C596/A17196), Astellas Pharma, and Worldwide Cancer Research (16-1194). S.W.L. is a founder and consultant for Mirimus, a company that has commercialized the inducible shRNA transgenic technology used in this study.

Received: November 28, 2016
Revised: March 15, 2017
Accepted: April 28, 2017
Published: May 18, 2017

## REFERENCES

Alexeyev, M.F., Fayzulin, R., Shokolenko, I.N., and Pastukh, V. (2010). A retro-lentiviral system for doxycycline-inducible gene expression and gene knockdown in cells with limited proliferative capacity. Mol. Biol. Rep. *37*, 1987–1991.

Baek, S.H., and Kim, K.I. (2017). Epigenetic control of autophagy: nuclear events gain more attention. Mol. Cell *65*, 781–785.

Barrow, J.J., Balsa, E., Verdeguer, F., Tavares, C.D., Soustek, M.S., Hollingsworth, L.R., 4th, Jedrychowski, M., Vogel, R., Paulo, J.A., Smeitink, J., et al. (2016). Bromodomain inhibitors correct bioenergetic deficiency caused by mitochondrial disease complex I mutations. Mol. Cell *64*, 163–175.

Baudot, A.D., Haller, M., Mrschtik, M., Tait, S.W., and Ryan, K.M. (2015). Using enhanced-mitophagy to measure autophagic flux. Methods *75*, 105–111.

Bauer, P.O., Goswami, A., Wong, H.K., Okuno, M., Kurosawa, M., Yamada, M., Miyazaki, H., Matsumoto, G., Kino, Y., Nagai, Y., and Nukina, N. (2010). Harnessing chaperone-mediated autophagy for the selective degradation of mutant huntingtin protein. Nat. Biotechnol. *28*, 256–263.

Bisgrove, D.A., Mahmoudi, T., Henklein, P., and Verdin, E. (2007). Conserved P-TEFb-interacting domain of BRD4 inhibits HIV transcription. Proc. Natl. Acad. Sci. USA *104*, 13690–13695.

Bolden, J.E., Tasdemir, N., Dow, L.E., van Es, J.H., Wilkinson, J.E., Zhao, Z., Clevers, H., and Lowe, S.W. (2014). Inducible in vivo silencing of Brd4 identifies potential toxicities of sustained BET protein inhibition. Cell Rep. *8*, 1919–1929.

Cantó, C., Gerhart-Hines, Z., Feige, J.N., Lagouge, M., Noriega, L., Milne, J.C., Elliott, P.J., Puigserver, P., and Auwerx, J. (2009). AMPK regulates energy expenditure by modulating NAD+ metabolism and SIRT1 activity. Nature *458*, 1056–1060.

Chang, C., Su, H., Zhang, D., Wang, Y., Shen, Q., Liu, B., Huang, R., Zhou, T., Peng, C., Wong, C.C., et al. (2015). AMPK-dependent phosphorylation of GAPDH triggers Sirt1 activation and is necessary for autophagy upon glucose starvation. Mol. Cell *60*, 930–940.

Chauhan, S., Goodwin, J.G., Chauhan, S., Manyam, G., Wang, J., Kamat, A.M., and Boyd, D.D. (2013). ZKSCAN3 is a master transcriptional repressor of autophagy. Mol. Cell *50*, 16–28.

Church, D.M., Schneider, V.A., Graves, T., Auger, K., Cunningham, F., Bouk, N., Chen, H.C., Agarwala, R., McLaren, W.M., Ritchie, G.R., et al. (2011). Modernizing reference genome assemblies. PLoS Biol. *9*, e1001091.

Dawson, M.A., Prinjha, R.K., Dittmann, A., Giotopoulos, G., Bantscheff, M., Chan, W.I., Robson, S.C., Chung, C.W., Hopf, C., Savitski, M.M., et al. (2011). Inhibition of BET recruitment to chromatin as an effective treatment for MLL-fusion leukaemia. Nature *478*, 529–533.

Filippakopoulos, P., Qi, J., Picaud, S., Shen, Y., Smith, W.B., Fedorov, O., Morse, E.M., Keates, T., Hickman, T.T., Felletar, I., et al. (2010). Selective inhibition of BET bromodomains. Nature *468*, 1067–1073.

Fisher, S., Barry, A., Abreu, J., Minie, B., Nolan, J., Delorey, T.M., Young, G., Fennell, T.J., Allen, A., Ambrogio, L., et al. (2011). A scalable, fully automated process for construction of sequence-ready human exome targeted capture libraries. Genome Biol. *12*, R1.

Floyd, S.R., Pacold, M.E., Huang, Q., Clarke, S.M., Lam, F.C., Cannell, I.G., Bryson, B.D., Rameseder, J., Lee, M.J., Blake, E.J., et al. (2013). The bromodomain protein Brd4 insulates chromatin from DNA damage signalling. Nature *498*, 246–250.

French, C.A. (2010). NUT midline carcinoma. Cancer Genet. Cytogenet. *203*, 16–20.

Füllgrabe, J., Lynch-Day, M.A., Heldring, N., Li, W., Struijk, R.B., Ma, Q., Hermanson, O., Rosenfeld, M.G., Klionsky, D.J., and Joseph, B. (2013). The histone H4 lysine 16 acetyltransferase hMOF regulates the outcome of autophagy. Nature *500*, 468–471.

Füllgrabe, J., Klionsky, D.J., and Joseph, B. (2014). The return of the nucleus: transcriptional and epigenetic control of autophagy. Nat. Rev. Mol. Cell Biol. *15*, 65–74.

Füllgrabe, J., Ghislat, G., Cho, D.H., and Rubinsztein, D.C. (2016). Transcriptional regulation of mammalian autophagy at a glance. J. Cell Sci. *129*, 3059–3066.

Galluzzi, L., Pietrocola, F., Bravo-San Pedro, J.M., Amaravadi, R.K., Baehrecke, E.H., Cecconi, F., Codogno, P., Debnath, J., Gewirtz, D.A., Karantza, V., et al. (2015). Autophagy in malignant transformation and cancer progression. EMBO J. *34*, 856–880.

Guan, B., Wang, T.L., and Shih, IeM. (2011). ARID1A, a factor that promotes formation of SWI/SNF-mediated chromatin remodeling, is a tumor suppressor in gynecologic cancers. Cancer Res. *71*, 6718–6727.

Hale, C.M., Cheng, Q., Ortuno, D., Huang, M., Nojima, D., Kassner, P.D., Wang, S., Ollmann, M.M., and Carlisle, H.J. (2016). Identification of modulators of autophagic flux in an image-based high content siRNA screen. Autophagy *12*, 713–726.

Itakura, E., and Mizushima, N. (2011). p62 Targeting to the autophagosome formation site requires self-oligomerization but not LC3 binding. J. Cell Biol. *192*, 17–27.

Jang, J.E., Eom, J.I., Jeung, H.K., Cheong, J.W., Lee, J.Y., Kim, J.S., and Min, Y.H. (2016). AMPK-ULK1-mediated autophagy confers resistance to BET inhibitor JQ1 in acute myeloid leukemia stem cells. Clin. Cancer Res. Published online November 18, 2016. http://dx.doi.org/10.1158/1078-0432.CCR-16-1903.

Kellner, W.A., Van Bortle, K., Li, L., Ramos, E., Takenaka, N., and Corces, V.G. (2013). Distinct isoforms of the Drosophila Brd4 homologue are present at enhancers, promoters and insulator sites. Nucleic Acids Res. *41*, 9274–9283.

Khaminets, A., Behl, C., and Dikic, I. (2016). Ubiquitin-dependent and independent signals in selective autophagy. Trends Cell Biol. *26*, 6–16.

Kim, D., Pertea, G., Trapnell, C., Pimentel, H., Kelley, R., and Salzberg, S.L. (2013). TopHat2: accurate alignment of transcriptomes in the presence of insertions, deletions and gene fusions. Genome Biol. *14*, R36.

Kimura, S., Noda, T., and Yoshimori, T. (2007). Dissection of the autophagosome maturation process by a novel reporter protein, tandem fluorescent-tagged LC3. Autophagy *3*, 452–460.

Klionsky, D.J., Abdelmohsen, K., Abe, A., Abedin, M.J., Abeliovich, H., Acevedo Arozena, A., Adachi, H., Adams, C.M., Adams, P.D., Adeli, K., et al. (2016). Guidelines for the use and interpretation of assays for monitoring autophagy (3rd edition). Autophagy *12*, 1–222.

Korb, E., Herre, M., Zucker-Scharff, I., Darnell, R.B., and Allis, C.D. (2015). BET protein Brd4 activates transcription in neurons and BET inhibitor Jq1 blocks memory in mice. Nat. Neurosci. *18*, 1464–1473.

Ktistakis, N.T., and Tooze, S.A. (2016). Digesting the expanding mechanisms of autophagy. Trends Cell Biol. *26*, 624–635.

Lamb, C.A., Yoshimori, T., and Tooze, S.A. (2013). The autophagosome: origins unknown, biogenesis complex. Nat. Rev. Mol. Cell Biol. *14*, 759–774.

Langmead, B., and Salzberg, S.L. (2012). Fast gapped-read alignment with Bowtie 2. Nat. Methods *9*, 357–359.

Love, M.I., Huber, W., and Anders, S. (2014). Moderated estimation of fold change and dispersion for RNA-seq data with DESeq2. Genome Biol. *15*, 550.

Lu, J., Qian, Y., Altieri, M., Dong, H., Wang, J., Raina, K., Hines, J., Winkler, J.D., Crew, A.P., Coleman, K., and Crews, C.M. (2015). Hijacking the E3 ubiquitin ligase cereblon to efficiently target BRD4. Chem. Biol. *22*, 755–763.

Maynard, C.J., Böttcher, C., Ortega, Z., Smith, R., Florea, B.I., Diaz-Hernández, M., Brundin, P., Overkleeft, H.S., Li, J.Y., Lucas, J.J., and Dantuma, N.P. (2009). Accumulation of ubiquitin conjugates in a polyglutamine

CellPress

disease model occurs without global ubiquitin/proteasome system impairment. Proc. Natl. Acad. Sci. USA *106*, 13986–13991.

McEwan, D.G., Popovic, D., Gubas, A., Terawaki, S., Suzuki, H., Stadel, D., Coxon, F.P., Miranda de Stegmann, D., Bhogaraju, S., Maddi, K., et al. (2015a). PLEKHM1 regulates autophagosome-lysosome fusion through HOPS complex and LC3/GABARAP proteins. Mol. Cell *57*, 39–54.

McEwan, D.G., Richter, B., Claudi, B., Wigge, C., Wild, P., Farhan, H., McGourty, K., Coxon, F.P., Franz-Wachtel, M., Perdu, B., et al. (2015b). PLEKHM1 regulates Salmonella-containing vacuole biogenesis and infection. Cell Host Microbe *17*, 58–71.

Mizushima, N., Levine, B., Cuervo, A.M., and Klionsky, D.J. (2008). Autophagy fights disease through cellular self-digestion. Nature *451*, 1069–1075.

Morgenstern, J.P., and Land, H. (1990). Advanced mammalian gene transfer: high titre retroviral vectors with multiple drug selection markers and a complementary helper-free packaging cell line. Nucleic Acids Res. *18*, 3587–3596.

Narain, Y., Wyttenbach, A., Rankin, J., Furlong, R.A., and Rubinsztein, D.C. (1999). A molecular investigation of true dominance in Huntington's disease. J. Med. Genet. *36*, 739–746.

Perera, R.M., Stoykova, S., Nicolay, B.N., Ross, K.N., Fitamant, J., Boukhali, M., Lengrand, J., Deshpande, V., Selig, M.K., Ferrone, C.R., et al. (2015). Transcriptional control of autophagy-lysosome function drives pancreatic cancer metabolism. Nature *524*, 361–365.

Premsrirut, P.K., Dow, L.E., Kim, S.Y., Camiolo, M., Malone, C.D., Miething, C., Scuoppo, C., Zuber, J., Dickins, R.A., Kogan, S.C., et al. (2011). A rapid and scalable system for studying gene function in mice using conditional RNA interference. Cell *145*, 145–158.

Rabinowitz, J.D., and White, E. (2010). Autophagy and metabolism. Science *330*, 1344–1348.

Reimand, J., Arak, T., and Vilo, J. (2011). g:Profiler—a web server for functional interpretation of gene lists (2011 update). Nucleic Acids Res. *39*, W307–W315.

Roczniak-Ferguson, A., Petit, C.S., Froehlich, F., Qian, S., Ky, J., Angarola, B., Walther, T.C., and Ferguson, S.M. (2012). The transcription factor TFEB links mTORC1 signaling to transcriptional control of lysosome homeostasis. Sci. Signal. *5*, ra42.

Rubinsztein, D.C., Codogno, P., and Levine, B. (2012). Autophagy modulation as a potential therapeutic target for diverse diseases. Nat. Rev. Drug Discov. *11*, 709–730.

Sanjana, N.E., Shalem, O., and Zhang, F. (2014). Improved vectors and genome-wide libraries for CRISPR screening. Nat. Methods *11*, 783–784.

Schwartz, B.E., Hofer, M.D., Lemieux, M.E., Bauer, D.E., Cameron, M.J., West, N.H., Agoston, E.S., Reynoird, N., Khochbin, S., Ince, T.A., et al. (2011). Differentiation of NUT midline carcinoma by epigenomic reprogramming. Cancer Res. *71*, 2686–2696.

Settembre, C., Di Malta, C., Polito, V.A., Garcia Arencibia, M., Vetrini, F., Erdin, S., Erdin, S.U., Huynh, T., Medina, D., Colella, P., et al. (2011). TFEB links autophagy to lysosomal biogenesis. Science *332*, 1429–1433.

Shen, H.M., and Mizushima, N. (2014). At the end of the autophagic road: an emerging understanding of lysosomal functions in autophagy. Trends Biochem. Sci. *39*, 61–71.

Shi, J., and Vakoc, C.R. (2014). The mechanisms behind the therapeutic activity of BET bromodomain inhibition. Mol. Cell *54*, 728–736.

Shin, H.J., Kim, H., Oh, S., Lee, J.G., Kee, M., Ko, H.J., Kweon, M.N., Won, K.J., and Baek, S.H. (2016). AMPK-SKP2-CARM1 signalling cascade in transcriptional regulation of autophagy. Nature *534*, 553–557.

Shinkai, Y., and Tachibana, M. (2011). H3K9 methyltransferase G9a and the related molecule GLP. Genes Dev. *25*, 781–788.

Stadel, D., Millarte, V., Tillmann, K.D., Huber, J., Tamin-Yecheskel, B.C., Akutsu, M., Demishtein, A., Ben-Zeev, B., Anikster, Y., Perez, F., et al. (2015). TECPR2 cooperates with LC3C to regulate COPII-dependent ER export. Mol. Cell *60*, 89–104.

Vaquero, A., Sternglanz, R., and Reinberg, D. (2007). NAD+-dependent deacetylation of H4 lysine 16 by class III HDACs. Oncogene *26*, 5505–5520.

Wang, C.Y., and Filippakopoulos, P. (2015). Beating the odds: BETs in disease. Trends Biochem. Sci. *40*, 468–479.

Wang, T., Wei, J.J., Sabatini, D.M., and Lander, E.S. (2014). Genetic screens in human cells using the CRISPR-Cas9 system. Science *343*, 80–84.

Wilkinson, S., Croft, D.R., O'Prey, J., Meedendorp, A., O'Prey, M., Dufès, C., and Ryan, K.M. (2011). The cyclin-dependent kinase PITSLRE/CDK11 is required for successful autophagy. Autophagy *7*, 1295–1301.

Williams, A., Sarkar, S., Cuddon, P., Ttofi, E.K., Saiki, S., Siddiqi, F.H., Jahreiss, L., Fleming, A., Pask, D., Goldsmith, P., et al. (2008). Novel targets for Huntington's disease in an mTOR-independent autophagy pathway. Nat. Chem. Biol. *4*, 295–305.

Zippo, A., Serafini, R., Rocchigiani, M., Pennacchini, S., Krepelova, A., and Oliviero, S. (2009). Histone crosstalk between H3S10ph and H4K16ac generates a histone code that mediates transcription elongation. Cell *138*, 1122–1136.

Zuber, J., Shi, J., Wang, E., Rappaport, A.R., Herrmann, H., Sison, E.A., Magoon, D., Qi, J., Blatt, K., Wunderlich, M., et al. (2011). RNAi screen identifies Brd4 as a therapeutic target in acute myeloid leukaemia. Nature *478*, 524–528.

# STAR★METHODS

## KEY RESOURCES TABLE

| REAGENT or RESOURCE | SOURCE | IDENTIFIER |
|---|---|---|
| Antibodies | | |
| Rabbit monoclonal anti-BRD4 (clone E2A7X) (human specific) (long isoform) | Cell Signaling Technology | Cat#: 13440S |
| Rabbit monoclonal anti-NUT (clone C52B1) | Cell Signaling Technology | Cat#: 3625S; RRID: AB_2066833 |
| Rabbit monoclonal anti-G9a (EHMT2/KMT1C) (clone C6H3) | Cell Signaling Technology | Cat#: 3306S; RRID: AB_2097647 |
| Rabbit monoclonal anti-SIRT1 (clone D1D7) | Cell Signaling Technology | Cat#: 9475P; RRID: AB_2617130 |
| Mouse monoclonal anti-DBC1 (clone 3G4) | Cell Signaling Technology | Cat#: 5857S; RRID: AB_10838138 |
| Rabbit monoclonal anti-AMPKα pT172 | Cell Signaling Technology | Cat#: 2535S; RRID: AB_331250 |
| Mouse monoclonal anti-AMPKα1/α2 | Cell Signaling Technology | Cat#: 2793S; RRID: AB_915794 |
| Rabbit polyclonal anti-LC3B | Cell Signaling Technology | Cat#: 2775S; RRID: AB_915950 |
| Rabbit monoclonal anti-LC3B (clone D11) | Cell Signaling Technology | Cat#: 3868S; RRID: AB_2137707 |
| Rabbit polyclonal anti-TFEB | Cell Signaling Technology | Cat#: 4240S; RRID: AB_11220225 |
| Rabbit monoclonal anti-LAMP1 (clone D2D11) | Cell Signaling Technology | Cat#: 9091P |
| Rabbit polyclonal anti-Cathepsin D | Cell Signaling Technology | Cat#: 2284S; RRID: AB_10694258 |
| Rabbit polyclonal anti-ASM | Cell Signaling Technology | Cat# 3687S; RRID: AB_1904135 |
| Rabbit monoclonal anti-Cathepsin B (clone D1C7Y) | Cell Signaling Technology | Cat#: 31718S |
| Rabbit monoclonal anti-ATG5 (clone D5F5U) | Cell Signaling Technology | Cat#: 12994S |
| Rabbit monoclonal anti-p70 S6K pT389 (clone 108D2) | Cell Signaling Technology | Cat#: 9234S; RRID: AB_2269803 |
| Rabbit monoclonal anti-p70 S6K (clone 49D7) | Cell Signaling Technology | Cat#: 2708S; RRID: AB_390722 |
| Rabbit monoclonal anti-Acetyl-Histone H4 (Lys16) (clone E2B8W) | Cell Signaling Technology | Cat#:13534S |
| Mouse monoclonal anti-Histone H4 (clone L64C1) | Cell Signaling Technology | Cat#: 2935P; RRID: AB_1147658 |
| Rabbit monoclonal anti-c-Myc (clone D84C12) | Cell Signaling Technology | Cat#: 5605S; RRID: AB_1903938 |
| Rabbit monoclonal anti-CDK9 (clone C12F7) | Cell Signaling Technology | Cat#: 2316T; RRID: AB_2291505 |
| Rabbit monoclonal anti-GFP (clone D5.1) | Cell Signaling Technology | Cat#: 2956S; RRID: AB_1196615 |
| Rabbit polyclonal anti-TFE3 | Cell Signaling Technology | Cat#: 14779S |
| Normal rabbit IgG | Cell Signaling Technology | Cat#: 2729S; RRID: AB_1031062 |
| Mouse IgG1 isotype control G3A1 | Cell Signaling Technology | Cat#: 5415S; RRID: AB_10829607 |
| Rabbit monoclonal anti-BRD4 (clone EPR5150(2)) (human and mouse) (long and short isoforms) | Abcam | Cat#: ab128874; RRID: AB_11145462 |
| Mouse monoclonal anti-GAPDH | Abcam | Cat#: ab9484; RRID: AB_307274 |
| Rabbit polyclonal anti-β-actin | Abcam | Cat#: ab8227; RRID: AB_2305186 |
| Rabbit polyclonal anti-G9a (EHMT2/KMT1C) | Abcam | Cat#: ab133482 |
| Mouse monoclonal anti-Histone H3 (di methyl K9) | Abcam | Cat#: ab1220; RRID: AB_449854 |
| Rabbit polyclonal anti-GAA (clone EPR4716(2)) | Abcam | Cat#: ab137068 |
| Mouse monoclonal Membrane Integrity WB Antibody Cocktail | Abcam | Cat#: ab110414 |
| Rabbit polyclonal anti-BRD4 (human and mouse) (long isoform) | Bethyl Laboratories | Cat#: A301-985A50; RRID: AB_2631449 |
| Rabbit polyclonal anti-BRD2 | Bethyl Laboratories | Cat#: A302-583A; RRID: AB_2034829 |
| Rabbit polyclonal anti-BRD3 | Bethyl Laboratories | Cat#: A302-368A; RRID: AB_1907251 |
| Rabbit polyclonal anti-hMOF (MYST1/KAT8) | Bethyl Laboratories | Cat#: A300-992A; RRID: AB_805802 |
| Rabbit polyclonal anti-Acetyl-Histone H4 (Lys16) | Millipore | Cat#: 07-329; RRID: AB_310525 |
| Rabbit polyclonal anti-Acetyl-Histone H4 (Lys16) | Active Motif | Cat#: 39167 |

(*Continued on next page*)

*Continued*

| REAGENT or RESOURCE | SOURCE | IDENTIFIER |
|---|---|---|
| Mouse monoclonal anti-LAMP2/CD107b | BD Biosciences | Cat#: 555803; RRID: AB_396137 |
| Mouse monoclonal anti-p62 | BD Biosciences | Cat#: 610833; RRID: AB_398152 |
| Mouse monoclonal anti-GFP | Covance | Cat#: MMS-118P-200; RRID: AB_10063778 |
| Goat polyclonal anti-LaminA/C | Santa Cruz | Cat#: sc-6215; RRID: AB_648152 |
| Goat polyclonal anti-HSP90β | Santa Cruz | Cat#: sc-1057; RRID: AB_2121392 |
| Mouse monoclonal anti-FLAG (clone M2) | Sigma-Aldrich | Cat#: F1804; RRID: AB_262044 |
| Mouse monoclonal anti-V5 | Invitrogen | Cat#: 46-0705 |
| Mouse monoclonal anti-WIPI2 | Bio-Rad | Cat#: MCA5780GA; RRID: AB_10845951 |
| Mouse monoclonal anti-LC3 | NanoTools | Cat#: 0231-100/LC3-5F10 |
| Bacterial and Virus Strains | | |
| *Salmonella enterica* serovar Typhimurium (strain 12023) | David Holden Lab (Imperial College London) | N/A |
| Chemicals, Peptides, and Recombinant Proteins | | |
| Chloroquine | Sigma-Aldrich | Cat#: C6628 |
| Doxycycline | Sigma-Aldrich | Cat#: D9891 |
| Antimycin A | Sigma-Aldrich | Cat#: A8674 |
| Oligomycin | Sigma-Aldrich | Cat#: O4876 |
| D-(+)-Trehalose dihydrate | Sigma-Aldrich | Cat#: T0167 |
| 4-Hydroxytamoxifen | Sigma-Aldrich | Cat#: H7904 |
| (+)-JQ1 | TOCRIS | Cat#: 4499 |
| I-BET151 | TOCRIS | Cat#: 4650 |
| OTX015 | Cayman | Cat#: 15947 |
| Compound C | EMD Millipore | Cat#: 171264 |
| Rapamycin | LC Laboratories | Cat#: R-5000 |
| ARV-825 | Chemietek | Cat#: CT-ARV825 |
| LysoTracker red DND-99 | Thermo Fisher Scientific | Cat# L7528 |
| Magic Red Cathepsin B | ImmunoChemistry Technologies | Cat#: 938 |
| Hoechst33342 | Thermo Fisher Scientific | Cat#: H3570 |
| Critical Commercial Assays | | |
| TruSeq RNA Sample Prep Kit v2 | Illumina | Cat#: RS-122-2001 |
| Click-iT EdU Flow Cytometry Assay Kit | Thermo Fisher Scientific | Cat#: C10633 |
| Deposited Data | | |
| Raw and processed data of the RNA-seq | This paper | GEO: GSE90444 |
| Full scans of western blot data and original microscopy images | This paper | Mendeley Data: http://dx.doi.org/10.17632/ksz4pmwkdb.1 |
| Experimental Models: Cell Lines | | |
| Human: KP-4 | RIKEN | RCB1005 |
| Human: PA-TU-8902 | DMSZ | ACC-179 |
| Human: SUIT2 | JCRB | JCRB1094 |
| Human: PA-TU-8988T | DMSZ | ACC-162 |
| Human: hTERT-HPNE | ATCC | CRL-4023 |
| Human: IMR90 ER-HRas G12V | Peter D. Adams Lab (Cancer Research UK Beatson Institute) | N/A |
| Human: HEK293T | ATCC | CRL-3216 |
| Human: PK-1 | RIKEN | RCB1972 |
| Human: TY-82 | JCRB | JCRB1330 |
| Human: Phoenix-AMPHO | ATCC | CRL-3213 |

(*Continued on next page*)

***Continued***

| REAGENT or RESOURCE | SOURCE | IDENTIFIER |
|---|---|---|
| Experimental Models: Organisms/Strains | | |
| Mouse: CAGs-rtTA3 | Scott W. Lowe Lab (Memorial Sloan Kettering Cancer Center) | Premsrirut et al., 2011 (also available from the Jackson Laboratory, Stock #: 016532) |
| Mouse: TRE-shRen | Scott W. Lowe Lab | N/A |
| Mouse: TRE-shBRD4 | Scott W. Lowe Lab | N/A |
| Mouse: C57BL/6J | The Jackson Laboratory | Stock #: 000664 |
| Oligonucleotides | | |
| siRNAs, see the Table S1 | N/A | N/A |
| pPCR primers, See the Table S2 | N/A | N/A |
| Recombinant DNA | | |
| pBabe-puro | Morgenstern and Land, 1990 | Addgene plasmid # 1764 |
| pRetrox-tight-puro-HA-BRD4 | MRC Protein Phosphorylation and Ubiquitylation Unit | Cat#: DU46347 |
| pBabe-puro-human BRD4 long variant | This paper | N/A |
| pLenti-puro | Guan et al., 2011 | Addgene plasmid # 39481 |
| pLenti-puro-human BRD4 long variant | This paper | N/A |
| pEGFP-C1+mRFP-LC3 | Tamotsu Yoshimori Lab (Osaka University) | Kimura et al., 2007 |
| pBabe-puro-mRFP-GFP-LC3 | This paper | N/A |
| pLZRS-YFP-Parkin | Baudot et al., 2015 | N/A |
| pcDNA3 | Invitrogen | N/A |
| pcDNA3-human BRD4 short variant | This paper | N/A |
| pLenti6-MK1-EHMT2 (G9a)-V5 (human G9a long variant) | Addgene | Addgene plasmid # 31113 |
| pTRE-tight | Clontech | Cat#: 631059 |
| pTRE-tight-Htt94Q-CFP | Maynard et al., 2009 | Addgene plasmid #23966 |
| pMA2640 | Alexeyev et al., 2010 | Addgene plasmid #25434 |
| pFlag-CMV2-Brd4 (1-1362) (human BRD4 long variant) | Bisgrove et al., 2007 | Addgene plasmid #22304, discontinued due to reason other than plasmid issue |
| psPAX2 | Addgene | Addgene plasmid #12260 |
| pMD2.G | Addgene | Addgene plasmid #12259 |
| pMXs-puro GFP-p62 | Itakura and Mizushima, 2011 | Addgene plasmid #38277 |
| pEGFP-N1 | Clontech | Cat#: 6085-1 |
| pEGFP-N1-TFEB | Roczniak-Ferguson et al., 2012 | Addgene plasmid #38119 |
| pEGFP-N1-TFE3 | Roczniak-Ferguson et al., 2012 | Addgene plasmid #38120 |
| pEGFP-N1-MITF-A | Roczniak-Ferguson et al., 2012 | Addgene plasmid #38132 |
| pEGFP-Q74 | Narain et al., 1999 | Addgene plasmid # 40262 |
| pLVX-TetOne-Puro | Clontech | Cat#: 631849 |
| pLVX-TetOne-Puro-GFP-HTT exon1 Q74 | This paper | N/A |
| lentiCRISPR v2 | Sanjana et al., 2014 | Addgene plasmid #52961 |
| lentiCRISPR v2-human hMOF/KAT8 #1 | This paper | N/A |
| lentiCRISPR v2-human hMOF/KAT8 #2 | This paper | N/A |
| lentiCRISPR v2-human SIRT1 | This paper | N/A |
| lentiCRISPR v2-human AMPK$\alpha$1/PRKAA1 | This paper | N/A |
| lentiCRISPR v2-human AMPK$\alpha$2/PRKAA2 | This paper | N/A |
| lentiCRISPR v2-human ATG5 | This paper | N/A |
| lentiCRISPR v2-non-targeting control (NTC) | This paper | N/A |
| pLKO.1-non-targeting control (NTC) | Sigma-Aldrich | Cat#: SHC002 |
| pLKO.1-human G9a shRNA #1 | Dharmacon | Cat#: TRCN0000115670 |

(*Continued on next page*)

*Continued*

| REAGENT or RESOURCE | SOURCE | IDENTIFIER |
|---|---|---|
| pLKO.1-human G9a shRNA #2 | Dharmacon | Cat#: TRCN0000115668 |
| pTRIPZ-non-targeting control (NTC) | Dharmacon | Cat#: RHS4743 |
| pTRIPZ-human BRD4 shRNA (targeting short and long variants) | Dharmacon | Cat#: V3THS326487 |
| Software and Algorithms | | |
| ImageJ64 | NIH | https://imagej.nih.gov/ij/ |
| CellProfiler | Anne Carpenter Lab (Broad Institute) | http://cellprofiler.org |
| Optimized CRISPR Design | Feng Zhang Lab (MIT) | http://crispr.mit.edu |
| FastQC | Babraham Bioinformatics | https://www.bioinformatics.babraham.ac.uk/projects/fastqc/ |
| FastQ Screen | Babraham Bioinformatics | http://www.bioinformatics.babraham.ac.uk/projects/fastq_screen/ |
| TopHat2 v.2.0.10 | Kim et al., 2013 | https://ccb.jhu.edu/software/tophat/index.shtml |
| Bowtie v.2.1.0 | Langmead and Salzberg, 2012 | http://bowtie-bio.sourceforge.net/bowtie2/index.shtml |
| HTSeq v.0.5.4p3 | Simon Anders (EMBL Heidelberg) | http://www-huber.embl.de/users/anders/HTSeq/doc/overview.html |
| DESeq2 | Love et al., 2014 | N/A |
| g:Profiler | Reimand et al., 2011 | N/A |
| ZEN 2010 software | Zeiss | N/A |
| ZEN 2012 software | Zeiss | N/A |
| StepOne software | Applied Biosystems | N/A |
| FlowJo software v.7.6.5 | FlowJo | N/A |
| BD CellQuest Pro software | BD Biosciences | N/A |
| GraphPad Prism 7 | GraphPad software | N/A |

## CONTACT FOR REAGENT AND RESOURCE SHARING

Further information and requests for resources and reagents should be directed to and will be fulfilled by the Lead Contact, Kevin M. Ryan (k.ryan@beatson.gla.ac.uk).

## EXPERIMENTAL MODEL AND SUBJECT DETAILS

### Cell Culture

KP-4 cells (RIKEN, Cat#: RCB1005) were cultured in IMDM (Thermo Fisher Scientific, Cat#: 21980065) supplemented with 20% FBS (Thermo Fisher Scientific, Cat#: 10270106) and antibiotics (Thermo Fisher Scientific, Cat#: 15140122) in a humidified atmosphere with 5% $CO_2$. PA-TU-8902 (DMSZ, Cat#: ACC-179), SUIT2 (JCRB, Cat#: JCRB1094), PA-TU-8988T (DMSZ, Cat#: ACC-162), hTERT-HPNE (ATCC, Cat#: CRL-4023), IMR90 ER-HRas G12V (a gift from Peter D. Adams, Cancer Research UK Beatson Institute, UK), and HEK293T (ATCC, Cat#: CRL-3216) cells were maintained in DMEM (Thermo Fisher Scientific, Cat#: 21969035) supplemented with 10% FBS, 2 mM L-Glutamine (Thermo Fisher Scientific, Cat#: 25030032), and antibiotics. PK-1 (RIKEN, Cat#: RCB1972) and TY-82 (JCRB, Cat#: JCRB1330) were maintained in RPMI-1640 (Thermo Fisher Scientific, Cat#: 31870074) supplemented with 10% FBS, 2 mM L-Glutamine, and antibiotics. For starvation experiments, cells were cultured in EBSS (Sigma-Aldrich, Cat#: E2888). Since amino acid-free and glucose-free IMDM media are not commercially available, we used amino acid-free and glucose-free DMEM media supplemented with 20% FBS. For amino acid starvation, DMEM low glucose amino acid free (USBiological, Cat#: D9800-13) was supplemented with Glucose (Thermo Fisher Scientific, Cat#: 15023021) to 25 mM, 20% dialized FBS (Thermo Fisher Scientific, Cat#: 26400044), 1 mM Sodium pyruvate (Sigma-Aldrich, Cat#: S8636), 3.7 g/L Sodium bicarbonate (Sigma-Aldrich, Cat#: S5761), and antibiotics. For glucose starvation, DMEM no glucose (Thermo Fisher Scientific, Cat#: 11966-025) was supplemented with 20% dialized FBS, 1 mM Sodium pyruvate, and antibiotics. DMEM supplemented with 20% dialized FBS, 2 mM L-Glutamine, and antibiotics was used as a control for amino acid and glucose starvation.

### Mice

6-8 week old TRE-shRen/CAG-rtTA3 and TRE-shBRD4/CAG-rtTA3 mice were fed with 625 mg/kg doxycycline-containing food pellets (Harlan Teklad) for 2 weeks. Tissues were harvested and fixed overnight in 10% neutral buffered formalin, followed by paraffin embedding and sectioning as described previously (Bolden et al., 2014). All experimental procedures were approved by, and adhered to guidelines of, the Memorial Sloan Kettering Cancer Center institutional animal care and use committee.

## METHOD DETAILS

### Reagents

Chloroquine (Cat#: C6628), Doxycycline (Cat#: D9891), Antimycin A (Cat#: A8674), Oligomycin (Cat#: O4876), D-(+)-Trehalose dihydrate (Cat#: T0167), and 4-Hydroxytamoxifen (Cat#: H7904) were from Sigma-Aldrich. (+)-JQ1 (Cat#: 4499) and I-BET151 (Cat#: 4650) were from TOCRIS. OTX015 (Cat#: 15947) was from Cayman. Compound C (Cat#: 171264) was from EMD Millipore. Rapamycin (Cat#: R-5000) was from LC Laboratories. ARV-825 was from Chemietek (Cat#: CT-ARV825).

### Plasmid Transfection

Plasmids were transfected into HEK293T cells using Lipofectamine2000 (Thermo Fisher Scientific, Cat#: 11668027) or GeneJuice (EMD Millipore, Cat#: 70967). KP-4 cells were transfected with plasmids using Lipofectamine3000 (Thermo Fisher Scientific, Cat#: L3000015).

### siRNA Transfection

Cells were reverse-transfected with 20 nM of siRNAs using Lipofectamine RNAiMAX reagent (Thermo Fisher Scientific, Cat#: 13778150) for 72 hr. siRNAs are listed in Table S1. BRD4 #1-#4 were used to knockdown both short and long isoforms. Since NUT is a testis-specific gene, NUT siRNAs were used to knockdown BRD4-NUT fusion gene (Schwartz et al., 2011).

### Western Blotting

Cells were lysed with cell lysis buffer (20 mM HEPES-KOH pH7.5, 150 mM NaCl, 2 mM EDTA, 1% Triton X-100) containing Halt protease inhibitor cocktail (Thermo Scientific, Cat#: 78430). Total protein concentration was determined by BCA assay using Copper (II) sulfate solution (Sigma-Aldrich, Cat#: C2284) and Bicinchoninic Acid solution (Sigma-Aldrich, Cat#: B9643). The cell extracts were mixed with 6x SDS-PAGE sample buffer (0.3 M Tris-HCl (pH6.8), 0.12 g/ml SDS, 0.1 M Dithiothreitol, 60% Glycerol, 0.6 mg/ml Bromophenol blue) and heated at 99°C for 5 min. The same amount of protein (10-30 μg) was loaded and run on SDS-PAGE. The following antibodies were used. BRD4 E2A7X (long isoform) (Cat#: 13440S, WB 1/1000, IP, ChIP), NUT (Cat#: 3625S, WB 1/1000), G9a (Cat#: 3306S, WB 1/1000), SIRT1 (Cat#: 9475P, WB 1/1000), DBC1 (Cat#: 5857S, WB 1/1000, IP), AMPKα pT172 (Cat#: 2535S, WB 1/1000), AMPKα1/α2 (Cat#: 2793S, WB 1/1000), LC3B (Cat#: 2775S, WB 1/1500), LC3B D11 (Cat#: 3868S, IF 1/200), TFEB (Cat#: 4240S, WB 1/1000), LAMP1 (Cat#: 9091P, WB 1/1000, IF 1/200), CTSD (Cat#: 2284S, WB 1/1000), ASM (Cat#: 3687S, WB 1/1000), CTSB (Cat#: 31718S, WB 1/1000), ATG5 (Cat#: 12994S, WB 1/1500), p70 S6K pT389 (Cat#: 9234S, WB 1/1000), p70 S6K (Cat#: 2708S, WB 1/1500), Histone H4K16Ac (Cat#: 13534S, WB 1/1000), Histone H4 (Cat#: 2935P, WB 1/1000), c-Myc (Cat#: 5605S, WB 1/1000), CDK9 (Cat#: 2316T, WB 1/1000), GFP (Cat#: 2956S, WB 1/2000), TFE3 (Cat#: 14779S, WB 1/1000), Normal rabbit IgG (Cat#: 2729S, IP, ChIP), Mouse IgG1 isotype control (Cat#: 5415S, IP), Anti-rabbit IgG HRP-linked Antibody (Cat#: 7074S, WB 1/5000), and Anti-mouse IgG HRP-linked Antibody (Cat#: #7076S, WB 1/5000) were from Cell Signaling Technology. BRD4 NT (short and long isoforms) (Cat#: ab128874, WB 1/1000), GAPDH (Cat#: ab9484, WB 1/2000), β-Actin (Cat#: ab8227, WB 1/2000), G9a (Cat#: ab133482, WB 1/1000, IP, ChIP), H3K9diMe (Cat#: ab1220, ChIP), GAA (Cat#: ab137068, WB 1/1000), Membrane Integrity WB Antibody Cocktail (Cat#: ab110414 (MS620), WB 1/5000), and Anti-Goat IgG H&L (HRP) (Cat#: ab6741, WB 1/5000) were from Abcam. BRD4 (long isoform) (Cat#: A301-985A50, ChIP, IHC 1/2000), BRD2 (Cat#: A302-583A, WB 1/5000), BRD3 (Cat#: A302-368A, WB 1/5000), and hMOF (Cat#: A300-992A, WB 1/1000) were from Bethyl Laboratories. H4K16Ac (Cat#: 07-329, WB 1/2000, ChIP) was from Millipore. H4K16Ac (Cat#: 39167, ChIP) was from Active motif. LAMP2/CD107b (Cat#: 555803, WB 1/2000) and p62 (Cat#: 610833, WB 1/5000) were from BD. GFP (Cat#: MMS-118P, WB 1/5000) was from Covance. LaminA/C (Cat#: sc-6215, WB 1/2000) and Hsp90β (Cat#: sc-1057, WB 1/2000) were from Santa Cruz. FLAG (Cat#: F1804, WB 1/2000) was Sigma-Aldrich. V5 (Cat#: 46-0705, WB 1/2000) was from Invitrogen. WIPI2 (Cat#: MCA5780GA, IF 1/200) was from Bio-Rad. LC3B (Cat#: 0231-100/LC3-5F10, IHC: 1/50) was from NanoTools. Proteins were detected using Pierce ECL Western Blotting Substrate (Thermo Fisher Scientific, Cat#: 32106) or SuperSignal West Femto Maximum Sensitivity Substrate (Thermo Fisher Scientific, Cat#: 34095). Signal intensity was measured using ImageJ64 software (https://imagej.nih.gov/ij/).

### Plasmids, sgRNAs, and shRNAs

cDNA encoding human BRD4 transcript variant long was excised from pRetrox-tight-puro-HA-BRD4 (obtained from MRC Protein Phosphorylation and Ubiquitylation Unit, Cat#: DU46347) and inserted into pBabe-puro (a gift from Hartmut Land & Jay Morgenstern & Bob Weinberg, Addgene plasmid # 1764) (Morgenstern and Land, 1990) and pLenti-puro (a gift from Ie-Ming Shih, Addgene plasmid # 39481) (Guan et al., 2011) vectors. Human BRD4 transcript variant short was cloned using pRetrox-tight-puro-HA-BRD4 as a template with BRD4 Short Fw (CGCGATATCACCATGGACTACAAAGACGATGACGACAAGATGTCTGCGGAGAGCGG) and BRD4 Short Rv (CGCGTCGACTTAGGCAGGACCTGTTTCGGAGTCTTCGCTG) primers. The fragment was digested with EcoRV and SalI and inserted into pcDNA3 vector (Invitrogen) (EcoRV and XhoI sites). The sequence was confirmed to be identical to BRD4 transcript variant short (RefSeq: NM_014299.2). mRFP-GFP-LC3 cDNA was excised from pEGFP-C1+mRFP-LC3 (a kind gift from Tamotsu Yoshimori, Osaka University, Japan) (Kimura et al., 2007) and inserted into pBabe-puro vector. pLZRS-YFP-Parkin was described in (Baudot et al., 2015). pLenti6-MK1-EHMT2 (G9a)-V5 was a gift from Bernard Futscher (Addgene plasmid # 31113). pTreTight-Htt94Q-CFP was a gift from Nico Dantuma (Addgene plasmid #23966) (Maynard et al., 2009). pMA2640 was a gift from Mikhail Alexeyev (Addgene plasmid #25434) (Alexeyev et al., 2010). pFlag-CMV2-Brd4 (1-1362) was a gift from Eric Verdin (Addgene plasmid #22304) (Bisgrove et al., 2007). psPAX2 and pMD2.G were gifts from Didier Trono (Addgene plasmid #12260 and #12259). pMXs-puro GFP-p62 was a gift from Noboru Mizushima (Addgene plasmid #38277) (Itakura and Mizushima, 2011). pEGFP-N1-TFEB, pEGFP-N1-TFE3 and pEGFP-N1-MITF-A were gifts from Shawn Ferguson (Addgene plasmid #38119, #38120 and #38132) (Roczniak-Ferguson et al., 2012). GFP-HTT exon1 Q74 cDNA was excised from pEGFP-Q74 (a gift from David Rubinsztein, Addgene plasmid #40262) (Narain et al., 1999) and inserted into pLVX-TetOne-puro vector (Clontech, Cat#: 631849). pTRE-tight and pEGFP-N1 vectors were from Clontech (Cat#: 631059 and 6085-1). lentiCRISPR v2 was a gift from Feng Zhang (Addgene plasmid #52961) (Sanjana et al., 2014).

The following sgRNA sequences were used in the experiments.

Human hMOF/KAT8 #1: CCTTCCCGCGATGGCGGCAC (Wang et al., 2014);
Human hMOF/KAT8 #2: GGCGGCACAGGGAGCTGCTG (Wang et al., 2014);
Human SIRT1: AGAGATGGCTGGAATTGTCC (Wang et al., 2014);
Human AMPK$\alpha$1/PRKAA1: AAGATCGGCCACTACATTCT (Wang et al., 2014);
Human AMPK$\alpha$2/PRKAA2: GCTGAGAAGCAGAAGCACGA (Wang et al., 2014);
Human ATG5: AAGAGTAAGTTATTTGACGT (Designed using Optimized CRISPR Design (http://crispr.mit.edu);
Non-targeting control (NTC): GTAGCGAACGTGTCCGGCGT (Wang et al., 2014).

pLKO.1-non-targeting control (NTC) (Sigma-Aldrich, Cat#: SHC002) and pLKO.1-shG9a #1 and #2 (Dharmacon, Cat#: TRCN0000115670 (#1) and TRCN0000115668 (#2)) were purchased from Sigma-Aldrich and Dharmacon, respectively. pTRIPZ-non-targeting control (NTC) (Cat#: RHS4743) and shBRD4 (Cat#: V3THS326487) were purchased from Dharmacon.

### Lentivirus and Retrovirus Production and Infection

Lentiviral plasmids were transfected into HEK293T cells together with packaging and envelope plasmids (psPAX2 and pMD2.G) using Lipofectamine2000 (Thermo Fisher Scientific, Cat#: 11668027) or Genejuice (EMD Millipore, Cat# 70967). At 2 days after transfection, the medium was passed through a 0.45 $\mu$m pore filter and mixed with Polybrene (Sigma-Aldrich, Cat#: H9268). The medium containing lentiviruses was transferred to the recipient cells. HEK293T cells were further cultured in fresh medium for 24 hr. After 6 hr of infection, medium was changed. Next day, infection was repeated as above. After lentivirus infection, cells were selected with 1 $\mu$g/ml of Puromycin (Sigma-Aldrich, Cat#: P9620) or 5 $\mu$g/ml of Blasticidin (Thermo Fisher Scientific, Cat# R21001) for 5-10 days. For retrovirus production, retroviral plasmids were transfected into Phoenix-AMPHO cells (ATCC, Cat#: CRL-3213) using Lipofectamine2000 or Genejuice. Retrovirus infection was carried out as described above.

### Immunofluorescence and Confocal Imaging

Cells seeded on coverslips (VWR 16mm, Thickness No.1, Cat# 631-0152) were fixed with 4% PFA/PBS (Electron microscopy science, Cat#: 1570) at RT for 15 min followed by permeabilization with 0.1% Triton X-100/PBS. For LC3 and WIPI2 staining, cells were fixed and permeabilized in 100% ice-cold methanol at $-20^{\circ}$C for 15min. After incubation in blocking solution (3% BSA/PBS) at room temperature for 1hr, cells were incubated with primary antibody at 4$^{\circ}$C overnight. Cells were washed in PBS three times and stained with 2 $\mu$g/ml Hoechst33342 (Thermo Fisher Scientific, Cat#: H3570) for 15min at room temperature, followed by wash in PBS three times. Cells were then incubated with Anti-rabbit IgG-Alexa 488 (Thermo Fisher Scientific, Cat#: A11008, 1/1000) or Anti-mouse IgG-Alexa 568 (Thermo Fisher Scientific, Cat#: A11031, 1/1000) for 1hr at room temperature. After cells were washed with PBS four times, the coverslips were mounted onto glass slides using Fluorescent Mounting Medium (DAKO, Cat#: S3023). To visualize acidic lysosome compartments, cells were stained with LysoTracker Red DND-99 (Thermo Fisher Scientific, Cat# L7528, 100 nM, 2 hr). To measure lysosomal Cathepsin B activity, cells were incubated with Magic Red CathepsinB (ImmunoChemistry Technologies, Cat#: 938) for 1 hr according to the manufacturer's instructions. After incubation with LysoTracker Red or Magic Red CathepsinB, cells were fixed in 4% PFA/PBS for 15 min at room temperature. Cells were then washed in PBS five times followed by staining with 2 $\mu$g/ml Hoechst33342 for 15 min at room temperature. Cells were washed with PBS four times and the coverslips were mounted onto glass slides using Fluorescent Mounting Medium. All confocal images were acquired and processed using a Zeiss 710 confocal microscope (Zeiss) and Zen2010 software (Zeiss). The number of LC3 and WIPI2 puncta were counted using

CellProfiler software (http://cellprofiler.org) and normalized to the number of nuclei. The area of LAMP-1-, LysoTracker Red-, and Magic Red CathepsinB-positive compartments was measured using ImageJ64 software (https://imagej.nih.gov/ij/) and normalized to the number of nuclei.

### Immunohistochemistry

Transgenic mice harboring inducible Renilla luciferase and BRD4 shRNAs whose expression is under the control of TRE promoter were generated as described previously using the same shRNA sequences (Bolden et al., 2014). Briefly ESCs containing a homing cassette at the Col1a1 locus were targeted with TRE-driven single-copy shRNAs and mice were generated by blastocytst injections. Resulting F1 mice were crossed to the CAG-rtTA3 strain (Premsrirut et al., 2011). Doxycycline was administered to 6-8 week old TRE-shRen/CAG-rtTA3 or TRE-shBRD4/CAG-rtTA3 mice via 625 mg/kg doxycycline-containing food pellets (Harlan Teklad) for 2 weeks. JQ1 preparation and administration were performed as described previously (Bolden et al., 2014). JQ1 powder was dissolved in DMSO to generate a concentrated 50 mg/mL stock solution. For administration to animals, a working solution was generated by diluting 1 part of the concentrated JQ1stock drop-wise into 9 parts 10% 2-(Hydroxypropyl)-β-cyclodextrin (Sigma-Aldrich, Cat#: C0926). C57BL/6 mice received once daily intraperitoneal injections of 100 mg/kg JQ1 for 2 weeks. Tissues were harvested and fixed overnight in 10% neutral buffered formalin, followed by paraffin embedding and sectioning as described previously (Bolden et al., 2014). All experimental procedures were approved by, and adhered to guidelines of, the Memorial Sloan Kettering Cancer Center institutional animal care and use committee.

Paraffin embedded sections were placed in Xylene for 5 min, 100% Ethanol for 1 min twice, 70% Ethanol for 1 min, and deionized water for 5 min. Antigen retrieval was performed in PT Module using Sodium citrate retrieval buffer pH 6 (Thermo Scientific, Cat#: TA-250-PM1X) at 98°C for 25 min followed by wash with Tris buffered saline and tween 20 (TBST) (Thermo Scientific, Cat#: TA-999-TT). The sections were then blocked for endogenous peroxidase using Peroxidase-blocking solution (Dako, Cat#: S2023) for 5 min followed by wash with TBST. The sections were incubated with LC3B (NanoTools, Cat#: 0231-100/LC3-5F10, 1/50) or BRD4 (Bethyl Laboratories, Cat#: A301-985A50, 1/2000) antibody diluted in Antibody diluent (Dako, Cat#: S2022) for 35 min. After wash with TBST twice, the sections were incubated with EnVision+ HRP, Mouse or Rabbit (Dako, Cat#: K4001 and K4003) for 30 min followed by wash with TBST twice. The sections were incubated with 3,3′-Diaminobenzidine tetrahydrochloride (DAB) (Dako, Cat#: K3468) for 10 min, washed with deionized water for 1 min, stained with Haematoxylin Z (CellPath, Cat#: RBA-4201-00A) for 7 min, washed with deionized water for 1min, differentiated in 1% Acid alcohol, washed with deionized water for 30 s, incubated in Scott's tap water substitute for 1 min, and washed with deionized water for 1 min. The sections were dehydrated, cleaned, and mounted with DPX. Images were acquired using a Zeiss Axio Scope.A1 microscope (Zeiss) and ZEN 2012 software (Zeiss).

To measure LC3 lipidation levels in BRD4 knockdown and JQ1-treated mice, proteins were extracted from formalin-fixed paraffin-embedded (FFPE) tissues using Qproteome FFPE Tissue Kit (QIAGEN, Cat#: 37623). Total protein concentration was determined by Bradford assay (Bio-Rad, Cat#: 500-0201). The cell extracts were mixed with 6x SDS-PAGE sample buffer and heated at 99°C for 5 min. The same amount of protein (20-30 μg) was loaded and run on SDS-PAGE. To confirm BRD4 knockdown, total RNA was isolated from FFPE tissues using RNeasy FFPE kit (QIAGEN, Cat#: 73504) followed by RT-qPCR analysis described below.

### RNA Sequencing

KP-4 cells were transfected with Control #1, BRD4 #1, or BRD4 #2 siRNA for 72 hr. At 72 hr after transfection, total RNA was isolated and purified using RNeasy mini kit (QIAGEN, Cat#: 74104). Quality of the purified RNA was assessed using an Agilent RNA 6000 Nano kit and 2100 Bioanalyzer. Libraries for cluster generation and DNA sequencing were prepared following an adapted method from (Fisher et al., 2011) using TruSeq RNA Sample Prep Kit v2 (Illumina, Cat#: RS-122-2001). Quality and quantity of the DNA libraries were assessed on an Agilent 2100 Bioanalyser and Qubit (Thermo Fisher Scientific), respectively. The libraries were run on the Illumina Next Seq 500 using the High Output 75 cycles kit (2x36 cycles, paired end reads, single index). The results were then analyzed as follows. Quality checks on the raw RNA-Seq data files were conducted using fastqc (https://www.bioinformatics.babraham.ac.uk/projects/fastqc/) and fastq_screen (http://www.bioinformatics.babraham.ac.uk/projects/fastq_screen/). RNA-Seq reads were aligned to the GRCh37 (Church et al., 2011) version of the human genome using tophat2 version 2.0.10 (Kim et al., 2013) with Bowtie version 2.1.0 (Langmead and Salzberg, 2012). Expression levels were determined and statistically analyzed by a combination of HTSeq version 0.5.4p3 (http://www-huber.embl.de/users/anders/HTSeq/doc/overview.html), the R 3.1.1 environment, utilizing packages from the Bioconductor data analysis suite and differential gene expression analysis based on a generalized linear model using the DESeq2 (Love et al., 2014). Enrichment analysis for Gene Ontology terms within this gene set was performed using g:Profiler (Reimand et al., 2011).

### RNA Isolation, Reverse Transcription, and Quantitative PCR (RT-qPCR)

The total RNA was isolated and purified using the RNeasy mini kit (QIAGEN, Cat#: 74104). 1 μg of total RNA was reverse-transcribed using the High-Capacity RNA-to-cDNA Kit (Applied Biosystems, Cat# 4387406) at 37°C for 1 hr. 1 μL of cDNA from 20 μL reaction volume was used for qPCR. qPCR was run on a StepOnePlus (Applied Biosystems) using Fast SYBR Green Master Mix (Applied Aiosystems, Cat#: 4385617). mRNA levels were determined by the relative standard curve method, normalized to 18S, GAPDH, or HPRT levels, and presented as relative mRNA levels. qPCR analyses were done in triplicate. Experiments were repeated at least twice. Primers are listed in Table S2.

CellPress

### Co-immunoprecipitation

Cells were lysed in cell lysis buffer (20 mM HEPES-KOH pH 7.5, 150 mM NaCl, 2 mM EDTA, 1% Triton X-100) containing Halt protease inhibitor cocktail (Thermo Fisher Scientific, Cat#: 78430). Lysates were incubated with 1 μg of antibody or control rabbit or mouse IgG (Cell Signaling Technology, Cat#: 2729S and 5415S) at 4°C overnight followed by incubation with 50 μL of Dynabeads Protein G (Thermo Fisher Scientific, Cat# 10004D) for 3 hr. After washing 3 times with cell lysis buffer containing 0.05% NP-40, immunoprecipitates were resuspended in 1x SDS-PAGE sample buffer and resolved by SDS-PAGE followed by western blot analysis.

### Chromatin Immunoprecipitation

Approximately $7x10^6$ cells were fixed with 1% Formaldehyde (Sigma-Aldrich, Cat#: F8775) at room temperature for 10 min and quenched by adding Glycine at a final concentration of 125 mM. Cells were then harvested and lysed in 500 μL of ChIP lysis Buffer (50 mM Tris-HCl pH8.0, 5 mM EDTA, 150 mM NaCl, 0.5% Triton X-100, 0.5% SDS, 0.5% NP-40, 1 mM Sodium butylate) containing Halt protease inhibitor cocktail. The lysates were subjected to sonication to shear DNA to the length of approximately between 150 and 900 bp using a Bioruptor (Diagenode). 300 μL of the lysate were then diluted in 1.2 mL of ChIP dilution buffer (50 mM Tris-HCl pH8.0, 5 mM EDTA, 150 mM NaCl, 0.5% Triton X-100, 0.5% NP-40, 1 mM Sodium butylate) containing Halt protease inhibitor cocktail, and incubated with control IgG (Cell Signaling Technology, Cat#: 2729S) or primary antibody together with 50 μL of Dynabeads protein G (Thermo Fisher Scientific, Cat# 10004D) at 4°C overnight. The beads were washed sequentially with the following buffers: ChIP dilution buffer, high salt wash buffer twice (50 mM Tris-HCl pH8.0, 5 mM EDTA, 600 mM NaCl, 0.5% Triton X-100, 0.5% NP-40), LiCl wash buffer twice (10 mM Tris-HCl pH 8.0, 250 mM LiCl, 1 mM EDTA, 0.5% NP-40, 0.5% sodium deoxycholate), ChIP dilution buffer, and wash buffer 4 (10 mM Tris-HCl, pH 8.0, 0.1% NP-40). The immunocomplexes were eluted with 75 μL of elution buffer (1% SDS, 0.1 M $NaHCO_3$) twice at 65°C for 30 min. After elution, the cross-link was reversed by adding NaCl to a final concentration of 200 mM and incubated together with Proteinase K (Thermo Fisher Scientific, Cat#: EO0491) for 6 hr at 65°C. 3M Sodium acetate solution pH5.2 (Thermo Fisher Scientific, Cat#: R1181) was added to the eluate to lower pH. DNA fragments were purified with the QIAquick PCR purification kit (QIAGEN, Cat#: 28104). The purified DNA was analyzed on a StepOnePlus using Fast SYBR Green Master Mix. The results are presented as percentage of input. qPCR analyses were done in triplicate. Experiments were repeated at least twice. Primers are listed in Table S2.

### RNAi in *Drosophila* S2R+ cells

Culture of *Drosophila* S2R+ cells, generation of S2R+ cells stably expressing GFP-LC3, delivery of control luciferase and Fs(1)h dsRNAs into GFP-LC3 expressing S2R+ cells, and subsequent confocal microscopic analysis were described previously (Wilkinson et al., 2011).

### β-Hexosaminidase Assay

Lysosomal β-Hexosaminidase activity was measured as described in (Chauhan et al., 2013). An equal number of KP-4 cells ($3x10^5$ cells) were lysed in 50 μL of 0.1% Triton X-100 containing Halt protease inhibitor cocktail. 20 μL of the cell extracts were then incubated with 1 mM 4-Nitrophenyl N-acetyl-β-D-glucosaminide (p-NAG) (Sigma-Aldrich, Cat#: N9376) at 37°C for 1.5 hr. The reaction was stopped by adding 0.1 M Carbonate/bicarbonate (Sigma-Aldrich, Cat#: C3041). The amount of the reaction product was measured by reading the absorbance at 405nm.

### Aggrephagy

Effects of BRD4 knockdown and overexpression on aggrephagy were examined as described in (Bauer et al., 2010). KP-4 cells harboring rtTA and Tre-tight-HTT Q94-CFP were treated with 1 μg/ml of Doxycycline (DOX) for 10 hr. Cells were then washed with PBS three times and cultured in fresh medium. At 48 hr after removal of DOX, cells were lysed in cell lysis buffer and separated into Triton X-100 soluble and insoluble fractions. Triton X-100 insoluble fraction was washed with lysis buffer three times. Triton X-100 soluble fraction was mixed with 6x SDS-PAGE sample buffer and Triton X-100 insoluble fraction was resuspended in 1x SDS-PAGE sample buffer followed by SDS-PAGE and western blot. To determine the effect of mutant HTT on cell number, HTT exon1 Q74 was overexpressed in cells as described in (Williams et al., 2008). KP-4 cells infected with pLVX-TetOne-GFP-HTT Q74 and control parental cells were treated with 100 ng/ml DOX for 60 hr. Cell number of mutant HTT expressing cells was normalized to that of parental cells and presented as percentage of reduction in cell number upon mutant HTT induction. Cell number of KP-4 pLVX-GFP-HTT Q74 and parental control cells was comparable in the absence of DOX (data is shown in Figure S6K first lane).

### Mitophagy

Effects of BRD4 knockdown and overexpression on mitophagy were examined as described in (Baudot et al., 2015). KP-4 cells stably expressing YFP-parkin were treated with 1 μM of Antimycin A and Oligomycin for 8 hr. Degradation of mitochondrial proteins was monitored as a readout for mitophagy.

### Xenophagy

KP-4 cells were plated in triplicates at $8x10^4$ cells in 6-well plates and reverse-transfected with 20 nM of siRNAs using Lipofectamine RNAiMAX. Infection with *Salmonella enterica* serovar Typhimurium (strain 12023) was performed 48 hr after siRNA transfection as described previously (McEwan et al., 2015b). Therefore, an overnight (stationary) culture of *Salmonella* was diluted 1:33 and incubated for 3 hr at 37°C prior to infection. The culture was diluted 1:250 to infect cells and *Salmonella* were allowed to invade cells for 15 min. Afterward, cells were washed with EBSS and incubated for 1 hr in media containing 100 μg/ml gentamycin. Media was replaced with 20 μg/ml gentamycin thereafter. To enumerate intracellular *Salmonella*, cells were lysed 2, 6 or 8 hr post infection in PBS with 0.1% Triton X-100. Lysates were serial diluted and plated in duplicates on Agar plates.

### Cell Proliferation and Cell Death Assays

For EdU staining, KP-4 cells were treated with 10 μM EdU for 2 hr before fixation. Cells were then subjected to EdU staining using Click-iT EdU Flow Cytometry Assay Kit (Thermo Fisher Scientific, Cat#: C10633). Samples were then stained with FxCycle PI/RNAase staining solution (Thermo Fisher Scientific, Cat#: F10797) and analyzed on a FACSCalibur (BD Biosciences). Percentage of EdU positive cells was calculated using FlowJo software. Cell number was determined by using a CASY cell counter (Roche Innovatis) or by Trypan blue exclusion test using Trypan blue solution (Sigma-Aldrich, Cat#: T8154). To determine the sub G1 population, cells were fixed with 10% methanol followed by staining with 50 μg/ml Propidium iodide (Sigma-Aldrich, Cat#: P4170) containing 50 μg/ml RNase A (QIAGEN, Cat#: 19101). Cells were then analyzed on a FACSCalibur using BD CellQuest Pro software (BD Biosciences).

## QUANTIFICATION AND STATISTICAL ANALYSIS

### Quantification of Western Blotting

Quantification of western blotting was performed using ImageJ64 software (https://imagej.nih.gov/ij/) using Gel analyzer script. Signal intensity of the protein of interest was normalized to that of loading control (GAPDH, Hsp90, or β-actin).

### Quantification of Microscopic Images

The number of LC3 and WIPI2 puncta were counted using CellProfiler software (http://cellprofiler.org) and normalized to the number of nuclei. The area of LAMP-1-, LysoTracker Red-, and Magic Red CathepsinB-positive compartments was measured using ImageJ64 software (https://imagej.nih.gov/ij/) and normalized to the number of nuclei.

### Quantification of the qPCR Results

Target mRNA levels were determined by relative standard curve method, normalized to 18S, GAPDH, or HPRT levels, and presented as relative mRNA levels compared to control. StepOne software (Applied Biosystems) was used to analyze the data.

### Statistical Analyses

All studies were performed on at least three independent occasions. Results are shown as mean ± SD unless mentioned otherwise. Statistical significance was determined by two-tailed unpaired Student's t test for two group comparison and one-way ANOVA with Tukey or Dunnett for multiple group comparison using GraphPad Prism 7 (GraphPad software). P values $< 0.05$ were considered significant. Significance in all figures is indicated as follows: * $p < 0.01$, ** $p < 0.05$, N.S.: no significance.

## DATA AND SOFTWARE AVAILABILITY

The raw and processed data of the RNA-Seq have been deposited in Gene Expression Omnibus under GEO: GSE90444. Full scans of western blot data and original microscopy images have been deposited in Mendeley Data (http://dx.doi.org/10.17632/ksz4pmwkdb.1).

Check for updates

# SIK2 orchestrates actin-dependent host response upon *Salmonella* infection

Marcel Hahn[a], Adriana Covarrubias-Pinto[a], Lina Herhaus[a], Shankha Satpathy[b,1], Kevin Klann[a], Keith B. Boyle[c], Christian Münch[a], Krishnaraj Rajalingam[d], Felix Randow[c], Chunaram Choudhary[b], and Ivan Dikic[a,e,2]

[a]Institute of Biochemistry II, Goethe University School of Medicine, 60590 Frankfurt am Main, Germany; [b]Department of Proteomics, The Novo Nordisk Foundation Center for Protein Research, Faculty of Health and Medical Sciences, University of Copenhagen, Blegdamsvej 3B, Copenhagen 2200, Denmark; [c]Division of Protein and Nucleic Acid Chemistry, Medical Research Council (MRC) Laboratory of Molecular Biology, CB2 0QH Cambridge, United Kingdom; [d]Cell Biology Unit, University Medical Center of the Johannes Gutenberg University Mainz, 55131 Mainz, Germany; and [e]Buchmann Institute for Molecular Life Sciences, Goethe University Frankfurt, 60438 Frankfurt, Germany

Edited by Vishva M. Dixit, Genentech, San Francisco, CA, and approved April 1, 2021 (received for review November 20, 2020)

**_Salmonella_ is an intracellular pathogen of a substantial global health concern. In order to identify key players involved in _Salmonella_ infection, we performed a global host phosphoproteome analysis subsequent to bacterial infection. Thereby, we identified the kinase SIK2 as a central component of the host defense machinery upon _Salmonella_ infection. SIK2 depletion favors the escape of bacteria from the _Salmonella_-containing vacuole (SCV) and impairs Xenophagy, resulting in a hyperproliferative phenotype. Mechanistically, SIK2 associates with actin filaments under basal conditions; however, during bacterial infection, SIK2 is recruited to the SCV together with the elements of the actin polymerization machinery (Arp2/3 complex and Formins). Notably, SIK2 depletion results in a severe pathological cellular actin nucleation and polymerization defect upon _Salmonella_ infection. We propose that SIK2 controls the formation of a protective SCV actin shield shortly after invasion and orchestrates the actin cytoskeleton architecture in its entirety to control an acute _Salmonella_ infection after bacterial invasion.**

*Salmonella* | actin cytoskeleton | Arp2/3 complex | host–pathogen interactions | *Salmonella*-containing vacuole

*Salmonella enterica* is a gram-negative, facultative intracellular human pathogen, annually causing more than 100 million food- and waterborne infections worldwide. *Salmonella* Typhimurium causes severe gastroenteritis, which could turn into a systemic infection in children, immune-compromised, or elderly people (1, 2). Concurrently, multidrug resistant bacteria are globally emerging and threatening our health systems, calling for a better understanding of the underlying virulence mechanism and host response.

Pathogenic bacteria have evolved the inherent ability to infect and to establish their niche within host cells. For colonizing nonphagocytic cells such as epithelial cells, *Salmonella* uses a trigger mechanism–based entry mode. Bacterial virulence factors are then injected via a Type III-secretion system (T3SS) into the host cell to induce cytoskeletal rearrangements leading to membrane ruffling and macropinocytosis-driven internalization into a sealed phagosome (3, 4). This specialized compartment is referred to as the *Salmonella*-containing vacuole (SCV) and serves as the intracellular replicative niche by hiding the bacteria from the humoral and cell-autonomous immune response (5). *Salmonella* invasion requires a cooperative action of several bacterial effector proteins hijacking multiple host targets. One of the main targets forcing *Salmonella*´s uptake is the actin cytoskeleton by subverting the host Rho GTPases system. Bacterial effector proteins such as SopE/SopE2 mimic host nucleotide exchange factors (GEFs) to stimulate Rac1 and CDC42 activity (6, 7). Once GTP-activated, Rho GTPases stimulate downstream pathways to drive actin filament (F-actin) assembly and rearrangement.

The actin cytoskeleton network is regulated by actin-binding proteins (ABPs), which orchestrate assembly and disassembly of actin in higher networks (8). Monomeric, globular actin (G-actin) is nucleated into new actin filaments, or the existing F-actin is elongated, stabilized, or disassembled by ABPs. The major actin nucleation factor is the multimeric Arp2/3 complex, which generates branched actin filament networks. Formins generate long unbranched actin filaments and represent another actin nucleation family. Together with actin nucleation-promoting factors, small Rho GTPases control ABPs in a spatiotemporal manner. Actin polymerization and membrane ruffling are necessary for *Salmonella* invasion. Following *Salmonella* internalization, the SCV undergoes SPI-1–dependent biogenesis and is transported to a juxtanuclear position at 1 to 2 h postinfection (pi). At later time-points (4 to 6 h pi), SPI-2–dependent effector proteins are expressed to further mature the SCV, allowing bacterial proliferation. Pioneering work described that, at later stages of the infection (≥6 h pi), an actin meshwork around the SCV stabilizes and protects the vacuolar niche (9–13).

Here, we report SIK2 as a *Salmonella* resistance factor and a regulator of the actin cytoskeleton. SIK2 belongs to the AMPK kinase family and was named after its homolog SIK1, found to be expressed upon high-salt diet-induced stress in rats (14, 15). SIK2 has been implicated into multiple biological roles including melanogenesis, cancer progression, and gluconeogenesis (16–18). SIK2 depletion results in a loss of SCV integrity and bacterial escape into the host cytosol, causing intracellular *Salmonella* hyperproliferation. Notably, SIK2 depletion results in a severe pathological cellular

## Significance

**Through conducting quantitative proteomics upon *Salmonella* infection, we identified a SIK2 signaling network, implementing the kinase into a so far concealed biological function. Our data exposed SIK2 as a central orchestrator of an actin regulatory network, coordinating the stability of *Salmonella*-containing vacuole (SCV) and cellular actin assembly, in order to limit the acute phase of the infection. Most strikingly, SIK2 is not exclusively acting locally on actin assembly associated with the SCV but impacts the actin cytoskeleton architecture in its entirety upon *Salmonella* infection. Our work provides a mechanistic framework for how the actin cytoskeleton is regulated and how it helps to control an acute *Salmonella* infection.**

Author contributions: M.H. and I.D. designed research; M.H., A.C.-P., L.H., and S.S. performed research; K.B.B., K.R., and F.R. contributed new reagents/analytic tools; M.H., S.S., K.K., C.M., and C.C. analyzed data; and M.H. and I.D. wrote the paper.

The authors declare no competing interest.

This article is a PNAS Direct Submission.



[1]Present address: Broad Proteomics, Broad Institute of Massachusetts Institute of Technology and Harvard, Cambridge, MA 02142.

[2]To whom correspondence may be addressed. Email: dikic@biochem2.uni-frankfurt.de.

This article contains supporting information online at https://www.pnas.org/lookup/suppl/doi:10.1073/pnas.2024144118/-/DCSupplemental.

Published May 4, 2021.

BIOCHEMISTRY

actin nucleation and polymerization defect upon *Salmonella* infection. Hence, SIK2 may represent a cellular safeguard, which controls the actin cytoskeleton and SCV integrity, thereby serving as a prime regulator of *Salmonella* proliferation subsequent to cellular internalization.

## Results

**Quantitative Phosphoproteomics in *Salmonella*-Infected Epithelial Cells.** In order to shed light on the signaling pathways underlying the *Salmonella* infection, we performed quantitative phosphoproteomics. HCT116 cells were metabolically labeled with stable isotope labeling of amino acid in cell culture (SILAC), allowing the relative quantification of peptides by high-resolution mass spectrometry (MS). To this end, we used a triple-SILAC labeling in which "light"-labeled cells were left uninfected and "heavy"- and "medium"-labeled cells were infected with *Salmonella* and subsequently analyzed (30 min or 2 h pi) (Fig. 1*A*). In total, we quantified around 17,900 phosphosites from 4,200 proteins that were modified in minimum two out of four experimental replicates. At 30 min pi, the up-regulation of phosphorylation events was most pronounced (Fig. 1 *B* and *C*). Across all experimental replicates, we mapped 964 phosphosites displaying $\log_2$ (heavy:light) ratios of $\geq$0.58 indicating a 1.5-fold increase; 626 proteins and 742 phosphosites with $\log_2$ (heavy:light) ratios of $\leq$0.58 indicating a 1.5-fold decrease; and 481 proteins at 30 min pi (Fig. 1*B*). Significant $\log_2$ values represent a $P$ value of $\leq$ 0.05. To obtain a general understanding of the host phosphoproteome changes upon *Salmonella* infection, we standardized the data set (*z*-score) and displayed relative changes of phosphopeptides in a heatmap (Fig. 1*D*). Our data indicates an acute modulation of phosphorylation events in various signaling pathways shortly after a *Salmonella* infection (Fig. 1*E*). Pathway analyses of the up-regulated functional interaction network 30 min pi revealed extensive remodeling of Rho GTPases, like CDC42- and/or Rac1-signaling (Fig. 1*E*). Among these, we identified over 20 proteins belonging to the Rho GTPase network (e.g., ARHGAP5 and ARHGEF2/11/12), confirming this distinct signaling network as a major target of *Salmonella* at early time points pi (19, 20). An additional functional analysis exhibited a direct association between bacterial invasion and the Rho GTPase pathway as a major cluster in our phosphoproteome data set (*SI Appendix*, Fig. S1*A*). Members of tumor necrosis factor (TNF)- and nucleotide-binding oligomerization domain (NOD)-like receptor signaling were also overrepresented pi (Fig. 1*E*) (*SI Appendix*, Fig. S1*A*). Among them were several components of the MAPK/IKK-pathway, followed by pattern recognition receptor activation. We validated the key phosphosites of these pathways using phospho-specific antibodies against components of the MAPK-signaling cascade (*SI Appendix*, Fig. S1 *B* and *C*). NOD-like receptors are intracellular PPRs, which recognize bacterial peptidoglycan and SopE-mediated Rho GTPase activation and represent one of the main proinflammatory pathways activated by *Salmonella* infection (21, 22). Our MS data confirm previously published results, indicating that NF-κB-signaling sets a proinflammatory state to dampen bacterial proliferation in host cells (23).

**SIK2 Signaling Network Is Triggered upon *Salmonella* Infection.** Analyzing the reproducible and significantly regulated phosphorylation sites 30 min pi, we identified and confirmed the innate immunity kinase TAK1 (MAP3K7) as a central target of *Salmonella*-induced phosphosite modulation (24, 25). Strikingly, we identified the AMPK-related kinase SIK2 as a target of potential similar importance (Fig. 1*F*). We found SIK2 to be phosphorylated at S117, which represents a phosphorylation site within the kinase domain. Since AMPK-related kinases are poorly characterized and SIK2 has not yet been associated with *Salmonella* infection, we focused on the

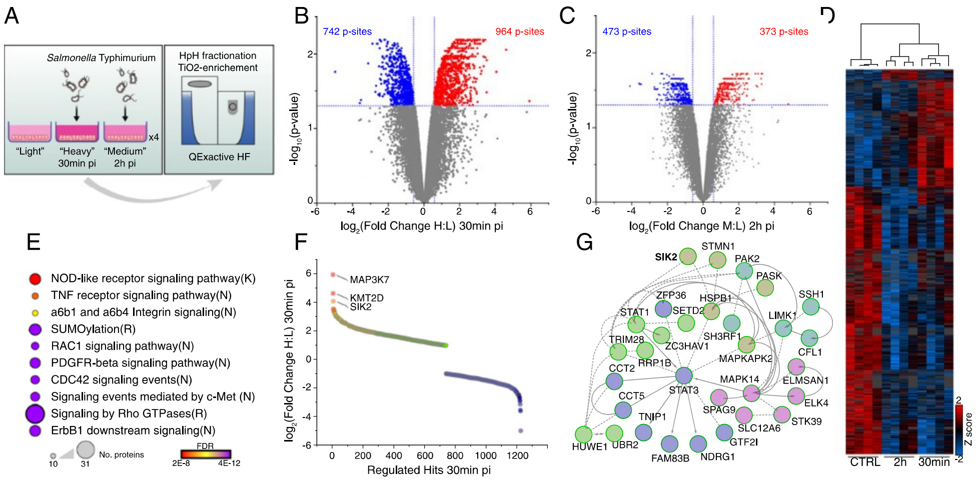


**Fig. 1.** Global host phosphoproteome reveals SIK2 signaling network upon *Salmonella* infection. (*A*) The phosphoproteome workflow for 30 min and 2 h pi ($n$ = 4). (*B*) Volcano plot showing relative phosphorylation changes 30 min pi versus noninfected. Log2 ratios were plotted against −log10 $P$ values. (*C*) Volcano plot showing relative phosphorylation changes 2 h pi versus noninfected. Log2 ratios were plotted against −log10 $P$ values. (*D*) Heatmap and hierarchical clustering summarizing results from Fig. 1*A*. *Z*-Scores were calculated and hierarchical clustering performed using Euclidean distance between the samples. Only ANOVA-significant peptides were used ($P$ value $\leq$ 0.05). (*E*) Reactome pathway analysis of proteins with up-regulated phospho-sites 30 min pi (log2 $\geq$ 1 and $P$ value $\leq$ 0.05). Pathway results are shown with the number of proteins found in dataset and computed FDR for pathway enrichment (FDR < 0.001). (*F*) Scatter plot showing regulated phosphosites (log2 $\leq$1 or $\geq$ 1 and $P$ value $\leq$ 0.05) from 30 min pi. (*G*) Reactome FI-based SIK2-associated cluster analysis. Up-regulated hits from 30 min pi were FI annotated, clustered, and SIK2-associated cluster isolated.

SIK2-associated functional network in the same dataset (Fig. 1*G*). In this cluster, we identified several constituents of the Rac1-signaling network (Cofilin-1, PAK2, LIMK1, STAT3, and p38a) (Fig. 1*G*) (*SI Appendix*, Fig. S1*D*). Rac1-signaling is one of the major pathways targeted by SPI-1 *Salmonella* effector proteins to establish an intracellular niche within the host cell, enabling protected proliferation of bacteria (6, 7). This prompted us to further investigate the role of SIK2 during *Salmonella* infection.

**SIK2 Is Essential for Restriction of Intracellular *Salmonella* Proliferation.** To test whether SIK2 is required for antibacterial defense in epithelial cells, we used short interfering RNAs (siRNA) to deplete cells of SIK2 (*SI Appendix*, Fig. S2*A*). Cells lacking SIK2 failed to restrict proliferation of bacteria within the SCV (Fig. 2*A*). This phenotype was characterized by bacterial hyperproliferation rather than bacterial hyper-invasion (Fig. 2*B*). The hyperproliferation of intracellular *Salmonella* was already evident at 6 h pi and increased further at 8 h pi. The phenotype was confirmed by an alternative second siRNA targeting SIK2, which depletes SIK2 protein levels as well (*SI Appendix*, Fig. S2*B*). To further characterize the phenotype, we generated a functional HA-SIK2 doxycycline-inducible HeLa cell line, resistant to anti-SIK2 siRNAs. To obtain SIK2 expression levels mimicking endogenous levels, we titrated the doxycycline concentration (*SI Appendix*, Fig. S2*C*). Using a low concentration of doxycycline, we observed a full phenotypic rescue by re-expressing SIK2 wild-type levels (Fig. 2*C*). Thus, wild-type SIK2 controls *Salmonella* infection and functions as a central host defense kinase. Next, we investigated whether besides SIK2 expression, SIK2 kinase activity is required for restricting *Salmonella* proliferation. To this end, we generated a HeLa cell line expressing an inducible and SIK2-siRNA–resistant kinase-inactive (K49A) HA-SIK2. Again, we titrated the doxycycline concentration to mimic endogenous protein levels (*SI Appendix*, Fig. S2*D*). Expression of the kinase-inactive mutant failed to restrict bacterial proliferation (Fig. 2*D*). Therefore, the kinase activity of SIK2 is mandatory to limit bacterial proliferation during an acute infection. By using Phos-Tag gels, we were able to validate the phosphorylation of SIK2 directly following bacterial infection at 15 min pi and at 30 min at endogenous levels (*SI Appendix*, Fig. S2 *E* and *F*). The phosphorylation of SIK2 appeared independent of its kinase activity, suggesting a transphosphorylation event of SIK2 by an unidentified up-stream kinase, which was not investigated further (*SI Appendix*, Fig. S2*E*). Notably, we observed at 2 h pi an increase in the phosphorylation status of the wild-type kinase, in contrast to



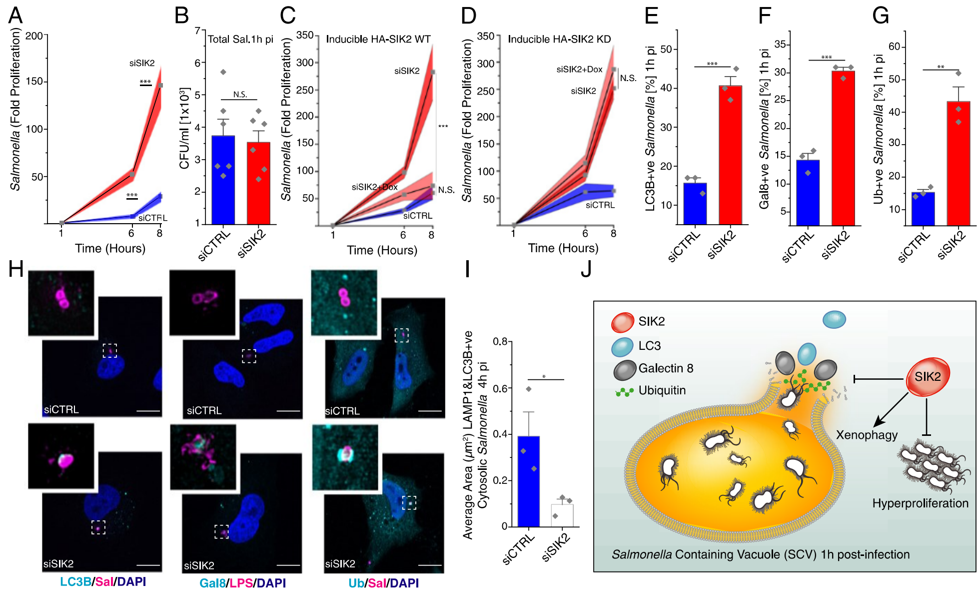


**Fig. 2.** SIK2 is essential for restriction of intracellular *Salmonella* proliferation. (*A*) Kinetics of intracellular *Salmonella* replication in HeLa cells. (*B*) *Salmonella* burden at 1 h pi in HeLa cells. Data are depicted as total CFU/mL at 1 h pi and presented as means + SEM, $n = 3$. (*C*) Kinetics of intracellular *Salmonella* replication in HeLa cells expressing HA-SIK2 wild type under a doxycycline-inducible promotor. (*D*) Kinetics of intracellular *Salmonella* replication in HeLa cells expressing HA-SIK2 kinase–deficient (K49A) under a doxycycline-inducible promotor. (*E*) Quantification of LC3B-positive *Salmonella* from Fig. 2*H*. (*F*) Quantification of Galectine8-positive *Salmonella* from Fig. 2*H*. (*G*) Quantification of Ubiquitin-positive *Salmonella* from Fig. 2*H*. (*H*) Immunofluorescence of siRNA-transfected and *Salmonella*-infected HeLa cells 1 h pi. Cells were stained for endogenous LC3B or Galectine8 or Ubiquitin (ubiquitin FK2 antibody), *Salmonella* (anti-*Salmonella* common structural antigens (CSA) or anti-*Salmonella* lipopolysaccharides (LPS) antibody) and DAPI. Images are maximum intensity projections of confocal z-stacks. (Scale bar, 10 μm.) (*I*) HeLa cells were siRNA transfected and infected with *Salmonella* SFH2 4 h pi. Cells were stained for LC3B and LAMP1. Average area (micrometers squared) of colocalization of both markers on cytosolic (GFP+-ve) *Salmonella* was quantified. (*J*) Model of observed SIK2 depletion phenotype in HeLa cells 1 h pi. SIK2 depletion results in loss of SCV integrity and favors bacterial escape from the vacuole into the host cytosol, resulting into *Salmonella* hyperproliferation. (*A*–*D*) Bacteria were counted on the basis of their ability to form colonies on agar plates. (*A*, *C*, and *D*) Data are depicted as fold proliferation normalized to 1 h pi and presented as means ± SD, $n = 3$, and $^{***}P \leq 0.001$ as analyzed by Student's *t* test. (*E*–*G* and *I*) Data presented as mean + SEM, $n = 3$, >100 bacterial counts per condition, $^{***}P \leq 0.001$, $^{**}P \leq 0.01$. and $^{*}P \leq 0.05$ as analyzed by Student's *t* test. (*C* and *D*) Gene expression was induced with 100 ng/mL doxycycline for 24 h preinfection. (*A*–*I*) Cells were transfected with nontargeting control- and anti-SIK2 siRNA.

the kinase-inactive version, indicating a cis-phosphorylation (*SI Appendix*, Fig. S2*E*). By using a SPI-1 deletion *Salmonella* strain, we showed that the phosphorylation depends on SPI-1 effector proteins (*SI Appendix*, Fig. S2*F*). To further investigate SIK2 phosphorylation, we made use of GFP-SopA– and GFP-SopE–inducible HeLa cell lines to test whether these SPI-1 effector proteins mediate SIK2 activation (*SI Appendix*, Fig. S2*G*). Our data indicates that SIK2 is being phosphorylated in a SopE-dependent manner and activated further during the early phase of a *Salmonella* infection.

**SIK2 Controls SCV Integrity and Bacterial Evasion.** To understand the SIK2 depletion phenotype, we studied the fate of intracellular bacteria using confocal microscopy. The autophagy modifier LC3B selectively targets autophagic cargo (such as bacteria) to the autophagosome to promote it's autophagic degradation. Therefore, we monitored endogenous LC3B recruitment to *Salmonella* 1 h pi. In accordance with literature (26), siCTRL-transfected cells showed an LC3B–*Salmonella* colocalization rate of ∼15%. In contrast, cells depleted of SIK2 showed a significantly higher percentage of LC3B-positive *Salmonella* (close to 40%) (Fig. 2 *E* and *H*). Using Galectin-8 as a marker of vesicle, endosomal, or lysosomal integrity revealed a significant increase in Galectin-8–positive *Salmonella* after depleting SIK2 from cells (Fig. 2 *F* and *H*). Using ubiquitin as an alternative damage marker, we confirmed this finding (Fig. 2 *G* and *H*). Thus, SIK2 depletion causes SCV damage, enabling enhanced bacterial access to the host cytosol. To study the fate of cytosolic bacteria, we used a *Salmonella* strain expressing green fluorescent protein (GFP) only, when exposed to the host cytosol, controlled by a glucose-6-phospate–inducible promoter (27). By studying endogenous LC3B and LAMP1 recruitment at 4 h pi, we found significant less colocalization of both markers on cytosolic bacteria after SIK2 depletion (Fig. 2*I*). SIK2 ensures the integrity of the SCV, thus preventing *Salmonella* from entering the host cytosol in HeLa cells, in which bacterial hyperproliferation occurs (28). Furthermore, SIK2 is required for autolysosome formation and therefore for the degradation of cytosolic bacteria via the autophagy–lysosomal system (Fig. 2*J*).

**Recruitment of SIK2 upon Infection to Actin Cytoskeleton Network.** To understand the role of SIK2 during the course of a *Salmonella* infection, we tagged endogenous SIK2 with an HA tag at its C terminus in a HeLa cell line, using CRISPR/Cas12–assisted PCR-tagging (29). This cell line was used for immunoprecipitation and subsequent quantitative TMT-based mass spectrometry (IP-MS) (Fig. 3*A*). Under basal, noninfected conditions we were able to identify 21 significant interaction partners of SIK2, which fulfilled our stringent criteria (Fig. 3*B*). As expected, the bait SIK2 was the most enriched protein. Among the SIK2-interacting partners were the Rho GTPase CDC42, ACTBL2 encoding kappa-actin, CLTB/Clathrin light chain B, TPM2/Tropomyosin-beta, MYL3/Myosin light chain 3, and CORO1C/Coronin-1C, pointing toward a potential role in the basal cytoskeleton dynamics (Fig. 3*B*). Upon *Salmonella* infection, the SIK2 interactome profile changed to a much higher degree of complexity, and we observed 175 cointeracting partners of SIK2. This indicates that SIK2 is recruited to a larger protein interactome at 1 h pi (Fig. 3*C*). To rule out technical reasons for this increased complexity, we plotted the fold-changes of uninfected versus infected samples on a scatter plot. Our data demonstrated equal immunoprecipitation of SIK2 in both settings and a pronounced shift in the interactome triggered by *Salmonella* infection (*SI Appendix*, Fig. S3*C*). Functional pathway analysis of the SIK2 interactome upon infection revealed strong enrichment of bacterial/*Salmonella* infection pathway components, such as Rho GTPases and the regulation of the actin cytoskeleton (Fig. 3*D*) (*SI Appendix*, Fig. S3*A*). The hits from both categories were clustered hierarchically, revealing that SIK2 is interacting with the entire Arp2/3 complex (Arp2/ACTR2, Arp3/ACTR3, p41/ARPC1A&B, p34/ARPC2, p21/ARPC3, p20/ARPC4, and p16/ARPC5) and additional known modulators of this complex, such as CDC42, CTTN/Cortactin, and IQGAP1 (Fig. 3*E*) (*SI Appendix*, Fig. S3*B*) (30). Arp2/3 complex represents the main F-actin nucleation factor generating branched actin networks (31, 32). We also identified the Formin FMNL2 as another actin nucleation factor, required for linear actin polymerization (33). Additionally, several factors encoding type II myosin like MYH9, MYH11, MYH14, and molecular constituents involved in actin stress fiber formation (e.g., ACTN1&4/α-actinin, FLNA/Filamin-A, CALD1/Caldesmon and Tropomyosin) were identified (Fig. 3*E*) (*SI Appendix*, Fig. S3 *A* and *B*) (34). Together with F-actin bundles, myosins form actin stress fibers, which are stabilized by α-actinin (35).

Functional pathway analysis revealed SIK2 recruitment to well-known *Salmonella* targets, such as the Arp2/3 complex, Filamin-A, or type II myosin (MYH9 and MYH10), forming the basis for functional categorization, such as "*Salmonella* infection (K)" (Fig. 3*D*) (*SI Appendix*, Fig. S3*A*). Upon *Salmonella* infection, SIK2 is recruited to a central actin hub and to a large number of essential factors for *Salmonella* colonization within the host cell (36, 37). To verify the IP-MS results, we used the same set-up as described before and performed a hemagglutinin (HA) immunoprecipitation (IP), followed by sodium dodecyl sulphate–polyacrylamide gel electrophoresis (SDS-PAGE) and Western blot. We were able to confirm the *Salmonella*-dependent recruitment of SIK2 to actin, cortactin, and the Arp2/3 complex (ARPC2) under endogenous settings (Fig. 3*F*). In additional IP results, we demonstrated the interaction of SIK2 with FMNL2 and actin under basal, noninfected conditions.

**Impact of SIK2 on the Actin Cytoskeleton during Infection.** Since the SIK2 kinase activity is required to rescue the siRNA-mediated hyperproliferative phenotype, we explored pathways/networks regulated by SIK2 upon *Salmonella* infection. To this end, we established a SIK2-dependent TMT-based phosphoproteome screen in HeLa cells, in which siRNA-transfected cells were lysed at 30 min pi. Extracted proteins were digested, TMT 16–plexed and used for iron-nitrilotriacetic acid complex (Fe-NTA) phosphopeptide enrichment (Fig. 4*A*). A principal component analysis (PCA) showed clustering of the respective replicates, which was further analyzed by a Pearson-based column correlation (*SI Appendix*, Fig. S4 *A* and *B*). To illustrate changes in the phosphoproteome under basal and infection conditions, we calculated *z*-scores and hierarchically clustered the ANOVA-significant phosphopeptides fulfilling our stringency criteria (Fig. 4*B*). The data showed a strong effect of SIK2 depletion in the global phosphoproteome, as already evident in the PCA (*SI Appendix*, Fig. S4*A*). Since the endogenous SIK2 interactome already revealed significant changes upon *Salmonella* infection, we were looking for an infection- and SIK2-dependent cluster in the phosphoproteome (Fig. 4*B*). Cluster I identifies peptides exhibiting reduced phosphorylation status, whereas cluster II exhibits those with an increased phosphorylation status upon *Salmonella* infection after SIK2 depletion. The overall cluster profile, however, did not change and was not significantly different from control settings (*SI Appendix*, Fig. S4*C*). To understand the infection-induced phosphorylation events, we performed a functional pathways cluster analysis (Fig. 4*C*). Most strikingly, the second most pronounced functional cluster was composed of a major fraction of genes regulating the actin cytoskeleton, which runs in parallel to the cluster "signaling by RhoGTPases (R)" (Fig. 4*C*). Given the background of the endogenous, infection-triggered SIK2 interactome, we filtered cluster I and II to identify all cytoskeleton components. From this information we were able to construct a dense protein–protein network centered around the cytoskeleton elements (Fig. 4*D*). To narrow down the impact of SIK2 on the cytoskeleton, we calculated the intersection between phosphoproteome clusters I and II and the endogenous SIK2 interactome at 1 h pi (Fig. 4*E*). Notably, almost one-third of the whole interactome

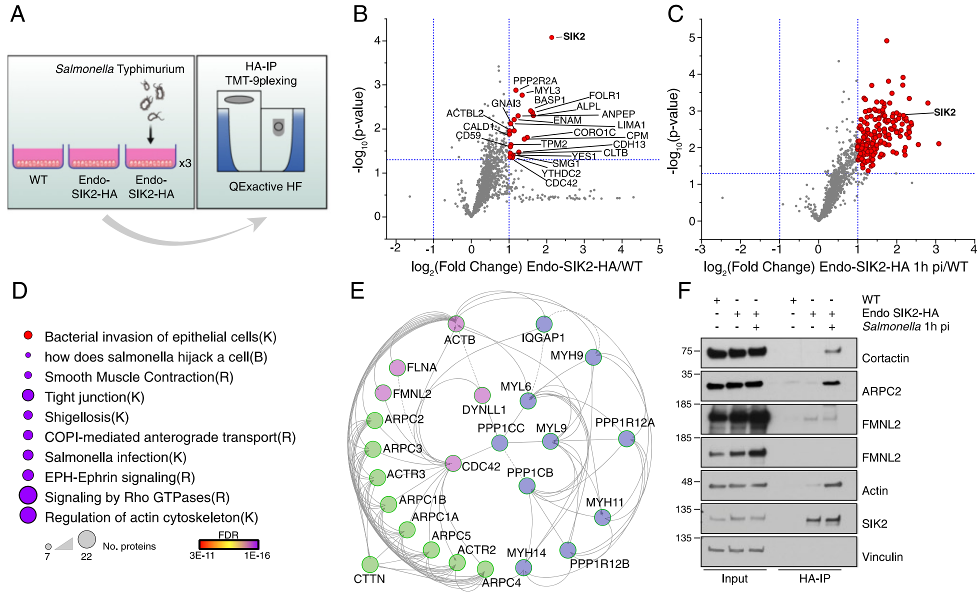


**Fig. 3.** Recruitment of SIK2 upon infection to an actin cytoskeleton hub. (*A*) The endogenously tagged SIK2-HA IP workflow. HeLa wild-type or endogenous SIK2-HA–tagged HeLa cells were left uninfected or infected with *Salmonella* and analyzed 1 h pi ($n = 3$). (*B*) Volcano plot showing relative interaction partners between HeLa endogenous SIK2-HA versus HeLa wild type. Log2 ratios were plotted against −log10 *P* values. (*C*) Volcano plot showing relative interaction partners between HeLa endogenous SIK2-HA infected with *Salmonella* 1 h pi versus HeLa wild type. Log2 ratios were plotted against −log10 *P* values. (*D*) Reactome pathway analysis of regulated interactome of endogenous SIK-HA upon infection at 1 h pi (log2 ≥ 1 and *P* value ≤ 0.05). Pathway results are shown with number of proteins found in dataset and computed FDR for pathway enrichment (FDR < 0.001). (*E*) Reactome FI-based cluster analysis. Endogenous SIK2-HA–interacting partners upon infection at 1 h pi were FI annotated, clustered, and pathway analyzed (q-value < 0.001). The most prominent pathway (from Fig. 3*D*: signaling by Rho GTPases [R]) was filtered and hierarchically clustered. (*F*) Endogenous SIK2-HA IP followed by SDS-PAGE and Western blotting. Lysates were probed with the indicates antibodies.

could be assigned to these phosphoproteome clusters. The cytoskeleton-associated intersection was then clustered hierarchically (Fig. 4*F*). These proteins showed a significantly altered phosphorylation pattern compared to control infection settings. Among these proteins, we found a cluster of proteins required for building up and stabilizing F-actin, including lamellipodia and stress fibers (e.g., ACTN4, FLNA, FNLB, ARPC1B, CTTN, MYO9, MYO10, CALD1/Caldesmon, EMD/Emerin, PDLIM1/Elfin, and LIMA1/EPLIN). Taken together, we identified a SIK2-interacting, actin cytoskeleton–centered network, which shows pronounced changes in the phosphorylation pattern upon SIK2 depletion and *Salmonella* infection.

**Endogenous SIK2 Is Colocalized with Actin Filaments and the SCVs.** To validate MS and biochemical data, we performed microscopic analysis of cells (MEFs) with a focus on endogenous localization of SIK2 (Fig. 3 *E* and *F*). SIK2 showed a localization in the cell periphery, forming foci with a linear arrangement (Fig. 5*A*). By costaining with Phalloidin, we found SIK2 to colocalize with F-actin–rich regions in MEFs. Thereby, SIK2 decorates polymerized actin fibers with distinct SIK2 foci in MEFs (Fig. 5*A*). The data showed SIK2 colocalizes with F-actin within the areas undergoing pronounced remodeling and/or de-novo assembly of the actin cytoskeleton under basal, noninfected conditions (Fig. 5 *A* and *B*). This finding raised the questions of the localization of SIK2 under an infection scenario. Therefore, we infected MEFs with *Salmonella* and stained for endogenous SIK2. Most strikingly, we found SIK2 to be recruited to *Salmonella* at 30 min pi, decorating the SCV (Fig. 5*B*) (*SI Appendix*, Fig. S5 *A* and *B*). The endogenous SIK2 localization was verified by two different anti-SIK2 antibodies (Fig. 5*B*) (*SI Appendix*, Fig. S5*A*). Quantitative analysis showed that more than 50% of the intracellular *Salmonella* colocalized with SIK2 at early time-points pi (*SI Appendix*, Fig. S5*C*). The SIK2 interactome revealed interactions with actin nucleation factors such as the Arp2/3 complex or well-established modulators of this complex, such as cortactin. Accordingly, we were able to show by microscopic analysis that these factors also colocalized with the SCV (*SI Appendix*, Fig. S5 *D* and *E*). This is in accordance with SIK2 being recruited to the SCV directly after cellular invasion and corecruitment to the actin network.

**SIK2 Impacts Actin Nucleation and Polymerization during *Salmonella* Infection.** To address the role of SIK2 in regulating the actin cytoskeleton, we depleted SIK2 by an siRNA approach in HeLa cells and stained for F-actin using Phalloidin. Under noninfected conditions, changes in the structure of the actin cytoskeleton compared to control cells are readily visible (*SI Appendix*, Fig. S5*F*). In contrast, after *Salmonella* infection, we observed significantly less F-actin in SIK2-depleted cells, suggesting a breakdown of actin polymerization upon infection (*SI Appendix*, Fig. S5*G*). Overall, cortical actin structures and actin stress fibers were dramatically reduced in SIK2-depleted cells; however, the

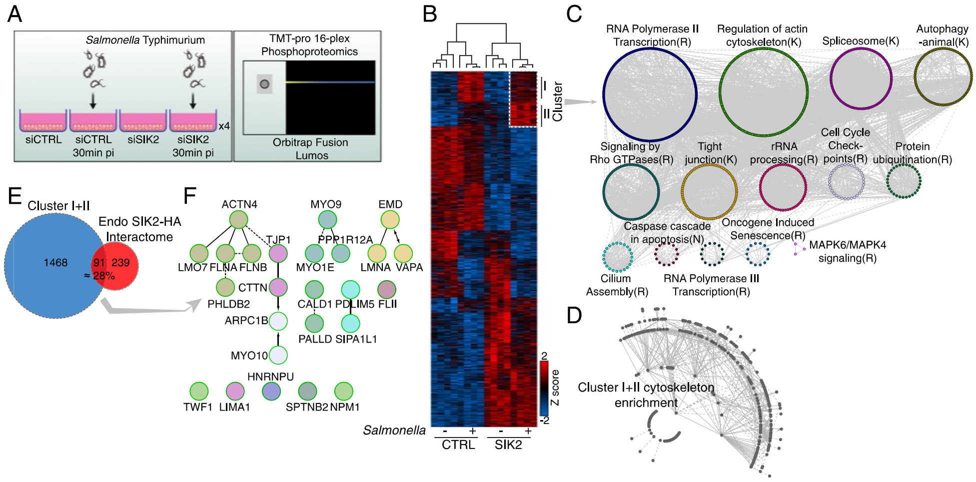


**Fig. 4.** Impact of SIK2 on the actin cytoskeleton during infection. (*A*) SIK2-dependent phosphoproteomics workflow ($n = 4$). (*B*) Heatmap and hierarchical clustering summarizing results from Fig. 4*A*. *Z*-Scores were calculated and hierarchical clustering performed using Euclidean distance between the samples. Only ANOVA-significant peptides were used (*P* value $\leq 0.05$). (*C*) ReactomeFI cluster analysis of proteins isolated from cluster I and II. Proteins were FI annotated, clustered, and clusters analyzed for significantly enriched Reactome pathways (q-value < 0.001). A representative pathway of each cluster is indicated. Connecting lines show interaction of protein nodes. (*D*) STRING network analysis of proteins from cluster I and II. Network was filtered using cytoskeleton compartment filter (filter set to 3.0) in STRING and clustered. (*E*) Venn diagram of phosphoproteome cluster I and II and regulated interacting proteins from the endogenous SIK2-HA interactome upon infection (log2 $\geq 0.5$ and *P* value $\leq 0.05$). (*F*) Intersection of Fig. 4*E* was loaded into STRING and filtered using cytoskeleton compartment filter (filter set to 3.0) and clustered.

microtubules (visualized by tubulin staining) remained unaffected (*SI Appendix*, Fig. S5*H*). To corroborate the observed defects in actin polymerization, we were able to mimic the microscopic phenotype of SIK2 depletion after *Salmonella* infection by using 2 μM of the actin polymerization inhibitor Cytochalasin B for 30 min (*SI Appendix*, Fig. S5*I*). Using a confocal microscopic quantitative image cytometer platform and subsequent automated analysis, we were able to validate these findings (Fig. 5*C*). Further biochemical analysis by separating G- and F-actin showed higher levels of G-actin after SIK2 depletion in cells (*SI Appendix*, Fig. S5*J*). This indicates that SIK2 depletion under basal conditions and particularly in combination with *Salmonella* infection phenocopies a strong actin nucleation and polymerization defect. By using the inducible HA-SIK2 HeLa cell line, resistant to SIK2 siRNAs, we tested whether we can phenotypically rescue the actin polymerization defect upon *Salmonella* infection. In accordance with the *Salmonella* proliferation assay, we were only able to phenotypically rescue actin polymerization with HA-SIK2 wild type, whereas the kinase inactive mutant failed to rescue the phenotype (Fig. 5*D*). Thus, SIK2 kinase activity is controlling F-actin formation and rearrangements. Overall, our data show that SIK2 is an actin cytoskeleton–modulating effector protein, which is activated upon *Salmonella* infection and recruited to the actin hub centered around the Arp2/3 complex to control F-actin formation in the cell and especially around the SCV in an early phase of *Salmonella* infection.

## Discussion

The actin cytoskeleton is central to cell-autonomous immunity during bacterial infections (22). In the present study, we identified a role of SIK2 as a host-defense kinase, regulating the actin cytoskeleton upon *Salmonella* entry into the host cell and restricting the intra-SCV proliferation of *Salmonella*. Our data from cell systems, working at the endogenous protein levels, indicate that SIK2 represents a central orchestrator of the actin regulatory network, coordinating SCV stability and cellular actin assembly, in order to limit the acute phase of the infection.

To gain access into epithelial cells, *Salmonella* injects effector proteins via its T3SS to modulate the host cytoskeleton by inducing membrane ruffling, resulting in bacterial uptake. SopE and SopE2 are central to *Salmonella*-induced activation of Rac1 and CDC42 by molecularly mimicking host GEFs (7, 38). In addition, SopB, a phosphoinositide phosphatase, is essential for *Salmonella* invasion and activation of RhoG (20). Activated Rac1 and CDC42 recruit the WAVE-regulatory complex to induce the Arp2/3 complex–dependent F-actin polymerization (39, 40). Notably, two *Salmonella* effectors (SipA and SipC) are direct actin-binding proteins, which results in the nucleation and bundling of the actin filaments (41, 42). To ensure spatiotemporal actin rearrangements, *Salmonella* reverses the effects of SopE via the GTPase-activating protein (GAP) SptP, thus normalizing the actin cytoskeleton (43). This study identifies SIK2 as an actin effector protein, controlling F-actin polymerization and limiting the intracellular proliferation of bacteria by restricting it to the SCV. We show that SopE mediates SIK2 phosphorylation and activation. However, it remains unknown how SopE exactly activates SIK2, probably through the exploitation of anther host kinase. Given the high similarity with SopE, it is certainly possible that SopE2 might as well trigger SIK2 phosphorylation. Both effector proteins activate directly Rac1 and CDC42, although with different GEF activities and stimulate p21-activated kinase (PAK) signaling, which might be upstream of SIK2 activation.

During a *Salmonella* infection, the SIK2 interactome profile dramatically changes and recruits SIK2 to a dense actin-regulating network, centered around CDC42, the Arp2/3 complex, and actin

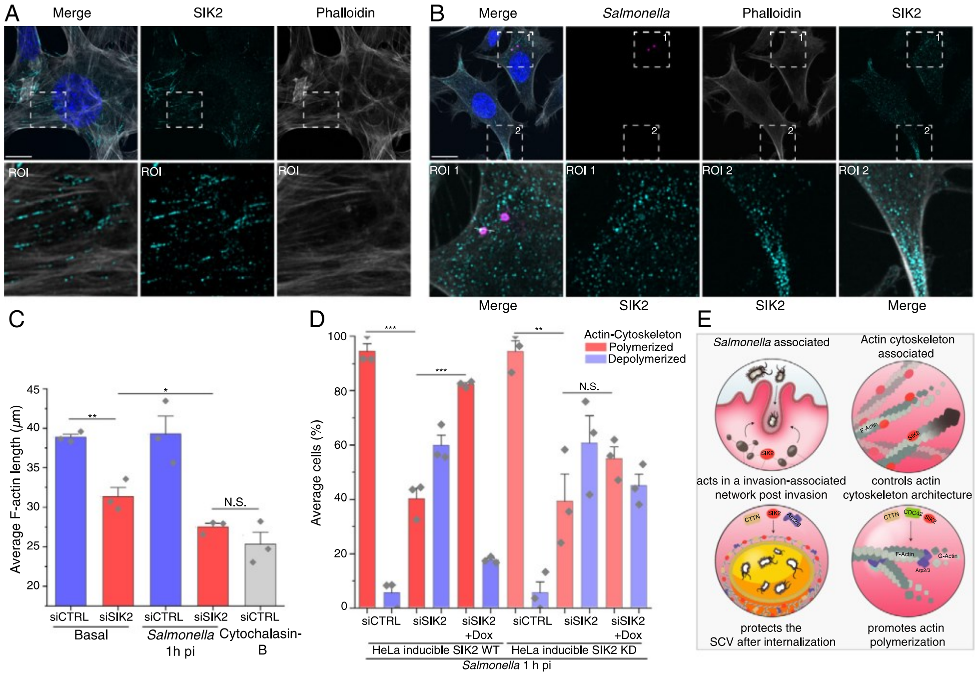


**Fig. 5.** SIK2 is required for the actin cytoskeleton integrity. (*A*) Immunofluorescence of MEFs stained for endogenous SIK2, Phalloidin, and DAPI. (*B*) Immunofluorescence of MEFs infected with *Salmonella* 30 min pi and stained for endogenous SIK2, *Salmonella* (anti-*Salmonella* CSA antibody), Phalloidin, and DAPI. (*C*) Quantification of Phalloidin-stained F-actin length. HeLa cells were siRNA transfected and infected with *Salmonella* 1 h pi and stained with Phalloidin, Tubulin, *Salmonella*, and DAPI and quantitively analyzed. Cells transfected with control siRNA were treated with Cytochalasin B (2 μM) for 30 min where indicated. Data presented as mean + SEM, $n = 3$, > 500 cell counts per condition, $^{**}P \leq 0.01$, and $^{*}P \leq 0.05$ as analyzed by Student's *t* test. (*D*) Quantification of phenotypic analysis of cells showing defective actin polymerization. HeLa cells expressing HA-SIK2 wild type or SIK2 K49A under a doxycycline-inducible promotor were transfected with siCTRL or siSIK2, $^{-/+}$ doxycycline, and infected with *Salmonella* 1 h pi. Cells were stained with Phalloidin and DAPI and phenotypically analyzed by confocal microscopy. Data presented as mean + SEM, $n = 3$, 100 cell counts per condition, $^{***}P \leq 0.001$, and $^{**}P \leq 0.01$ as analyzed by Student's *t* test. (*E*) Proposed functions of SIK2 upon *Salmonella* infection. (*A* and *B*) Images are maximum intensity projections of confocal z-stacks. (Scale bar, 10 μm.)



stabilization factors. The Arp2/3 complex, Formins, type II myosins, IQGAP, and CDC42 are all required for the efficient *Salmonella* invasion (37, 44, 45). This event was not affected by SIK2 depletion. In contrast, we were able to demonstrate that SIK2 acts at a later stage of infection.

It is intriguing to recognize that SIK2 takes on a central role in the *Salmonella* invasion–associated network, in which it assumes a different function acting on the SCV postinvasion. This is supported by our findings, which show that SIK2 depletion is causing bacterial hyperproliferation rather than bacterial hyper- or hypoinvasion. SIK2 is recruited to the SCV shortly after the invasion, in which it colocalizes with the elements of the actin machinery. Based on our data, we propose a model of SIK2-induced actin de novo synthesis around the SCV, which may establish a protective shield to prevent the evasion of bacteria out of the SCV and into the cytosol or SCV fusion that may establish a larger intracellular compartment for bacterial proliferation. Furthermore, SIK2 depletion impairs fusion of the autolysosome with cytosolic bacteria. The combination of enhanced SCV escape into the cytosol and the impaired lysosomal degradation of cytosolic bacteria leads to a fatal cellular outcome, resulting into hyperproliferative *Salmonella*. Strikingly, SIK2 is not acting exclusively on the local actin assembly associated with SCV but impacts the actin cytoskeleton architecture in its entirety (*SI Appendix*, Fig. S6). We demonstrated that SIK2 binds actin under the basal conditions and decorates filamentous actin in fibroblasts and in the areas undergoing rearrangements (e.g., Lamellipodia or actin stress fibers). In this process, FMNL2 (FHOD2) may represent, along with FHOD1, the second Formin playing a crucial role in *Salmonella* infection process (46). FMNL2 is critical for Lamellipodia and stress fiber formation and may act cooperatively with the Arp2/3 complex in the analogy to previous reports for other Formins (47, 48). SIK2 deletion results in reduction of filamentous actin, an effect which becomes even more pronounced upon *Salmonella* infection, resulting in a major defect in actin polymerization.

SIK2 is a central regulator/modulator of actin assembly and polymerization, with its role becoming most prominent upon *Salmonella* infection. Our work provides mechanistic insights into the regulation of the actin cytoskeleton and its role in controlling the acute *Salmonella* infection (Fig. 5*E*).

These results provide a solid foundation for the future work that will focus on understanding the molecular dynamics of the protein–protein interaction, in order to precisely delineate and define the temporal regulation of the early SIK2-controlled events of the intracellular propagation of *Salmonella*. What remains to be defined are the direct substrates of SIK2 and how these substrate interactions relate to the observed, here described, effects on actin assembly/formation.

It is unknown whether SIK2 activation also protects against other intracellular intruders. Upon *Chlamydia* infection, the cytoskeletal network surrounding and stabilizing the bacterial vacuole hours after the invasion has been reported (49). After *Salmonella* infection, an actin meshwork around the SCV assembles in a SPI-2 (SteC)–dependent manner (≥6 h pi) (9–13). Here we report that SIK2 acts directly postinvasion in a SPI-1 (SopE)–dependent way to build up an actin shield around the SCV. In addition, the more recent work reported an analogous actin network, which builds up a cocoon-like actin structure after *Shigella* infection. The *Shigella*-triggered actin network (e.g., Arp2/3 complex, CDC42, and Cortactin) protects the bacterial vacuole and seems to function as a gatekeeper (50, 51). In contrast to *Salmonella*, *Shigella* actively destabilizes the SCV to help escape into the host cytosol <10 min pi (52, 53). It may be interesting to analyze the role of SIK2 upon *Shigella* infection and compare the sequence of molecular events in the early process pi between *Salmonella* and *Shigella*. This may help to obtain insights into potential targets valuable for therapeutic strategies and anti-bacterial defense of intracellular bacteria/parasites in general.

Studying the cellular host response to *Salmonella* infection identified SIK2 as a critical host defense kinase, which modulates a fundamental cellular process (e.g., F-actin polymerization) in a way that it limits intracellular proliferation of bacteria, may provide an exciting starting point for those future studies.

## Materials and Methods

**Bacterial Strains.** *S. enterica* serovar Typhimurium strain SL1344 (gift from David Holden, Imperial College London), SL1344 ΔSPI-1 described earlier (54) (gift from Jorge Galan, Yale School of Medicine), SL1344 puHpT-GFP (SFH2) expressing GFP when exposed to the host cytosol, controlled by a glucose-6-phospate–inducible promoter described earlier (27) (gift from Dirk Bumann, Biozentrum, University of Basel), and *S.* Typhimurium 12023 pFPV25.1-mCherry described earlier (55) (gift from Felix Randow, LMB) were used in this study.

***Salmonella* Culturing and Infections.** Single *Salmonella* colonies were picked from a lysogeny broth (LB) Agar plate and inoculated into 1 mL LB medium (plus the respective antibiotic) and grown overnight to a stationary phase at 37 °C. Next day, *Salmonella* was diluted 1:33 and grown for 3.5 h at 37 °C before infection. Cells were infected in antibiotic-free medium with a multiplicity of infection of 100 for 10 min and washed afterward twice with phosphate-buffered saline (PBS). Subsequently, cells were cultured further in medium containing 100 μg/mL Gentamycin for 1 h and thereafter reduced to 20 μg/mL Gentamycin for the remaining time of the experiment.

**Cell Lines.** HeLa, HCT116, HEK293T, MEFs, and HeLa Flp-In T-Rex GFP-SopA or GFP-SopE [described earlier (56, 57)] were grown in Iscove's Modified Dulbecco's Media (IMDM) or Dulbecco's Modified Eagle Medium (DMEM), supplemented with 10% fetal calf serum (FCS) (heat-inactivated at 56 °C for 30 min) and 20 μg/mL Gentamycin at 37 °C and 5% $CO_2$. All cell lines were routinely checked for mycoplasma infections using MycoAlert (Lonza). The cells were passaged two to three times a week and were used for experiments at passages between 2 to 35.

**Colony-forming unit (CFU) Assay.** HeLa cells were seeded in triplicates with $2 \times 10^4$ cells into a 24-well and siRNA-transfected in antibiotic-free medium. The experiment was performed 48 to 72 h posttransfection. After the infection, cells were washed with PBS and cultured with Gentamycin-containing medium. At 1, 6, or 8 h pi, cells were lysed in 0.1% (vol/vol) Triton X-100 in PBS and serial diluted in PBS. Diluted lysates were plated in technical duplicates on Agar plates and incubated for colony formation overnight at 37 °C. The number of colonies (within the linear range of the assay) was enumerated using a colony counter apparatus and software (aCOLyte 3, Synbiosis).

**SDS-PAGE and Immunoblotting.** Cells were washed twice with cold PBS and lysed in Lysis Buffer (50 mM Hepes, pH 7.5, 150 mM NaCl, 1 mM EDTA, 1 mM EGTA, 1% Triton X-100, 25 mM NaF, 5% glycerol, and 10 μM ZnCl2) or SDS Lysis Buffer (30 mM Tris·HCl, pH 7.4, 120 mM NaCl, 2 mM EDTA, 2 mM KCl, 0.5% CHAPS, 1% SDS, 50 mM NaF, and 5 mM Na3VO4) supplemented with complete protease inhibitors (cOmplete, EDTA-free; Roche Diagnostics) and phosphatase inhibitors (P5726, P0044; Sigma-Aldrich). Cell lysates were cleared by spinning at 20,000 g for 15 min at 4 °C in a centrifuge. Cell extracts were incubated with SDS sample buffer (50 mM Tris·HCl, pH 6.8, 10% glycerol, 2% SDS, 0.02% bromophenol blue, and 5% β-mercaptoethanol) and heated at 95 °C for 5 min. Samples were loaded onto 4 to 20% precast gradient Gels (BioRad) or self-casted 8% or 10% acrylamide gels and separated by SDS-PAGE. Proteins were plotted by wet-\ transfer onto a Nitrocellulose or PVDF membrane and blocked with 5% low-fat milk or 5% bovine serum albumin (BSA) in Tris-buffered saline (TBS) (150 mM NaCl, 20 mM Tris, and pH 8.0) for 1 h. Primary antibodies were diluted in 5% BSA in TBS-T (TBS + 0.1% Tween 20) and secondary antibodies in 5% low-fat milk in TBS-T.

**Protein Immunoprecipitation.** Following cell lysis under nondenaturing conditions, cleared cell extracts were incubated with Lysis Buffer–equilibrated antibody-coupled resin. Therefore, HA agarose beads (Sigma-Aldrich) were used and incubated with lysates for 2 h at 4 °C on a rotating platform. Protein-bound beads were washed four times with Lysis Buffer. Immunoprecipitated and input samples were reduced in SDS sample buffer and heated at 95 °C for 5 min.

**G-Actin/F-Actin Fractionation.** G-actin and F-actin fractions were extracted from HeLa cell lysates by ultracentrifugation at 100,000 rpm using the G-actin/F-actin in vivo assay biochem kit (Cytoskeleton, Inc., BK037) according to the manufacture protocol. The levels of G-actin and F-actin were quantified by Western blotting using the anti-actin antibody provided in the kit.

**Immunofluorescence, Confocal Microscopy.** Cells were seeded on glass coverslips and washed after the treatment twice with PBS before fixation with 4% paraformaldehyde in PBS for 10 min. Cells were permeabilized with 0.2% (vol/vol) Triton X-100 in PBS for 10 min and blocked with 5% BSA in PBS for 1 h. Primary and secondary (including 4′,6-diamidino-2-phenylindole [DAPI] and Phalloidin) antibodies were incubated in 5% BSA in PBS for 1 h with three PBS washes in between. Before mounting in Mowiol (Sigma), cells were washed three times and once with distilled water. Images were acquired on a Leica TCS SP8 microscope with a 63× oil immersion objective. For an automatic quantitive analysis, images were taken using the Yokogawa CQ1 confocal quantitative image cytometer platform (63× magnification). Cells were seeded onto black, clear flat-bottom 24-well plates and stained with indicated antibodies. The images were analyzed using the CQ1 Yokogawa CellPathfinder, high-content analysis software with the built-in plugin for cytoskeleton fiber detection. DAPI and Tubulin staining were used for determining the cell body of each cell.

**CRISPR/Cas12-Assisted PCR Tagging.** Endogenous tagging was performed as described (29) and on http://www.pcr-tagging.com. Briefly, the PCR cassette was amplified from pMaCTag-P27 (1 × HA) plasmid in combination with M1_SIK2_fwd and M2_SIK2_AsCpf1_TATV_rev primer using a Velocity polymerase (Bioline) and High-Fidelity (HiFi) buffer (20 mM Tris·HCl, pH 8.8, 10 mM $[NH_4]_2SO_4$, 50 mM KCl, 0.1% [vol/vol] Triton X-100, 0.1 mg/mL BSA, and 2 mM $MgCl_2$) on a gradient PCR cycler. The PCR product was gel purified with GeneJET Gel Extraction Kit. HeLa cells were transiently transfected with 1 μg of the PCR cassette and 1 μg pcDNA3.1-hAsCpf1(TATV) (pY220) using GeneJuice (Merck Millipore) according to the manufacture protocol and selected with 0.5 μg/mL Puromycin 72 h posttransfection.

**Lentiviral Transduction and Cell Line Generation.** HEK293T cells were cotransfected with the lentiviral plasmid (pLTD N-term HA cloned with SIK2 WT or SIK2 K49A) together with the packaging vectors pPAX2 and pMD2. The medium containing the lentivirus was exchanged after 24 h, and after another 24 h, medium was collected for transduction of the recipient cells. Recipient cells were transduced with 1 mL of the virus containing medium with polybrene (8 μg/mL; Sigma-Aldrich, H9268-5G). Cells were selected 48 h posttransduction with 1 μg/mL Puromycin.

**RNA Interference.** Cells were transfected 24 h postseeding with 20nM siRNA (ON TARGETplus anti-SIK2 siRNA [Horizon Discovery] and AllStars Negative Control siRNA [Qiagen]) using Lipofectamine RNAiMAX (Life Technologies) according to the manufacture protocol. Experiments were performed 48 to

72 h posttransfection. Transfection efficiency was verified by Western blotting.

**Phos-Tag Gels.** Phos-tag acrylamide (Wako) gels were prepared and used according to manufactures protocol. Gels were prepared with 6% acrylamide, 25 μM Phos-tag reagent, and 100 μM MnCl2. Cells were lysed in SDS Lysis Buffer.

**SILAC-Based Phosphoproteomics.** HCT116 cells were grown in SILAC-DMEM (arginine and lysine-free medium), supplemented with dialyzed FCS (10%) and lysine (74 μg/mL) and arginine (42 μg/mL) as "light K0, R0," "medium K4, R6," or "heavy K8, R10." Cells were lysed in 6 M Guanidinhydrochlorid buffer (100 mM Tris HCL pH 8.5, 5 mM TCEP, and 10 mM chloracetamide), heated at 95 °C for 15 min, and sonicated with Sonics Vibra-Cell (1 s ON/1 s OFF pulse for 30 s using 30% amplitude). Phosphoproteomic analysis was performed as previously described (58). The cell lysates were diluted to 2 M guanidium hydrochloride with 50 mM Hepes buffer at pH 8.5 and incubated with Lys-C (1 ug for 100 ug protein lysate) for 2 h followed by further dilution to 1 M guanidium hydrochloride and overnight digestion with Trypsin (1 ug for 100 ug protein lysate). Peptides were desalted and quantified using bicinchoninic acid assay (BCA) assay. Equal peptide amounts from the three SILAC states were mixed at 1:1:1 ratio and dried down. This was followed by fractionation on a high-pH gradient into a total of 12 fractions. TiO2-based phospho-enrichment was performed, followed by data acquisition on a Q Exactive HF instrument.

**TMT Labeling.** After tryptic digestion peptides were cleaned up using Sep-Pak tC18 (Waters, 50 mg) according to the manufactures protocol. Peptides were resuspended into TMT-labeling buffer (0.2 M EPPS pH8.2 and 10% Acetonitrile) and peptide concentration determined by μBCA-assay (Thermo Fisher Scientific). Peptides were labeled with a 1:2 ratio (1mg peptide and 2 mg TMT reagent) with TMT reagents (Thermo Fisher Scientific, 90110 and A44520) for 1 h at room temperature (RT). The reaction was quenched with 0.5% (final concentration) hydroxylamine for 15 min at RT. Samples were multiplexed with equimolar ratios (unless stated otherwise) and cleaned up using Empore C18 (Octadecyl) resin material (3M Empore) as described earlier (59).

**TMT-Based Phosphoproteomics.** HeLa cells were lysed in (2% SDS, 50 mM Tris·HCl pH8, 150 mM NaCl, 10 mM TCEP, and 40 mM chloracetamide), heated at 95 °C for 10 min, and sonicated with Sonics Vibra-Cell (1 s ON/1 s OFF pulse for 30 s using 30% amplitude). Protein lysates were precipitated by methanol/chloroform using four volumes of ice-cold methanol, one volume of chloroform, and three volumes of water. The mixture was centrifuged at 20,000 g for 30 min, and the upper aqueous phase was removed and three volumes of ice-cold methanol added. Proteins were pelleted by centrifugation and washed twice with one volume of ice-cold methanol and air dried. The resulting protein pellet was resuspended in 8 M urea with 10 mM EPPS pH 8.2. Protein concentration was determined by Bradford assay. For digestion, 300 μg proteins were diluted to 1 M urea and incubated 1:50 with LysC (Wako Chemicals) for 3 h and 1:100 with sequencing grade trypsin (Promega) overnight. The reaction was acidified using TFA (0.5%) and purified using Sep-Pak tC18 (Waters, 50 mg) according to manufacturer's protocol. A total 100 μg of peptides were TMT labeled and channels adjusted to equimolar ratios as jugged by single-injection measurements by liquid chromatography (LC)-mass spectrometry (MS). Ratio-adjusted peptides were multiplexed and used for phosphopeptide enrichment using High-Select Fe-NTA Phosphopeptide Enrichment Kit (Thermo Fisher Scientific) according to manufactures protocol. Phosphopeptides were cleaned up by C8 stage tip and fractionated using C18 stage tips. After washing (80% acetonitrile) and equilibration step with 0.1% TFA, peptides were loaded on C18 stage tips in 0.1% TFA solution and washed twice with 0.1% TFA in water. Peptides were fractionated into 16 fractions with an acetonitrile gradient from 2.5 to 50% in 0.1% Triethylamine and cross-concatenated into eight fractions. Samples were vacuum dried for LC-MS measurements.

**HA-IP, On-Bead Digest, and TMT Labeling.** Cells were lysed in 1% Triton X-100–based Lysis Buffer and incubated with HA agarose beads (Sigma) for 2 h at 4 °C on a rotating platform. Protein-bound beads were washed three times with Lysis Buffer and three times with Lysis Buffer without detergents. Samples were incubated with 25 μl SDC buffer (2% sodium deoxycholate [SDC], 1 mM TCEP, 4 mM chloracetamide, and 50 mM Tris pH 8.5) and heated at 95 °C for 10 min. Samples were mixed 1:1 with 500 ng LysC and 500 ng Trypsin (50 mM Tris and pH 8.5) and digested overnight at 37 °C. Reaction was stopped with 150 μl of isopropanol with 1% TFA. Peptides were cleaned up by loading them onto styrenedivinylbenzene-reverse phase sulfonate (SDB-RPS) (Empore) stage tips. After one wash with 1% TFA in isopropanol and one wash with 0.2% TFA in water, peptides were eluted using 80% acetonitrile and 1.25% ammonia. Eluted peptides were dried, TMT labeled, and processed for LC-MS measurements.

**Liquid Chromatography MS.** For Q Exactive HF: Peptides were separated on an easy nLC 1200 (Thermo Fisher) and a 15 cm long, 75 μm inner diameter (ID)-fused silica column, which has been packed in house with 1.9 μm C18 particles (ReproSil-Pur, Dr. Maisch), and kept at 45 °C using an integrated column oven (Sonation). Peptides were eluted by linear gradient from 5 to 38% acetonitrile over 120 min and directly sprayed into a Q Exactive HF mass spectrometer equipped with a nanoFlex ion source (Thermo Fisher Scientific) at a spray voltage of 2.3 kV. Full-scan MS spectra (350 to 1,400 m/z) were acquired at a resolution of 120,000 at m/z 200, a maximum injection time of 100 ms and an automatic gain control (AGC) target value of $3 \times 10^6$ charges. Up to 10 most intense peptides per full scan were isolated using a 1 Th window and fragmented using higher-energy collisional dissociation (normalized collision energy of 35). MS/MS spectra were acquired with a resolution of 60,000 at m/z 200, a maximum injection time of 128 ms, and an AGC target value of $1 \times 10^5$. Ions with charge states of 1 and >6 as well as ions with unassigned charge states were not considered for fragmentation. Dynamic exclusion was set to 20 s to minimize repeated sequencing of already acquired precursors. Enriched phosphopeptides were analyzed on a Q Exactive HF instrument coupled to nLC 1200. A 15 cm column was used as described above. For SILAC phosphoproteome analysis, the MS parameters are as follows: MS1: 60,000 resolution, AGC: 3e6, and injection time: 20 ms and MS2: resolution: 30,000, AGC: 1e5, injection time: 110 ms, and TOP N: 12.

Data were acquired in centroid mode on an Orbitrap Fusion Lumos mass spectrometer hyphenated to an easy nLC 1200 nano high-performance liquid chromatography (HPLC) system using a nanoFlex ion source (Thermo Fisher Scientific) applying a spray voltage of 2.6 kV with the transfer tube heated to 300 °C and a funnel radio frequency (RF) of 30%. Internal mass calibration was enabled (lock mass 445.12003 m/z). Peptides were separated on a self-made, 32 cm long, 75 μm ID-fused silica column, packed in house with 1.9 μm C18 particles (ReproSil-Pur, Dr. Maisch), and heated to 50 °C using an integrated column oven (Sonation). HPLC solvents consisted of 0.1% formic acid in water (Buffer A) and 0.1% formic acid, 80% acetonitrile in water (Buffer B). For phosphopeptide analysis, each peptide fraction was eluted by a linear gradient from 5 to 32% B over 120 min followed by a step-wise increase to 95% B in 8 min which was held for another 7 min. Full-scan MS spectra (350 to 1,400 m/z) were acquired with a resolution of 120,000 at m/z 200, maximum injection time of 100 ms, and AGC target value of 4 × 105. The 20 most intense precursors per full scan with a charge state between 2 and 5 were selected for fragmentation ("Top 20"), isolated with a quadrupole isolation window of 0.7 Th, and fragmented via high energy collision-induced dissociation (HCD) applying an normalized collision energy (NCE) of 38%. MS2 scans were performed in the Orbitrap using a resolution of 50,000 at m/z 200, maximum injection time of 86 ms, and AGC target value of 1 × 105. Repeated sequencing of already-acquired precursors was limited by setting a dynamic exclusion of 60 s and 7 ppm, and advanced peak determination was deactivated.

**MS Data Analysis.** Raw files were analyzed using Proteome Discoverer (PD) 2.4 software (Thermo Fisher Scientific). Spectra were selected using default settings and database searches performed using SequestHT node in PD. Database searches were performed against trypsin-digested Homo Sapiens SwissProt database and *Salmonella* typhimurium (strain LT2/SGSC1412/ATCC 700720) database. Static modifications were set as TMT6 at the N terminus and lysines and carbamidomethyl at cysteine residues. Search was performed using Sequest HT taking the following dynamic modifications into account: Oxidation (M), Phospho (S,T,Y), Met-loss (N-term), Acetyl (N-term), and Met-loss acetyl (N-term). For whole-cell proteomics, the same settings were used, except phosphorylation was not allowed as dynamic modification. For phosphoproteomics, all peptide groups were normalized by summed intensity normalization and then analyzed on peptide level. For whole-cell proteomics, normalized peptide-spectrum matches (PSMs) were summed for each accession and data exported for further use. For SILAC phosphoproteomics data, MaxQuant was used with default SILAC parameters. Methionine oxidation, N-terminal acetylation, and phosphorylation (pSTY) were used as the variable modifications.

**Significance Testing.** Statistical significance was assessed with two-sided Student's *t* test. *P* values ≤ 0.05 were considered as significant. Adjusted *P* values were corrected by Benjamini–Hochberg false discovery rate (FDR). Differences with $P \leq 0.05$ are annotated as *$P \leq 0.01$, **$P \leq 0.01$, and ***$P \leq 0.001$. $P > 0.05$ are annotated N.S. (not significant) Data are presented as the mean of replicates with error bars indicating the SD or SEM. For clustering and enrichment analyses (see below), q-value cutoffs of 0.001 were used for significance definition. N represents number of independent replicates.

BIOCHEMISTRY

**Hierarchical Clustering.** Hierarchical cluster analysis was performed using Perseus software (version 1.6.5.0) with default settings after centering and scaling of data (*z*-scores).

**Interaction Network and Pathway Enrichment Analysis.** Identified genes were analyzed with Cytoscape with plugins for ReactomeFI, STRING, and Omics-Visualizer. Pathway enrichment analysis was performed by ReactomeFI Cytoscape plugin. Networks were generated with ReactomeFI or STRING (confidence cutoff of 0.9), as indicated.

**Data Availability.** The MS proteomics data have been deposited to the ProteomeXchange Consortium via the PRIDE (60) partner repository (https://www.ebi.ac.uk/pride/archive) with the dataset identifier PXD023703 (Fig. 1) and PXD021859 (Figs. 3 and 4).

**ACKNOWLEDGMENTS.** We thank Karl-Richard Reuter for help with illustration work, Evgenij Fiskin for initial project support, Katarzyna Bogucka for providing protocols/reagents, and all members of the I.D. laboratory for support and constructive discussions. We thank Andrea Gubas for critical proofreading of the manuscript. We thank the q-Proteomics platform at the Institute of Biochemistry II (Frankfurt) for excellent support. Furthermore, we thank the Kraiczy laboratory (University Hospital of Frankfurt) for help with *Salmonella* work. This project has received funding from the European Research Council under the European Union's Horizon 2020 research and innovation program (Grant Agreement 742720), the grants from Else Kroener Fresenius Stiftung–Dr. Rolf M. Schwiete Stiftung, and was supported by the Deutsche Forschungsgemeinschaft (German Research Foundation) Projects 173096411–SPP 1580 and 259130777–SFB 1177. The Novo Nordisk Foundation Center for Protein Research is financially supported by the Novo Nordisk Foundation (NNF14CC0001).


1. S. E. Majowicz *et al.*; International Collaboration on Enteric Disease 'Burden of Illness' Studies, The global burden of nontyphoidal Salmonella gastroenteritis. *Clin. Infect. Dis.* **50**, 882–889 (2010).
2. L. A. Knodler, J. R. Elfenbein, Salmonella enterica. *Trends Microbiol.* **27**, 964–965 (2019).
3. J. E. Galán, Salmonella interactions with host cells: Type III secretion at work. *Annu. Rev. Cell Dev. Biol.* **17**, 53–86 (2001).
4. P. Cossart, P. J. Sansonetti, Bacterial invasion: The paradigms of Enteroinvasive pathogens. *Science* **304**, 242–248 (2004).
5. F. Randow, J. D. MacMicking, L. C. James, Cellular self-defense: How cell-autonomous immunity protects against pathogens. *Science* **340**, 701–706 (2013).
6. R. C. Orchard, N. M. Alto, Mimicking GEFs: A common theme for bacterial pathogens. *Cell. Microbiol.* **14**, 10–18 (2012).
7. W.-D. Hardt, L.-M. Chen, K. E. Schuebel, X. R. Bustelo, J. E. Galán, S. typhimurium encodes an activator of Rho GTPases that induces membrane ruffling and nuclear responses in host cells. *Cell* **93**, 815–826 (1998).
8. S. J. Winder, K. R. Ayscough, Actin-binding proteins. *J. Cell Sci.* **118**, 651–654 (2005).
9. S. Méresse *et al.*, Remodelling of the actin cytoskeleton is essential for replication of intravacuolar Salmonella. *Cell. Microbiol.* **3**, 567–577 (2001).
10. K. E. Unsworth, M. Way, M. McNiven, L. Machesky, D. W. Holden, Analysis of the mechanisms of Salmonella-induced actin assembly during invasion of host cells and intracellular replication. *Cell. Microbiol.* **6**, 1041–1055 (2004).
11. J. A. Wasylnka *et al.*, Role for myosin II in regulating positioning of Salmonella-containing vacuoles and intracellular replication. *Infect. Immun.* **76**, 2722–2735 (2008).
12. C. Odendall *et al.*, The Salmonella kinase SteC targets the MAP kinase MEK to regulate the host actin cytoskeleton. *Cell Host Microbe* **12**, 657–668 (2012).
13. J. Poh *et al.*, SteC is a Salmonella kinase required for SPI-2-dependent F-actin remodelling. *Cell. Microbiol.* **10**, 20–30 (2008).
14. Z. Wang, H. Takemori, S. K. Halder, Y. Nonaka, M. Okamoto, Cloning of a novel kinase (SIK) of the SNF1/AMPK family from high salt diet-treated rat adrenal. *FEBS Lett.* **453**, 135–139 (1999).
15. J. M. Lizcano *et al.*, LKB1 is a master kinase that activates 13 kinases of the AMPK subfamily, including MARK/PAR-1. *EMBO J.* **23**, 833–843 (2004).
16. F. Chen, L. Chen, Q. Qin, X. Sun, Salt-inducible kinase 2: An oncogenic signal transmitter and potential target for cancer therapy. *Front. Oncol.* **9**, 18 (2019).
17. K. Sakamoto, L. Bultot, O. Göransson, The salt-inducible kinases: Emerging metabolic regulators. *Trends Endocrinol. Metab.* **29**, 827–840 (2018).
18. J. Sakamaki *et al.*, Role of the SIK2-p35-PJA2 complex in pancreatic β-cell functional compensation. *Nat. Cell Biol.* **16**, 234–244 (2014).
19. E. Fiskin, T. Bionda, I. Dikic, C. Behrends, Global analysis of host and bacterial ubiquitinome in response to Salmonella typhimurium infection. *Mol. Cell* **62**, 967–981 (2016).
20. J. C. Patel, J. E. Galán, Differential activation and function of Rho GTPases during Salmonella-host cell interactions. *J. Cell Biol.* **175**, 453–463 (2006).
21. A. M. Keestra *et al.*, Manipulation of small Rho GTPases is a pathogen-induced process detected by NOD1. *Nature* **496**, 233–237 (2013).
22. S. Mostowy, A. R. Shenoy, The cytoskeleton in cell-autonomous immunity: Structural determinants of host defence. *Nat. Rev. Immunol.* **15**, 559–573 (2015).
23. S. J. L. van Wijk *et al.*, Linear ubiquitination of cytosolic Salmonella Typhimurium activates NF-κB and restricts bacterial proliferation. *Nat. Microbiol.* **2**, 17066 (2017).
24. J. Ninomiya-Tsuji *et al.*, The kinase TAK1 can activate the NIK-I kappaB as well as the MAP kinase cascade in the IL-1 signalling pathway. *Nature* **398**, 252–256 (1999).
25. W. Liu *et al.*, Activation of TGF-beta-activated kinase 1 (TAK1) restricts Salmonella Typhimurium growth by inducing AMPK activation and autophagy. *Cell Death Dis.* **9**, 570 (2018).
26. C. L. Birmingham, A. C. Smith, M. A. Bakowski, T. Yoshimori, J. H. Brumell, Autophagy controls Salmonella infection in response to damage to the Salmonella-containing vacuole. *J. Biol. Chem.* **281**, 11374–11383 (2006).
27. M. Polajnar, M. S. Dietz, M. Heilemann, C. Behrends, Expanding the host cell ubiquitylation machinery targeting cytosolic *Salmonella*. *EMBO Rep.* **18**, 1572–1585 (2017).
28. O. Steele-Mortimer, The salmonella-containing vacuole: Moving with the times. *Curr. Opin. Microbiol.* **11**, 38–45 (2008).
29. J. Fueller *et al.*, CRISPR-Cas12a-assisted PCR tagging of mammalian genes. *J. Cell Biol.* **219**, 615 (2020).
30. K. G. Campellone, M. D. Welch, A nucleator arms race: Cellular control of actin assembly. *Nat. Rev. Mol. Cell Biol.* **11**, 237–251 (2010).
31. L. M. Machesky, S. J. Atkinson, C. Ampe, J. Vandekerckhove, T. D. Pollard, Purification of a cortical complex containing two unconventional actins from Acanthamoeba by affinity chromatography on profilin-agarose. *J. Cell Biol.* **127**, 107–115 (1994).
32. R. D. Mullins, J. A. Heuser, T. D. Pollard, The interaction of Arp2/3 complex with actin: Nucleation, high affinity pointed end capping, and formation of branching networks of filaments. *Proc. Natl. Acad. Sci. U.S.A.* **95**, 6181–6186 (1998).
33. J. Block *et al.*, FMNL2 drives actin-based protrusion and migration downstream of Cdc42. *Curr. Biol.* **22**, 1005–1012 (2012).
34. S. Tojkander, G. Gateva, P. Lappalainen, Actin stress fibers–assembly, dynamics and biological roles. *J. Cell Sci.* **125**, 1855–1864 (2012).
35. P. Hotulainen, P. Lappalainen, Stress fibers are generated by two distinct actin assembly mechanisms in motile cells. *J. Cell Biol.* **173**, 383–394 (2006).
36. S. Vorwerk, V. Krieger, J. Deiwick, M. Hensel, N. Hansmeier, Proteomes of host cell membranes modified by intracellular activities of Salmonella enterica. *Mol. Cell. Proteomics* **14**, 81–92 (2015).
37. P. J. Hume, V. Singh, A. C. Davidson, V. Koronakis, Swiss army pathogen: The *Salmonella* entry toolkit. *Front. Cell. Infect. Microbiol.* **7**, 348 (2017).
38. S. Stender *et al.*, Identification of SopE2 from Salmonella typhimurium, a conserved guanine nucleotide exchange factor for Cdc42 of the host cell. *Mol. Microbiol.* **36**, 1206–1221 (2000).
39. D. Zhou, J. Galán, Salmonella entry into host cells: The work in concert of type III secreted effector proteins. *Microbes Infect.* **3**, 1293–1298 (2001).
40. D. Humphreys, A. Davidson, P. J. Hume, V. Koronakis, Salmonella virulence effector SopE and Host GEF ARNO cooperate to recruit and activate WAVE to trigger bacterial invasion. *Cell Host Microbe* **11**, 129–139 (2012).
41. R. D. Hayward, V. Koronakis, Direct nucleation and bundling of actin by the SipC protein of invasive Salmonella. *EMBO J.* **18**, 4926–4934 (1999).
42. E. J. McGhie, R. D. Hayward, V. Koronakis, Cooperation between actin-binding proteins of invasive Salmonella: SipA potentiates SipC nucleation and bundling of actin. *EMBO J.* **20**, 2131–2139 (2001).
43. Y. Fu, J. E. Galán, A salmonella protein antagonizes Rac-1 and Cdc42 to mediate host-cell recovery after bacterial invasion. *Nature* **401**, 293–297 (1999).
44. J. Hänisch *et al.*, Activation of a RhoA/myosin II-dependent but Arp2/3 complex-independent pathway facilitates Salmonella invasion. *Cell Host Microbe* **9**, 273–285 (2011).
45. M. D. Brown, L. Bry, Z. Li, D. B. Sacks, IQGAP1 regulates Salmonella invasion through interactions with actin, Rac1, and Cdc42. *J. Biol. Chem.* **282**, 30265–30272 (2007).
46. D. Truong *et al.*, Formin-mediated actin polymerization promotes Salmonella invasion. *Cell. Microbiol.* **15**, 2051–2063 (2013).
47. K. Rottner, J. Faix, S. Bogdan, S. Linder, E. Kerkhoff, Actin assembly mechanisms at a glance. *J. Cell Sci.* **130**, 3427–3435 (2017).
48. S. Tojkander *et al.*, A molecular pathway for myosin II recruitment to stress fibers. *Curr. Biol.* **21**, 539–550 (2011).
49. Y. Kumar, R. H. Valdivia, Actin and intermediate filaments stabilize the Chlamydia trachomatis vacuole by forming dynamic structural scaffolds. *Cell Host Microbe* **4**, 159–169 (2008).
50. S. Ehsani *et al.*, Hierarchies of host factor dynamics at the entry site of Shigella flexneri during host cell invasion. *Infect. Immun.* **80**, 2548–2557 (2012).
51. S. Kühn *et al.*, Actin assembly around the Shigella-containing vacuole promotes successful infection. *Cell Rep.* **31**, 107638 (2020).
52. I. Paz *et al.*, Galectin-3, a marker for vacuole lysis by invasive pathogens. *Cell. Microbiol.* **12**, 530–544 (2010).
53. N. Mellouk, J. Enninga, Cytosolic access of intracellular bacterial pathogens: The Shigella paradigm. *Front. Cell. Infect. Microbiol.* **6**, 35 (2016).
54. V. M. Bruno *et al.*, Salmonella Typhimurium type III secretion effectors stimulate innate immune responses in cultured epithelial cells. *PLoS Pathog.* **5**, e1000538 (2009).
55. B. J. Ravenhill *et al.*, The cargo receptor NDP52 initiates selective autophagy by recruiting the ULK complex to cytosol-invading bacteria. *Mol. Cell* **74**, 320–329.e6 (2019).
56. E. Fiskin *et al.*, Structural basis for the recognition and degradation of host TRIM proteins by Salmonella effector SopA. *Nat. Commun.* **8**, 14004 (2017).
57. K. E. Yuki *et al.*, CYRI/FAM49B negatively regulates RAC1-driven cytoskeletal remodelling and protects against bacterial infection. *Nat. Microbiol.* **4**, 1516–1531 (2019).
58. A. Camgoz *et al.*, STK3 is a therapeutic target for a subset of acute myeloid leukemias. *Oncotarget* **9**, 25458–25473 (2018).
59. J. Rappsilber, M. Mann, Y. Ishihama, Protocol for micro-purification, enrichment, pre-fractionation and storage of peptides for proteomics using StageTips. *Nat. Protoc.* **2**, 1896–1906 (2007).
60. Y. Perez-Riverol *et al.*, The PRIDE database and related tools and resources in 2019: Improving support for quantification data. *Nucleic Acids Res.* **47**, D442–D450 (2019).

**IKK-β inhibits the integrated stress response to prevent bacterial proliferation**

Marcel Hahn[1,*], Kevin Klann[1,*], Ines Gössner[1], Ivan Dikic[1,+] and Christian Münch[1,+]

[1]Institute of Biochemistry II, Faculty of Medicine, Goethe University, Frankfurt am Main, Germany

* These authors contributed equally to this work

+ Corresponding authors

* Correspondence should be addressed to:

Ivan Dikic: dikic@biochem2.uni-frankfurt.de

Christian Münch: ch.muench@em.uni-frankfurt.de

**Summary**

Infection with the *Salmonella* bacterium is common across the globe and can lead to serious disease. During infection, host cell and pathogen both rapidly and dynamically reshape the cellular protein networks to control pathogen proliferation. A number of key pathways have been identified so far. However, molecular connections across these pathways remain unclear. Here, we reveal that *Salmonella*-induced NF-kB signaling inhibits the integrated stress response (ISR) to prevent bacterial proliferation. Monitoring host cell and bacterial proteome and translatome changes over time during *Salmonella* infection revealed a highly time-resolved translation response modulating IKK/NF-κB activation. In addition, we identified a regulatory link between the IKK kinase complex and the ISR. IKK activity inhibited the ER-resident kinase PERK, which resulted in ISR inhibition that halted bacterial proliferation in cells. In turn, inhibition of IKK activity induced the ISR and caused bacterial hyperproliferation in a PERK and ATF4-dependent mechanism. Our results show that *Salmonella* infection critically depends on this IKK-PERK-ATF4 signaling axis for proliferation. Furthermore, the link between these two key host cell response pathways suggests that the ISR likely contributes to a range of cellular stresses elicited IKK/NF-κB signaling.

**Main Text**

Infection with *Salmonella enterica* (*Salmonella*) and the resulting salmonellosis is a common disease, causing around 100 million diarrheal diseases worldwide[1]. *Salmonella* are intracellular bacteria and consequently engage in a complex network of interactions with the host cell affecting their proliferation[2]. The IKK/NF-κB pathway has been shown to be a key component of host cell responses. The IKK kinase complex is the gatekeeper for activation of the transcription NF-κB , which induces antimicrobial and pro-inflammatory genes[3]. NF-κB signaling cooperates with other pro-inflammatory pathways, such as type I interferon signaling, and has been found to play a crucial role during pathogen infection in the past, including *Salmonella*[4,5]. In addition, bacterial pathogens are known to modulate the host protein synthesis machinery directly or indirectly via host defenses[6,7]. Tuning protein translation rates is a rapid way to change the cellular proteome in order to react to an eminent threat. Changes in translation patterns can induce signaling changes and lead to preferentially expressed proteins needed for the host cell response[6,8]. Such mechanisms are also common responses to other types of infections or cell stress in general and can potentially be exploited by pathogens[9–11]. However, how these different cellular machineries integrate, potentially including the activation of additional pathways, to control *Salmonella* proliferation remains unclear.

**Infection with *Salmonella* translationally modulates the NF-κB pathway**

To globally profile host cell changes during *Salmonella* infection, we quantified changes in total protein levels and protein synthesis over time using mePROD proteomics – a combination of tandem mass tag multiplexing and pulse-labeling of newly synthesized proteins (Figure 1A, Table S1)[10]. Interestingly, based on bacterial protein synthesis and total protein level profiles, we observed two distinct phases during intracellular *Salmonella* proliferation (Figure 1B, S1A). While the early phase was defined by largely constant bacterial protein synthesis and levels, the late phase was shaped by a burst of bacterial protein synthesis that consequently manifested in high levels of bacterial proteins, indicating the onset of bacterial proliferation. To better characterize these two phases, we monitored two time points of each phase in more detail and measured translation changes in triplicates (Figure S1B, Table S2). We found significant translation changes for proteins of the extracellular matrix (ECM), which is important for host cell invasion by pathogens[12] (Table S3). We next focused on the proteins induced during the second infection phase as their induction coincided with the observed burst of bacterial proliferation. This set of regulated proteins was significantly enriched for the NF-kappa B signaling pathway (Figure 1C, S1C, D). We therefore analyzed the complete set of proteins associated with the TNFα/NF-κB pathway and found extensive translational rearrangements throughout the whole pathway (Figure 1D, S1D). This showed that the NF-kB pathway was highly controlled by translational mechanisms during *Salmonella* infection.

**Inhibition of the IKK complex leads to integrated stress response activation**

Recent worked showed a key role of IKK/NF-κB signaling in the cell-autonomous defense that restricts *Salmonella* proliferation[13,14]. Since the underlying molecular mechanism remains unknown, we further examined the effects of IKK/NF-κB signaling on the host cell translatome. We used the IKK-ß inhibitor TPCA-1[15,16] to prevent IKK-dependent signaling and measured the host cell translatome response upon basal and infection conditions (Table S4). In accordance with previous literature[13,14], our functional assays showed that IKK inhibition led to hyperproliferative *Salmonella* in our system (Figure 2A, S2A). Surprisingly, we also observed global protein synthesis attenuation upon TPCA-1 treatment (Figure 2B), which had not yet been associated with IKK/NF-κB signaling. Comparable changes are typically observed upon activation of stress response pathways, such as the integrated stress response (ISR) or mTORC1[17–19]. We observed this phenomenon upon basal conditions as well as during infection, suggesting that translation attenuation was independent of infection. To test whether specific translation rearrangements or general global host translation inhibition were driving *Salmonella* hyperproliferation, we titrated low doses of cycloheximide (CHX) and performed colony formation assays after *Salmonella* infection of cells (Figure 2C). CHX treatment did not affect *Salmonella* proliferation, indicating that the phenotype was caused by specific regulatory mechanisms and not general protein synthesis inhibition. In parallel to the global translation repression, we also observed increased translation of proteins that are ISR targets controlled by the effector transcription factor ATF4 (Figure 2D, S2B). Additional functional cluster analyses suggested an upregulation of proteins involved in amino acid synthesis and metabolism, which are also known to be controlled by ISR-mediated ATF4 increases[20] (Figure S2C). Thus, we hypothesized that IKK links the IKK/NF-κB signaling pathway with the ISR and that IKK inhibition results in an ISR-mediated translational reprograming of cellular protein expression favoring *Salmonella* proliferation (Figure 2E).

**An IKK-PERK signaling axis modulates the integrated stress response**

To confirm whether IKK inhibitors were capable of inducing the ISR, we examined the classical markers of the ISR – phosphorylation of eIF2α (EIF2S1) at serine 51 and ATF4 levels. Two different IKK-β inhibitors rapidly activated the ISR (Figure 3A). Notably, phosphorylation of the mTORC1 substrate EIF4EBP1 remained stable showing that mTORC1 did not contribute to the observed translation attenuation. To facilitate a quantitative readout for ISR activation in cells, we generated a stable HeLa ATF4-GFP reporter gene cell line compatible with FACS-based readouts[21]. TPCA-1 treatment induced ATF4-GFP, which was reduced when adding the ISR inhibitor ISRIB (Figure 3B, S3A)[18,22–24]. Hence, our data suggested a negative regulatory role of IKK-β to block the ISR and subsequently eIF2α phosphorylation and ATF4 induction. This interpretation was further supported by overexpression of a dominant negative IKK-β mutant being sufficient to induce the ISR (Figure 3C). Notably, IKK-mediated ISR activation was not dependent on downstream NF-κB signaling, since knockdown of p65 (RELA) did not induce the ISR itself nor influenced the TPCA-1-dependent ISR induction (Figure S3B). While TPCA-1 treatment led to increased mRNA expression of ISR genes, such as *ATF4* or *DDIT3* (also known as *CHOP*), it did not cause increased *BiP* expression, showing that the ISR activation observed upon IKK inhibition was not part of a general activation of the ER unfolded protein response (UPR) (Figure 3D)[25]. To further confirm that the IKK-induced ISR activation was independent of UPR induction, we compared the cell-wide phosphorylation changes upon IKK inhibition with thapsigargin-mediated UPR activation using phospho-proteomics (Figure 3E, Table S5). TPCA-1 treated cells exhibited a distinct phosphorylation pattern indicating ISR activation without UPR induction. The ISR is induced by activation (phosphorylation) of one of the four eIF2a kinases (EIF2AK1-4) leading to eIF2a phosphorylation[26]. When monitoring the phosphorylation status of the eIF2a kinases, we observed a significant decrease in phosphorylation of EIF2AK3, better known as PERK, at serine 1,094 (Figure 3F). This site is located in the very C-terminal region of the protein, which is exposed to the cytosol and therefore might be targeted by cytosolic kinases through a yet unknown mechanism. We observed a phosphorylation-induced PERK SDS-page mobility shift after TPCA-1 treatment, orthogonally confirming PERK activation (Figure 3G). To test if PERK was responsible for the observed ISR induction, we depleted PERK by siRNA and treated the ATF4-GFP reporter cell line with TPCA-1. We saw a significant reduction of ATF4 or eIF2α phosphorylation in PERK-depleted cells (Figure 3H, S3C). We further investigated whether the IKK kinase complex was directly responsible for PERK modulation by performing co-immunoprecipitation experiments in HEK293T cells expressing Flag-tagged IKK-β and myc-tagged PERK (Figure 3I). Indeed, we saw co-precipitation of IKK-β when pulling down myc-PERK, indicating a functional protein interaction. Hence, our data strongly suggested PERK to drive ISR induction after IKK inhibition.

**IKKs protect the host cell during infection by blocking the ISR**

We next asked whether the IKK-PERK-ISR axis protected host cells during *Salmonella* infection and whether it modulated *Salmonella* proliferation. Infection with intracellular bacteria is known to induce the ISR by various mechanisms[27]. Accordingly, after infecting cells with *Salmonella*, we observed a strong induction of eIF2α phosphorylation and ATF4 expression (Figure 4A). To test whether the IKK-PERK-ISR axis was driving the previously seen *Salmonella* hyperproliferation during IKK inhibition (Figure 2), we monitored proliferation after depletion of PERK or ATF4. We found that depleting these ISR core genes prevented IKK-induced hyperproliferation (Figure 4B-D). Strikingly, we also observed a general defect in bacterial proliferation in the absence of PERK or ATF4, indicating that the IKK-mediated ISR restriction played an important role to restrain bacterial proliferation. For other intracellular pathogens, it was already reported that bacterial effector proteins can target the IKK complex to restrain inflammatory responses[28]. However, our data suggested that targeting the IKK complex might also facilitate bacterial proliferation via the ISR. To test this hypothesis, we expressed the E3-Ligase IpaH9.8 from *Shigella flexineri*, which has been shown to target the essential IKK subunit NEMO for proteasomal degradation, thereby diminishing NF-κB activation in cells[28]. A functional *Salmonella* homologue has not been described, yet. When overexpressing IpaH9.8, we observed a robust activation of the ISR (Figure 4E). These experiments suggested that the observed IKK-PERK-ISR axis is crucial to control *Salmonella* proliferation and that bacteria can modulate this axis (Figure 4F).

**Discussion**

IKK signaling and the ISR are well-established mediators of bacterial infection determining cellular fate. So far, the integration of these pathways remained unclear. Recent reports demonstrated, that an ISR activation displays cytoprotective features and can co-regulate NF-κB-dependent innate immune signaling [27,29,30]. While profiling the translatomic landscape of *Salmonella*-infected cells, we discovered an IKK-PERK-ATF4 signaling axis, which protects the host and is critically exploited by intercellular bacteria required for proper bacterial proliferation (Figure 4F). The IKK complex acts upstream of NF-κB signaling and is crucial to fight bacterial infection. So far, it remained unknown how IKK/NF-κB signaling mediates cell-autonomous immunity upon *Salmonella* infection[13,14]. Here we demonstrated, that the kinase activity of IKK-ß negatively regulated the ISR pathway via the eIF2α kinase PERK, both under basal and *Salmonella* infection conditions. The UPR had been shown to activate NF-κB signaling via the ER kinase IRE1[31,32]. However, our data clearly shows, that an IKK inhibition triggers the ISR via PERK, eliciting a translational and transcriptional program distinct from the UPR and IRE1 activation. Previous work suggested that the UPR induction favors bacterial proliferation[33]. We show that *Salmonella* hyperproliferation in response to impaired IKK/NF-KB signaling is mainly driven by the ISR, explaining the cell-autonomous defense-effect of IKK signaling. In the context of bacterial infection, we showed that the ISR favored pathogen replication and was actively restrained by the IKK complex to counteract bacterial proliferation. Strikingly, while no IKK-targeting protein has been identified in *Salmonella* yet, other intracellular bacteria, such as *Shigella*, actively target the IKK complex. Our data suggests competition between host-driven IKK signaling and the ISR, activated by bacterial pathogens to exploit the ISR to favor bacterial proliferation[28,34]. This link explains how *Salmonella* infection activates the ISR and has wide-ranging consequences as numerous conditions have been shown to modulate IKKs and consequently have the potential to modulate the ISR in parallel. Both pathways can switch between supporting cellular survival or death and could thus have implications in in disease models[35]. Based on these findings, we postulate a new paradigm of how IKK signaling protects the host cell by balancing inflammation and ISR activation. Moreover, our data suggest that the link to the ISR pathway should be further investigated as a target for therapeutic intervention of intracellular bacterial infections. In addition, the IKK-PERK-ISR link contributes towards a better understanding of the complex roles of the IKK complex in human diseases.

**Acknowledgements**

We thank the q-Proteomics platform at the Institute of Biochemistry II (Frankfurt) for excellent support. Furthermore, we thank the Kraiczy lab (KGU, Frankfurt) for help with *Salmonella* work. We thank Yves Matthess for help with molecular cloning. I.D. received funding from the European Research Council (ERC) under the European Union´s Horizon 2020 research and innovation program (grant agreement No 742720), the grants from Else Kroener Fresenius Stiftung; Dr. Rolf M. Schwiete Stiftung and was supported by the Deutsche Forschungsgemeinschaft (DFG, German Research Foundation) - Project number 173096411 - SPP 1580, Project number 259130777 – SFB 1177, and Project number 403765277. C.M. was supported by the European Research Council under the European Union's Seventh Framework Programme (ERC StG 803565), CRC 1177 and the Emmy Noether Programme of the Deutsche Forschungsgemeinschaft (DFG, MU 4216/1-1), the Johanna Quandt Young Academy at Goethe and an Aventis Foundation Bridge Award.

**References**

1. Majowicz, S. E. *et al.* The Global Burden of Nontyphoidal *Salmonella* Gastroenteritis. *Clin. Infect. Dis.* **50**, 882–889 (2010).
2. Haraga, A., Ohlson, M. B. & Miller, S. I. *Salmonella*e interplay with host cells. *Nat. Rev. Microbiol.* **6**, 53–66 (2008).
3. Oeckinghaus, A., Hayden, M. S. & Ghosh, S. Crosstalk in NF-κB signaling pathways. *Nat. Immunol.* **12**, 695–708 (2011).
4. Robinson, N. *et al.* Type I interferon induces necroptosis in macrophages during infection with *Salmonella* enterica serovar Typhimurium. *Nat. Immunol.* **13**, 954–962 (2012).
5. Ivashkiv, L. B. & Donlin, L. T. Regulation of type I interferon responses. *Nat. Publ. Gr.* **14**, 36–49 (2014).
6. Lemaitre, B. & Girardin, S. E. Translation inhibition and metabolic stress pathways in the host response to bacterial pathogens. *Nat. Rev. Microbiol.* **11**, 365–369 (2013).
7. Selkrig, J. *et al.* Spatiotemporal proteomics uncovers cathepsin-dependent macrophage cell death during *Salmonella* infection. *Nat. Microbiol.* **16**, 1–15 (2020).
8. Fontana, M. F. *et al.* Secreted Bacterial Effectors That Inhibit Host Protein Synthesis Are Critical for Induction of the Innate Immune Response to Virulent Legionella pneumophila. *PLOS Pathog.* **7**, e1001289 (2011).
9. Stern-Ginossar, N., Thompson, S. R., Mathews, M. B. & Mohr, I. Translational control in virus-infected cells. *Cold Spring Harb. Perspect. Biol.* **11**, (2019).
10. Klann, K., Tascher, G. & Münch, C. Functional Translatome Proteomics Reveal Converging and Dose-Dependent Regulation by mTORC1 and eIF2α. *Mol. Cell* **77**, (2020).
11. Bojkova, D. *et al.* Proteomics of SARS-CoV-2-infected host cells reveals therapy targets. *Nature* **583**, 469–472 (2020).
12. Singh, B., Fleury, C., Jalalvand, F. & Riesbeck, K. Human pathogens utilize host extracellular matrix proteins laminin and collagen for adhesion and invasion of the host. *FEMS Microbiol. Rev.* **36**, 1122–1180 (2012).
13. Van Wijk, S. J. L. L. *et al.* Linear ubiquitination of cytosolic *Salmonella* Typhimurium activates NF-kappaB and restricts bacterial proliferation. *Nat. Microbiol.* **2**, 17066

(2017).

14. Noad, J. *et al.* LUBAC-synthesized linear ubiquitin chains restrict cytosol-invading bacteria by activating autophagy and NF-κB. *Nat. Microbiol.* **2**, 17063 (2017).

15. Du, Z. *et al.* Inhibition of Type I Interferon-Mediated Antiviral Action in Human Glioma Cells by the IKK Inhibitors BMS-345541 and TPCA-1. *J. Interf. Cytokine Res.* **32**, 368–377 (2012).

16. Nan, J. *et al.* TPCA-1 Is a Direct Dual Inhibitor of STAT3 and NF-κB and Regresses Mutant EGFR-Associated Human Non–Small Cell Lung Cancers. *Mol. Cancer Ther.* **13**, 617 LP – 629 (2014).

17. Pakos-Zebrucka, K. *et al.* The integrated stress response. *EMBO Rep.* **17**, 1374–1395 (2016).

18. Klann, K., Tascher, G. & Münch, C. Functional Translatome Proteomics Reveal Converging and Dose-Dependent Regulation by mTORC1 and eIF2α. *Mol. Cell* **77**, 913-925.e4 (2020).

19. Thoreen, C. C. *et al.* A unifying model for mTORC1-mediated regulation of mRNA translation. *Nature* **485**, 109–113 (2012).

20. Harding, H. P. *et al.* An Integrated Stress Response Regulates Amino Acid Metabolism and Resistance to Oxidative Stress. *Mol. Cell* **11**, 619**–**633 (2003).

21. Lu, P. D., Harding, H. P. & Ron, D. Translation reinitiation at alternative open reading frames regulates gene expression in an integrated stress response. *J. Cell Biol.* **167**, 27–33 (2004).

22. Sidrauski, C., McGeachy, A. M., Ingolia, N. T. & Walter, P. The small molecule ISRIB reverses the effects of eIF2α phosphorylation on translation and stress granule assembly. *Elife* **2015**, e05033 (2015).

23. Rabouw, H. H. *et al.* Small molecule ISRIB suppresses the integrated stress response within a defined window of activation. *Proc. Natl. Acad. Sci.* **116**, 2097–2102 (2019).

24. Halliday, M. *et al.* Partial restoration of protein synthesis rates by the small molecule ISRIB prevents neurodegeneration without pancreatic toxicity. *Cell Death Dis.* **6**, e1672–e1672 (2015).

25. Ron, D. & Walter, P. Signal integration in the endoplasmic reticulum unfolded protein response. *Nat. Rev. Mol. Cell Biol.* **8**, 519–529 (2007).

26. Taniuchi, S., Miyake, M., Tsugawa, K., Oyadomari, M. & Oyadomari, S. Integrated stress response of vertebrates is regulated by four eIF2α kinases. *Sci. Rep.* **6**, 32886 (2016).

27. Knowles, A., Campbell, S., Cross, N. & Stafford, P. Bacterial Manipulation of the Integrated Stress Response: A New Perspective on Infection. *Frontiers in Microbiology* vol. 12 463 (2021).

28. Ashida, H. *et al.* A bacterial E3 ubiquitin ligase IpaH9.8 targets NEMO/IKKγ to dampen the host NF-κB-mediated inflammatory response. *Nat. Cell Biol.* **12**, 66–73 (2010).

29. Abdel-Nour, M. *et al.* The heme-regulated inhibitor is a cytosolic sensor of protein misfolding that controls innate immune signaling. *Science (80-. ).* **364**, eaaw4144 (2019).

30. Tattoli, I. *et al.* Amino acid starvation induced by invasive bacterial pathogens triggers an innate host defense program. *Cell Host Microbe* **11**, 563–575 (2012).

31. Hu, P., Han, Z., Couvillon, A. D., Kaufman, R. J. & Exton, J. H. Autocrine Tumor

Necrosis Factor Alpha Links Endoplasmic Reticulum Stress to the Membrane Death Receptor Pathway through IRE1α-Mediated NF-κB Activation and Down-Regulation of TRAF2 Expression. *Mol. Cell. Biol.* **26**, 3071–3084 (2006).

32. Schmitz, M. L., Shaban, M. S., Albert, B. V., Gökçen, A. & Kracht, M. The crosstalk of Endoplasmic Reticulum (ER) stress pathways with NF-κB: Complex mechanisms relevant for cancer, inflammation and infection. *Biomedicines* vol. 6 (2018).

33. Antoniou, A. N. *et al. Salmonella* exploits HLA-B27 and host unfolded protein responses to promote intracellular replication. *Ann. Rheum. Dis.* **78**, 74–82 (2019).

34. Rahman, M. M. & McFadden, G. Modulation of NF-κB signalling by microbial pathogens. *Nat. Rev. Microbiol.* **9**, 291–306 (2011).

35. Senegas, A., Gautheron, J., Maurin, A. G. D. & Courtois, G. IKK-related genetic diseases: Probing NF-κB functions in humans and other matters. *Cell. Mol. Life Sci.* **72**, 1275–1287 (2015).

**Figure 1: Infection with *Salmonella* translationally modulates the NF-κB pathway**

**A)** Scheme of experimental design. HeLa cells were infected with *Salmonella* and lysed at the indicated time-points post infection (pi). One hour before lysis cells were SILAC-pulsed. **B)** Profile plot of *Salmonella* translation after Z-scoring (upper plot) and *Salmonella* proteome in log2 fold changes (lower plot) over the indicated infection time-points. **C)** Functional KEGG pathway analysis of upregulated hits (log2 ≥ 0.5 and p-value ≤ 0.05) at 8 h and 10 h post-infection. **D)** Heatmap and hierarchical clustering of combined datasets after Z-score calculation and clustering based on Euclidean distance between the samples. Z-scores are shown for indicated time-points and replicates (n=3).

**Figure 2: Inhibition of the IKK complex leads to integrated stress response activation**

**A)** Fold proliferation of intracellular *Salmonella* in DMSO, TPCA-1 (10μM) or IKK-16 (1μM) treated HeLa cells at 8 h pi.. **B)** Translation rate in HeLa cells at the indicated time-points and treatments (DMSO, TPCA-1 (10μM) and -/+ *Salmonella* infection). Median intensity (arbitrary units (AU)) of heavy SILAC-peptides as means ±SD, n=3. **C)** Fold proliferation of intracellular *Salmonella* in DMSO and cycloheximide (CHX) (100-1 μM) treated HeLa cells at 8 h pi. **D)** Volcano plot showing relative translation changes (log2) for TPCA-1 (10μM) versus control treated HeLa cells plotted against p-values (n=3). ATF4 pathway enrichment was calculated from upregulated genes against the Reactome pathway set ATF4 induced gene expression by a hypergeometric test with the whole dataset as background. **E)** Model illustrating the observed effects upon IKK complex inhibition.

**B&D)** Data are depicted as fold proliferation normalized to 1 h pi and presented as means ± SD, n=3. Bacteria were counted on the basis of their ability to form colonies on agar plates. Cells were treated with respective drugs during the time of the experiment.

**Figure 3: IKK/PERK signaling axis modulates the integrated stress response**

**A)** Western blot showing ATF4 and eIF2α S51-induction and stable EIF4EB1 phosphorylation in TPCA-1(10µM) or IKK-16 (1µM) treated HeLa cells at the indicated time-points. **B)** ATF4-GFP induction in DMSO, ISRIB (500nM), thapsigargin (1µM) or TPCA-1 (10µM) treated (overnight) cells. **C)** ATF4-GFP induction in mock, Flag-IKK-β or Flag- IKK-β K44A transfected cells. **D)** Quantitative-PCR of Hela cells after 4h of DMSO and TPCA-1 (10µM) treatment. Relative expression of target genes was normalized to ACTB **E)** Heatmap after phosphoproteome profiling of UPR genes upon DMOS, TPCA-1 (10mM) or thapsigargin treatment (1 h). Phosphopeptides were filtered through a Reactome molecular signature database and displayed as log2 fold changes for treatments versus control (n=5). **F)** Heatmap of EIF2AKs after PTM profiling. Shown are log2 fold changes for TPCA-1 or thapsigargin treatment versus control. **G)** Western blot showing PERK mobility shift and eIF2α S51 phosphorylation after TPCA-1 treatment in HeLa cells. **H)** ATF4-GFP induction in siControl or siPERK transfected and DMSO or TPCA-1 treated (overnight) cells. **I)** Co-IP of Flag- IKK-β with Myc-PERK. Lysates from HEK293T cells expressing the indicated constructs were subjected to anti-Myc IP followed by western blotting.

**B,C&H)** Stable HeLa ATF4-GFP reporter cell line was analyzed by FACS after indicated treatments. Data shown as median GFP intensity (AU) ± SD, n=3.

**Figure 4: Bacterial infection targets IKKs to induce the ISR**

**A)** Western blot showing ATF4 induction and eIF2α S51 phosphorylation in MEFs upon *Salmonella* infection at the indicated time-points. **B)** Fold proliferation of intracellular *Salmonella* in siCTRL or siPERK transfected HeLa cells at 8 h pi. **C)** Fold proliferation of intracellular *Salmonella* in wild-type or ATF4-knockout HeLa cells at 8 h pi.. **D)** Fold proliferation of intracellular *Salmonella* in siCTRL or siATF4 transfected HeLa cells at 8 h pi.. **E)** ATF4-GFP induction in mock, Flag- IKK-β, Flag- IKK-β K44A or GST-IpaH9.8 transfected cells. **F)** Model illustrating the dual protective role of functional IKK signaling by activating pro-inflammatory signaling and simultaneously dampening the PERK/ATF4 ISR signaling axis.

**B-D)** Data are depicted as fold proliferation normalized to 1 h pi and presented as means ± SD, n = 3. Bacteria were counted on the basis of their ability to form colonies on agar plates. Cells were treated with DMSO, TPCA-1 (10µM) or IKK-16 (1µM) during the time of the experiment.

**E&F)** Stable HeLa ATF4-GFP reporter cell line was analyzed by FACS after indicated treatments. Data shown as median GFP intensity (AU) ± SD, n=3.

**Supplementary Figure Legends**

**Figure S1:**

**A)** Principal component analysis of time-course data. (left) Translation data measured by mePROD after 1 – 8 hours of infection with *Salmonella*. (right) Total protein data measured by proteomics after 1 – 8 hours of infection. **B)** Heatmap representation of replicate translation data measured by mePROD after 1, 4, 8 and 10 hours of *Salmonella* infection. Data is shown as gene-wise Z scores. Clustering was performed using hierarchical clustering with Euclidean distance. **C)** Pathway representation of the interferon/STAT signaling pathway, overlaid with translation data measured by mePROD. Stacked layers around the proteins represent the different time-points from B and are colored after the log2 fold change. **D)** Pathway representation of the NF-κB pathway overlaid with translation data. Stacked layers around the proteins represent the different time-points from B and are colored after the log2 fold change. (see Figure 1)

**Figure S2:**

**A)** Log2 fold changes of total protein levels from *Salmonella* proteins after 8 hours of infection plotted between DMSO treated cells and TPCA-1 treated cells. The trendline shows higher induction of *Salmonella* proteins in the TPCA-1 treated cells after 8 hours, indicating higher proliferation rates. **B)** Volcano plot showing fold changes in protein translation between TPCA-1 and DMSO treated cells after 8 hours of infection and their corresponding P values (log10 transformed). Blue dots indicate significantly decreased proteins ($P < 0.05$, $|FC| > 0.58$), red dots indicate significant increase in protein translation. **C)** GO term enrichment result of significantly increased protein translation upon TPCA-1 treatment at both time-points. For each pathway the number of found proteins is plotted and the bars are colored according the FDR. All shown pathways are significantly enriched with an FDR < 0.05. (see Figure 2)

**Figure S3:**

**A)** ATF4 reporter assay using Flow cytometry over time after TPCA-1, thapsigargin and DMSO treatment. Shown is the median GFP reporter intensity in arbitrary units in dependency of the treatment time. **B)** Western blot showing ISR activation upon TPCA treatment with and without the siRNA knockdown of RELA (p65). **C)** Western blot showing ISR activation upon TPCA treatment in EIF2AK3 (PERK) CRISPR KO cells (cell pool after KO). (see Figure 3)

**Figure S4:**

**A)** CFU assay showing *Salmonella* proliferation after TPCA-1 and IKK-16 treatment in wildtype cells and ATF4 knockout cells. Data shown as *Salmonella* proliferation in fold changes (Drug/DMS0), n=3. **B)** Western Blot showing the ISR activation after transfection of either the empty vector (EV) or overexpression plasmids containing coding sequences for IKK, IKK K44A (catalytically inactive) or the *Shigella flexneri* IpaH9.8 protein. (see Figure 4)

**Supplementary Table Legends:**

Table S1: mePROD translatome data for infection kinetics. Given are total protein levels and mePROD translation values for all measured samples.

Table S2: mePROD translatome data in biological triplicates for Mock, 1h, 4h, 8h and 10h of *Salmonella* infection. Replicate translation data are given together with log2 fold changes and P values for each time-point compared to mock control.

Table S3: Reactome pathway enrichment for cluster found in data of Table S2 (Figure S1B). Significantly enriched pathways are given with description and FDR.

Table S4: mePROD translatome data of biological triplicates for cells treated with either DMSO or TPCA-1 under basal and infection conditions at two different time-points (2h, 8h).

Replicates were split across three multiplexes and normalized using the IRS method before statistical inference. Log2 fold changes and P values are given for statistical comparisons.

Table S5: Phospho-proteomic data of cells treated with either DMSO, TPCA-1 or thapsigargin for one hour. Data is on peptide level and normalized TMT intensities for each peptide is given together with peptide annotations (modification and position), log2 fold changes for statistical comparisons, P values and Benjamini-Hochberg adjusted P values.

## Methods

### Cell culture

HeLa, HEK293T and MEFs cells were cultivated in IMDM (Gibco) containing 10% Fetal Bovine Serum (FBS, Gibco) at 37°C/5% $CO_2$. For translation measurements cells were shifted to IMDM for SILAC medium, supplemented with isotope labelled Arginine (R10) and Lysine (K8) containing 10% FBS. To label newly synthesized proteins a SILAC pulse of one hour was applied before harvest. All cell lines were routinely checked for mycoplasma infections using MycoAlert (Lonza).

### Lentiviral Transduction and Cell Line Generation

HEK293T cells were co-transfected with the lentiviral plasmid together with the packaging vectors psPAX2 and pMD2.G. The medium containing the lentivirus was exchanged after 24 h and after another 24 h, medium was collected for transduction of the recipient cells. Recipient cells were transduced with 1 mL of the virus containing medium with polybrene (8 µg/mL; Sigma-Aldrich, H9268-5G). Cells were selected 48 h post-transduction with 10 µg/mL Blasticidin or 1 µg/ml Puromycin.

### Generation of ATF4 Knockout cell line

Gene knockout of ATF4 was conducted in HeLa cells by CRISPR-Cas-9-mediated genome editing. The sgRNA sequence for ATF4 (5′-TCT CTT AGA TGA TTA CCT GG-3′) was cloned into eSpCas9(1.1) (plasmid 71814, addgene). HeLa cells were co-transfected with a puromycin containing plasmid and selected for 24 h with 1 µg/ml puromycin. After selection, single cells were seeded into 96-well plates and incubated for 2 weeks. Resulting colonies were expanded and gene knockout was confirmed by Sanger sequencing and Western blot analysis.

### Generation of EIF2AK3 CRISPR cells

Gene knockout of EIF2AK3 was performed by co-transfection of three lentiviral vectors containing gRNAs against EIF2AK3 (GAATATACCGAAGTTCAAAG, TTATCTACCATACTACAAGA, GTACCACCCATTACCTATTG) and pCW-Cas9-Blast for 24 hours in HeLa cells, followed by changing the medium to IMDM + 10% FBS containing 10µg/mL blasticidin and 2µg/mL puromycin. After induction of Cas9 expression by addition of 0.5µg/mL doxycycline, the cells were cultured for two days and subsequently doxycycline was removed from medium. The resulting cell pool was cultured for several days and used for experiments.

**Reagents and antibodies**

TPCA-1 (#S2824, Selleckchem), IKK-16 (#1186195-62-9, Abcam), Cycloheximide (#A0879, Applichem), ISRIB (#SML0843-5MG, Sigma Aldrich), Thapsigargin (#ab120286, Abcam), PERK (#5683S, Cell Signaling Technology), EIF2S1 (phospho S51) (#ab32157, Abcam), EIF2S1 (#ab5369, Abcam), ATF-4 (#11815, Cell Signaling Technology), α-Tubulin (#T9026, Sigma-Aldrich), FLAG (#F3165, Sigma-Aldrich), c-Myc (#5605, Cell Signaling Technology), p65/RELA (#sc-372, Santa Cruz), GST (#sc-138, Santa Cruz)

**Plasmids**

pCR-2FLAG-mIKK-ß (lab plasmid #1497), pCR-2FLAG-mIKK-ß K44A (lab plasmid #1498), pEBG6P-IPAH9.8 (#32827, PPU-MRC, University of Dundee), PERK 6: PERK.9E10.pBABE was a gift from David Ron (Addgene plasmid # 21819), EIF2AK3 gRNA vectors were a gift from John Doench & David Root (AddGene plasmids #77166, #77167, #77168), pCW-Cas9-Blast was a gift from Mohan Babu (Addgene plasmid #83481), ATF4-GFP coding sequence was cloned out of ATF4 5 plasmid (5'ATF4.GFP was a gift from David Ron (Addgene plasmid # 21852)) and inserted in frame into pLenti CMV Blast DEST (706-1), which was a gift from Eric Campeau & Paul Kaufman (Addgene plasmid # 1745), psPAX2 was a gift from Didier Trono (Addgene plasmid # 12260), pMD2.G was a gift from Didier Trono (Addgene plasmid # 12259).

**Quantitative PCR**

Cells were harvested in 250µL lysis buffer from a RNA extraction kit (NucleoSpin) and RNA was extracted following the provided protocol. 1µg of RNA was used to synthesize cDNA with random hexamer primers with the High-Capacity cDNA synthesis kit (ThermoFisher, 4368814) following the provided protocol. cDNA was subsequently diluted and 4ng of cDNA were used for qPCR using the primaQUANT SYBR Green kit (#SL-9902, Steinbrenner Laborsysteme).

**Salmonella culturing and infections**

*Salmonella enterica serovar* Typhimurium strain 12023 pFPV25.1-mCherry (gift from Felix Randow, LMB, Cambridge, UK) was used in this study as described earlier.[1,2] Single Salmonella colonies were picked from a lysogeny broth (LB) agar plate and inoculated into 1 mL LB medium (plus the respective antibiotic) and grown overnight to a stationary phase at 37 °C. Next day, Salmonella was diluted 1:33 and grown for 3.5 h at 37 °C before infection. Cells were infected in antibiotic-free medium with a multiplicity of infection of 100 for 10 min and washed afterward twice with phosphate-buffered saline (PBS). Subsequently, cells were cultured further in medium containing 100 µg/mL gentamycin for 1 h and thereafter reduced to 20 µg/mL gentamycin for the remaining time of the experiment.

**Colony-forming unit (CFU) Assay**

HeLa cells were seeded in triplicates with $2 \times 10^4$ cells into a 24-well and siRNA-transfected in antibiotic-free medium. Experiments were performed 72 h post transfection. After the infection, cells were washed with PBS and cultured with gentamycin-containing medium. At 1 or 8 h pi, cells were lysed in 0.1% (vol/vol) Triton X-100 in PBS and serial diluted in PBS. Diluted lysates were plated in technical duplicates on agar plates and incubated for colony formation overnight at 37 °C. The number of colonies (within the linear range of the assay) was enumerated using a colony counter device (aCOLyte3, Synbiosis).

**SDS-PAGE and Immunoblotting**

Cells were washed twice with cold PBS and lysed in lysis buffer (50 mM Hepes, pH 7.5, 150 mM NaCl, 1 mM EDTA, 1 mM EGTA, 1% Triton X-100, 25 mM NaF, 5% glycerol, and 10 µM $ZnCl_2$) or SDS lysis buffer (30 mM Tris·HCl, pH 7.4, 120 mM NaCl, 2 mM EDTA, 2 mM KCl, 0.5% CHAPS, 1% SDS, 50 mM NaF, and 5 mM $Na_3VO_4$) supplemented with complete protease inhibitors (cOmplete, EDTA-free; Roche Diagnostics) and phosphatase inhibitors (P5726, P0044; Sigma-Aldrich). Cell lysates were cleared by spinning at 20,000 g for 15 min at 4 °C in a centrifuge. Cell extracts were incubated with SDS sample buffer (50 mM Tris·HCl, pH 6.8, 10% glycerol, 2% SDS, 0.02% bromophenol blue, and 5% β-mercaptoethanol) and heated at 95 °C for 5 min. Samples were loaded onto 4 to 20% precast gradient gels (BioRad) or self-casted 8% or 10% acrylamide gels and separated by SDS-PAGE. Proteins were plotted by wet-transfer onto a PVDF membrane and blocked with 5% low-fat milk or 5% bovine serum albumin (BSA) in Tris-buffered saline (TBS) (150 mM NaCl, 20 mM Tris, and pH 8.0) for 1 h. Primary antibodies were diluted in 5% BSA in TBS-T (TBS + 0.1% Tween 20) and secondary antibodies in 5% low-fat milk in TBS-T.

**Protein Immunoprecipitation**

Following cell lysis under non-denaturing conditions, cleared cell extracts were incubated with lysis-buffer-equilibrated antibody-coupled resin. Therefore, Myc-Trap agarose (Chromotek) was used and incubated with lysates for 2 h at 4°C on a rotating platform. Protein-bound beads were washed four times with lysis buffer. Immunoprecipitated and input samples were reduced in SDS sample buffer and heated at 95°C for 5 min.

**RNA interference**

Cells were transfected 24h post-seeding with 20nM siRNA siRNA

(ON-TARGETplus human EIF2AK3 siRNA smart pool (Horizon Discovery, # L-004883-00-0005), siRNA against ATF4 (Horizon Discovery, UUG GCC AUC UCC CAG AAA G), ON-TARGETplus Human RELA siRNA smart pool (Horizon Discovery #L-003533-00-0005) and AllStars Negative Control siRNA (#102728, Qiagen)) using Lipofectamine RNAiMAX (Life Technologies) according to the manufacturers protocol. Experiments were performed 72 h post-transfection. Transfection efficiency was verified by western blotting.

**Isotope labelling and cell lysis**

One hour before harvest cells were washed twice with warm PBS to remove interfering medium and cultured for one additional hour with IMDM medium containing 84 mg/L L-Arginine ($^{13}C6^{15}N4$; Cambridge Isotope Laboratories, Cat#CNLM-539-H) and 146 mg/L L-Lysine ($^{13}C6^{15}N2$, Cambridge Isotope Laboratories, Cat#CNLM-291-H) to label nascent proteins. After labelling culture, the cells were washed three times with warm PBS and lysed with 95°C hot lysis buffer (100mM Tris pH 8.0, 2% SDS, 1mM TCEP, 4mM 2-Chloracetamide, Protease inhibitor tablet mini EDTA-free [Roche]). Samples were then incubated for additional five minutes at 95°C, followed by sonication for 30s and further 10min incubation at 95°C.

**Sample preparation for mass spectrometry**

Samples were prepared as previously described[3]. Briefly, proteins were precipitated using methanol/chloroform precipitation and resuspended in 8M Urea/10mM EPPS pH 8.2. Isolated proteins were digested with 1:50 wt/wt LysC (Wako Chemicals) and 1:100 wt/wt Trypsin (Promega, Sequencing grade) overnight at 37°C after dilution to a final Urea concentration of 1M. Digests then were acidified (pH 2-3) using TFA. Peptides were purified using C18 (50mg) SepPak columns (Waters) as previously described. Desalted peptides were dried and 25µg of peptides were resuspended in TMT labelling buffer (200mM EPPS pH 8.2, 10% acetonitrile). Peptides were subjected to TMT labelling with 1:2 Peptide TMT ratio (wt/wt) for one hour at RT. Labelling reaction was quenched by addition of hydroxylamine to a final concentration of 0.5% and incubation at RT for additional 15min. All multiplexes were mixed with a bridge channel, that consists of control sample labelled in one reaction and split to all multiplexes in equimolar amounts. 250 µg of pooled peptides were dried for offline High pH Reverse phase fractionation by HPLC (whole cell proteome) and remaining 1 mg of multiplexed peptides were used for phospho-peptide enrichment by High-Select Fe-NTA Phosphopeptide enrichment kit (Thermo Fisher) after manufacturer`s instructions. After enrichment, peptides were dried and resuspended in 70% acetonitrile/0.1% TFA and filtered through a C8 stage tip to remove contaminating Fe-NTA particles. Dried phospho-peptides then were fractionated on C18 (Empore) stage-tip. For fractionation C18 stagetips were washed with 100% acetonitrile twice, followed by equilibration with 0.1% TFA solution. Peptides were loaded in 0.1% TFA solution and washed with water. Elution was performed stepwise with different acetonitrile concentrations in 0.1% Triethylamine solution (5-30% in 11 steps, 50%). The 12 fractions were concatenated into six fractions and dried for LC-MS.

**Offline high pH reverse phase fractionation**

Peptides were fractionated using a Dionex Ultimate 3000 analytical HPLC. 250 µg of pooled and purified TMT-labeled samples were resuspended in 10 mM ammonium-bicarbonate (ABC), 5% ACN, and separated on a 250 mm long C18 column (X-Bridge, 4.6 mm ID, 3.5 µm particle size; Waters) using a multistep gradient from 100% Solvent A (5% ACN, 10 mM ABC in water) to 60% Solvent B (90% ACN, 10 mM ABC in water) over 70 min. Eluting peptides were collected every 45 s into a total of 96 fractions, which were cross-concatenated into 24 fractions and dried for further processing.

**Liquid chromatography mass spectrometry**

Peptides were resuspended in 0.1% FA and separated on an Easy nLC 1200 (ThermoFisher Scientific) and a 22 cm long, 75 µm ID fused-silica column, which had been packed in house with 1.9 µm C18 particles (ReproSil-Pur, Dr. Maisch), and kept at 45°C using an integrated column oven (Sonation). Peptides were eluted by a non-linear gradient from 5-38% acetonitrile over 120 min and directly sprayed into a QExactive HF mass spectrometer equipped with a nanoFlex ion source (ThermoFisher Scientific) at a spray voltage of 2.3 kV. Full scan MS spectra (350-1400 m/z) were acquired at a resolution of 120,000 at m/z 200, a maximum injection time of 100 ms and an AGC target value of 3 x $10^6$. Up to 20 most intense peptides per full scan were isolated using a 1 Th window and fragmented using higher energy collisional dissociation (normalized collision energy of 35). MS/MS spectra were acquired with a resolution of 45,000 at m/z 200, a maximum injection time of 80 ms and an AGC target value of 1 x $10^5$. Ions with charge states of 1 and > 6 as well as ions with unassigned charge states were not considered for fragmentation. Dynamic exclusion was set to 20 s to minimize repeated sequencing of already acquired precursors.

Phospho-peptide data was acquired in centroid mode on an Orbitrap Fusion Lumos mass spectrometer hyphenated to an easy-nLC 1200 nano HPLC system using a nanoFlex ion source (ThermoFisher Scientific) applying a spray voltage of 2.6 kV with the transfer tube heated to 300°C and a funnel RF of 30%. Internal mass calibration was enabled (lock mass 445.12003 m/z). Peptides were separated on a self-made, 32 cm long, 75µm ID fused-silica column, packed in house with 1.9 µm C18 particles (ReproSil-Pur, Dr. Maisch) and heated to 50°C using an integrated column oven (Sonation). HPLC solvents consisted of 0.1% Formic acid in water (Buffer A) and 0.1% Formic acid, 80% acetonitrile in water (Buffer B). For phosphopeptide analysis, each peptide fraction was eluted by a linear gradient from 5 to 32% B over 120 minutes followed by a step-wise increase to 95% B in 8 minutes which was held for another 7 minutes. Full scan MS spectra (350-1400 m/z) were acquired with a resolution of 120,000 at m/z 200, maximum injection time of 100 ms and AGC target value of 4 x $10^5$. The 20 most intense precursors per full scan with a charge state between 2 and 5 were selected for fragmentation ("Top 20"), isolated with a quadrupole isolation window of 0.7 Th and fragmented via HCD applying an NCE of 38%. MS2 scans were performed in the Orbitrap using a resolution of 50,000 at m/z 200, maximum injection time of 86ms and AGC target value of 1 x $10^5$. Repeated sequencing of already acquired precursors was limited by setting a dynamic exclusion of 60 seconds and 7 ppm and advanced peak determination was deactivated. An $MS^2$ based method was chosen, because of higher precision and identification rates[4]. Phospho-peptide fractions intrinsically exhibit lower complexity, rendering them less prone to ratio compression by isolation interference.

**Mass spectrometry data analysis**

Raw files were analyzed using Proteome Discoverer (PD) 2.4 software (ThermoFisher Scientific). Spectra were selected using default settings and database searches performed using SequestHT node in PD. Database searches were performed against trypsin digested Homo Sapiens SwissProt database , Salmonella typhimurium (strain LT2/SGSC1412/ATCC

700720) and FASTA files of common contaminants (`contaminants.fasta` provided with MaxQuant) for quality control. Fixed modifications were set as TMT6 at the N-terminus and carbamidomethyl at cysteine residues. One search node was set up to search with TMT6 (K) and methionine oxidation as static modifications to search for light peptides and one search node was set up with TMT6+K8 (K, +237.177), Arg10 (R, +10.008) and methionine oxidation as static modifications to identify heavy peptides. Searches were performed using Sequest HT. After search, posterior error probabilities were calculated and PSMs filtered using Percolator using default settings. Consensus Workflow for reporter ion quantification was performed with default settings, except the minimal signal-to-noise ratio was set to 5. Results were then exported to Excel files for further processing. For proteome quantification all peptides were summed intensity normalized, and peptides corresponding to a given UniProt Accession were summed including all modification states.

For translatome measurements, Excel files were processed in Python, as previously described[3]. Python 3.6 was used together with the following packages: pandas 0.23.4[5], numpy 1.15.4[6], scipy 1.3.0. Excel files with normalized PSM data were read in and each channel was normalized to the lowest channel based on total intensity. For each peptide sequence, all possible modification states containing a heavy label were extracted and the intensities for each channel were averaged between all modified peptides. Baseline subtraction was performed by subtracting the measured intensities for the non-SILAC-labeled sample from all other values. Negative intensities were treated as zero. The heavy label incorporation at the protein level was calculated by summing the intensities of all peptide sequences belonging to one unique protein accession. These values were combined with the standard protein output of PD 2.4 to add annotation data to the master protein accessions.

For TPCA-1 treated data (Figure 2, Table S3) the three measured multiplexes were processed individually as described above, followed by IRS normalisation on protein level to adjust for technical variance[7].

For phospho-peptide analysis static modifications were set as TMT6 at the N-terminus and lysines and carbamidomethyl at cysteine residues. Search was performed using Sequest HT taking the following dynamic modifications into account: Oxidation (M), Phospho (S, T, Y), Met-loss (Protein N-terminus), Acetyl (Protein N-terminus) and Met-loss acetyl (Protein N-terminus).

**Statistical analysis**

Significance was, unless stated otherwise, tested using unpaired two-sided students t-tests with equal variance assumed in cases where only two conditions are compared. For CFU and reporter assays with more than two samples, ANOVA was performed with post-hoc Bonferroni test for mean comparison. Statistical analysis was performed using OriginPro 2020 analysis software. For network and GO analysis all statistical computations were performed by the corresponding packages.

**Pathway enrichment analysis**

Pathway enrichment analysis was performed by ReactomeFI cytoscape plugin or by STRING functional enrichment analysis. Both analysis used Reactome database for pathway annotations.

**Hierarchical clustering and profile comparison**

Hierarchical cluster analysis and comparison with viral protein profiles for all samples was performed using Perseus[8] software package (version 1.6.5.0) after centering and scaling of data (Z scores).

**Additional references**

1. Ravenhill, B. J. *et al.* The Cargo Receptor NDP52 Initiates Selective Autophagy by Recruiting the ULK Complex to Cytosol-Invading Bacteria. *Mol. Cell* (2019).

2. Hahn, M. *et al.* SIK2 orchestrates actin-dependent host response upon Salmonella infection. *Proc. Natl. Acad. Sci. U. S. A.* **118**, e2024144118 (2021).

3. Klann, K., Tascher, G. & Münch, C. Functional Translatome Proteomics Reveal Converging and Dose-Dependent Regulation by mTORC1 and eIF2α. *Mol. Cell* **77**, 913-925.e4 (2020).

4. Hogrebe, A. *et al.* Benchmarking common quantification strategies for large-scale phosphoproteomics. *Nat. Commun.* **9**, 1045 (2018).

5. McKinney, W. Data Structures for Statistical Computing in Python. 51–56 (2010).

6. van der Walt, S., Colbert, S. C. & Varoquaux, G. The NumPy Array: A Structure for Efficient Numerical Computation. *Comput. Sci. Eng.* **13**, 22–30 (2011).

7. Plubell, D. L. *et al.* Extended Multiplexing of Tandem Mass Tags (TMT) Labeling Reveals Age and High Fat Diet Specific Proteome Changes in Mouse Epididymal Adipose Tissue. *Mol. Cell. Proteomics* **16**, 873–890 (2017).

8. Tyanova, S. *et al.* The Perseus computational platform for comprehensive analysis of (prote)omics data. *Nat. Methods* **13**, 731–740 (2016).

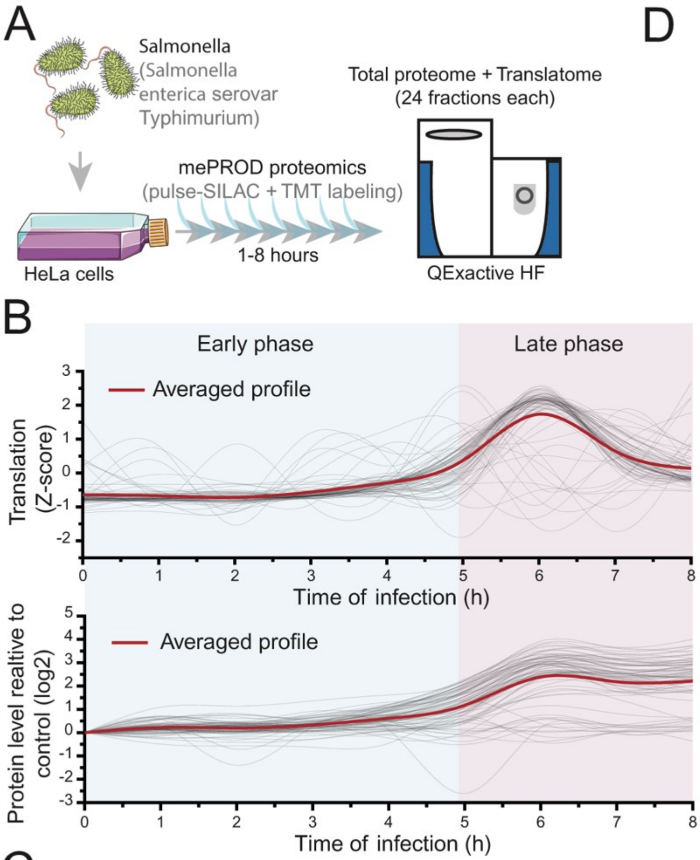


C

| Kegg pathway (late phase) | FDR |
|---|---|
| NF-kappa B signaling pathway | 7.93E-5 |
| Fluid shear stress and atherosclerosis | 0.0043 |
| Epstein-Barr virus infection | 0.0118 |
| TNF signaling pathway | 0.0195 |

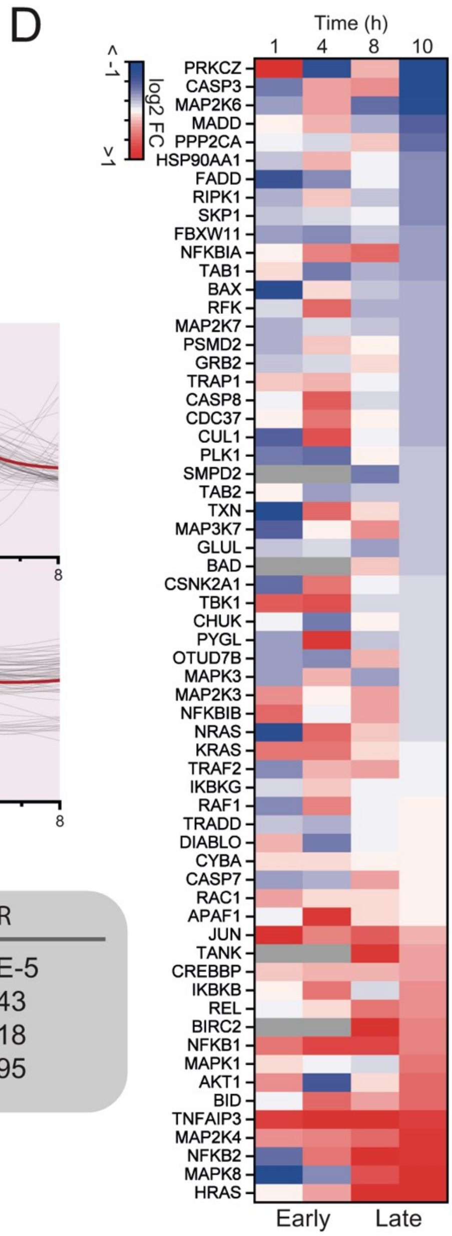


Fig. 1: Infection with Salmonella translationally modulates the NF-κB pathway

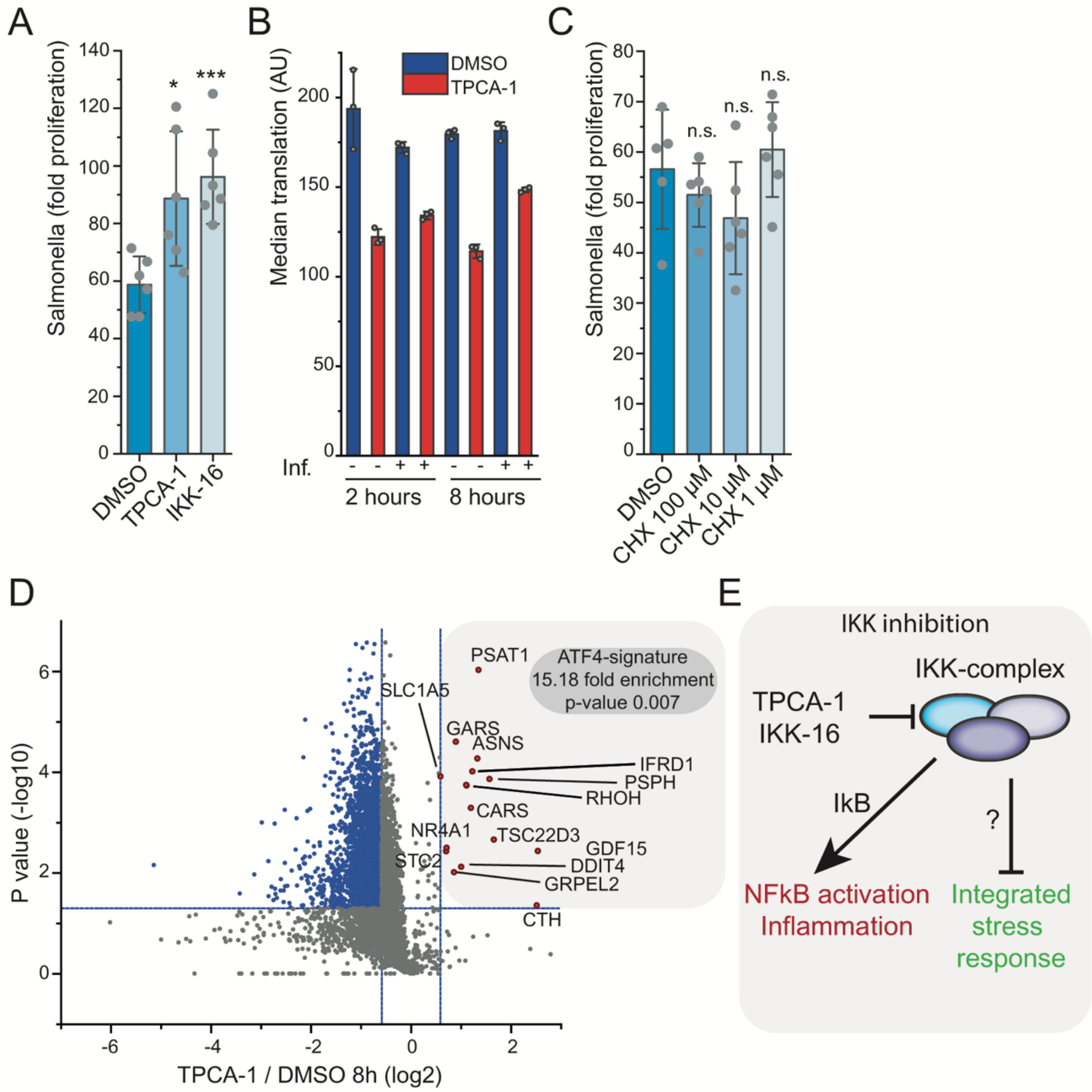


Fig. 2: Inhibition of the IKK complex leads to integrated stress response activation

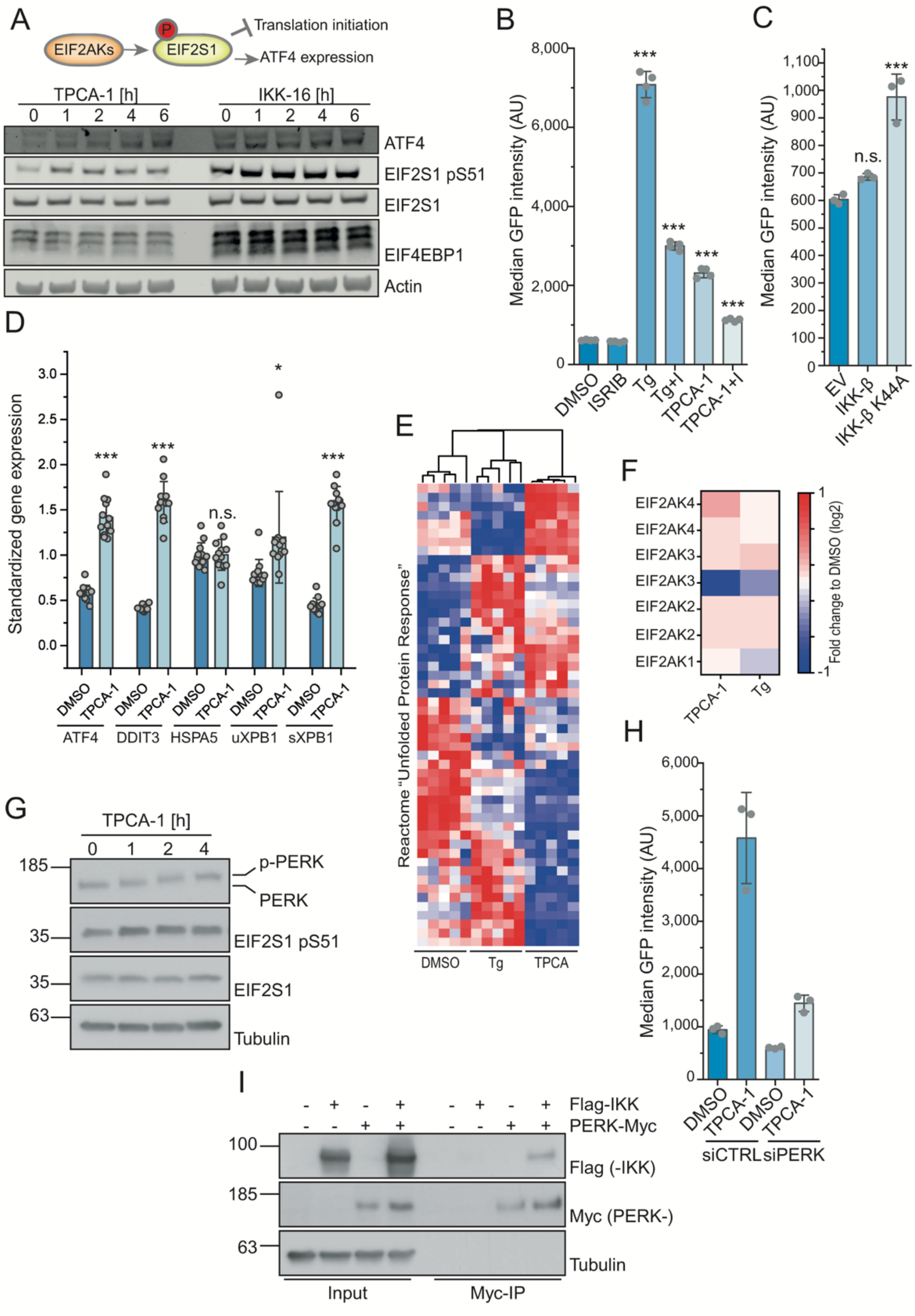


Fig. 3: A novel IKK/PERK signaling axis modulates the integrated stress response

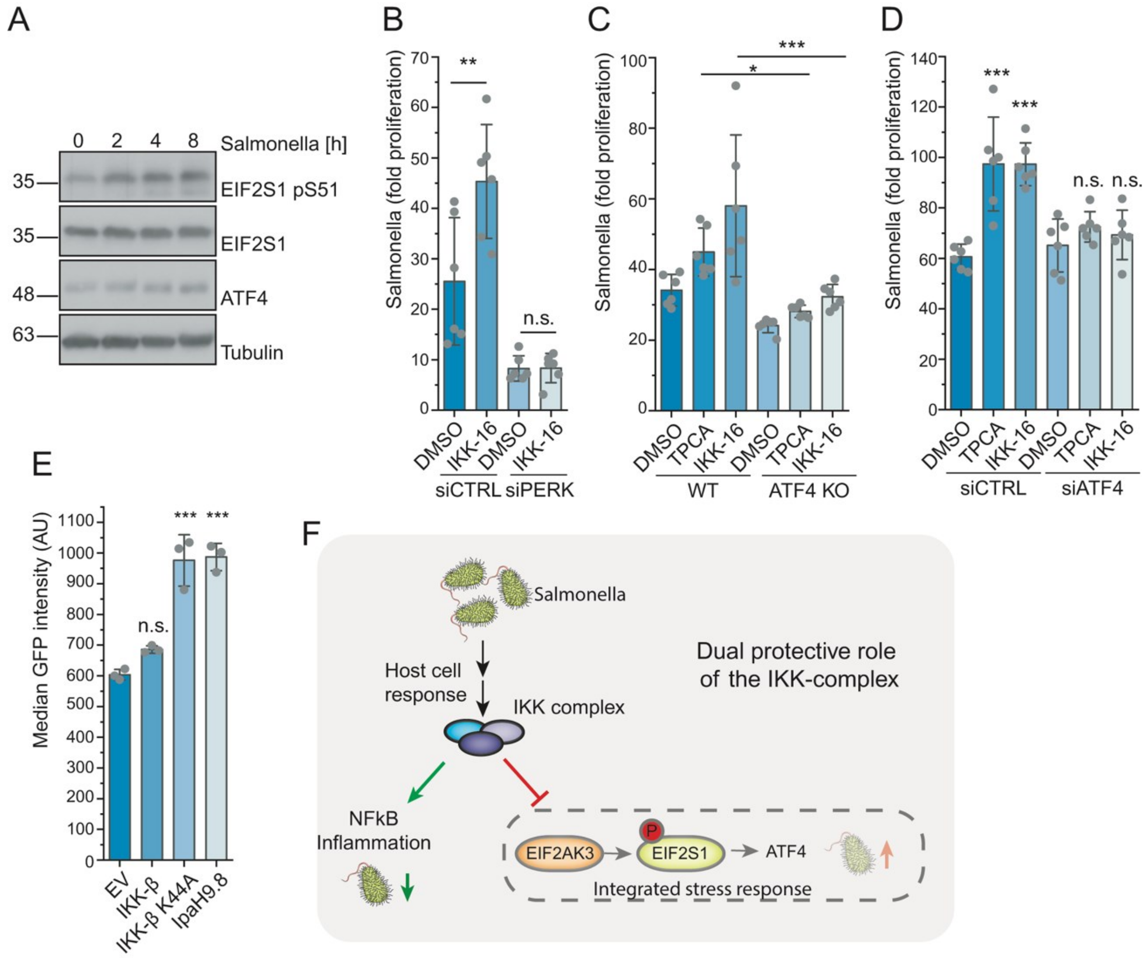


Fig. 4: Bacterial infection targets IKKs to induce the ISR

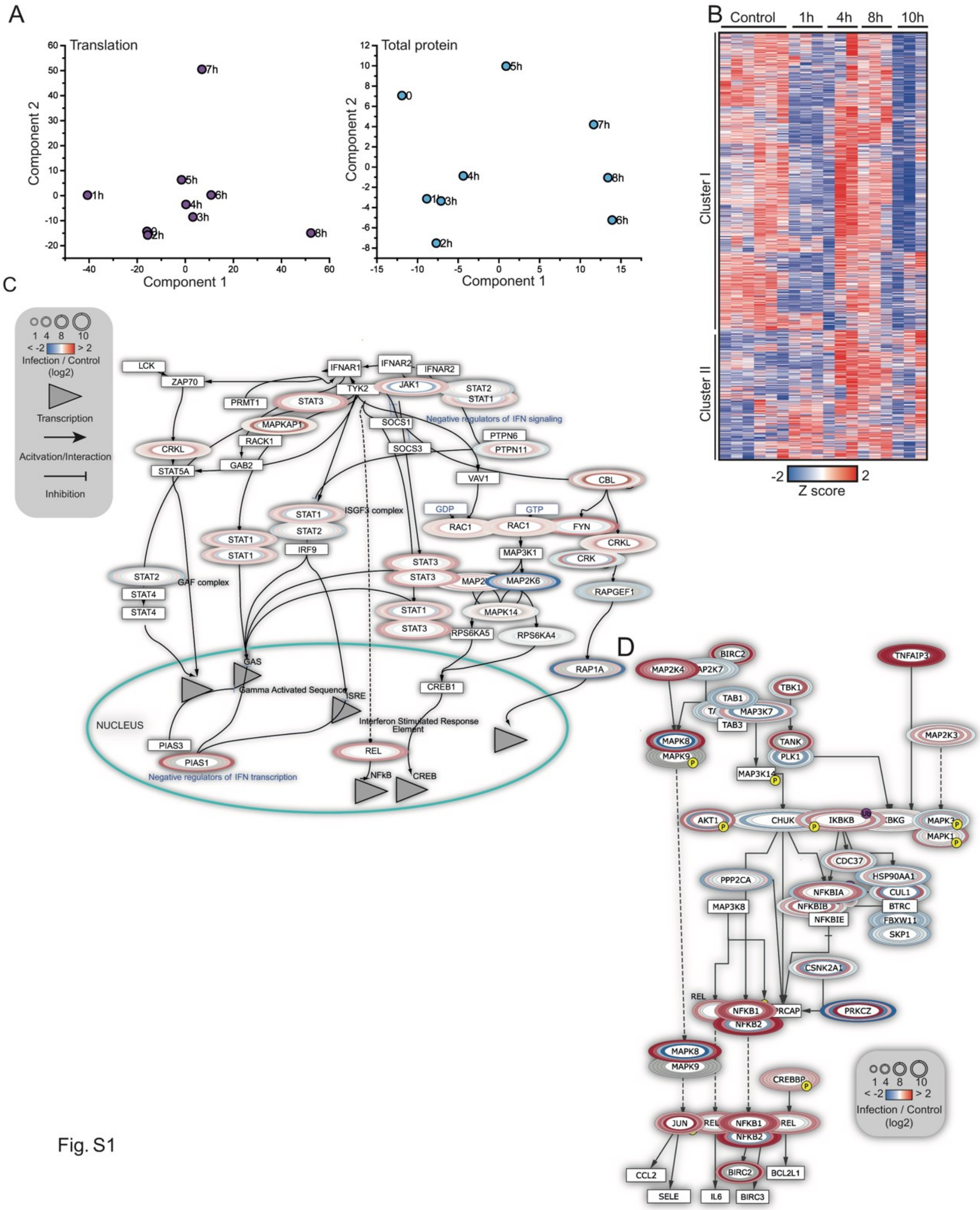

Fig. S1

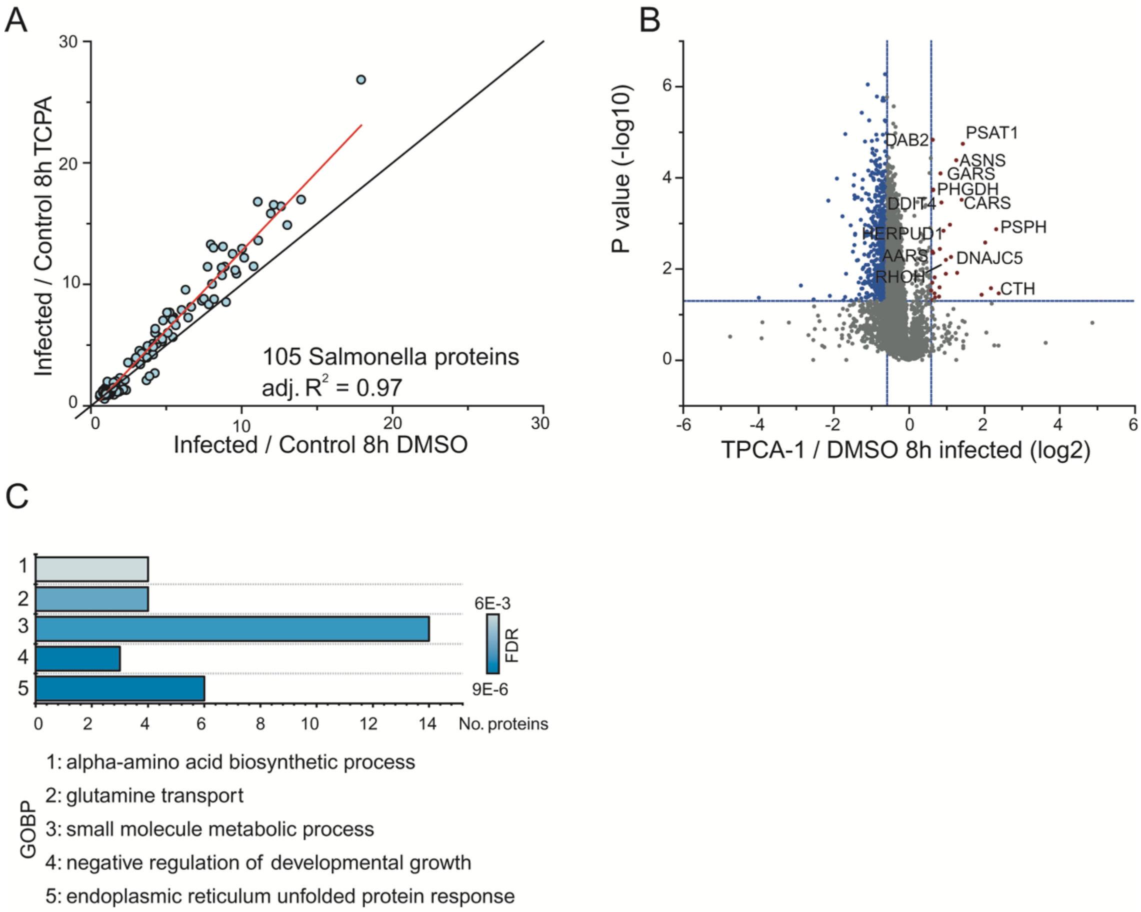
A
Infected / Control 8h TCPA
Infected / Control 8h DMSO
105 Salmonella proteins
adj. $R^2$ = 0.97
B
P value (-log10)
TPCA-1 / DMSO 8h infected (log2)
PSAT1
DAB2
ASNS
GARS
PHGDH
CARS
DDIT4
PSPH
HERPUD1
AARS
DNAJC5
RHOB
CTH
C
6E-3
FDR
9E-6
No. proteins
GOBP
1: alpha-amino acid biosynthetic process
2: glutamine transport
3: small molecule metabolic process
4: negative regulation of developmental growth
5: endoplasmic reticulum unfolded protein response

Fig. S2

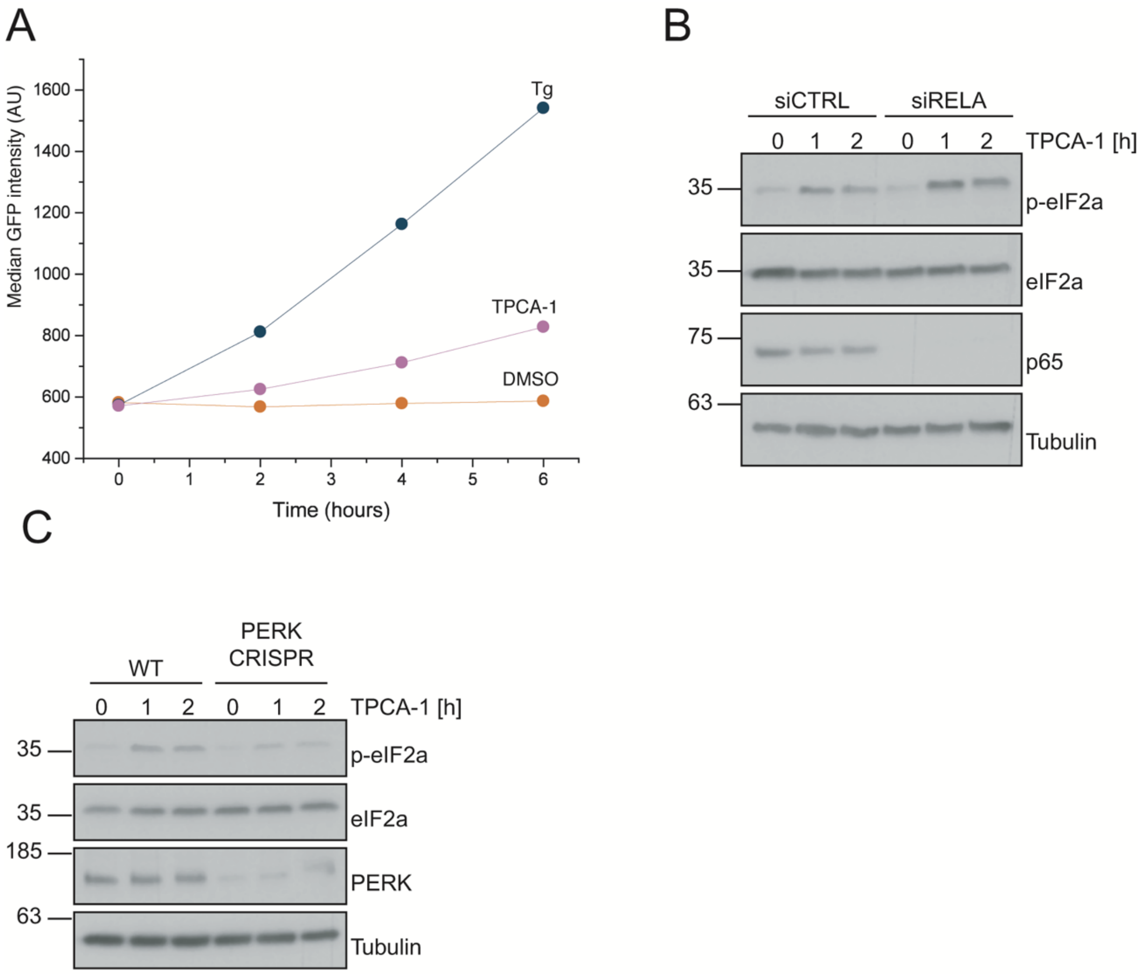
A
Median GFP intensity (AU)
1600
1400
1200
1000
800
600
400
0
1
2
3
4
5
6
Time (hours)
Tg
TPCA-1
DMSO
B
siCTRL
siRELA
0 1 2 0 1 2 TPCA-1 [h]
35
p-eIF2a
35
eIF2a
75
p65
63
Tubulin
C
WT
PERK CRISPR
0 1 2 0 1 2 TPCA-1 [h]
35
p-eIF2a
35
eIF2a
185
PERK
63
Tubulin

Fig. S3

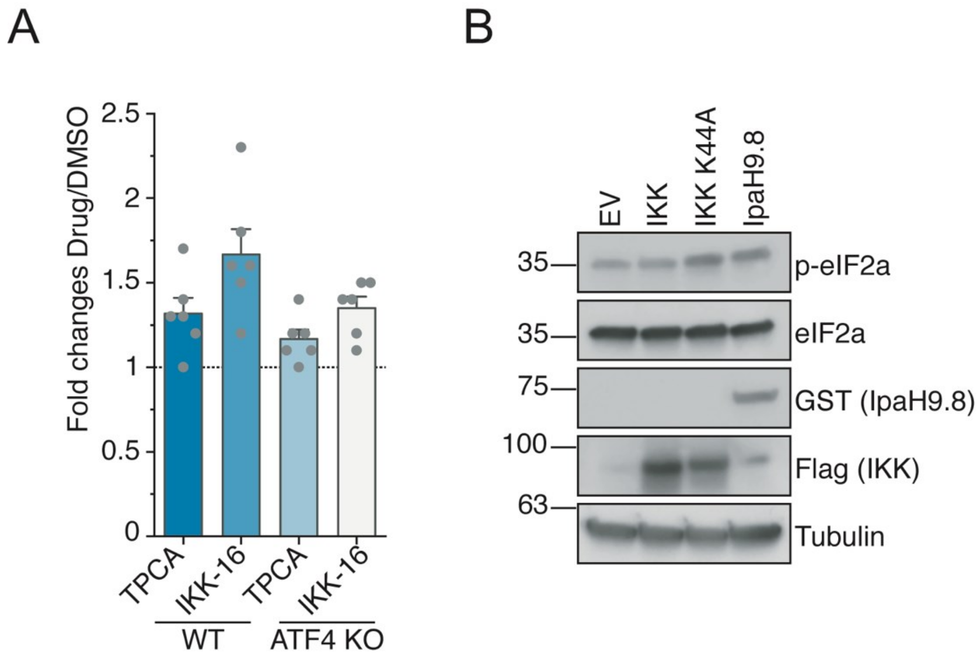
A
B
Fold changes Drug/DMSO
2.5
2
1.5
1
0.5
0
TPCA
IKK-16
TPCA
IKK-16
WT
ATF4 KO
EV
IKK
IKK K44A
IpaH9.8
35
35
75
100
63
p-eIF2a
eIF2a
GST (IpaH9.8)
Flag (IKK)
Tubulin

Fig. S4

Curriculum vitae